Dissertation zur Erlangung des Doktorgrades
der Fakultät für Chemie und Pharmazie
der Ludwig-Maximilians-Universität München

Assembly and regulation of kinetochore complexes at the budding yeast point centromere

Mia Potočnjak

aus

Rijeka, Primorsko-goranska, Croatia

2021

Erklärung

Diese Dissertation wurde im Sinne von § 7 der Promotionsordnung vom 28. November 2011 von Herrn Dr. Franz Herzog betreut.

Eidesstattliche Versicherung

Diese Dissertation wurde eigenständig und ohne unerlaubte Hilfe erarbeitet.

München, 26.01.2021

Mia Potočnjak

Dissertation eingereicht am 14.12.2020

1. Gutachter: Dr. Franz Herzog

2. Gutachter: Prof. Dr. Karl Peter Hopfner

Mündliche Prüfung am 19.01.2021

Abstract

Growth and propagation of all organisms depend on the accurate dissemination of the genetic material to the progeny. During the eukaryotic cell cycle the duplicated DNA condenses into chromosomes followed by their equal distribution to the daughter cells. The kinetochore is a multi-protein structure that creates a link between chromosomes and spindle microtubules and serves as a platform for feedback control mechanisms to ensure the fidelity of this process. The kinetochore is also required for replenishing the levels of the histone H3 variant CENP-A^{Cse4} and maintaining centromere identity. CENP-A^{Cse4} (budding yeast orthologues are superscripted) containing nucleosomes specify the assembly of the entire kinetochore which is composed of the Constitutive Centromere-Associated $Network^{Ctf19C}$ (CCAN) at the inner kinetochore and the $KNL1^{SPC105}$/$MIS12^{MTW1}$/$NDC80^{NDC80}$ (KMN) network at the outer kinetochore harbouring the main microtubule attachment site. Major efforts on the reconstitution and structural analysis resulted in a more detailed understanding of kinetochore assembly and its role in chromosome segregation. At the beginning of this thesis the protein interactions of CENP-C^{Mif2}, a backbone of kinetochore assembly had not been fully understood. CENP-C^{Mif2} was described as the only direct link between CENP-A^{Cse4} nucleosomes and the outer kinetochore MTW1 complex. Yet, it was clear that a link of a single centromeric nucleosome to only one microtubule attachment site does not withstand the pulling forces of depolymerising microtubules.

The goal of this thesis was to obtain a comprehensive understanding of the native kinetochore architecture in order to reveal its function in generating the mechanical link between chromosomes and microtubules and in integrating feedback control mechanisms that align chromosome segregation with cell cycle progression. The budding yeast point centromere is thought to represent a single kinetochore unit, as only one nucleosome is linked to a single microtubule. The budding yeast centromere is determined by a conserved DNA sequence recognised by Cep3, a subunit of the CBF3 complex. The Ndc10 subunit of the same complex is essential for Cse4 loading and provides the foundation for the recruitment of the inner and outer kinetochore. Using *in vitro* reconstituted kinetochore complexes, I identified two kinetochore components, Ame1/Okp1 and Ndc10, that in addition to Mif2 establish a direct link between the Cse4 nucleosome and the outer kinetochore MTW1c. Characterisation of their binding interfaces revealed a similar mode of interaction as Mif2. All three MTW1c

recruiters bind the helix-loop-helix region of the Mtw1 protein and their interactions are stabilized by phosphorylation of Dsn1 at S240 and S250, which released the masking of the Mtw1 site by Dsn1. Moreover, I showed that the simultaneous interaction of Mif2 and Ame1/Okp1 with MTW1c is important for the cooperative stabilization of the inner kinetochore at the centromeric nucleosome in mitosis. Mtw1 recruitment through the N-terminal domain of Ame1 is essential for cell viability, whereas Mtw1 binding by the N-termini of Mif2 or Ndc10 is dispensable and those two pathways only become important when either of them is impaired.

In a second independent project, I investigated the assembly and cooperative stabilization of the outer kinetochore KMN network. I identified the motifs in the Mtw1 C-terminus required for the recruitment of the SPC105 and NDC80 subcomplexes and showed that in contrast to human kinetochores, the budding yeast SPC105c was recruited through Kre28. Notably, I identified the protein interactions that generate cooperativity stabilizing the KMN network. In addition to interactions formed by the C-terminal motifs of the MTW1c, a weak direct interaction between the NDC80 and SPC105 subcomplexes significantly contributed to the cooperative stabilization.

My analysis of full-length multi-subunit kinetochore complexes allowed the identification and characterisation of two kinetochore complexes, Ame1/Okp1 and CBF3c, which directly connect the outer kinetochore microtubule binding interface to centromeric chromatin.

In particular, the finding that Ndc10, which so far has been implicated in Cse4 incorporation and nucleosome formation, contributes to kinetochore assembly by recruiting an additional microtubule binding unit in mitosis, is crucial for establishing a stable kinetochore architecture on the budding yeast point centromere that withstands the microtubule pulling forces in order to biorient chromosomes and to accurately distribute the genetic information.

List of publications and contributions

Potocnjak M, Singh S, Speljko T, Kumar CN, Brandstetter K, Harz H, Leonhardt H, Herzog F. Ndc10 recruits the outer kinetochore MTW1 complex through its N terminus in mitosis. Manuscript in preparation.

M.P. designed the project and the experiments. She cloned and purified kinetochore proteins, performed binding assays, size exclusion, *in vivo* immunoprecipitation assays and cross-linking mass spectrometry analysis. She participated in writing the manuscript.

Ghodgaonkar-Steger M*, **Potocnjak M***, Zimniak T, Fischböck-Halwachs J, Solis-Mezarino V, Singh S, Speljko T, Hagemann G, Drexler DJ, Witte G, Herzog F. C-Terminal Motifs of the MTW1 Complex Cooperatively Stabilize Outer Kinetochore Assembly in Budding Yeast. Cell Reports. 2020; 32, 108190. (*equal contribution)

M.P. participated in the design of the experiments. She cloned and purified various kinetochore proteins, performed binding assays and size exclusion experiments. She designed the crosslinked model. She participated in writing the manuscript.

Fischböck-Halwachs J*, Singh S*, **Potocnjak M***, Hagemann G, Solis-Mezarino V, Woike S, Ghodgaonkar-Steger M, Weissmann F, Gallego LD, Rojas J, Andreani J, Köhler A, Herzog F. The COMA complex interacts with Cse4 and positions Sli15/Ipl1 at the budding yeast inner kinetochore. Elife. 2019; 8. (*equal contribution)

M.P. cloned and expressed various kinetochore complexes and nucleosome reconstitution. She performed electrophoretic mobility shift assay (EMSA) of the CCAN subunits and obtained the cross-linking mass spectrometry network. She also performed EMSA and size exclusion analysis of the Okp1 mutants. She participated in design of the study and writing the manuscript.

Hagemann G*, Solis-Mezarino V*, Singh S, **Potocnjak M**, Kumar C, Herzog F. Quantitative Crosslinking and Mass Spectrometry Detect Phospho-Induced Kinetochore Stabilization. Manuscript under review.

M.P. expressed kinetochore proteins and mutants and performed the binding assays.

Kratzat H*, Mackens-Kiani T*, Ameismeier M, **Potocnjak M**, Cheng J, Dacheux E, Namane A, Berninghausen O, Herzog F, Fromont-Racine M, Becker T and Beckmann R. A structural inventory of native ribosomal ABCE1-43S pre-initiation complexes. EMBO J. 2020 e105179 .
M.P. carried out cross linking mass spectrometry analysis using DSSG of the ABCE1 43S pre-initiation complex.

Ivic N, **Potocnjak M,** Solis-Mezarino V, Herzog F, Bilokapic S, Halic M. Fuzzy Interactions Form and Shape the Histone Transport Complex. Mol Cell. 2019; 73(6):1191-1203.
M.P. carried out cross linking mass spectrometry analysis using DSSG and DMTMM of the Imp7:Impβ:H1.0 complex.

Acknowledgements

I want to thank Dr. Franz Herzog for the opportunity to work in his lab where I really had a chance to develop my expertise in any direction in found interesting and learn to independently work and design projects. Thank you!

I would like to also thank all of the members of the Herzog lab for a great atmosphere. It was always interesting, funny, creative and I truly am happy to have worked with such a great group of scientists.
Medini for teaching me a lot of different techniques as well as critical thinking. It was always fun to work with you! Victor for constant help with any bioinformatical question even after you finished your PhD and left the lab. Sylvie, Tea and Chandni for all the help in the lab especially during my last project. Josef and Gotz for the fun time at work together and every discussion we had.

I would also like to thank Silvija and Mario Halic who thought me so much even though our work together did not result in the publication we wanted.

Finally, I am truly grateful to my family Ines, Zarko, Matea and grandparents for their constant support throughout my life and knowing that they always have my back. And last, but the best, Przemek who set the course of my life in a direction I never dreamt of and would never change.

Contents

1 Introduction

1.1 Mitosis

The accurate dissemination of the genetic material during cell division is a prerequisite for all organisms to proliferate and develop from a single fertilized egg. Two identical copies of the genetic material must be equally distributed to the two daughter cells to avoid abnormal growth and cancer (Hanahan and Weinberg 2000). In eukaryotes, the cell is preparing and duplicating its genetic material prior to the mitotic cell division. Interphase is a longer period of the cell cycle during which the cell grows, and duplicates its genetic material. The cell grows by protein and organelle production in G1 phase, duplicates the chromosomes in S phase which is followed by further growth, DNA repair in preparation of mitosis. Finally, the mitotic cyclin-dependent kinase Cdk1 associated with cyclin B, promotes mitosis (M), the chromosomes segregate and the new cell cycle begins (Barnum and O'Connell 2014). This process was observed and described during the 18th and 19th century by a number of scientists. The term mitosis was coined by Walther Flemming from the Greek word mitos "thread", probably referring to the observation of the thread like chromosome structure (Sharp 1921).

The cell cycle rhythm is orchestrated by cyclins and cyclin-dependent kinases (Cdks). Cdks are serine/threonine protein kinases that remain inactive until cyclin binding occurs. Active Cdks phosphorylate key substrates thereby promoting mitotic progression. Cell cycle checkpoints in G1- and G2/M phase control the cell size and nutritional status before allowing the cell to progress further (Figure 1). Upon lack of nutrients the cell can leave the cell cycle and enter G0 phase. DNA damage is also one factor that is controlled during interphase and will slow down cell cycle progression. During S phase the cell is especially sensitive as DNA polymerases duplicate the genetic material and DNA damage acts as a physical barrier delaying DNA replication (Sullivan and Morgan 2007, Barnum and O'Connell 2014).

In higher eukaryotes, the mitotic phase occurs in the following stages: prophase, prometaphase, metaphase, anaphase and telophase. In prophase the DNA is condensed into chromosomes, through prometaphase the nuclear membrane breaks down and the chromosomes are attached to the spindle microtubules. The spindle

assembly checkpoint does not allow progression until all chromosomes have proper amphitelic attachments with the spindle and are aligned at the metaphase plate. Once this is satisfied, the E3 ubiquitin-protein ligase known as the anaphase-promoting complex or cyclosome (APC/C) targets cyclin B and securin for degradation (Murray 2004). The sister chromatids are then separated in anaphase, degradation of securin allows separase to cleave cohesin and the chromatids are pulled towards the opposing spindle poles. During telophase sister chromatids are surrounded by a nuclear membrane, and the cell is split into two identical daughter cells also known as cytokinesis. Yeast cells undergo a closed mitosis where the nuclear envelope remains intact as opposed to higher eukaryotes. However, the key phases of mitosis are conserved (Boettcher and Barral 2013).

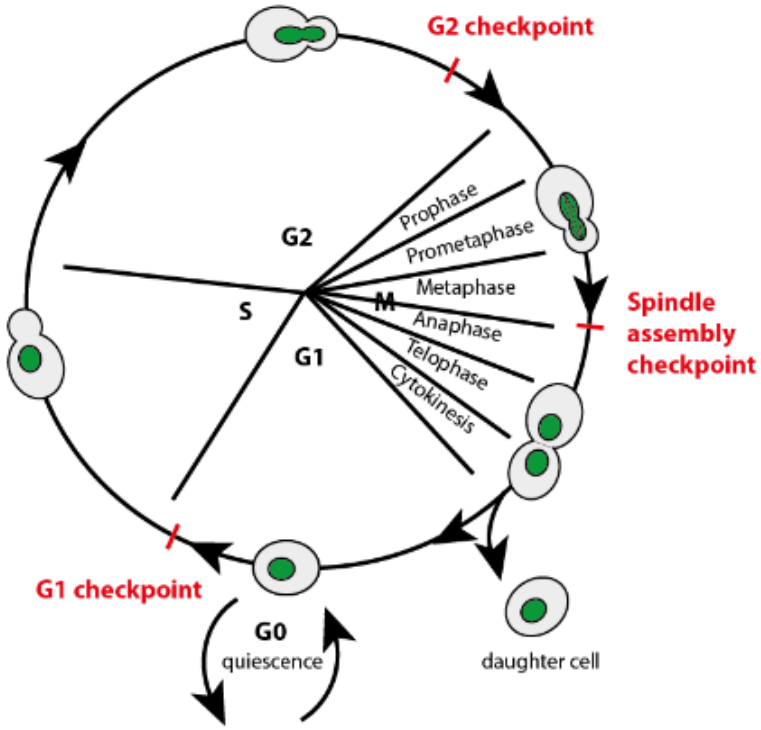

Figure 1 **Budding yeast cell cycle**

Cyclins and Cdks drive the cell irreversibility and unidirectionally through the phases of the cell cycle while checkpoints (G1-, G2- and the Spindle assembly checkpoint) ensure proper cell growth, accurate DNA replication and division of the DNA (adapted from (Nasmyth 1996, Delobel and Tesnière 2014)).

1.2 The centromere

The centromere is a region of specialized chromatin that links the two sister chromatids and allows their separation during mitosis by providing an attachment site for spindle microtubules. Its name suggests it is localized in the middle of the chromosome (Greek centro "central" and mere "part"), however that does not have to be the case (O'Connor 2008). Only metacentric chromosomes are characterised by a central centromere as opposed to submetacentric, acrocentric and telocentric with centromeres gradually approaching the telomeric region of the chromosome. This feature is useful for karyotyping and the mapping of gene positions. The centromere represents a point of constriction where the two sister chromatids meet and are linked by the cohesin protein complex until anaphase onset. Eukaryotic chromosomes have a single centromere where the kinetochore assembles prior to cell division (Levan 1964, Guacci, Koshland and Strunnikov 1997, Michaelis, Ciosk and Nasmyth 1997). Chromosomes without centromeres or with two centromeres will not be accurately divided and will be lost either after mitosis or result in chromosomal errors.

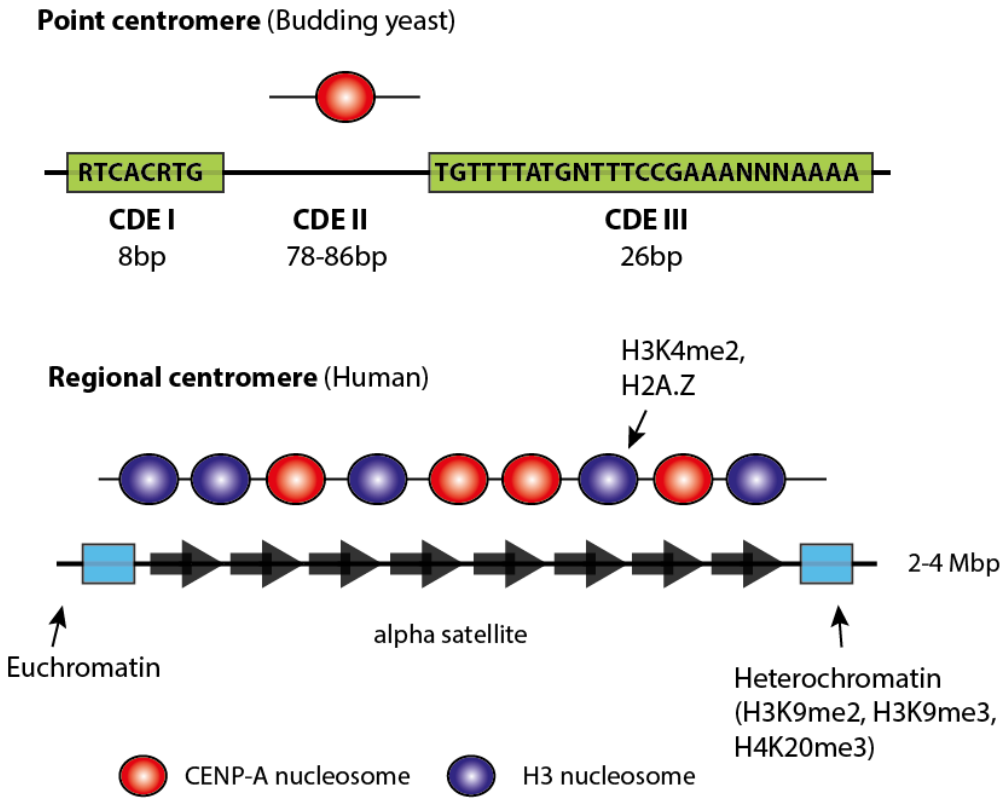

Figure 2 Point versus regional centromeres

The budding yeast point centromere is determined by a specific ~125 bp DNA sequence with a single Cse4 nucleosome linked to a single microtubule. DNA sequence is composed of 8bp long CDEI, AT rich CDEII and 26bp long CDEIII. Regional centromeres, as found in humans and more complex organisms, are assembled on alpha satellite DNA with 20-30 CENP-A nucleosomes forming a binding site for roughly 20 microtubules (adapted from (Verdaasdonk and Bloom 2011).

Formation of chromosomes is possible due to tight wrapping of the DNA around a histone octamer known as nucleosome. It is formed by two copies of H2A, H2B, H3 and H4 histones. However, centromeric chromatin is characterized by the incorporation of the histone H3 variant CENP-A. CENP-A was initially discovered in patients that suffered from CREST syndrome, an autoimmune disease due to which they developed anti-centromere antibodies. The proteins that reacted with those antibodies were termed CENPs (CENtromere Proteins) (Black et al. 2010, Earnshaw and Rothfield 1985). In vertebrates, a region spanning 0.5-2 Mb with multiple CENP-A nucleosomes defines regional centromeres. In contrast, the centromere found in *S. cerevisiae* and related fungi is composed of a single Cse4 nucleosome assembled on a conserved ∼125 bp long DNA segment (CEN) which is thus termed point centromere and is sufficient for kinetochore assembly (Hieter et al. 1985, Pluta et al. 1995). The three conserved DNA elements are the 8 bp Centromere Defining Element I (CDEI), the ∼ 90% AT rich CDEII, and the 26 bp long CDEIII sequence (Stoler et al. 1995, Clarke 1998) (Figure 2). The CDEI and CDEIII regions are necessary and sufficient for active centromere formation stabilizing the CDEII loop of the Cse4 nucleosomes. Those regions are occupied by Cbf1 and the CBF3 complex (CBF3C), respectively. The later has been proven to be essential for centromere function.

1.3 The kinetochore

The supramolecular kinetochore complex assembled at centromeres is a key cellular structure guiding faithful chromosome segregation (Cheeseman 2014, Nagpal and Fukagawa 2016). The kinetochore has four different functions in this process: 1) it establishes a physical link between chromosomal DNA and spindle microtubules. 2) it

integrates an error correction mechanism that discerns proper from improper spindle attachments and corrects erroneous attachments promoting bi-orientation of sister chromatids in metaphase (Foley and Kapoor 2013): 3) it provides a platform for a feedback control mechanism, known as the spindle assembly checkpoint, which coordinates chromosome alignment with mitotic exit (London and Biggins 2014, Musacchio 2015) and 4) it is part of a machinery that replenishes CENP-A levels at the centromere and thus, maintains centromere identity over generations (Swartz et al. 2019).

The kinetochore architecture is assembled at centromeric chromatin and composed of the inner kinetochore Constitutive Centromere-Associated Network (CCAN) and the outer kinetochore KNL1/MIS12/NDC80 (KMN) network. The former is tightly associated with centromeric nucleosomes throughout the cell cycle and provides a platform for building up the latter. The outer kinetochore facilitates the load-bearing interaction with dynamic microtubules and controls their attachment (Figure 3) (Musacchio and Desai 2017).

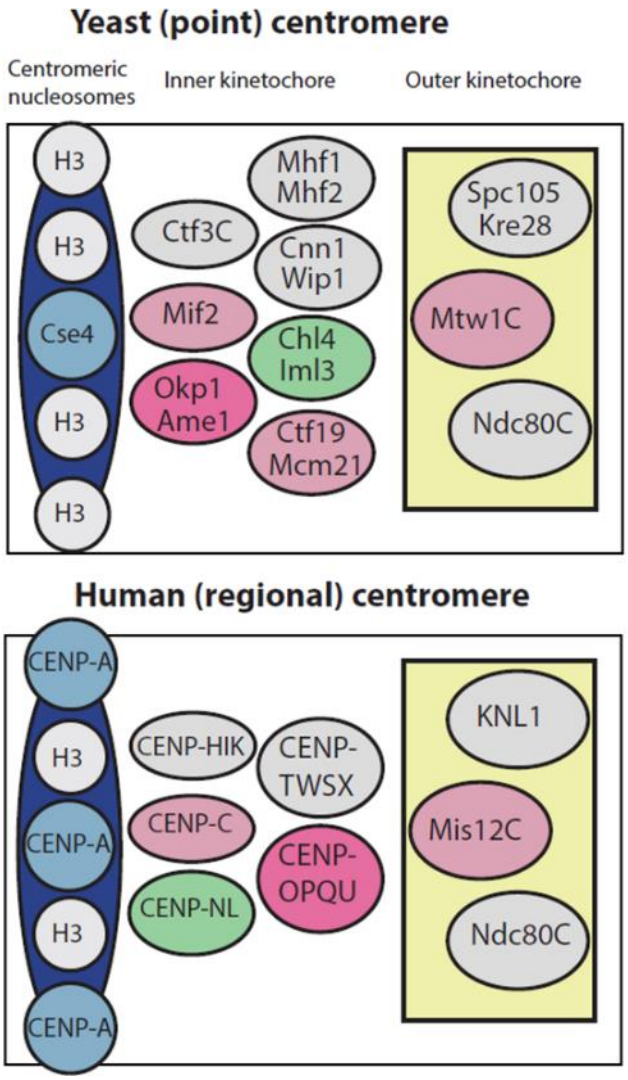

Figure 3 Kinetochore schematic

Illustration of kinetochore sub-complexes from budding yeast (upper panel) and human (lower panel), excluding proteins involved in cell cycle regulation (adapted from (Musacchio and Desai 2017)).

1.3.1 Nucleosome proximal CCAN subunits

Cse4^{CENP-A} containing nucleosomes, serve as the foundation for kinetochore assembly, its distinct structural properties allow selective binding of certain CTF19C^{CCAN} proteins. Homology between histone H3-like proteins is limited to the histone fold domain (HFD) (Henikoff et al. 2000). Unlike H3, Cse4 has a unique 135 amino acid long N-terminus essential for cell viability (Mann and Grunstein 1992, Keith et al. 1999, Chen et al. 2000). Based on the structure of H3 and CENP-A nucleosomes the HFD of Cse4 assembles into

the octamer with the N-terminus extending away from the core (Luger et al. 1997, Kato et al. 2013, Arimura et al. 2014). Recently two structures of the Cse4 nucleosome were published, however they were not able to resolve the flexible N-terminal tail harbouring the most interesting region that carries the difference between H3 and Cse4 nucleosome (Yan et al. 2019, Migl et al. 2020). The deletion of the first 36 to 50 amino acids is lethal to the cell and proposed to recruit the Ctf19 protein complex (Ortiz et al. 1999, Chen et al. 2000). This region might also be a target for the posttranslational modifications required for the integrity of the kinetochore architecture and/or function (Wolffe and Hayes 1999, Chen et al. 2000).

Advances in cryo-electron microscopy provided insights into the inner kinetochore architecture (Hinshaw and Harrison 2019, Yan et al. 2019). So far, two CCAN proteins were described as selective and direct binders of the human CENP-A nucleosome: CENP-C and CENP-N (Kato et al. 2013, Pentakota et al. 2017, Chittori et al. 2018). In contrast, for the yeast Cse4 nucleosome only the CENP-C homologue Mif2 has been identified as direct interactor. Although (Yan et al. 2019) report the interaction of Chl4/Iml3 the yeast orthologue of CENP-L/N, with the unwrapped DNA of the Cse4 nucleosome, no interaction was observed with Cse4 nucleosomes under *in vitro* conditions (Fischbock-Halwachs et al. 2019). CENP-N binds directly to the CENP-A centromere-targeting domain (CATD) (Carroll et al. 2009). CENP-C with the central region and CENP-C motif targets the acidic patch of H2A and H2B and the C-terminal tail of CENP-A (Carroll, Milks and Straight 2010, Kato et al. 2013, Falk et al. 2016). The budding yeast homolog Mif2 lacks the central region, but displays a conserved CENP-C motif and the dimerization domain (Cohen et al. 2008). Apart from $Mif2^{CENP\text{-}C}$, Ame1/Okp1 was identified as a selective interactor of Cse4 nucleosomes, while this was not confirmed for its human orthologue CENP-U/Q. Ame1/Okp1 directly docks on the extended N-terminal tail of Cse4 via interaction through Okp1 (Fischbock-Halwachs et al. 2019, Anedchenko et al. 2019). CENP-H/I/K is also a known, yet non-selective binding partner of CENP-A nucleosomes, as it equally binds to H3 nucleosomes (Weir et al. 2016). These proteins create a $CTF19C^{CCAN}$ foundation for kinetochore assembly.

Apart from the members of the $CTF19C^{CCAN}$ complex the CBF3 complex is only found in budding yeast without its known human orthologue. It specifically binds the

centromeric DNA and is required for localization of other kinetochore proteins (Ng and Carbon 1987).

Table 1 **Overview of the known kinetochore subunits in budding yeast and human cells**

Comparison of the known kinetochore subunits in budding yeast and human cells (Biggins 2013, Musacchio and Desai 2017).

Kinetochore layer	Subcomplex	Kinetochore proteins	
		S. cerevisiae	*H. sapiens*
Centromeric DNA binding components	CBF3 complex	Ndc10	
		Cep3	
		Ctf13	
		Skp1	
		Cbf1	
		Cse4	CENP-A
			CENP-B
CCAN network	COMA	Mif2	CENP-C
		Mcm21	CENP-O
		Ctf19	CENP-P
		Okp1	CENP-Q
		Ame1	CENP-U
		Chl4	CENP-N
		Iml3	CENP-L
	HIK complex	Mcm16	CENP-H
		Ctf3	CENP-I
		Mcm22	CENP-K
			CENP-M
	CENP-TWSX	Cnn1	CENP-T
		Wip1	CENP-W
		Mhf1	CENP-S
		Mhf2	CENP-X
		Nkp1	
		Nkp2	
KMN network	Mis12/MIND	Dsn1	Dsn1
		Nsl1	Nsl1
		Mtw1	Mis12
		Nnf1	Pmf1
	KNL1	Spc105	Knl1
		Kre28	Zwint
	Ndc80	Ndc80	Ndc80

		Nuf2 Spc24 Spc25	Nuf2 Spc24 Spc25
Microtubule binding components	Dam1/DASH complex	Ask1 Dad1 Dad2 Dad3 Dad4 Dam1 Duo1 Spc19	
	Ska1		Ska1 Ska2 Ska3

1.3.2 The CBF3 complex

The CBF3 complex (CBF3c) was only identified in inter-related budding yeasts as CEN DNA sequence binding complex (Ng and Carbon 1987). The *S. cerevisiae* centromeric DNA consists of three distinct regions, 8 bp long CDEI, 78-86 bp AT rich CDEII and 25 bp CDEII sequence (Hegemann and Fleig 1993). CBF3c binds the CDEIII sequence in such a sequence specific manner that a single mutation in the sequence leads to loss of interaction. The CCG triplet was shown to be the essential element and its mutation inhibits the binding of CBF3c *in vitro* and localization of Ndc10 and Mif2 proteins *in vivo* (Ng and Carbon 1987, Hegemann and Fleig 1993, Lechner and Carbon 1991, Meluh and Koshland 1997). Apart from Cbf1 all kinetochore proteins require CBF3c for their recruitment. It consists of four essential subunits assembled as Skp1:Ctf13 (Suppressor of kinetochore protein mutant 1: Chromosome transmission fidelity 13) heterodimer, Cep3 (Centromere protein 3) homodimer, and Ndc10 (Nuclear division cycle 10-1) homodimer. All four proteins are essential for kinetochore function (Doheny et al. 1993, Goh and Kilmartin 1993, Russell, Grancell and Sorger 1999, Strunnikov, Kingsbury and Koshland 1995, Jiang, Lechner and Carbon 1993). The CBF3 core refers to the Skp1:Ctf13:(Cep3)2 subassembly which is stable *in vitro* (Leber, Nans and Singleton 2018). Skp1, the only conserved CBF3 protein, was identified a few years after the other three components as a suppressor of CBF3 mutations (Connelly and Hieter 1996). It is better known as a subunit of the Skp1/Cullin1/F-box ubiquitin ligase family (SCF ligases) and a part of the 'regulator of the (H+)-ATPase of the vacuolar and endosomal membranes' (RAVE)

complex (Deshaies 1999, Seol et al. 2001). Skp1 is able to bind multiple different F-box proteins with its C-terminus (Tang et al. 2012, Purvis and Singleton 2008). The N-terminus of Ctf13 contains an F-box responsible for Skp1 binding, this interaction is indispensable for Ctf13 which is unstable on its own (Russell et al. 1999). The function of Skp1 and Ctf13 in the kinetochore context has not been clarified. Skp1 promotes Ctf13 phosphorylation as demonstrated in insect cells and activates the CBF3c to form a CBF3–CEN DNA complex *in vitro* (Kaplan, Hyman and Sorger 1997). Assembly of the CBF3 complex is highly regulated by posttranslational modifications (Stemmann and Lechner 1996, Kaplan et al. 1997, Kitagawa et al. 1999). Three subunits of the CBF3c (Cep3, Ctf13 and Ndc10) interact with DNA (Yan et al. 2018). Cep3 is a homodimer with an N-terminal Gal-4 like domain. The two zinc finger domains from each of the two Cep3 proteins display specificity for CCG triplets in the CDEIII region of centromeric DNA (Bellizzi, Sorger and Harrison 2007, Purvis and Singleton 2008). It also contains an αMN helix required for CBF3 binding that displays specificity for the conserved TGT motif (Russell et al. 1999). Cep3 carries the specificity of the CBF3c for CEN DNA binding while Ctf13 and Ndc10 enhance overall binding affinity, by non-specific DNA binding (Perriches and Singleton 2012). Crystal and cryo-EM structures were determined for the full CBF3c together with DNA as well as for individual components of the CBF3c (Yan et al. 2018, Lee et al. 2019, Zhang et al. 2019, Leber et al. 2018, Purvis and Singleton 2008, Perriches and Singleton 2012, Cho and Harrison 2011, Orlicky et al. 2003). The Ndc10 protein is described as a part of the CBF3c, however, it does not belong to the CBF3 core complex as it is not stable without DNA and does not easily purify as a part of the complex *in vitro* as its N-terminal region interacts only with a small surface of Ctf13 (Leber 2018, Yan et al. 2018). *Kluyveromyces lactis* Ndc10 has been subdivided into five distinct functional domains. The N-terminal domain 1 interacts with Cbf1 and CBF3c, domain 2 enables CDEII DNA contacts, domain 3 is responsible for Ndc10 dimerization while domains 4 and 5 associate with Scm3/HJURP (Cho and Harrison 2011) (**Figure 4**). Its C-terminal tail also contains a degron motif which is triggered by erroneous protein folding. It leads to rapid degradation via HSP70 and the ubiquitin system (Furth et al. 2011). Ndc10 association with $Scm3^{HJURP}$ has a crucial function for the cell as it is responsible for Cse4 deposition (Camahort et al. 2007). It also interacts with the chromosomal passenger complex through $Bir1^{Survivin}$ (Bouck and Bloom 2005, Yoon and Carbon 1999).

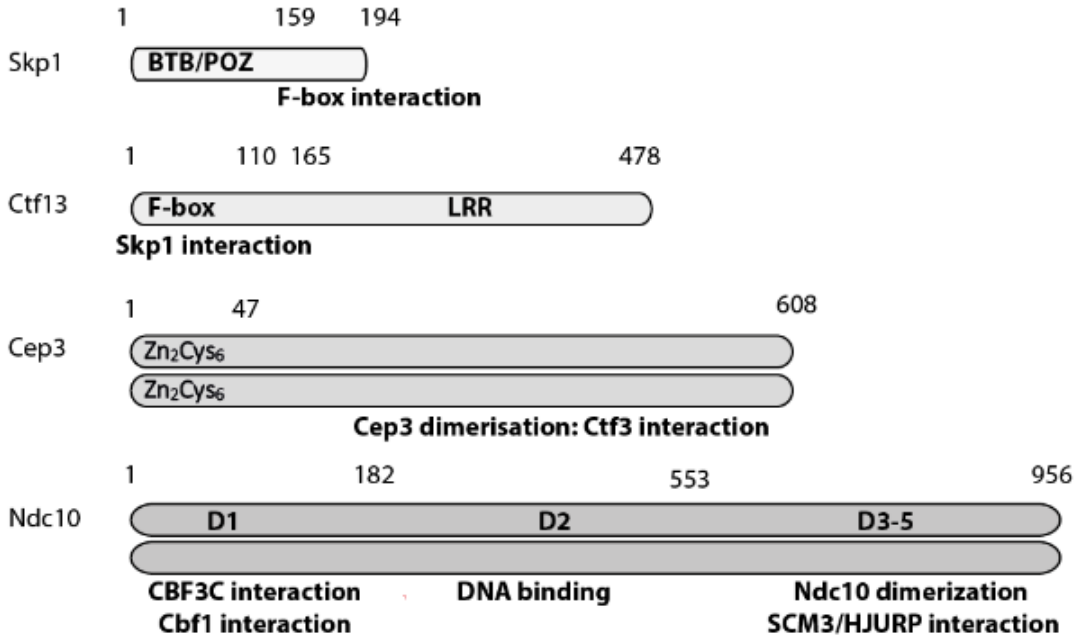

Figure 4 Components of the CBF3 complex.

Protein domains of *S. cerevisiae* CBF3c, their reported functions and interaction partners are annotated. Adapted from (Zhang et al. 2019).

1.3.3 The Constitutive Centromere Associated Network

1.3.3.1 Mif2

Mif2^{CENP-C} is specifically recruited to the centromere through a hydrophobic region at the C-terminus of Cse4^{CENP-A}, H2A and H2B histones (Kato et al. 2013) and the CBF3c (Westermann et al. 2003). Conserved structural features between human CENP-A and the budding yeast orthologue Mif2 include the PEST domain, characterised by a high percentage of proline (P), glutamic acid (E), serine (S),and threonine (T) required for protein stability (Lanini and McKeon 1995), the CENP-C motif responsible for targeting the CENP-A C-terminal region and the dimerization domain (Carroll et al. 2010, Kato et al. 2013). Two regions are required for nucleosome binding, the 'CENP-C central region' or 'DNA binding domain' (DBD) whose function is taken over by the 'AT-hook' in budding yeasts which preferentially binds to the CDEII region of the centromeric DNA with a higher AT content (Cohen et al. 2008, Brown 1995, Xiao et al. 2017, Ali-Ahmad et al. 2019) and the CENP-C motif. The CENP-C motif is not able to properly localize in the absence of the dimerization domain while the DNA binding domain is sufficient for centromere targeting *in vivo* (Musacchio and Desai 2017, Milks, Moree and

Straight 2009). It represents a crucial link between the centromeric nucleosome and the kinetochore architecture (Weir et al. 2016) and is indispensable for chromosome segregation (Milks et al. 2009, Song et al. 2002). Mif2^{CENP-C} provides a binding site for the Ame1/Okp1 inner kinetochore complex (Hornung et al. 2014). It has been proposed that Mif2 and Ame1 N-termini create mutually exclusive docking sites for the Mtw1 complex and thus recruit two individual outer kinetochore KMN networks (Hornung et al. 2014, Dimitrova et al. 2016, Killinger et al. 2020). Mif2 is one of the few essential CCAN proteins, however, its interaction with the Mtw1 complex is dispensable (Hornung et al. 2014). This interaction is regulated through an auto-inhibitory mechanism that is released upon Cse4 binding which prevents the mis-localized binding of the outer kinetochore (Killinger et al. 2020).

1.3.3.2 The COMA complex

The four subunit COMA complex is composed of Ctf19^{CENP-P}, Okp1^{CENP-Q}, Mcm21^{CENP-O} and Ame1^{CENP-U} (Hyland et al. 1999, De Wulf, McAinsh and Sorger 2003, Ortiz et al. 1999). Members of the COMA complex were the first components identified of the Ctf19 complex. They are recruited to the budding yeast centromere through the Cse4 containing nucleosome, CBF3c and Mif2 (Ortiz et al. 1999). Ame1/Okp1 are essential proteins while Ctf19/Mcm21 are required for accurate chromosome segregation, but not essential (Hyland et al. 1999, Hornung et al. 2014). CENP-U and CENP-Q are not reported to be essential, although CENP-U deletion leads to mouse embryonic stem cell death (Kagawa et al. 2014). Localization of Ame1/Okp1 is independent of Ctf19/Mcm21 as its deletion does not impair Ame1/Okp1 localisation. Vice versa mutation of Ame1/Okp1 causes mis-localisation of Ctf19/Mcm21 (De Wulf et al. 2003, Knockleby and Vogel 2009). Okp1 binds to the Ctf19/Mcm21 double RWD domain (found in RING finger and WD repeat containing proteins and DEAD-like helicases) through the Ctf19/Mcm21 binding domain on its C-terminus. The Ame1/Okp1 heterodimer selectively interacts with the N-terminal END domain of Cse4 nucleosomes through the Okp1 core domain (Anedchenko et al. 2019, Fischbock-Halwachs et al. 2019). The Ame1 N-terminus, along with the N-terminus of Mif2 represents the only known link from the inner kinetochore to the Mtw1 complex of the outer kinetochore in budding yeast (Hornung et al. 2014). Yet, no link to the outer kinetochore has been detected for the human orthologue CENP-OPQUR (Pesenti et al. 2018).

1.3.3.3 Chl4/Iml3

The human orthologues of Chl4/Iml3, CENP-N and CENP-L are involved in selective binding of CENP-A nucleosomes and nucleosome stabilization. With its N-terminal region CENP-N interacts with the RG loop of CENP-A as well as the centromeric DNA (Guo et al. 2017, Pentakota et al. 2017, Chittori et al. 2018, Tian et al. 2018). The RG loop comprises differences in accessibility for CENP-N resulting in cell cycle dependent recruitment (Fang et al. 2015, Hellwig et al. 2011). CENP-LN also directly interacts with CENP-C and the CENP-H-I-K-M complex, both required for its localization (McKinley et al. 2015). So far, the only evidence of Chl4/Iml3 interaction with the Cse4 nucleosome is via the CENP-N DNA binding groove with the unwrapped DNA (Yan et al. 2019), however there is no indication of a stable complex formation with Cse4 or H3 nucleosomes assembled on the *in vitro* nucleosome positioning Widom 601 sequence (Fischbock-Halwachs et al. 2019, Lowary and Widom 1998). Deletion of Chl4 results in viable cells displaying chromosome loss and instability (Kouprina et al. 1993). The budding yeast Chl4/Iml3 complex requires Mif2 and Ctf19/Mcm21 for proper centromere localization (Schmitzberger et al. 2017).

1.3.3.4 The CTF3 complex (Mcm16/Ctf3/Mcm22)

The budding yeast CTF3c consists of Mcm16^{CENP-H}, Ctf3^{CENP-I} and Mcm22^{CENP-K} (Measday et al. 2002). In humans it is referred to as CENP-HIKM complex, with CENP-M so far not being recognised in budding yeast (Basilico et al. 2014). It is also known as a part of a larger stable complex known as CENP-CHIKMLN (Weir et al. 2016). CENP-HIK interacts with CENP-A nucleosomes, however, it does not display specificity as it equally interacts with H3 nucleosomes and DNA. Formation of a large CENP-CHIKMLN complex introduces selectivity towards CENP-A nucleosomes, probably through CENP-C and CENP-N (Carroll et al. 2009, Kato et al. 2013, Tian et al. 2018, Weir et al. 2016). The role of the budding yeast CTF3c is less understood. Kinetochore localization of CTF3c is cell cycle dependent, displaying the highest levels in late anaphase and dropping before S phase (Pot et al. 2003). CTF3c can be purified as a stable complex *in vitro*. It interacts through anti-parallel interaction of Ctf3 N-terminal HEAT repeats and C-terminal helical knob with Mcm16/22 coiled coils (Hinshaw, Dates and Harrison 2019). The complex recruits the Cnn1/Wip1 dimer as a stable five subunit assembly through

the Cnn1 histone fold domain. As such it is able to bind two subunits of the microtubule binding Ndc80 complex (Pekgoz Altunkaya et al. 2016b).

1.3.3.5 Cnn1/Wip1, Mhf1/Mhf2

The human orthologue of Cnn1/Wip1 and Mhf1/Mhf2 is the CENP-T/W/S/X complex. CENP-T-W associates as a stable complex with CENP-S-X (Amano et al. 2009). They contain histone fold domains and it is proposed that they create a nucleosome-like structure wrapping the centromeric DNA (Hori et al. 2008, Nishino et al. 2012). The CENP-T/W/S/X complex induces positive supercoiling in the DNA, as opposed to canonical nucleosomes, but without evidence of sequence selectivity. Therefore, there is still a certain level of scepticism whether it forms a second nucleosome adjacent to CENP-A. When incubated with CENP-A or H3 di-nucleosomes it does not localise with the nucleosome-bound DNA or create familiar patterns upon nuclease cleavage (Takeuchi et al. 2014). It does also not require any histone chaperones for its localization, which seems to be dependent on CENP-A and CENP-HIKM (Thakur and Henikoff 2016, Basilico et al. 2014, Pekgoz Altunkaya et al. 2016b, McKinley et al. 2015). Accordingly, Cnn1/Wip1 and Mhf1/Mhf2 do not form a stable complex under *in vitro* conditions or interact with chromatin (Pekgoz Altunkaya et al. 2016a). However, presumably specific, yet unidentified conditions are required for this interaction to occur in budding yeast. The elongated N-terminal region of CENP-T-W provides a binding interface for outer kinetochore proteins (Gascoigne et al. 2011, Suzuki et al. 2011). It has been shown that in budding yeast $Cnn1^{CENP\text{-}T}$ binds the Ndc80 complex and this pathway becomes essential when the Mis12 pathway is impaired (Lang, Barber and Biggins 2018). CENP-T-W requires CENP-A for its localization, but does not directly bind to it.

1.3.3.6 Nkp1/Nkp2

The Nkp1/Nkp2 heterodimer was identified as “non-essential kinetochore protein 1 and 2” without its human orthologue (Cheeseman et al. 2002). It associates with the COMA complex via the C-termini of Okp1 and Ame1. This interaction stabilizes the termini consequently aiding kinetochore stability. The human orthologue of the COMA complex, CENP-OPQU copurifies with CENP-R which might carry out a similar function (Schmitzberger et al. 2017).

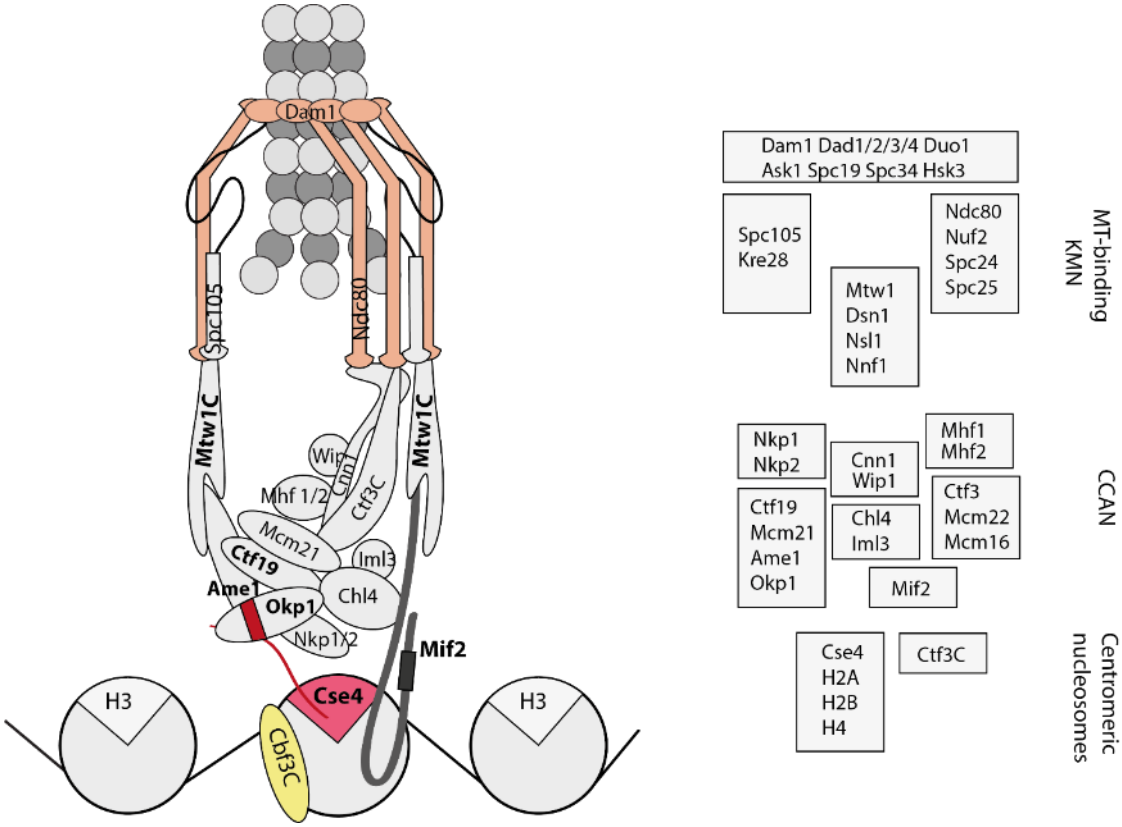

Figure 5 **Architecture of the budding yeast kinetochore**

The budding yeast kinetochore is assembled on a single Cse4 nucleosome wrapped with CEN3 DNA. The CBF3 complex is responsible for the recruitment of Cse4 to the centromere and ensures tight wrapping of the DNA surrounding the nucleosome. The inner kinetochore is bound to the nucleosome via Ame1/Okp1 and Mif2 interactions. With their N-termini Ame1 and Mif2 provide a docking site for the outer kinetochore through interaction with the MTW1 complex. The C-terminal regions of MTW1 and CTF3c:Cnn1/Wip1 provide a binding interface for the microtubule binding NDC80 complex (Fischbock-Halwachs et al. 2019, Lang et al. 2018, Musacchio and Desai 2017).

1.3.4 The outer kinetochore

The outer kinetochore or KMN network is assembled of Kinetochore null 1 ($SPC105^{KNL1}$), Mis-segregation 12 ($MTWc^{MIS12}$) and Nuclear division cycle 80 ($NDC80^{NDC80}$) complexes which interact with the $CTF19^{CCAN}$ complex (Pagliuca et al. 2009, Foley and Kapoor 2013). The 4-subunit MTW1 complex (consisting of Dsn1, Mtw1, Nsl1 and Nnf1 in budding yeast) directly docks to the $Mif2^{CENP-C}$ and Ame1 N-termini and serves as a structural backbone of the kinetochore (Przewloka et al. 2011, Hornung et al. 2014, Hinshaw and Harrison 2018). Crystal

structures of human and *K. lactis* MTW1c revealed an elongated Y shaped heterotetrametric complex. Branching of the heterodimers Mtw1:Nnf1 and Dsn1:Nsl1 creates globular modules of head I and head II in the N-terminus, respectively (Dimitrova et al. 2016). Phosphorylation of Dsn1 S240/S250 (S213/S223 in *K. lactis*) releases a binding site on head I which mediates binding of Mif2 and Ame1. Phospho-regulation of Dsn1 by Ipl1^{AuroraB} is essential for budding yeast and a phosphorylation deficient Dsn1-S240A/S250A mutant is targeted for degradation. Mutation of the Cdk1 phosphorylation site S264 prevents degradation of Dsn1-S240A/S250A suggesting its role in regulation of Dsn1 levels (Akiyoshi et al. 2013b, Akiyoshi, Nelson and Biggins 2013a, Dimitrova et al. 2016). The binding of Mif2 and Ame1 to the MTW1c seems to be mutually exclusive indicating that they bind two separate MTW1 complexes (Killinger et al. 2020). The MTW1c C-terminus seems to be essential for establishing the KMN network, since it promotes the assembly of the other two outer kinetochore complexes, Spc105^{KNL1}/Kre28^{ZWINT} and Ndc80C (Ndc80, Nuf2, Spc24, Spc25) (Cheeseman et al. 2006). Motifs in the C-termini of human NSL1 and the yeast Dsn1, Mtw1 and Nsl1 subunits, provide binding sites for the C-terminal RWD domains of the Spc24/25 heterodimer of the Ndc80 complex (Petrovic et al. 2010, Malvezzi et al. 2013, Dimitrova et al. 2016, Ghodgaonkar-Steger et al. 2020). The MIS12^{MTW1c} complex provides a binding site for KNL1C^{Spc105c} involving a C-terminal motif in the human NSL1 protein or short helices in budding yeast Mtw1 and Nsl1, respectively (Petrovic et al. 2014, Ghodgaonkar-Steger et al. 2020).

The budding yeast SPC105^{KNL1} complex consists of Spc105 and Kre28 assembled in a 1:2 ratio. The N-terminal region of Spc105^{KNL1} contains a patch of multiple Met-Glu-Leu-Thr amino acids termed MELT repeats, which serve as a binding motif for spindle assembly checkpoint proteins crucial for correct microtubule-kinetochore attachments (Primorac et al. 2013, London and Biggins 2014, Foley and Kapoor 2013, Kiyomitsu, Murakami and Yanagida 2011). It also aids in providing a microtubule binding interface along with NDC80c, however the details of the interaction are yet to be investigated (Pagliuca et al. 2009). The C-terminal region of human KNL1 establishes a connection to the inner kinetochore via the MIS12^{MTW1} complex (Pagliuca et al. 2009, Foley and Kapoor 2013). In budding yeast this interaction is carried out by the coiled coil 2 domain of Kre28, while the human Kre28 orthologue Zwint-1 was shown to be redundant for the interaction which is solely accomplished through the KNL1 protein (Petrovic et al. 2014, Ghodgaonkar-Steger et al. 2020).

The NDC80 complex is the main microtubule binding site of the kinetochore. It consists of Ndc80/Nuf2 and Spc24/Spc25 heterodimers which are connected through elongated coiled coils forming a heterotetramer (Musacchio and Desai 2017). The positively charged N-terminal region of Ndc80 and the calponin homology domains of Ndc80 and Nuf2 account for the main microtubule contact sites (Alushin et al. 2010, Wang et al. 2008). On the opposite side it docks to the inner kinetochore via binding of the Spc24/25 RWD domains to the C-terminus of the Mtw1C involving Dsn1-, Nsl1- and Mtw1 short helical motifs. All of the motifs are required and crucial for cell viability. Spc24/25 also forms weak interactions with SPC105c^{KNL1C} aiding to overall stability of the outer kinetochore (Malvezzi et al. 2013, Petrovic et al. 2010, Ghodgaonkar-Steger et al. 2020). When the Mtw1 pathway is impaired the same Spc24/25 binding site is occupied and rescued via Cnn1 binding. However, phosphorylated Cnn1 is not able to bind Spc24/25 and it has been proposed that phosphorylation of Cnn1, which peaks in anaphase, serves as a mechanism to disassemble Ndc80 from the KMN (Lang et al. 2018, Malvezzi et al. 2013, Bock et al. 2012).

The budding yeast specific essential DAM1 complex creates a ring around microtubules and increases kinetochore affinity for microtubule binding. In vertebrates a similar role is carried out by the spindle and kinetochore-associated (SKA) complex, however its function is redundant. The difference probably lies in the fact that the budding yeast point centromere associated kinetochore binds only a single microtubule, while in vertebrates regional centromeres provide attachment sites for ~20 microtubules (Westermann et al. 2006, Helgeson et al. 2018) (Figure 5).

1.3.5 Error correction of incorrect microtubule attachments

Proper separation of the sister chromatids is a crucial task for healthy cell division and proliferation. In humans, all 46 chromosomes have to be accurately and faithfully duplicated and divided with each cell cycle to prevent aneuploidy and abnormalities including cancer (Walczak, Cai and Khodjakov 2010, Weaver and Cleveland 2006). In order for chromosomes to be accurately divided they have to be properly attached to microtubules, this is called amphitelic attachment where kinetochores are attached to both spindle poles. Spindle microtubules stochastically search for attachment sites which also leads to inevitable false attachments. Microtubules are inherently unstable and if the correct tension is not detected

by the kinetochore they will not get stabilised and will detach. Monotelic (one sided kinetochore binding) and syntelic (both kinetochores are anchored to the same spindle pole) attachments are generally more easily detected and corrected due to incorrect tension. However, human kinetochores bind approximately 20 microtubules and correcting merotelic (where one kinetochore is attached to both poles while the other kinetochore is properly attached to one pole) attachments represents a bigger challenge and thus is the major cause of aneuploidy. The recognition of a false merotelic attachment will also depend on the number of microtubules that are improperly attached thereby changing the tension (Cimini 2008, Musacchio and Salmon 2007, Nicklas 1997) (Figure 5).

Proper kinetochore – microtubule attachment is monitored by the chromosomal passenger complex (CPC), which consists of the Ipl1$^{\text{AURORA B}}$ kinase, Sli15$^{\text{INCENP}}$, Bir1$^{\text{SURVIVIN}}$ and Nbl1$^{\text{BOREALIN}}$ (Biggins and Murray 2001, Tanaka et al. 2002). The CPC acts as a tension sensor phosphorylating the tensionless microtubule binding interface. Aurora B kinase phosphorylates the outer kinetochore complexes KNL1C, Ndc80C, Dam1 and SKAc which leads to reduced microtubule binding and depolymerization (DeLuca and Musacchio 2012, Nicklas 1997, Zaytsev et al. 2014). If the microtubule attachment is recognised as accurate it will be stabilised. Intra kinetochore stretching results in reduction of Aurora B activity allowing phosphatases such as PP1 to be recruited via KNL1 (Joglekar, Bloom and Salmon 2009, Francisco, Wang and Chan 1994, Liu et al. 2010).

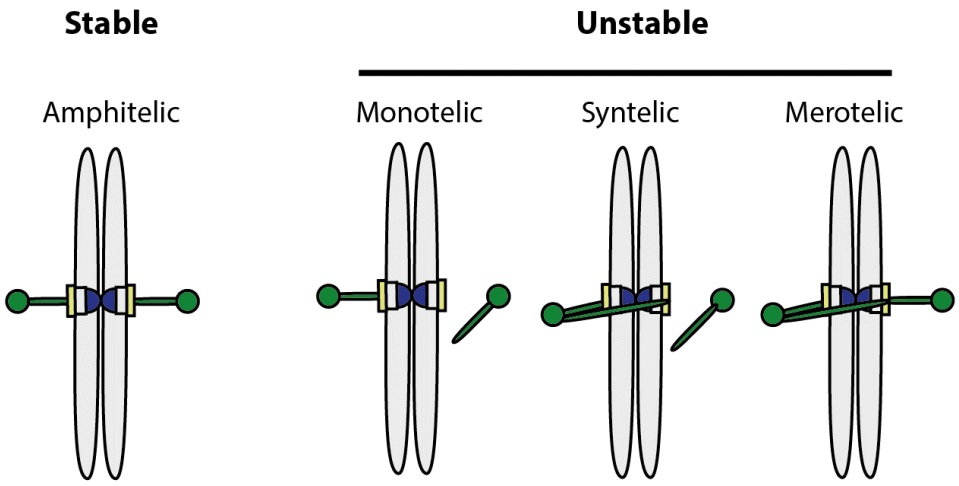

Figure 6 Types of kinetochore microtubule attachments

Proper stable bi-polar attachment of the sister chromatids is called amphitelic attachment. Besides, microtubule binding can adopt various unstable attachments which tend to be

corrected. Monotelic attachments: only one sister chromatid is attached to a single kinetochore; synthelic attachments: both kinetochores are attached to the same spindle pole; merotelic attachments: microtubules from opposite spindle poles are attached to a single kinetochore (Kelly and Funabiki 2009).

1.3.6 The spindle assembly checkpoint

The spindle assembly checkpoint (SAC) (**Figure 1**) acts as a mitotic quality control before anaphase onset ensuring proper chromosome bi-orientation. As long as kinetochores are not stably bound to microtubules the SAC is activated and anaphase onset is delayed (Li and Murray 1991). This is achieved by recruitment of specific SAC proteins, Bub3, Mad2, BubR1^{Mad3} and Cdc20, that form the mitotic checkpoint complex (MCC). Apart from MCC proteins Mad1, Bub1, Mps1, and Aurora B kinase are required for SAC function. The MCC targets and inhibits the APC/C apoenzyme, but once Cdc20 is bound anaphase is initiated (Murray 2004, Fujimitsu, Grimaldi and Yamano 2016, Qiao et al. 2016).

The Mps1 kinase in yeast acts as a regulator of the SAC proteins, it allows recruitment of Bub1 and Bub3 proteins to the outer kinetochore KNL1^{Spc105} complex by phosphorylating its N-terminus (Weiss and Winey 1996). Bub1 recruitment is required for the majority of the SAC proteins, BubR1^{Mad3}, Bub3, Mad1 and Mad2 and subsequent formation of the MCC (Taylor, Ha and McKeon 1998). Mad2 exists in two conformational forms, inactive O-Mad2 (open) and active C-Mad2 (closed). O-Mad2 in the cytosol is converted into its active form by Mad1 binding. Only C-Mad2 is able to bind Cdc20. Formation of the core MCC formed by C-Mad2, BubR1, Bub3 and Cdc20 proteins results in depletion of free Cdc20 as well as inactivation of the Cdc20 bound APC/C (Faesen et al. 2017).

Upon proper microtubule attachment to the kinetochore there is a reduction in the local amount of Mps1 and spatial separation of KNL1 and Ndc80. Ndc80 binding physically prevents Mps1 from phosphorylating KNL1 (Joglekar et al. 2009, Joglekar and Aravamudhan 2016). Protein phosphatases 1 (PP1) and 2A (PP2A) are recruited to KNL1 and dephosphorylate its N-terminus. This prevents further recruitment of SAC proteins to the kinetochore and MCC formation. Cdc20 is now free to activate the APC/C which swiftly leads to degradation of securin and cyclin B. Degradation of securin releases separase which cleaves the cohesin kleisin subunit between the sister chromatids leading to anaphase (Meadows and Millar 2015, London et al. 2012, Espert et al. 2014, Kim and Yu 2011).

2 Project aims

Previous studies reported substantial knowledge about individual kinetochore subunits and the regulation of kinetochore function by posttranslational modifications. High resolution structures of isolated kinetochore complexes using cryo-electron microscopy and crystallography have been published (reviewed in (Pesenti, Weir and Musacchio 2016, Nagpal and Fukagawa 2016, Schalch and Steiner 2017)). However, a comprehensive topological map of the kinetochore core structure was still missing. My colleagues were working on obtaining a network of the native budding yeast kinetochore using chemical cross-linking and mass spectrometry. The results obtained from this protein network confirmed many of the known interactions, and provided new information which is the foundation of this thesis.

We observed a large number of crosslinks within the outer kinetochore KMN network, specifically at the C-terminus of the MTW1c. This area is unstructured and flexible, and thus it was unlikely to obtain this information by high resolution structural analysis. This is when I joined the project to investigate the connectivity in the outer kinetochore using biochemical and genetic analysis to address the following questions:

1. Is the putative helix motif in the Mtw1 C-terminus required for with the assembly of the SPC105c and NDC80c at the outer kinetochore?
2. What is the contribution of the Mtw1 helix to the binding sites provided by the Nsl1 and Dsn1 helices and do these motifs cooperate to stabilize the outer kinetochore assembly?
3. How is SPC105c bound to MTW1c and is this interaction essential?
4. Do SPC105c and NDC80c associate and does this affinity enhance the overall KMN stability?

In the second project I focused on the nucleosome-associated kinetochore complexes. Budding yeast Mif2 was the only known direct link between the centromeric nucleosome and the outer kinetochore MTW1c. However, a single connection would not facilitate the stable transmission of the pulling forces of the depolymerizing microtubules. Thus, it is was likely that Mif2 was not the only attachment site. In order to obtain further insights, I addressed the following questions:

1. Is there another link between Cse4 nucleosomes and the outer kinetochore apart from Mif2?
2. Is the yeast orthologue of CENP-LN, Chl4/Iml3, involved in Cse4 binding as described for human CENP-A nucleosomes?
3. Does the budding yeast CTF3c bind centromeric nucleosomes as described for the human CENP-HIK complex?
4. Which domain of the Ame1/Okp1 complex mediates the direct interaction with the Cse4 nucleosome?

During the course of my efforts to study the nucleosome-assembled inner kinetochore I discovered that Ndc10, a subunit of the CBF3 complex forms a yet unknown link between the Cse4 nucleosome and the outer kinetochore MTW1 complex. This implied that there might be a third pathway of tethering the outer kinetochore to the nucleosome, apart from Mif2 and Ame1/Okp1 interactions. The aim of this third project was to understand the importance of this interaction for kinetochore assembly and characterise the molecular basis of this interaction.

1. Is the Ndc10 link between the Cse4 nucleosome and the MTW1c crucial for cell viability?
2. What are the sequence motifs mediating the Ndc10 – MTW1c interaction?
3. How does the Ndc10 binding mode compare to interactions with Mif2 and Ame1/Okp1 and is there a binding hierarchy of the three MTW1c recruiters?
4. Are there binding interdependencies between Mif2, Ame1/Okp1 and Ndc10 how do they affect MTW1c recruitment?

The work on these 3 projects are described in the thesis as follows. The first two projects resulted in joint publications which are included in the thesis as well as the manuscript on the Ndc10 project which is under preparation.

3 Results

3.1 The COMA complex interacts with Cse4 and positions Sli15/Ipl1 at the budding yeast inner kinetochore

Fischböck-Halwachs J*, Singh S*, **Potocnjak M***, Hagemann G, Solis-Mezarino V, Woike S, Ghodgaonkar-Steger M, Weissmann F, Gallego LD, Rojas J, Andreani J, Köhler A, Herzog F. The COMA complex interacts with Cse4 and positions Sli15/Ipl1 at the budding yeast inner kinetochore. Elife. 2019; 8. doi: 10.7554/eLife.42879. (*equal contribution)

eLIFE elifesciences.org

RESEARCH ARTICLE

The COMA complex interacts with Cse4 and positions Sli15/Ipl1 at the budding yeast inner kinetochore

Josef Fischböck-Halwachs[1,2†], Sylvia Singh[1,2†], Mia Potocnjak[1,2†], Götz Hagemann[1,2], Victor Solis-Mezarino[1,2], Stephan Woike[1,2], Medini Ghodgaonkar-Steger[1,2], Florian Weissmann[3], Laura D Gallego[4], Julie Rojas[5], Jessica Andreani[6], Alwin Köhler[4], Franz Herzog[1,2*]

[1]Gene Center Munich, Department of Biochemistry, Ludwig-Maximilians-Universität München, Munich, Germany; [2]Department of Biochemistry, Ludwig-Maximilians-Universität München, Munich, Germany; [3]Research Institute of Molecular Pathology (IMP), Vienna Biocenter (VBC), Vienna, Austria; [4]Max F Perutz Laboratories, Medical University of Vienna, Vienna, Austria; [5]Laboratory of Chromosome Biology, Max Planck Institute of Biochemistry, Martinsried, Germany; [6]Institute for Integrative Biology of the Cell (I2BC), CEA, CNRS, Université Paris-Sud, Université Paris-Saclay, Gif-sur-Yvette, France

Abstract Kinetochores are macromolecular protein complexes at centromeres that ensure accurate chromosome segregation by attaching chromosomes to spindle microtubules and integrating safeguard mechanisms. The inner kinetochore is assembled on CENP-A nucleosomes and has been implicated in establishing a kinetochore-associated pool of Aurora B kinase, a chromosomal passenger complex (CPC) subunit, which is essential for chromosome biorientation. By performing crosslink-guided in vitro reconstitution of budding yeast kinetochore complexes we showed that the Ame1/Okp1$^{CENP-U/Q}$ heterodimer, which forms the COMA complex with Ctf19/Mcm21$^{CENP-P/O}$, selectively bound Cse4^{CENP-A} nucleosomes through the Cse4 N-terminus. The Sli15/Ipl1$^{INCENP/Aurora-B}$ core-CPC interacted with COMA in vitro through the Ctf19 C-terminus whose deletion affected chromosome segregation fidelity in Sli15 wild-type cells. Tethering Sli15 to Ame1/Okp1 rescued synthetic lethality upon Ctf19 depletion in a Sli15 centromere-targeting deficient mutant. This study shows molecular characteristics of the point-centromere kinetochore architecture and suggests a role for the Ctf19 C-terminus in mediating CPC-binding and accurate chromosome segregation.

DOI: https://doi.org/10.7554/eLife.42879.001

***For correspondence:** herzog@genzentrum.lmu.de

[†]These authors contributed equally to this work

Competing interests: The authors declare that no competing interests exist.

Funding: See page 22

Received: 16 October 2018
Accepted: 20 May 2019
Published: 21 May 2019

Reviewing editor: Jennifer G DeLuca, Colorado State University, United States

Introduction

Kinetochores enable the precise distribution of chromosomes during the eukaryotic cell division to avoid aneuploidy (***Santaguida and Musacchio, 2009***) which is associated with tumorigenesis, congenital trisomies and aging (***Baker et al., 2005***; ***Pfau and Amon, 2012***). Faithful segregation of the duplicated sister chromatids relies on their exclusive attachment to spindle microtubules emerging from opposite spindle poles (***Foley and Kapoor, 2013***). The physical link between chromosomal DNA and microtubules is the kinetochore, a macromolecular protein complex that mediates the processive binding to depolymerizing microtubules driving the sister chromatids apart into the two emerging cells (***Biggins, 2013***; ***Musacchio and Desai, 2017***). Kinetochore assembly is restricted to centromeres, chromosomal domains that are marked by the presence of the histone H3 variant Cse4^{CENP-A} (human ortholog names are superscripted if appropriate) (***Earnshaw and Rothfield,***

1985; *Fukagawa and Earnshaw, 2014*). In humans, regional centromeres span megabases of DNA embedding up to 200 CENP-A containing nucleosomal core particles (NCPs) (*Bodor et al., 2014*; *Musacchio and Desai, 2017*). In contrast, *Saccharomyces cerevisiae* has point centromeres, which are characterized by a specific ~125 bp DNA sequence wrapped around a single Cse4-containing histone octamer (*Fitzgerald-Hayes et al., 1982*; *Camahort et al., 2009*; *Hasson et al., 2013*).

The budding yeast kinetochore is composed of about 45 core subunits which are organized in different stable complexes (*De Wulf et al., 2003*; *Westermann et al., 2003*) of which several are present in multiple copies (*Joglekar et al., 2006*). The kinetochore proteins are evolutionary largely conserved between yeast and humans (*Westermann and Schleiffer, 2013*; *van Hooff et al., 2017*) and share a similar hierarchy of assembly from DNA to the microtubule binding interface (*De Wulf et al., 2003*). The centromere proximal region is established by proteins of the Constitutive Centromere Associated Network (CCAN), also known as the CTF19 complex (CTF19c) in budding yeast. The CTF19c comprises the Chl4/Iml3$^{CENP-N/L}$, Mcm16/Ctf3/Mcm22$^{CENP-H/I/K}$, Cnn1/Wip1$^{CENP-T/W}$, Mhf1/Mhf2$^{CENP-S/X}$ and Ctf19/Okp1/Mcm21/Ame1$^{CENP-P/Q/O/U}$ (COMA) complexes plus Mif2^{CENP-C} (*Cheeseman et al., 2002*; *Westermann et al., 2003*; *Biggins, 2013*; *Musacchio and Desai, 2017*) and the budding-yeast specific Nkp1/Nkp2 heterodimer. Another yeast inner kinetochore complex, the CBF3 (Ndc10/Cep3/Ctf13/Skp1) complex, has been identified as sequence-specfic binder of the centromeric DNA sequence CDEIII (*Ng and Carbon, 1987*; *Lechner and Carbon, 1991*). The CTF19c^{CCAN} provides a cooperative high-affinity binding environment for the Cse4^{CENP-A}-NCP (*Weir et al., 2016*), where distinct subunits selectively recognize Cse4^{CENP-A} specific features. Across different species the CENP-C signature motif interacts with divergent hydrophobic residues of the CENP-A C-terminal tail (*Musacchio and Desai, 2017*). Electron microscopy studies have recently resolved the interaction of CENP-N with the CENP-A centromere-targeting domain (CATD) in vertebrates (*Carroll et al., 2009*; *Guse et al., 2011*; *Pentakota et al., 2017*; *Chittori et al., 2018*; *Tian et al., 2018*). For budding yeast Cse4, a direct interaction has so far only been demonstrated with Mif2 (*Westermann et al., 2003*; *Xiao et al., 2017*). Apart from Mif2, the only essential CTF19c^{CCAN} proteins are Ame1 and Okp1 (*Meluh and Koshland, 1997*; *Ortiz et al., 1999*; *De Wulf et al., 2003*), with the N-terminus of Ame1 binding the N-terminal domain of Mtw1 and thus serving as docking site for the outer kinetochore KMN network (KNL1^{SPC105}-/MIS12^{MTW1}-/NDC80^{NDC80}-complexes) (*Hornung et al., 2014*; *Dimitrova et al., 2016*).

The kinetochore is also a hub for feedback control mechanisms that ensure high fidelity of sister chromatid separation by relaying the microtubule attachment state to cell cycle progression, known as spindle assembly checkpoint (SAC), and by destabilizing improper kinetochore-microtubule attachments and selectively stabilizing the correct bipolar attachments, referred to as error correction mechanism (*Foley and Kapoor, 2013*; *Krenn and Musacchio, 2015*). A major effector of both regulatory feedback loops is the kinase Ipl1$^{Aurora\ B}$, a subunit of the evolutionary conserved tetrameric chromosomal passenger complex (CPC) which associates close to the centromere from G1 until anaphase (*Biggins and Murray, 2001*; *Widlund et al., 2006*; *Carmena et al., 2012*). The kinase subunit Ipl1$^{Aurora\ B}$ binds to the C-terminal IN-box domain (*Adams et al., 2000*; *Kaitna et al., 2000*) of the scaffold protein Sli15^{INCENP}, and Nbl1^{Borealin} and Bir1^{Survivin} form a three-helix bundle with the Sli15 N-terminus (*Klein et al., 2006*; *Jeyaprakash et al., 2007*). All known mechanisms for recruitment of the CPC to the yeast centromere rely on Bir1, which directly associates with Ndc10 (*Cho and Harrison, 2011*) and is recruited through Sgo1 to histone H2A phosphorylated at S121 by Bub1 which so far has only been established in fission yeast (*Kawashima et al., 2010*). Based on previous reports we refer to the CPC recruited through Ndc10 or H2A-P as centromere-targeted CPC pool, notwithstanding that the centromere-targeted Sli15^{INCENP} scaffold may extend to, and Ipl1$^{Aurora\ B}$ may operate at, the kinetochore structure. CPC lacking the centromere-targeting domain (CEN) of Sli15^{INCENP} is indicated as inner kinetochore-localized CPC (*Knockleby and Vogel, 2009*; *Musacchio and Desai, 2017*).

During early mitosis incorrect microtubule attachment states are resolved by Ipl1$^{Aurora\ B}$ which phosphorylates Ndc80 and Dam1 sites within the microtubule binding interface and thereby reduces their affinity towards microtubules (*Cheeseman et al., 2002*; *Miranda et al., 2005*; *Westermann et al., 2005*; *Cheeseman et al., 2006*; *DeLuca et al., 2006*; *Santaguida and Musacchio, 2009*). The selective destabilization promotes the establishment of a correctly bi-oriented kinetochore configuration at the mitotic spindle, referred to as amphitelic attachment (*Tanaka et al., 2002*). The spatial separation model for establishing biorientation (*Krenn and Musacchio, 2015*)

implies that centromere-targeting of Sli15 allows substrate phosphorylation by Ipl1$^{Aurora\ B}$ within the span of the Sli15^{INCENP} scaffold and that tension dependent intra-kinetochore stretching (**Joglekar et al., 2009**) pulls the microtubule binding interface out of reach of Ipl1$^{Aurora\ B}$ resulting in dephosphorylation of outer kinetochore substrates and stabilization of amphitelic kinetochore-microtubule attachments (**Liu et al., 2009**; **Lampson and Cheeseman, 2011**).

A recent study challenged this model by showing that a Sli15 mutant lacking the centromere-targeting domain, Sli15ΔN2-228 (Sli15ΔN), suppressed the deletion phenotypes of Bir1, Nbl1, Bub1 and Sgo1 that mediate recruitment of the CPC to the centromere (**Campbell and Desai, 2013**). In contrast to wild-type Sli15, which localized between sister kinetochore clusters, Sli15ΔN showed weak localization overlapping with Nuf2 at kinetochores (**Campbell and Desai, 2013**). Apart from the altered localization, Sli15ΔN was indistinguishably viable from wild-type and displayed no significant chromosome segregation defects (**Campbell and Desai, 2013**; **Hengeveld et al., 2017**). Similarly, a survivin mutant in chicken DT40 cells that failed to localize INCENP and Aurora B to centromeres from prophase to metaphase displayed normal growth kinetics (**Yue et al., 2008**). These findings suggest that centromere-targeting of Sli15/Ipl1 is largely dispensable for error correction and SAC signaling. But a molecular understanding of how the inner kinetochore-localized Sli15ΔN/Ipl1 retains its biological function is missing.

We describe here the use of chemical crosslinking and mass spectrometry (XLMS) (**Herzog et al., 2012**) together with biochemical reconstitution to characterize the CTF19c^{CCAN} subunit connectivity and the protein interfaces that establish a selective Cse4-NCP binding environment. Subunits of the COMA complex were previously implicated in CPC function at kinetochores (**De Wulf et al., 2003**; **Knockleby and Vogel, 2009**) and the Sli15ΔN mutant showed synthetic lethality with deletions of Ctf19 or Mcm21 (**Campbell and Desai, 2013**). Thus, we investigated whether the COMA complex directly associates with Sli15/Ipl1. We demonstrate that the Cse4-N-terminus (**Chen et al., 2000**) binds Ame1/Okp1 through the Okp1 core domain (**Schmitzberger et al., 2017**) and that dual recognition of budding yeast Cse4-NCP is established through selective interactions of the essential CTF19c^{CCAN} proteins Mif2 and Ame1/Okp1 with distinct Cse4 motifs. We further show that Sli15/Ipl1 interacts with the Ctf19 C-terminus and that synthetic lethality upon Ctf19 depletion in the *sli15ΔN* background is rescued by fusing Sli15ΔN to the COMA complex. Our findings show contacts important for CTF19c^{CCAN} architecture assembled at budding yeast point centromeres and indicate that the interaction of CPC and COMA is important for faithful chromosome segregation.

Results

The Ame1/Okp1 heterodimer selectively binds Cse4 containing nucleosomes

To screen for direct interaction partners of Cse4-NCPs we reconstituted the individual CTF19c^{CCAN} subcomplexes (Mif2, Ame1/Okp1, Ctf19/Mcm21, Chl4/Iml3, Mcm16/Ctf3/Mcm22, Cnn1/Wip1, Nkp1/Nkp2, Mhf1/Mhf2) with Cse4- or H3-NCPs in vitro. The CTF19c^{CCAN} complexes were purified either from bacteria or insect cells as homogenous and nearly stoichiometric complexes (**Figure 1B**). Consistent with a recent study (**Xiao et al., 2017**), using electrophoretic mobility shift assays (EMSA), we observed that Mif2 selectively interacted with Cse4-NCPs and not with H3-NCPs (**Figure 1A**). We also found that Ame1/Okp1 bound specifically to Cse4-NCPs (**Figure 1A**). The lack of interaction with H3-NCPs, which were reconstituted using the same 601 DNA sequence (**Tachiwana et al., 2011**), suggests that Ame1/Okp1 directly and selectively binds Cse4 and that the interaction does not require AT-rich DNA sequences as previously proposed (**Hornung et al., 2014**). In contrast to the EMSA titration of human CCAN complexes with CENP-A-NCP (**Weir et al., 2016**) using 10 nM NCP mixed with up to 20-fold excess of the respective subcomplexes, we could not detect Cse4-NCP band shifts with Chl4/Iml3, the orthologs of human CENP-NL, and with Mcm16/Ctf3/Mcm22, the orthologs of human CENP-HIK (no *S. cerevisiae* ortholog of CENP-M has been identified) using 500 nM NCP incubated with a twofold excess of the complexes. Ctf19/Mcm21, Cnn1/Wip1, Nkp1/Nkp2 and Mhf1/Mhf2 did also not form distinct complexes with either Cse4- or H3-NCPs in the EMSA indicating that Mif2 and Ame1/Okp1 possess a higher relative binding affinity to Cse4-NCPs than the other CTF19c subcomplexes (**Figure 1A**).

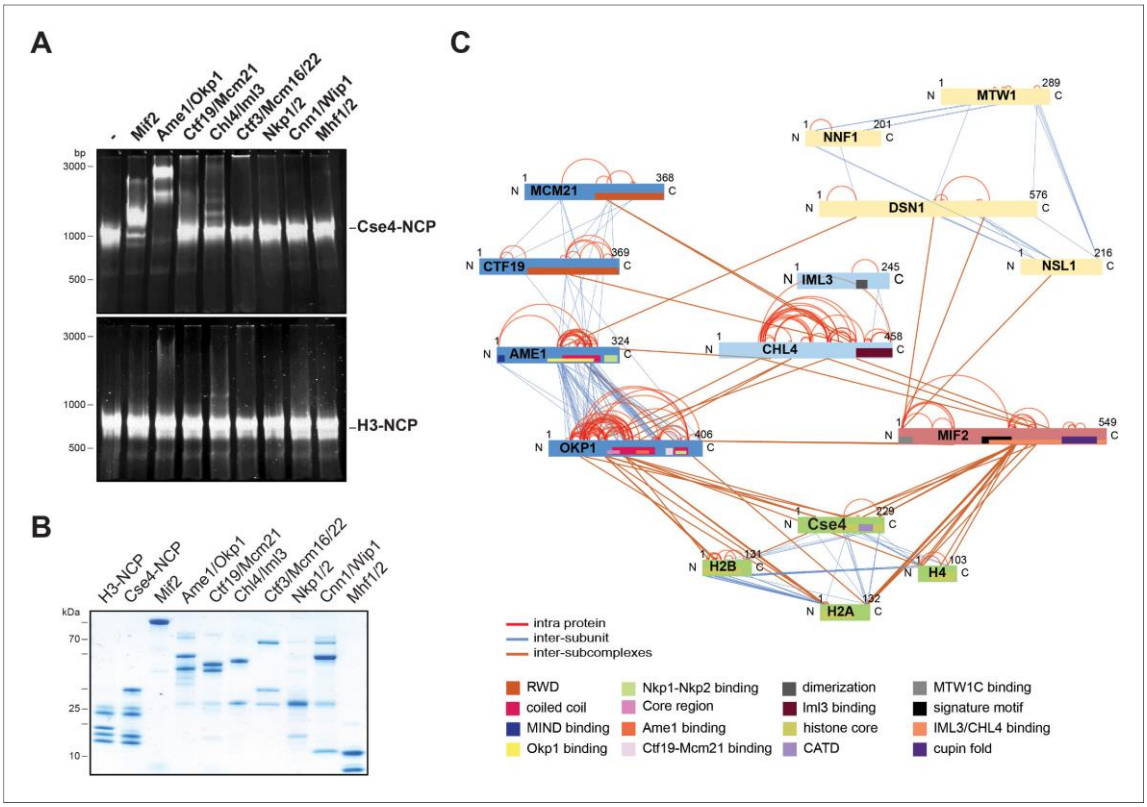

Figure 1. The heterodimeric Ame1/Okp1 complex directly and selectively binds the Cse4-NCP. (**A**) Electrophoretic mobility shift assays (EMSAs) of the indicated CTF19c^{CCAN} subunits and subcomplexes mixed in a 2:1 molar ratio with either Cse4- or H3-NCPs. DNA/protein complexes were separated on a 6% native polyacrylamide gel. The DNA is visualized by SYBR Gold staining. (**B**) Coomassie stained gel of the individual inner kinetochore components, recombinantly purified from *E. coli*, used in the EMSA in (**A**). (**C**) XLMS analysis of the in vitro reconstituted Cse4-NCP:Mif2:COMA:Chl4/Iml3:MTW1c complex. Proteins are represented as bars indicating annotated domains (***Supplementary file 3***) according to the color scheme in the legend. Subunits of a complex are represented in the same color and protein lengths and cross-link sites are scaled to the amino acid sequence.

DOI: https://doi.org/10.7554/eLife.42879.002

The following figure supplement is available for figure 1:

Figure supplement 1. Size exclusion chromatography (SEC) of the in vitro reconstituted Ctf19/Mcm21/Ame1/Okp1 (COMA):Chl4/Iml3:Mif2:MTW1c:Cse4-NCP complex.

DOI: https://doi.org/10.7554/eLife.42879.003

To identify the binding interfaces of the Ame1/Okp1:Cse4-NCP complex we performed XLMS analysis. We reconstituted a complex on Cse4-NCP composed of Ame1/Okp1, Mif2, Ctf19/Mcm21, Chl4/Iml3 and the MTW1c which links the KMN network to the inner kinetochore receptors Ame1 and Mif2 (***Przewloka et al., 2011***; ***Screpanti et al., 2011***; ***Hornung et al., 2014***). Size-exclusion chromatography (SEC) analysis showed that MTW1c forms a complex with Ame1/Okp1, Mif2, Ctf19/Mcm21 and Chl4/Iml3 and the peak fraction shifted to a higher molecular weight upon addition of Cse4-NCPs depicting nearly stoichiometric protein levels of all subunits (***Figure 1—figure supplement 1***). In all in vitro reconstitution and XLMS experiments we used wild-type MTW1c lacking the phosphorylation mimicking mutations of Dsn1 S240 and S250, which have been shown to stabilize the interaction with Mif2^{CENP-C} and Ame1^{CENP-U} (***Akiyoshi et al., 2013***; ***Dimitrova et al., 2016***), but were not required for complex formation on SEC columns (***Figure 2C***, ***Figure 1—figure supplement***

For purification of FLAG-tagged kinetochore complexes, insect cells were extracted in lysis buffer [50 mM Tris (pH 7.5), 150 mM NaCl, 5% glycerol] supplemented with cOmplete ULTRA EDTA-free Protease Inhibitor Cocktail (Roche) using a Dounce homogenizer. Cleared extracts were incubated with M2 anti-FLAG agarose (Sigma-Aldrich) for 2 hr, washed three times with lysis buffer and eluted in lysis buffer containing 1 mg/ml 3xFLAG peptide (Ontores).

High Five cells expressing Strep-tagged Sli15/Ipl1 were lysed in 50 mM NaH_2PO_4(pH 8.0), 300 mM NaCl, 5% glycerol supplemented with cOmplete ULTRA EDTA-free Protease Inhibitor Cocktail (Roche). Subsequent to incubating the cleared lysates with Strep-Tactin Superflow agarose (Qiagen), protein bound beads were washed three times with lysis buffer and the bound protein complex was eluted in lysis buffer containing 8 mM biotin. FLAG peptide or biotin was either removed via PD10 desalting columns (GE Healthcare) or SEC using a Superdex 200 HiLoad 16/60 column (GE Healthcare) and isocratic elution in lysis buffer.

Acknowledgements

We are grateful to Andrea Musacchio (MPI Dortmund) and Stefan Westermann (University of Essen) for discussions and sharing reagents. We thank Wolfgang Zachariae (MPI Munich) for help with fluorescence microscopy. JFH and GH were funded by the Graduate School (GRK 1721) and MP and VS were funded by the Graduate School (Quantitative Biosciences Munich) of the German Research Foundation (DFG). LDG was a recipient of a DOC Fellowship of the Austrian Academy of Sciences and AK was funded by ERC Grant 281354 (NPC GENEXPRESS). FH was supported by the European Research Council (ERC-StG no. 638218), the Human Frontier Science Program (RGP0008/2015), by the Bavarian Research Center of Molecular Biosystems and by an LMU excellent junior grant.

Additional information

Funding

Funder	Grant reference number	Author
Deutsche Forschungsgemeinschaft	Graduate School Quantitative Biosciences Munich	Mia Potocnjak Victor Solis-Mezarino
Deutsche Forschungsgemeinschaft	Graduate School GRK 1721	Götz Hagemann Franz Herzog
Austrian Academy of Sciences	DOC Fellowship	Laura D Gallego
European Research Council	281354 (NPC GENEXPRESS)	Alwin Köhler
European Research Council	ERC-StG MolStruKT, no. 638218	Franz Herzog
Human Frontier Science Program	RGP0008/2015	Franz Herzog
Bavarian Research Center for Molecular Biosystems		Franz Herzog
Ludwig-Maximilians-Universität München	Excellent Junior grant	Franz Herzog

The funders had no role in study design, data collection and interpretation, or the decision to submit the work for publication.

Author contributions

Josef Fischböck-Halwachs, Sylvia Singh, Formal analysis, Investigation, Methodology, Writing—original draft; Mia Potocnjak, Formal analysis, Methodology; Götz Hagemann, Victor Solis-Mezarino, Formal analysis, Investigation; Stephan Woike, Formal analysis, Investigation, Methodology; Medini Ghodgaonkar-Steger, Jessica Andreani, Formal analysis; Florian Weissmann, Laura D Gallego, Julie Rojas, Alwin Köhler, Methodology; Franz Herzog, Conceptualization, Funding acquisition, Writing—original draft

sample buffer containing 75 mM Tris (pH 8.8). Samples were boiled (10 min, 95˚C) and centrifuged at 10800 x g for 3 min at RT and supernatants were separated on 10% or 15% (Cse4 containing samples) SDS-PAGE gels. Immunoblotting was performed with the following antibodies: Anti-FLAG M2 (Sigma-Aldrich), Anti-PGK1 (ThermoFisher) and visualized by HRP-conjugated anti-mouse secondary antibodies (Santa Cruz).

Live cell microscopy

For localisation analysis of endogenously tagged Ctf19-GFP and Ctf19ΔC-GFP proteins, cells were grown in synthetic medium without tryptophan at 30˚C. For localisation analysis of ectopically expressed Ctf19-Okp1-GFP and Ctf19ΔC-Okp1-GFP proteins in the Ctf19-anchor-away (Ctf19-FRB) strain, cells were grown in selective medium (–His/-Trp) until OD_{600} ~0.4, then rapamycin (1 µg/ml) was added and cells were grown for another 3 hr at 30˚C. For imaging cells were immobilized on concanavalin-A (Sigma-Aldrich) coated slides (Ibidi). Microscopy was performed using a DeltaVision microscopy system (Applied precision) with a Olympus IX71 microscope controlled by softWoRx software (GE Healthcare). Images were processed using Fiji (***Schindelin et al., 2012***).

Protein expression and purification

Expression constructs for 6xHis-Chl4/Iml3, 6xHis-Cnn1/Wip1-1xFlag, 6xHis-Nkp1/Nkp2 and Mhf1/Mhf2-1xStrep were created by amplification of genomic DNA and cloned into pETDuet-1 vector (Novagen). Expression was performed in BL21 (DE3) cells (New England Biolabs). Cells were grown at 37˚C until OD_{600} 0.6, followed by induction with 0.5 mM IPTG for Chl4/Iml3 or 0.2 mM IPTG for all other protein expressions. Protein expression was induced overnight at 18˚C, or for 3 hr at 23˚C, respectively.

Cells were lysed using a French Press in lysis buffer [50 mM Hepes (pH 7.5), 400 mM NaCl, 3% glycerol, 0.01% Tween20 and cOmplete ULTRA EDTA-free Protease Inhibitor Cocktail (Roche)]. 6xHis-tagged proteins were purified using Ni-NTA agarose (Qiagen), whereby 30 mM imidazole were added to the lysis buffer in the washing step, followed by protein elution in 50 mM Hepes pH 7.5, 150 mM NaCl, 300 mM imidazole, and 5% glycerol. Strep-tag purification was performed using Strep-Tactin Superflow agarose (Qiagen) and eluted in a buffer containing 50 mM Hepes (pH 7.5), 150 mM NaCl, 8 mM biotin and 5% glycerol.

Buffer exchange into a buffer containing 50 mM Hepes (pH 7.5), 150 mM NaCl and 5% glycerol was performed using a Superdex 200 HiLoad 16/60 column (GE Healthcare) for Chl4/Iml3 and Cnn1/Wip1 or using a PD10 desalting column (GE Healthcare) for Nkp1/2 and Mhf1/2 protein complexes.

Ame1/Okp1 expression and purification

Ame1-6xHis/Okp1 wild-type and mutant protein expression and purification in *E. coli* was performed as described previously (***Hornung et al., 2014***).

In vitro reconstitution of Cse4- and H3-NCPs

Octameric Cse4 and H3 containing nucleosomes were *in vitro* reconstituted from budding yeast histones which were recombinantly expressed in *E. coli* BL21 (DE3) and assembled on 167 bp of the 'Widom 601' nucleosome positioning sequence according to a modified protocol (***Turco et al., 2015***).

Affinity-purification of recombinant protein complexes from insect cells

C-terminal 6xHis-6xFLAG-tags on Mcm21, Mif2, Dsn1, Mcm16 and C-terminal 2xStrep- tags on Sli15 were used to affinity-purify Ctf19/Mcm21, Mif2, MTW1c, CTF3c and Sli15/Ipl1 complexes. Open reading frames encoding the respective subunits were amplified from yeast genomic DNA and cloned into the pBIG1/2 vectors according to the biGBac system (***Weissmann et al., 2016***). The pBIG1/2 constructs were used to generate recombinant baculoviral genomes by Tn7 transposition into the DH10Bac *E. coli* strain (ThermoFisher) (***Vijayachandran et al., 2011***). Viruses were generated by transfection of Sf21 insect cells (ThermoFisher) with the recombinant baculoviral genome using FuGENE HD transfection reagent (Promega). Viruses were amplified by adding transfection supernatant to Sf21 suspension cultures. Protein complexes were expressed in High Fiveinsect cell (ThermoFisher) suspension cultures.

hydrolysable analog AMP-PNP (Santa Cruz Biotechnology) was applied. To remove basal phosphorylation, Sli15/Ipl1 was treated with lambda phosphatase (New England Biolabs) at 30˚C for 30 min. Subsequently, non-phosphorylated as well as phosphorylated or dephosphorylated Sli15/Ipl1 complexes were washed three times with binding buffer [50 mM NaH_2PO_4(pH 8), 120 mM NaCl, 5% glycerol].

Testing of binding between Ame1/Okp1, Ctf19/Mcm21 and Sli15/Ipl1 was performed in binding buffer at 4˚C, 1000 rpm for 1 hr in a thermomixer (Eppendorf). Unbound proteins were removed by washing three times with binding buffer. The complexes were either eluted with 8 mM biotin in 50 mM NaH_2PO_4(pH 8), 500 mM NaCl, 5% glycerol or by boiling in 2x SDS loading buffer.

To quantify the ratios of bound proteins to the bait protein SDS page band intensities were analyzed by using the Fiji software (**Schindelin et al., 2012**).

Amino acid sequence alignment

Multiple sequence alignment of Cse4 or Okp1 protein sequences from interrelated budding yeast species was conducted with Clustal Omega (**Sievers et al., 2011**). Only protein sequences with the highest similarity to *S. cerevisiae* Cse4 or *S. cerevisiae* Okp1 as determined by a protein BLAST search were included in the search. In addition three mammalian and the *Schizosaccharomyces pombe* homologous CENP-A protein sequences were included in the Cse4 alignment.

Yeast strains and methods

All plasmids and yeast strains used in this study are listed in **Supplementary file 4** and **Supplementary file 5**, respectively. Yeast strains were created in the S288c background. The generation of yeast strains and yeast methods were performed by standard procedures. The anchor-away technique was performed as previously described (**Haruki et al., 2008**).

For anchor-away rescue experiments, the respective promoters and coding sequences were PCR amplified from yeast genomic DNA and cloned into the vector pRS313 either via the Gibson assembly or the restriction/ligation method. In order to artificially target Sli15ΔN2-228 to the kinetochore, the individual promoters and genes were PCR amplified and the respective gene fusions [*CTF19*, *AME1*, *OKP1*, *CTF3*, *CNN1*, *MIF2*, *DSN1*, *MTW1*]-[*SLI15ΔN2-228*]-[*6xHis-7xFLAG*] (**Supplementary file 4**) were generated and cloned into pRS313 using the Gibson assembly reaction The same strategy was applied in order to generate the *CTF19* or *CTF19ΔC* gene fusions to *AME1* or *OKP1*, respectively (**Supplementary file 4**).

The individual deletion mutants were generated using the Q5 site-directed mutagenesis kit (New England Biolabs). The rescue constructs were transformed into Cse4-, Ctf19-, Okp1-, or Sli15 anchor-away strains (**Supplementary file 5**) and cell growth was tested in 1:10 serial dilutions on YPD plates in the absence or presence of rapamycin (1 µg/ml) at 30˚C for 3 days.

Minichromosome loss assay

The Ctf19 anchor-away strain containing a minichromosome (*pYCF1/CEN3.L*) (**Spencer et al., 1990**) and the Ctf19 anchor-away strains containing a minichromosome (*pYCF1/CEN3.L*) and the respective rescue plasmid were grown overnight in selective medium (-Ura selecting for the minichromosome, or –His/-Ura selecting for the rescue plasmid and the minichromosome) and then diluted into YPD medium and cultured for 4 hr. The yeast cultures were then plated onto synthetic medium containing rapamycin (1 µg/ml) and low (6 µg/ml) adenine to enhance the red pigmentation (**Hieter et al., 1985**) and incubated for 3 days at 30˚C. Colonies retaining the minichromosome are white, and loss events result in the formation of red/red sectored colonies. The minichromosome loss frequency was quantified by determining the percentage of red/red sectored colonies in relation to the total colony number (white and red/red sectored) of three biological replicates.

Western blot analysis

For western blot analysis an equivalent of 10 OD_{600} of cells logarithmically grown in liquid culture was collected by centrifugation at 3140 x g for 5 min at RT and the pellet was washed once with aqua dest. For protein extraction, the pellet was resuspended in 1 ml ice-cold 10% trichloroacetic acid and incubated on ice for 1 hr. Samples were pelleted at 20000x g for 10 min, 4˚C and washed twice with ice-cold 95% ethanol. Pellets were air-dried and resuspended in 100 µl 1x SDS-PAGE

Chemical cross-linking and mass spectrometry of kinetochore complexes

The complex containing Cse4-NCP, Mif2, Ame1/Okp1, Ctf19/Mcm21, Chl4/Iml3 and MTW1c was assembled in solution. It was cross-linked using an equimolar mixture of isotopically light (hydrogen) and heavy (deuterium) labeled bis[sulfosuccinimidyl]suberate (BS3, H12/D12) (Creative Molecules) at a final concentration of 0.25–0.5 mM at 10˚C for 30 min. The reaction was quenched by adding ammonium bicarbonate to a final concentration of 100 mM for 10 min at 10 ˚C. The sample was subjected to SEC on a Superose 6 Increase 10/300 GL column (GE Healthcare) and the fractions corresponding to the cross-linked complex were selected for the subsequent protein digest and mass spectrometry (see below).

The complex of Sli15-2xStrep-HA-6xHis/Ipl1 with Ame1/Okp1 and Ctf19/Mcm21 was assembled on Strep-Tactin Superflow agarose (Qiagen) by incubation at room temperature (RT), 1000 rpm for 1 hr in a thermomixer (Eppendorf). Unbound proteins were removed by washing three times with binding buffer [50 mM NaH_2PO_4(pH 8.0), 500 mM NaCl, 5% glycerol] and the complex was eluted in binding buffer containing 8 mM biotin. The eluted complex was re-isolated on Ni-NTA beads (Qiagen), washed twice with binding buffer and then cross-linked by resuspending the protein bound beads in BS3 cross-linker at a final concentration of 0.25–0.5 mM at 30˚C for 30 min. The cross-linking reaction was stopped by adding ammonium bicarbonate to a final concentration of 100 mM for 20 min at 30˚C.

Cross-linked samples were denatured by adding two sample volumes of 8 M urea, reduced with 5 mM TCEP (ThermoFisher) and alkylated by the addition of 10 mM iodoacetamide (Sigma-Aldrich) for 40 min at RT in the dark. Proteins were digested with Lys-C (1:50 (w/w), FUJIFILM Wako Pure Chemical Corporation) at 35˚C for 2 hr, diluted with 50 mM ammonium bicarbonate, and digested with trypsin (1:50 w/w, Promega) overnight. Peptides were acidified with trifluoroacetic acid (TFA) at a final concentration of 1% and purified by reversed phase chromatography using C18 cartridges (Sep-Pak, Waters). Cross-linked peptides were enriched on a Superdex Peptide PC 3.2/30 column using water/acetonitrile/TFA (75/25/0.1, v/v/v) as mobile phase at a flow rate of 50 µl/min and were analyzed by liquid chromatography coupled to tandem mass spectrometry (LC-MS/MS) using an Orbitrap Elite instrument (ThermoFisher). Fragment ion spectra were searched and cross-links were identified by the dedicated software *xQuest* (***Walzthoeni et al., 2012***). The results were filtered according to the following parameters: Δscore $\leq$ 0.85, MS1 tolerance window of -4 to 4 ppm and score $\geq$ 22. The quality of all cross-link spectra passing the filter was manually validated and cross-links were visualized as network plots using the webserver *xVis* (***Grimm et al., 2015***).

Electrophoretic mobility shift assay

Reconstituted nucleosomes (0.5 µM) were mixed in a 1:2 molar ratio with the respective protein complexes in a buffer containing 20 mM Hepes (pH 7.5) and incubated for 1 hr on ice. The interaction was analyzed by electrophoresis at 130 V for 70–90 min on a 6% native polyacrylamide gel in a buffer containing 25 mM Tris and 25 mM boric acid. After electrophoresis, gels were stained with SYBR Gold (ThermoFisher).

Analytical size exclusion chromatography for interaction studies

Analytical SEC experiments were performed on a Superdex 200 Increase 3.2/300 or a Superose 6 Increase 3.2/300 column (GE Healthcare). To detect the formation of a complex, proteins were mixed at equimolar ratios and incubated for 1 hr on ice before SEC. All samples were eluted under isocratic conditions at 4˚C in SEC buffer [50 mM HEPES (pH 7.5), 150 mM NaCl, 5% glycerol]. Elution of proteins was monitored by absorbance at 280 nm. 100 µl fractions were collected and analyzed by SDS-PAGE and Coomassie staining.

In vitro protein binding assay of Sli15/Ipl1 to Ame1/Okp1 and/or Ctf19/Mcm21

Phosphorylated or non-phosphorylated wild-type or mutant Sli15-2xStrep-HA-6xHis/Ipl1 was immobilized on Strep-Tactin Superflow agarose (Qiagen). For prephosphorylation, Sli15/Ipl1 was incubated at 30˚C for 30 min in the presence of 3 mM $MgCl_2$ and 3 mM ATP. Samples for non-phosphorylated Sli15/Ipl1 were treated the same way, but instead of 3 mM ATP the non-

Continued

Reagent type (species) or resource	Designation	Source or reference	Identifiers	Additional information
Peptide, recombinant protein	3xFLAG peptide	Ontores		
Peptide, recombinant protein	lambda phosphatase	New England Biolabs	P0753S	
Commercial assay or kit	Q5 Site-Directed Mutagenesis Kit	New England Biolabs	E0552S	
Chemical compound, drug	BS3-H12/D12 cross-linker	Creative Molecules	001SS	
Chemical compound, drug	Iodoacetamide	Sigma-Aldrich	I6125	
Chemical compound, drug	Lysyl Endopeptidase	FUJIFILM Wako Pure Chemical Corporation	125–05061	
Chemical compound, drug	Trypsin Sequencing Grade Modified	Promega	V5111	
Chemical compound, drug	SYBR Gold	ThermoFisher	S11494	
Chemical compound, drug	AMP-PNP	Santa Cruz Biotechnology	CAS 72957-42-7	
Chemical compound, drug	Rapamycin	Invitrogen	PHZ1235	
Chemical compound, drug	Concanavalin A from *Canavalia ensiformis*	Sigma-Aldrich	C2010	
Chemical compound, drug	FuGENE HD Transfection Reagent	Sigma-Aldrich	E2311	
Chemical compound, drug	cOmplete ULTRA EDTA-free Protease Inhibitor Cocktail	Roche	5892953001	
Chemical compound, drug	Ni-NTA Agarose	Qiagen	30210	
Chemical compound, drug	Strep-Tactin Superflow Plus Agarose	Qiagen	30004	
Chemical compound, drug	M2 anti-FLAG agarose	Sigma-Aldrich	A4596	
Other	Sep-Pak tC18 cartridges	Waters	WAT054960	
Other	PD-10 Desalting Columns	GE Healthcare	17085101	
Other	µ-Slide 8 Well	Ibidi	80826	
Software, algorithm	xQuest	(**Walzthoeni et al., 2012**)		
Software, algorithm	xVis	(**Grimm et al., 2015**)		
Software, algorithm	Fiji	(**Schindelin et al., 2012**)		
Software, algorithm	Clustal Omega	(**Sievers et al., 2011**)		
Software, algorithm	SoftWoRx	GE Healthcare		

Figure 7 continued

INCENP affected the correction of erroneous kinetochore-microtubule attachments (***Haase et al., 2017***). Centromere-targeting deficient CPC resulted in an imperfect inner kinetochore composition that failed to sense tension-loss and in intermediate Ndc80 phosphorylation levels that indicated the incapability of establishing a sharp phosphorylation gradient according to the spatial separation model. Flat Ndc80 phosphorylation levels could be sufficient for the non-selective turnover of erroneous kinetochore attachments, especially at budding yeast kinetochores which are attached to a single microtubule, unless cells are challenged by microtubule poisons.
DOI: https://doi.org/10.7554/eLife.42879.013

has recently been shown to promote accurate chromosome alignment by interaction with microtubules (***Pesenti et al., 2018***). If the observed interaction between the CPC and COMA is conserved in higher eukaryotes or is facilitated by other kinetochore proteins remains to be addressed.

In the spatial separation model the CPC is anchored at the centromere and substrate access of the Ipl1$^{Aurora\ B}$ kinase is regulated by tension-dependent intra-kinetochore stretching upon the biorientation of sister kinetochores. Whether the Ctf19-Sli15 interaction is required for CPC stabilization or for the precise positioning of Ipl1 activity at a distinct kinetochore conformation, competent for tension sensing and error correction, poses an interesting future question (***Figure 7***). Our findings place COMA at the center of kinetochore assembly in budding yeast and contribute to the molecular understanding of the fundamental process of how cells establish correct chromosome biorientation at the mitotic spindle.

Materials and methods

Key resources table

Reagent type (species) or resource	Designation	Source or reference	Identifiers	Additional information
Gene (*S. cerevisiae*)	See ***Supplementary file 5***			
Strain, strain background (*S. cerevisiae*)	S288c			
Strain, strain background (*E. coli*)	BL21(DE3)	New England Biolabs	C2527	
Strain, strain background (*E. coli*)	DH10Bac	ThermoFisher	10361012	
Cell line (*S. frugiperda*)	SF21; *Spodoptera frugiperda*	ThermoFisher	11497013	
Cell line (*Trichoplusia ni*)	High five; *Trichoplusia ni*	ThermoFisher	B85502	
Genetic reagent (*S. cerevisiae*)	See ***Supplementary file 5***			
Antibody	Anti-FLAG M2 (mouse monoclonal)	Sigma-Aldrich	F1804 RRID:AB_262044	1:5000
Antibody	Anti-PGK1 (mouse monoclonal)	Invitrogen	22C5D8 RRID:AB_2532235	1:10000
Antibody	goat anti-mouse IgG-HRP	Santa Cruz Biotechnology	sc-2005 RRID:AB_631736	1:10000
Recombinant DNA reagent	See ***Supplementary file 4***			

Continued on next page

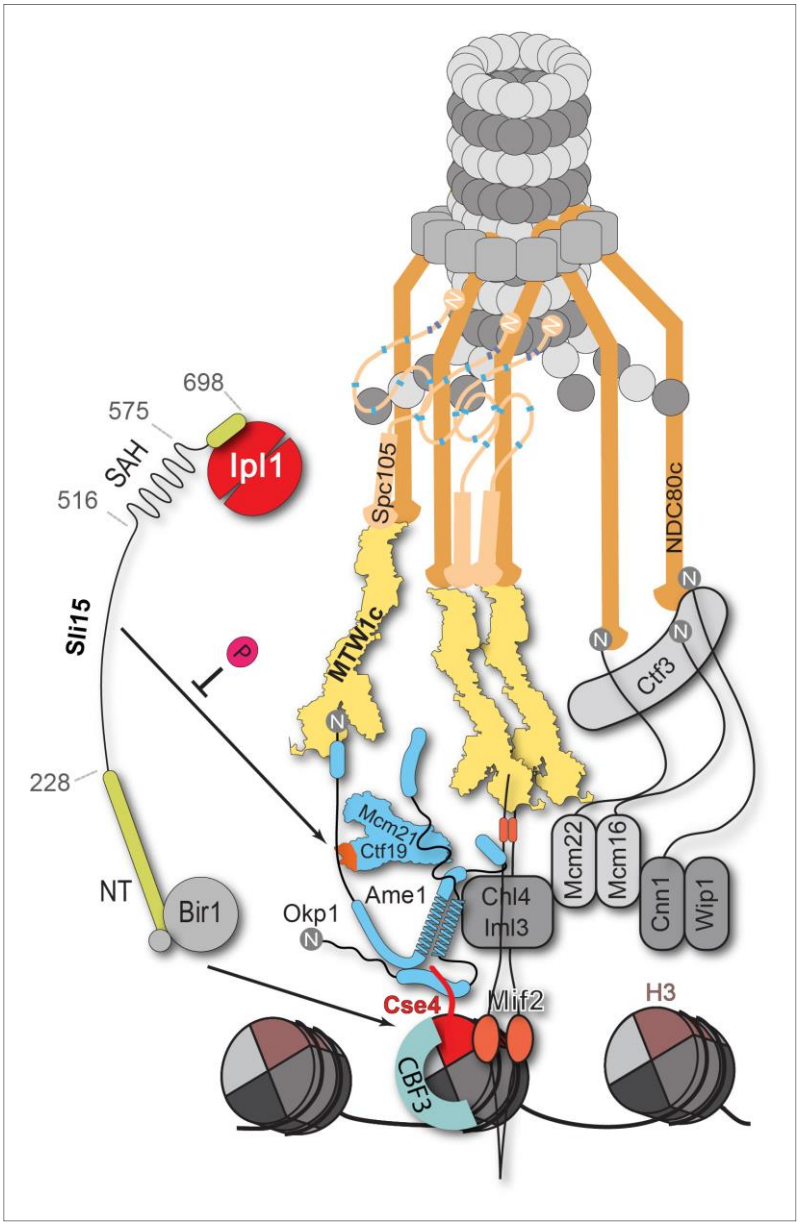

Figure 7. Schematic model of the budding yeast kinetochore subunit architecture. The Okp1 core domain directly binds the essential motif of the Cse4 END suggesting that in contrast to humans, the dual recognition of Cse4-NCPs in *S. cerevisiae* is established by the essential inner kinetochore subunits Ame1/Okp1 and Mif2 through interaction with distinct Cse4 motifs. Together with the observation that Ctf19 associates with Sli15/Ipl1, further CPC interactions with the inner and outer kinetochore could be part of a kinetochore conformation that is dependent on Sli15^{INCENP}. In line with the observed benomyl sensitivity of cells expressing Sli15ΔN as the only nuclear copy (***Figure 5C***), a recent study in Xenopus egg extracts found that CPC lacking the CEN domain of

Figure 7 continued on next page

essential CTF19c^{CCAN} proteins in budding yeast, whereas knockouts of CENP-U/Q in DT40 cells are viable (**Hori et al., 2008**).

The Ctf19 C-terminus is required for Sli15/Ipl1 binding in vitro and has a role in accurate chromosome segregation

Although the Ctf19/Mcm21 heterodimer is not essential, *ctf19Δ* and *mcm21Δ* mutants have chromosome segregation and cohesion defects (**Hyland et al., 1999**; **Ortiz et al., 1999**; **Poddar et al., 1999**; **Fernius and Marston, 2009**; **Hinshaw et al., 2017**). Moreover, Ctf19 and Mcm21 become essential when centromere-targeting of the CPC is lost in a *sli15ΔN* mutant. This observation has led to the hypothesis that centromere-targeted Sli15 might be involved in cohesin loading or in cohesion maintenance (**Campbell and Desai, 2013**). An alternative model posits that COMA is required for the localization and positioning of Sli15/Ipl1 at the kinetochore (**Knockleby and Vogel, 2009**).

Our work showed that COMA interacts directly with Sli15/Ipl1 and identified the Ctf19 RWD-C domain as the primary docking site (**Figure 4A,C**). Synthetic lethality upon Ctf19 or Mcm21 depletion in a *sli15ΔN* background was rescued by fusions of Sli15ΔN to COMA subunits, whereas fusions to other inner or outer kinetochore proteins did not (**Figure 5B**). This observation suggests that positioning Sli15/Ipl1 proximal to Ame1/Okp1 is important in vivo. Because of the requirement of a functional Ipl1-binding IN-box on Sli15 for restoring viability we assume that the observed synthetic lethality is due to mislocalized Ipl1 kinase (**Figure 5D**). Tethering Sli15 to the inner kinetochore might ensure the spatial positioning of Ipl1 kinase activity towards outer kinetochore substrates (**Akiyoshi et al., 2013**; **Foley and Kapoor, 2013**; **Krenn and Musacchio, 2015**), required for correcting erroneous kinetochore-microtubule attachments (**Figure 7**). COMA-Sli15ΔN fusions lacking the SAH domain rescued growth, indicating that this domain is dispensable for CPC function at the inner kinetochore. Because the SAH domain is required for binding to spindle microtubules and critical for cell survival (**Samejima et al., 2015**; **van der Horst et al., 2015**; **Fink et al., 2017**), we infer that the observed rescue was mediated by the SAH domain of endogenous Sli15ΔN (**Figure 5D**).

We also showed that deletion of the Ctf19 RWD-C domain was sufficient to cause synthetic lethality with Sli15ΔN (**Figure 6A**) and that recombinant Ctf19ΔC in complex with Mcm21 (**Figure 4C**) does not interact with Sli15. Moreover, assessing the initially proposed model for the synthetic growth defect of Ctf19/Mcm21 deletion in a *sli15ΔN* background (**Campbell and Desai, 2013**), we observed that deletion of the Ctf19 N-terminus did not cause a synthetic effect in *sli15ΔN* mutant cells. This result indicated that the synthetic growth defect is mediated by a Ctf19 domain distinct from its N-terminus and its role in cohesin loading.

Apart from the synthetic condition we addressed whether the Ctf19 C-terminus is required for chromosome segregation in Sli15 wild-type cells by monitoring missegregation in a minichromosome loss assay (**Hieter et al., 1985**). We showed that loss of the centromeric plasmid upon Ctf19 depletion was rescued to 70% by the ectopic expression of Ctf19-Okp1 and this rescue was abrogated upon deletion of the Ctf19 RWD-C domain in the fusion protein (**Figure 6B**). Similar observations have been obtained in a concomitant study (**García-Rodríguez et al., 2019**) using a complementary approach. By performing a 'centromere re-activation' assay (**Tanaka et al., 2005**) the Tanaka lab showed that Bir1 deletion, and to a lesser extent Mcm21 depletion, reduced localization of Ipl1 at the centromere which was synergistic upon removal of both and the effect on Ipl1 localization correlated with the establishment of chromosome biorientation. This is consistent with our finding that the Ctf19 C-terminus has a role in accurate chromosome segregation and indicates that the Sli15-Ctf19 interaction contributes to the localization and stabilization of the CPC at the inner kinetochore (**Figure 7**).

Our findings also agree with the observations that the functionally active Aurora B pool is associated with the kinetochore rather than the centromere (**DeLuca et al., 2011**; **Bekier et al., 2015**; **Krenn and Musacchio, 2015**; **Hindriksen et al., 2017**). A recent study in humans demonstrated that a kinetochore-localized CPC pool lacking the INCENP CEN domain is sufficient to carry out error correction and biorientation, if cohesin removal, which was attributed to the loss of the CEN domain, is prevented (**Hengeveld et al., 2017**). Furthermore, retaining the human CPC at centromeres in anaphase resulted in the untimely recruitment of Bub1 and BubR1 (**Vázquez-Novelle and Petronczki, 2010**; **Vázquez-Novelle et al., 2014**) which suggests that centromere-localization of the CPC is required, and microtubule-association may not be sufficient, for fulfilling its function in the spindle assembly checkpoint and chromosome biorientation. The human CENP-OPQUR complex

Figure 6 continued

anchor-away (*SLI15/CTF19-FRB*) strain, containing a minichromosome, either untransformed (-) or transformed with the indicated rescue constructs in the absence or presence of 1 µg/ml rapamycin. The percentage and standard error of red/red sectored colonies to the total colony number (white plus red/red sectored) of three biological replicates is shown. The results of 100% red colonies may be indicative of non-optimal conditions for the chromosome loss assay in combination with the anchor-away technique. (**C**) Localisation of ectopically expressed Ctf19-Okp1-GFP and Ctf19ΔC-Okp1-GFP fusion proteins in the Ctf19 anchor-away strain (*SLI15/CTF19-FRB*) in the presence of 1 µg/ml rapamycin. Live cell fluorescence microscopy was performed 3 hr after rapamycin addition. Ndc80-mCherry was used as kinetochore marker. Merged mCherry and GFP signals are shown on the right. (BF: brightfield).

DOI: https://doi.org/10.7554/eLife.42879.009

The following source data and figure supplements are available for figure 6:

Source data 1. Quantification of the minichromosome loss assay in a *SLI15/CTF19-FRB* strain.

DOI: https://doi.org/10.7554/eLife.42879.012

Figure supplement 1. Ctf19ΔC-GFP does not localize to kinetochores.

DOI: https://doi.org/10.7554/eLife.42879.010

Figure supplement 2. The N-terminal fusion protein of Ctf19 with Okp1 does not rescue chromosome segregation defects upon nuclear depletion of Ctf19 in the Sli15 wild-type background.

DOI: https://doi.org/10.7554/eLife.42879.011

Cse4 N-terminus and the binding interface for Ame1/Okp1 are mediated by the same 13 amino acid motif (***Figure 2***) suggests that Ame1/Okp1 is an essential link between centromeric nucleosomes and the outer kinetochore (***Hornung et al., 2014***).

Recent studies have identified the same Cse4 region to interact with Ame1/Okp1 (***Anedchenko et al., 2019***; ***Hinshaw and Harrison, 2019***). Anedchenko et al. found that the affinity of Cse4 N-terminal peptides to Ame1/Okp1 increases with the peptide length up to the low nanomolar range and that methylation of Cse4 R37 and acetylation of Cse4 K49 significantly reduces the binding affinity. Similarly, this region is regulated by Ipl1 phosphorylation in vivo and phosphorylation-mimicking mutants have been found to suppress temperature-sensitive Ipl1 and phosphorylation-deficient Dam1 und Ndc80 mutations (***Boeckmann et al., 2013***), and to decrease the affinity of a Cse4 peptide to Ame1/Okp1 (***Hinshaw and Harrison, 2019***). This observation has interesting implications on the regulation of kinetochore assembly by Ipl1 destabilizing the Cse4-Ame1/Okp1 interaction in a cell cycle regulated manner. Moreover, weakening the interaction of Ame1/Okp1 with Cse4 may have a role in the tension sensing and error correction mechanisms (***Boeckmann et al., 2013***).

Dual recognition of Cse4 at point centromeres by a CTF19c^{CCAN} architecture distinct from vertebrate regional centromeres

In vertebrates, CENP-NL and CENP-C, interact directly and specifically with CENP-A. CENP-C binds divergent hydrophobic residues at the CENP-A C-terminus, whereas CENP-N associates with the CENP-A CATD (***Carroll et al., 2009***; ***Carroll et al., 2010***; ***Guse et al., 2011***; ***Kato et al., 2013***; ***Weir et al., 2016***; ***Pentakota et al., 2017***). Recently, electron microscopy reconstructions of human CENP-A nucleosomes in complex with CENP-N/L identified the RG motif in the L1 loops of the CATD (***Zhou et al., 2011***) as the CENP-N interaction site in CENP-A (***Pentakota et al., 2017***; ***Chittori et al., 2018***; ***Tian et al., 2018***). We did not detect complex formation of Chl4/Iml3 with Cse4-NCPs in our EMSA (***Figure 1A***). Whether this observation can be attributed to the lack of conservation of the RG motif in the corresponding Cse4 sequences in related budding yeasts (***Figure 2A***), and whether this reflects a different role of Chl4/Iml3 in Cse4 recognition and kinetochore assembly remains to be determined. Our crosslink-derived restraints are also in good agreement with a recent cryo-electron microscopy structure of a 13-subunit budding yeast inner kinetochore complex lacking the Cse4-NCP and Mif2 (***Hinshaw and Harrison, 2019***) showing for instance crosslinks between the C-terminal domain of Chl4 and central regions of Ctf19 and Mcm21.

Similarly in humans, recruitment of the CENP-OPQRU complex to kinetochores requires a joint interface formed by CENP-HIKM and CENP-LN (***Foltz et al., 2006***; ***Okada et al., 2006***; ***Pesenti et al., 2018***), but loss of the complex does not affect localization of other inner kinetochore proteins. Differences between vertebrate and budding yeast inner kinetochores are reflected by the physiological importance of the involved proteins, as Ame1/Okp1 together with Mif2 are the

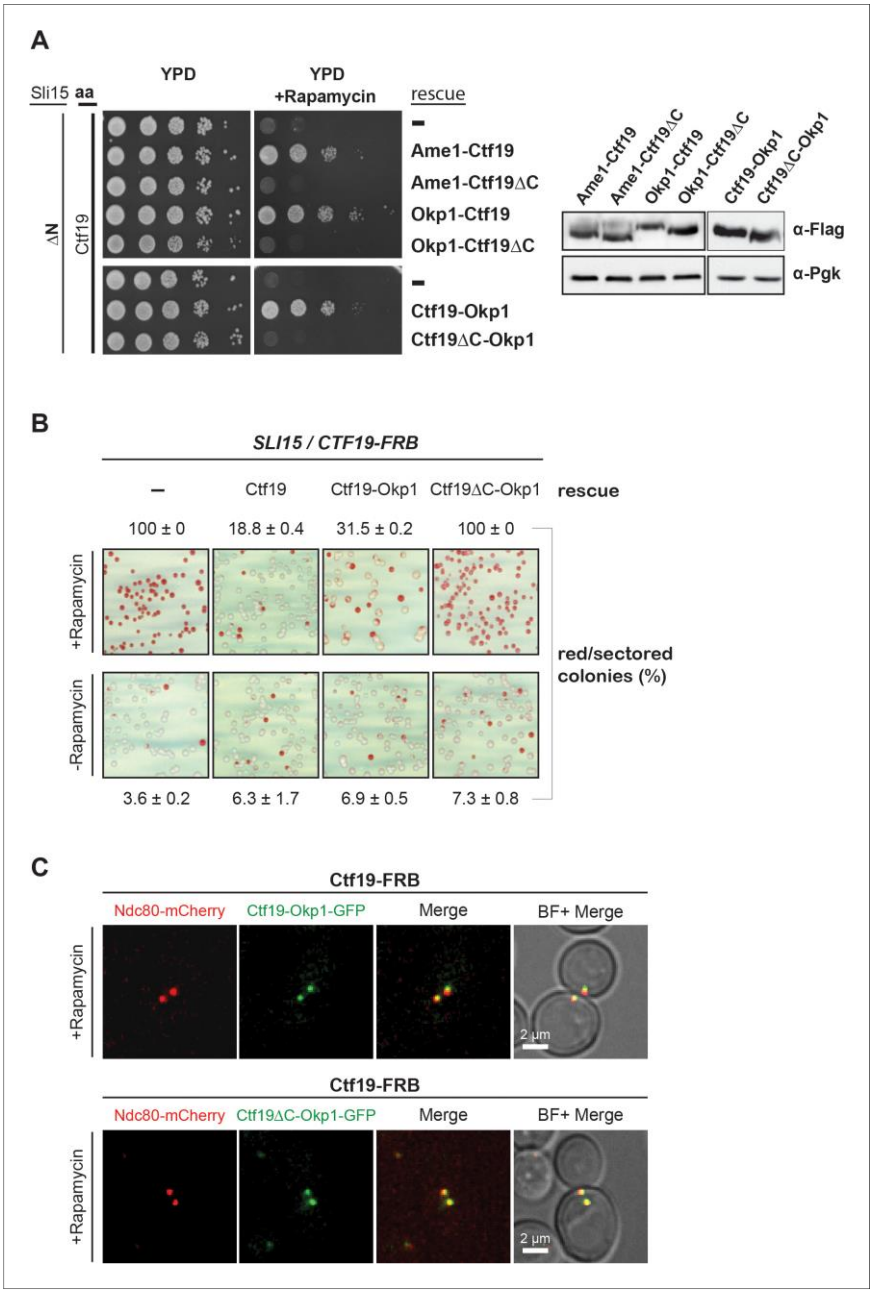

Figure 6. The Ctf19 C-terminus is important for chromosome segregation in the Sli15 wild-type background. (**A**) Left panel: Growth assay of the *sli15ΔN/CTF19-FRB* strain expressing Ame1-Ctf19, Ame1-Ctf19ΔC, Okp1-Ctf19, Okp1-Ctf19ΔC, Ctf19-Okp1 and Ctf19ΔC-Okp1 fusion proteins from the rescue plasmid. Right panel: Western blot analysis visualizing the levels of the ectopically expressed, C-terminally 7xFLAG-tagged fusion proteins. Pgk1 levels are shown as loading control. (aa: Anchor-away) (**B**) Minichromosome loss assay. Chromosome segregation fidelity was determined in the Ctf19

Figure 6 continued on next page

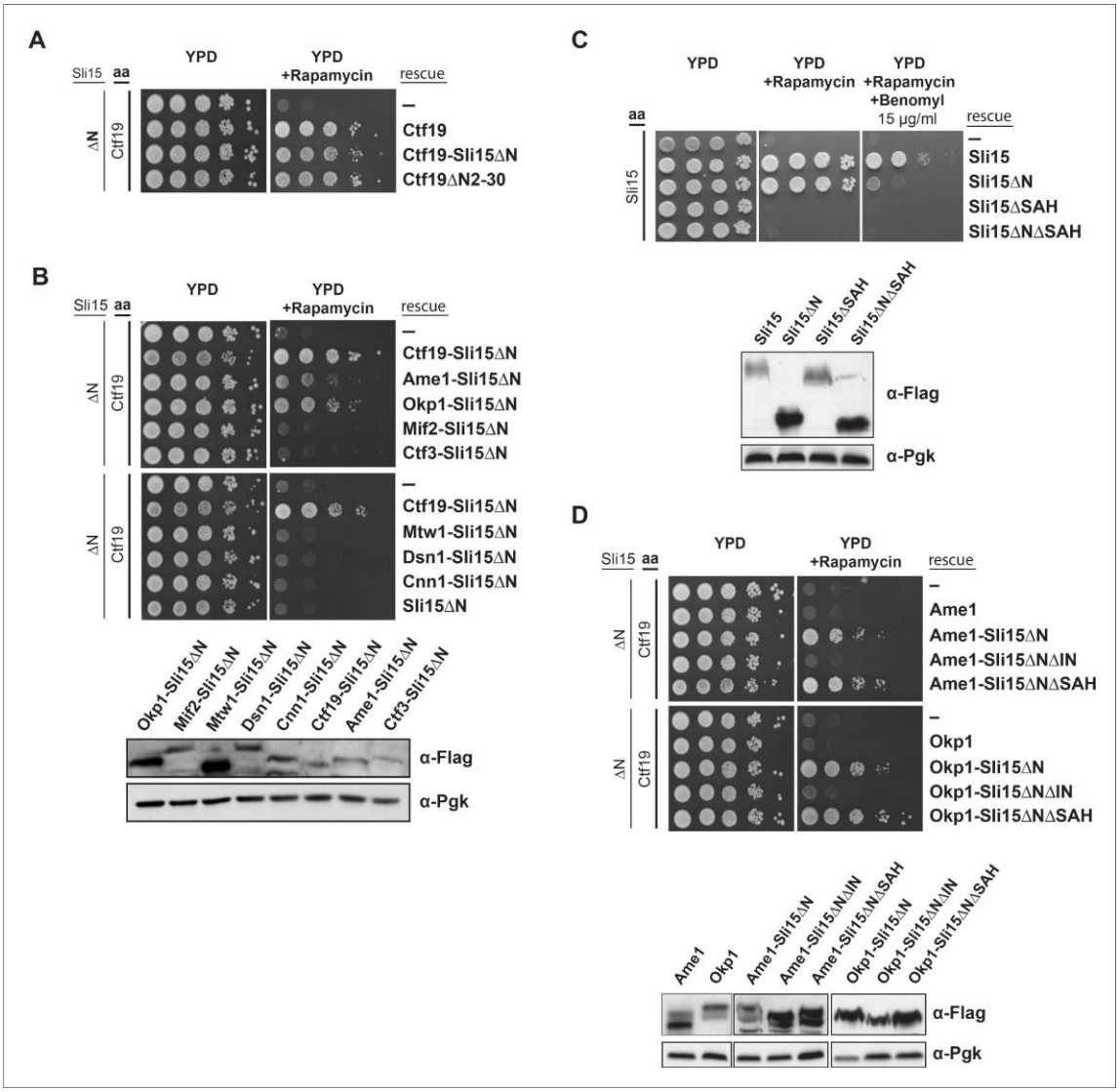

Figure 5. Synthetic lethality of Sli15ΔN and Ctf19 depletion is rescued by fusing Sli15ΔN to Ame1/Okp1 and is independent of Ctf19's role in cohesin loading. (**A**)-(**D**) Cell viability assays studying the rescue of synthetic lethality of a *sli15ΔN/CTF19-FRB* strain using the anchor-away system. The indicated constructs were transformed into a Ctf19 anchor-away (aa) strain (Ctf19-FRB) carrying *sli15ΔN* (ΔN) at the endogenous locus (A, B, D,) or into a Sli15 anchor-away strain (Sli15-FRB) (**C**). Yeast growth was tested in serial dilutions either untransformed (-) or transformed with the indicated rescue constructs on YPD medium in the absence or presence of 1 µg/ml rapamycin at 30˚C. The lower panels in (**B**), (**C**) and (**D**) show western blot analysis of the ectopically expressed protein levels. Pgk1 levels are shown as loading control. (**A**) Deletion of the Ctf19 N-terminus (Ctf19ΔN2-30) does not affect cell viability in a *sli15ΔN* background. (**B**) Artificial tethering of Sli15ΔN to Ame1 or Okp1 rescued synthetic lethality of *sli15ΔN* cells upon Ctf19-FRB depletion from the nucleus. (**C**) Growth phenotypes of Sli15 wild-type, Sli15ΔSAH, Sli15ΔN, and Sli15ΔNΔSAH tested in a Sli15-FRB anchor-away strain. (**D**) Rescue of cell growth by ectopic Ame1-Sli15ΔN or Okp1-Sli15ΔN fusion proteins is dependent on the Sli15 Ipl1-binding domain (IN-box), whereas the SAH domain is dispensable.

DOI: https://doi.org/10.7554/eLife.42879.008

Figure 4 continued

Recombinant Sli15-2xStrep/Ipl1 was immobilized on Streptavidin beads and incubated with Ctf19/Mcm21, Ame1/Okp1 or Ame1/Okp1/Ctf19/Mcm21. Autophosphorylation (p) of Sli15/Ipl1 largely reduced bound protein levels. Dephosphorylation (dp) of Sli15/Ipl1 did not alter the bound proteins levels, which were visualized by SDS-PAGE and Coomassie staining. (**C**) In vitro binding assay analyzing the interaction of Sli15/Ipl1 with Ctf19/Mcm21 or Ctf19ΔC/Mcm21. Ctf19ΔC lacks the last 100 amino acids which form the C-terminal RWD domain. This panel is representative of three independent experiments.

DOI: https://doi.org/10.7554/eLife.42879.007

Ame1- or Okp1-Ctf19 fusion proteins require the Ctf19 RWD-C domain to rescue synthetic lethality of a *sli15ΔN* mutant strain upon Ctf19 depletion

Since the RWD-C domain of Ctf19 was required for association with Sli15/Ipl1 in vitro (***Figure 4C***), we asked whether its deletion would cause synthetic lethality with *sli15ΔN*. As recently described, the Ctf19 C-terminus is involved in formation of the COMA complex through binding to Okp1 (***Schmitzberger et al., 2017***) and consequently, its deletion abrogates kinetochore localization of Ctf19 (***Figure 6—figure supplement 1***). To circumvent loss of Ctf19 from kinetochores, we tested whether Ame1 or Okp1 fusions to wild-type Ctf19 or Ctf19ΔC were able to rescue synthetic lethality in the *sli15ΔN/CTF19-FRB* background. Fusions to both, the N- or C-terminus, of wild-type Ctf19 restored viability, whereas fusions to Ctf19ΔC resulted in synthetic lethality (***Figure 6A***) suggesting that recruitment of Ipl1 activity to the inner kinetochore mediated by the Ctf19 C-terminus is important for CPC function.

Deletion of the Ctf19 RWD-C domain causes a chromosome segregation defect in the Sli15 wild-type background

Since Ctf19 mutants display normal growth, but have chromosome segregation defects (***Hyland et al., 1999***), we tested whether the Ctf19 C-terminus is important for this function using the minichromosome loss assay (***Hieter et al., 1985***). The Ctf19 anchor-away strain was transformed simultaneously with the various Ctf19 rescue constructs and a centromeric plasmid carrying the *SUP11* gene as a marker which indicated loss of the minichromosome by red pigmentation (***Hieter et al., 1985***). Depletion of Ctf19 from the nucleus resulted in a severe chromosome segregation defect that was not observed by growing cells on medium lacking rapamycin which showed 4% red/sectored colonies (***Figure 6B***). Ectopic expression of the Ctf19 wild-type protein decreased the segregation defect to 19% red/sectored colonies (***Figure 6B***, ***Figure 6B—source data 1***) and fusion of Okp1 to the C-terminus of wild-type Ctf19 reduced the red/sectored colonies to 32%. But the fusion of Okp1 to the Ctf19 N-terminus (Okp1-Ctf19 and Okp1-Ctf19ΔC) did not rescue the segregation defect (***Figure 6—figure supplement 2***, ***Figure 6B—source data 1***), indicating that the function of the Ctf19 N-terminus is compromised by fusing it to Okp1 (***Figure 6B***, ***Figure 6B—source data 1***). Thus, the Ctf19-Okp1 fusion rescued the segregation defect, albeit to a slightly lesser extent than the Ctf19 wild-type protein. In contrast, Ctf19ΔC-Okp1, which was localized at the kinetochore (***Figure 6C***), was unable to rescue the segregation defect (***Figure 6B***, ***Figure 6B—source data 1***) suggesting that the Ctf19 C-terminus has a role in mediating accurate chromosome segregation.

Discussion

The Ame1/Okp1 heterodimer directly links Cse4 nucleosomes to the outer kinetochore

We investigated the subunit connectivity of the inner kinetochore assembled at budding yeast point centromeres at the domain level using in vitro reconstitution and XLMS. We found that in addition to Mif2 (***Xiao et al., 2017***), the Ame1/Okp1 heterodimer of the COMA complex is a direct and selective interactor of Cse4-NCPs. We identified the conserved motifs aa 163–187 of the Okp1 core domain (***Figure 3B,C***) (***Schmitzberger et al., 2017***) and aa 34–46 (***Figure 2D,E***) of the Cse4 END to establish the interaction. Although, we did not address whether the Cse4 residues 34–46 are required for the Ame1/Okp1 kinetochore recruitment, the notion that the essential function of the

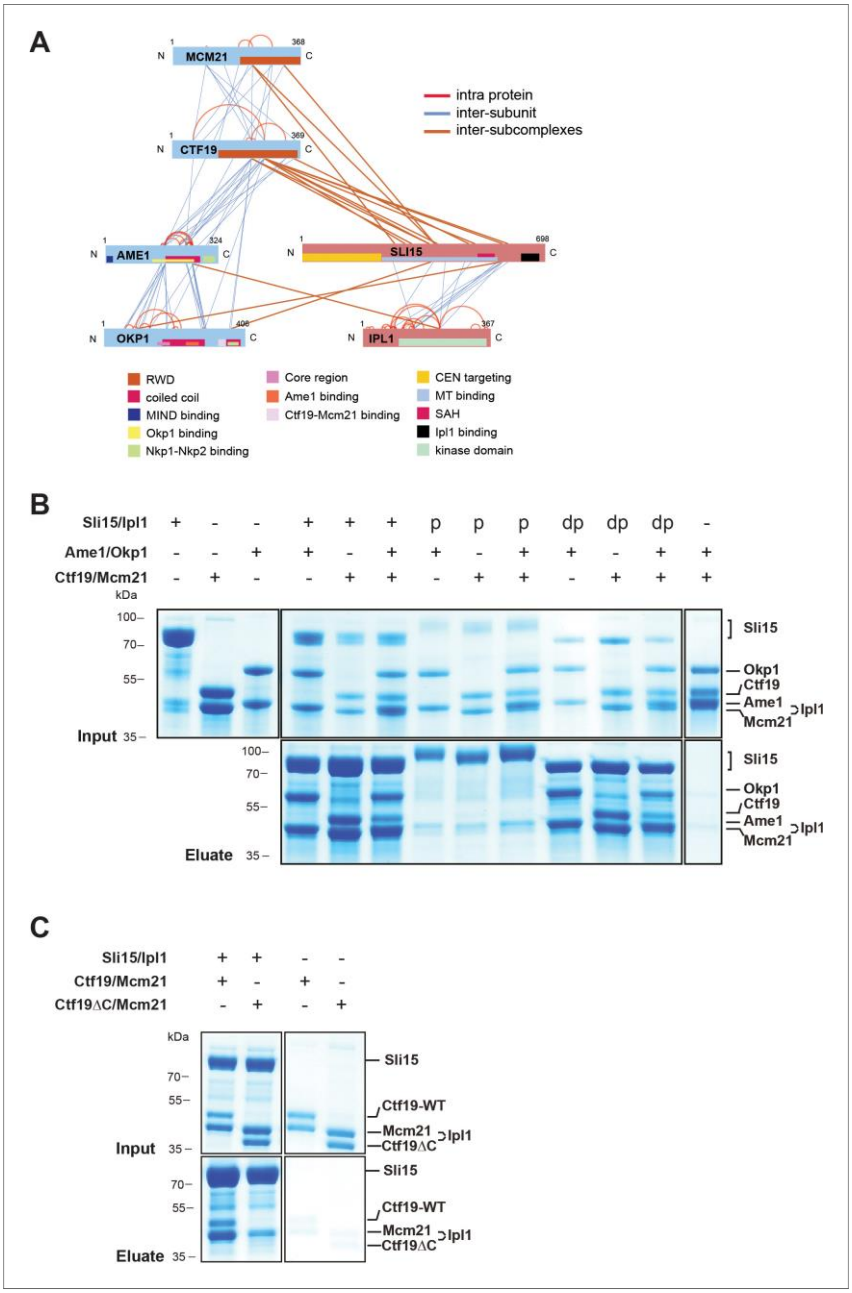

Figure 4. The core-CPC Sli15/Ipl1 associates with the COMA complex through the Ctf19 C-terminal RWD domain in vitro. (**A**) Network representation of lysine-lysine cross-links identified on recombinant Sli15/Ipl1 in complex with COMA. Proteins are represented as bars indicating annotated domains (***Supplementary file 3***) according to the color scheme in the legend. Subunits of a complex are represented in the same color. Protein lengths and cross-link sites are scaled to the amino acid sequence. (**B**) In vitro binding assay analyzing the interaction of Sli15/Ipl1 with the COMA complex.
Figure 4 continued on next page

Figure 3 continued

DOI: https://doi.org/10.7554/eLife.42879.005

The following figure supplement is available for figure 3:

Figure supplement 1. Identification of the Cse4 binding site on Okp1.

DOI: https://doi.org/10.7554/eLife.42879.006

microtubules, phosphorylation of Sli15 by Ipl1 may prevent and regulate its binding to the COMA complex (***Figure 4B***).

In summary, crosslink-derived restraints identified the Ctf19 RWD-C domain as a Sli15/Ipl1 docking site within the COMA complex, a conclusion supported by the loss of interaction upon deletion of the Ctf19 C-terminus in vitro.

Tethering Sli15ΔN selectively to COMA rescues the synthetic lethality of a *sli15ΔN* mutant upon Ctf19 depletion

As deletions of Ctf19 or Mcm21 were synthetically lethal in a *sli15ΔN* background (***Campbell and Desai, 2013***) and Sli15 associated with the Ctf19 RWD-C in vitro (***Figure 4***), we investigated the relevance of this interaction by performing yeast viability assays. First, we reproduced the reported synthetic lethality by anchoring-away Ctf19-FRB in a yeast strain, in which the endogenous *SLI15* copy was replaced by *sli15ΔN* (***Haruki et al., 2008***). We found that in the presence of Ctf19-FRB, cells expressing Sli15ΔN are viable, but display synthetic lethality on rapamycin containing medium, consistent with previous findings (***Campbell and Desai, 2013***) (***Figure 5A***).

Recently, the Ctf19 N-terminus has been identified as the receptor domain of the cohesin loading complex Scc2/4 in late G1 phase (***Hinshaw et al., 2017***). To address whether Sli15/Ipl1 has an active role in this process, we deleted 30 amino acids of Ctf19 (Ctf19ΔN2-30) which have been shown to contain phosphorylation sites of the Dbf4-dependent kinase required for Scc2/4 recruitment to the centromere (***Hinshaw et al., 2017***). Cells expressing Ctf19ΔN2-30 in the *sli15ΔN* background were just as viable upon depletion of Ctf19-FRB as those expressing intact Ctf19 (***Figure 5A***), demonstrating that the synthetic lethality is independent of the Ctf19 N-terminus and its role in cohesin loading.

If the synthetic effect is associated with the loss of interaction between Sli15ΔN and COMA, artificial tethering of Sli15ΔN to the kinetochore should restore growth. We generated fusions of Sli15ΔN to various inner and outer kinetochore proteins and investigated whether growth was restored in a *CTF19-FRB/sli15ΔN* background. Ectopic expression of Sli15ΔN fusions to the outer kinetochore subunits Mtw1 or Dsn1 and to the inner kinetochore subunits Mif2, Ctf3 or Cnn1 did not rescue viability (***Figure 5B***). But selectively tethering Sli15ΔN to Ame1 or Okp1 restored growth (***Figure 5B***).

We further tested whether the rescue of synthetic lethality depended on the Sli15 single alpha helix domain (SAH, aa 516–575) (***Samejima et al., 2015***; ***van der Horst et al., 2015***; ***Fink et al., 2017***) and the Ipl1 binding domain (IN-box, aa 626–698) (***Adams et al., 2000***; ***Kang et al., 2001***). Both domains are essential for cell growth in the Sli15 wild-type or the *sli15ΔN* background (***Figure 5C***) (***Kang et al., 2001***). Cells ectopically expressing the Sli15ΔN mutant protein grew like wild-type, but displayed sensitivity to 15 µg/ml benomyl which contrasted the previous observation that cells carrying the endogenous *sli15ΔN* allele were not sensitive to 12.5 µg/ml benomyl (***Campbell and Desai, 2013***). These deviating observations may be a result of different experimental conditions. To distinguish the requirement of one domain from that of the other in the context of inner kinetochore-localized Sli15/Ipl1, we generated Ame1- and Okp1-Sli15ΔN fusion constructs in which either the IN-box or the SAH domain of Sli15ΔN had been deleted. While expression of Ame1- or Okp1-Sli15ΔNΔSAH proteins rescued cell growth in the *sli15ΔN* background upon Ctf19 depletion, Ame1- and Okp1-Sli15ΔNΔIN fusions did not, indicating that Ipl1 kinase activity is required (***Figure 5D***). Since the ectopically expressed fusion proteins were tested in the *sli15ΔN* background, the result indicates that Ipl1 activity associated with endogenous Sli15ΔN could not rescue synthetic lethality and that tethering Ipl1 activity to COMA subunits is crucial. In contrast, deletion of the SAH domain in Ame1- and Okp1-Sli15ΔNΔSAH fusions was not lethal and was presumably rescued by the SAH domain of the endogenous Sli15ΔN protein (***Figure 5D***) suggesting that the SAH domain is not required for the function of the inner kinetochore-localized CPC pool.

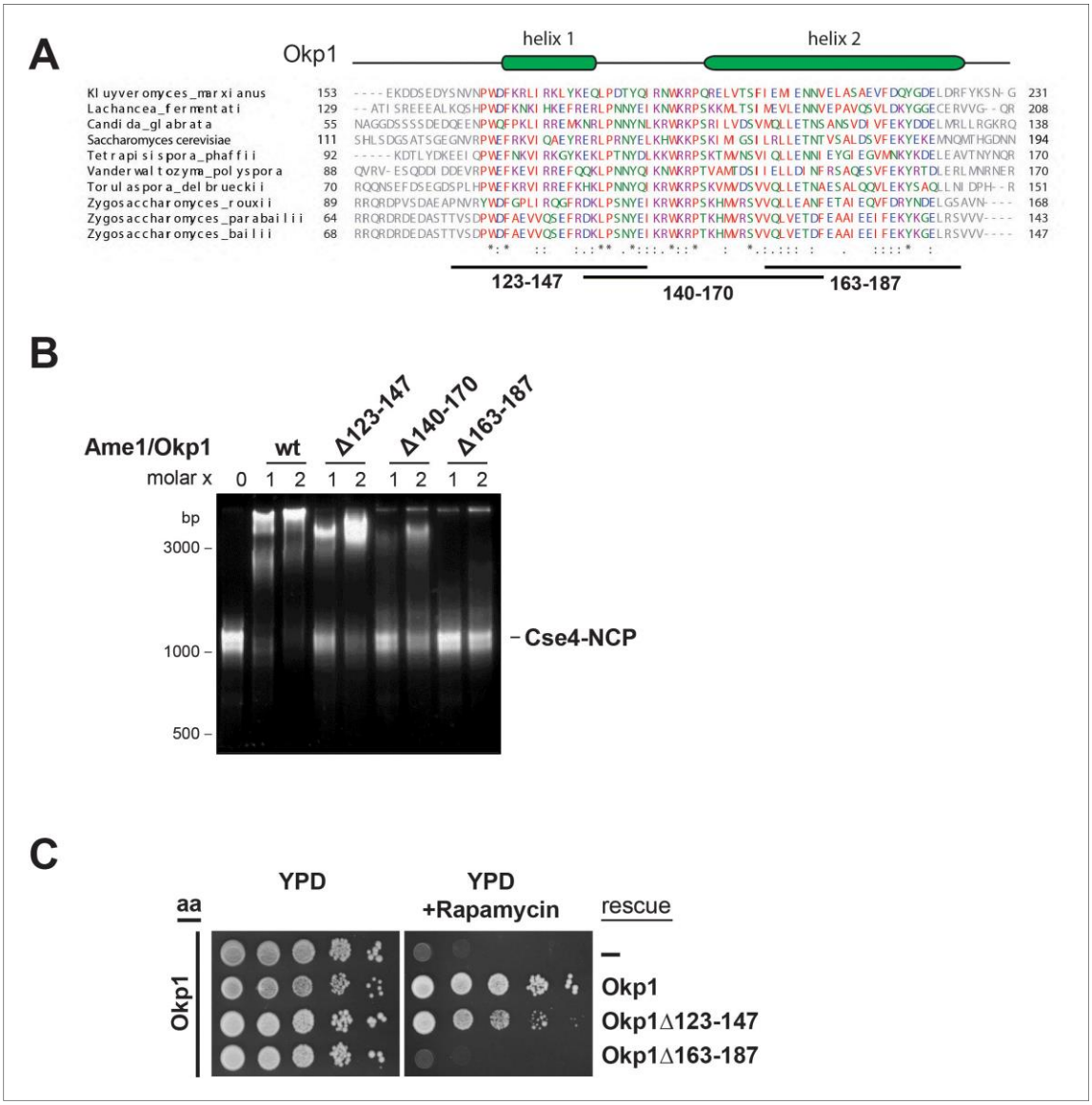

Figure 3. The essential core domain of Okp1 is required for the interaction with Cse4-NCPs. (**A**) Multiple sequence alignment of Okp1 amino acid sequences from related yeast species. Amino acid residues of the conserved region are colored and annotated according to the ClustalW color and annotation codes. Green bars above the alignment represent alpha helical regions predicted by Jpred (***Drozdetskiy et al., 2015***). Lines below the alignment indicate the overlapping Okp1 deletion mutants analysed in (**B**) and (**C**). Residues that are identical among aligned protein sequences (*), conserved substitutions (:), and semiconserved substitutions (.) are indicated. (**B**) EMSA assessing complex formation of Cse4-NCPs with Ame1/Okp1 including wild-type (wt) Okp1 and the indicated Okp1 deletion mutants. Recombinant Ame1/Okp1 complexes were tested in a 1:1 (1) and 2:1 (2) molar ratio with Cse4-NCPs. The DNA is visualized by SYBR Gold staining. (**C**) Cell viability assay of Okp1 deletion mutants using the anchor away (aa) technique. Yeast growth of either the untransformed (-) Okp1 anchor-away strain (Okp1-FRB) or of strains transformed with the indicated Okp1 rescue alleles was tested in 1:10 serial dilutions on YPD medium in the absence or presence of 1 µg/ml rapamycin for 72 hr at 30˚C.

Figure 3 continued on next page

away technique and performed rescue experiments by ectopically expressing the Cse4 mutants Cse4Δ34–46 and Cse4Δ48–61. Indeed, deletion of amino acids 34–46 was lethal, whereas the Cse4Δ48–61 mutant displayed wild-type growth rates (***Figure 2E***). The observation that deletion of the minimal Ame1/Okp1 interacting Cse4 motif (aa 34–46) correlates with the loss of cell viability, whereas the C-terminal half of the END (aa 48–61) is neither essential for viability nor required for Ame1/Okp1 association suggests that binding of the Ame1/Okp1 heterodimer to Cse4 residues 34–46 is essential for yeast growth. The Mif2 signature motif (***Xiao et al., 2017***) and Ame1/Okp1 recognize distinct motifs at the Cse4 C- and N-terminus (***Figure 1C***), respectively, and both are essential for viability (***Hornung et al., 2014***).

The Okp1 core domain interacts with Cse4

To characterize the Cse4 binding site in Okp1 we applied crosslink-derived restraints to narrow down the putative interface to amino acids 95–202 of Okp1 (***Figure 1C***, ***Supplementary file 1***). Based on MSA analysis of Okp1 sequences, this region harbors a conserved stretch (aa 127–184), including part of the previously described Okp1 core domain (aa 166–211) which is essential for cell growth and whose function is still elusive (***Schmitzberger et al., 2017***) (***Figure 3A***). Furthermore, a secondary structure analysis predicted two alpha helices within the conserved domain (helix1 aa 130–140, helix2 aa 156–188) (***Figure 3A***). Thus, we designed three deletion mutants (Okp1Δ123–147, Okp1Δ140–170, Okp1Δ163–187) and purified all Okp1 mutant proteins in complex with Ame1 from *E. coli*. In EMSAs Ame1/Okp1Δ123–147 bound to Cse4-NCPs as well as did the wild-type Ame1/Okp1 complex, whereas Ame1/Okp1Δ140–170 associated only weakly and Ame1/Okp1Δ163–187 failed to associate with Cse4-NCPs (***Figure 3B***). These results are consistent with monitoring protein complex formation by SEC (***Figure 3—figure supplement 1***). In addition, analysis of the Okp1 deletion mutants Δ123–147 and Δ163–187 in cell viability assays showed a tight correlation between their requirement for the interaction with Cse4 and being essential for yeast growth (***Figure 3C***) (***Schmitzberger et al., 2017***). This finding further supports the notion that the recognition of the Cse4 nucleosome by Ame1/Okp1 is essential in budding yeast.

The COMA complex interacts with Sli15/Ipl1 through the Ctf19 C-terminus

The COMA complex is composed of two essential, Ame1/Okp1, and two non-essential, Ctf19/Mcm21, subunits (***Ortiz et al., 1999***; ***Cheeseman et al., 2002***). Both, Ctf19 and Mcm21 contain C-terminal tandem-RWD (RING finger and WD repeat containing proteins and DEAD-like helicases) domains forming a rigid heterodimeric Y-shaped scaffold whose respective N-terminal RWDs of the tandems pack together as shown by a crystal structure of the *K. lactis* complex (***Schmitzberger and Harrison, 2012***). The *ctf19Δ* or *mcm21Δ* mutants become synthetically lethal in a *sli15ΔN* background (***Campbell and Desai, 2013***). Furthermore, Ame1 has been suggested to have a role in Sli15 localization close to kinetochores independently of Bir1 (***Knockleby and Vogel, 2009***). To investigate whether Sli15/Ipl1 associates with the COMA complex, in vitro reconstitution and XLMS analysis detected 98 inter-protein and 69 intra-protein crosslinks (***Figure 4A***, ***Supplementary file 2***). In particular, there were 10 crosslinks from the C-terminal RWD (RWD-C) domain of Ctf19 and 4 crosslinks from the Mcm21 RWD-C domain to the microtubule binding domain of Sli15 (aa 229–565) (***Figure 4A***, ***Supplementary file 2***, ***3***). In the Ame1/Okp1 heterodimer, we identified crosslinks from Sli15 to Okp1 and from Ipl1 to Ame1. The crosslink detected to lysine 366 of Okp1 is located near the identified Ctf19/Mcm21 binding site within Okp1 ('segment 1' aa 321–329) (***Schmitzberger et al., 2017***) and thus is close to the RWD-C domains of Ctf19 and Mcm21. We verified the interaction of Sli15 and the Ctf19 RWD-C domain by in vitro binding assays. Sli15-2xStrep/Ipl1 was immobilized on Streptavidin beads and incubated with a 2-fold molar excess of either Ame1/Okp1 and Ctf19/Mcm21 using wild-type Ctf19 protein or a C-terminal deletion mutant Ctf19Δ270–369 (Ctf19ΔC). Ame1/Okp1 and Ctf19/Mcm21 were both pulled down with Sli15/Ipl1 either as individual complexes or in combination (***Figure 4B***). In agreement with previous findings (***Schmitzberger et al., 2017***), recombinant Ctf19ΔC formed a stoichiometric complex with Mcm21, but lost its ability to bind Sli15/Ipl1 indicating that the RWD-C of Ctf19 is required for Sli15/Ipl1 interaction in vitro (***Figure 4C***). Autophosphorylation of Sli15/Ipl1 abrogated its interaction with Ame1/Okp1 and Ctf19/Mcm21 indicating that like the phosphorylation-regulated binding to

Figure 2 continued

according to the ClustalW color and annotation codes (S.: *Schizosaccharomyces*, C.: *Candida*, Z.: *Zygosaccharomyces*, L.: *Lachancea*). Residues that are identical among aligned protein sequences (*), conserved substitutions (:), and semiconserved substitutions (.) are indicated. (**B**) Scheme of the deletion mutants within the Cse4 N-terminus used in the SEC experiments in (**C**) and (**D**) and in the cell viability assays in (**E**). The conserved region (aa 34–61) is highlighted in pink. (**C**) SEC analysis of the indicated mixtures of recombinant Ame1/Okp1 (AO) and MTW1c and reconstituted H3-, Cse4-, Cse4Δ2–30- or Cse4Δ31–60-NCPs. Ame1/Okp1, MTW1c and the Cse4 proteins were mixed equimolar. Eluted proteins were visualized by SDS-PAGE and Coomassie staining. (**D**) SEC analysis of Ame1/Okp1 (AO) preincubated with Cse4Δ34–46- or Cse4Δ48–61-NCPs. Eluted complexes were analyzed by SDS-PAGE and Coomassie staining. (**E**) Left panel: Cell growth assay of Cse4 mutants in budding yeast using the anchor-away system. The Cse4 wild-type and indicated mutant proteins were ectopically expressed in a Cse4 anchor-away strain (Cse4-FRB) and cell growth was monitored by plating 1:10 serial dilutions on YPD medium at 30˚C in the absence or presence of 1 µg/ml rapamycin. Right panel: Western blot analysis of the ectopically expressed Cse4 wild-type and mutant protein levels in the yeast strains shown on the left. Pgk1 levels are shown as loading control.

DOI: https://doi.org/10.7554/eLife.42879.004

1). In total 349 inter-subunit crosslinks between the fifteen proteins were identified (***Figure 1C***, ***Supplementary file 1***). The majority of the crosslinks detected within the different subcomplexes MTW1c, COMA, Chl4/Iml3, and Cse4-NCP are in agreement with previous studies validating our crosslink map (***De Wulf et al., 2003***; ***Hinshaw and Harrison, 2013***; ***Hornung et al., 2014***). Moreover, crosslinks from the Mif2 N-terminus to the MTW1c (***Przewloka et al., 2011***; ***Screpanti et al., 2011***), from the Mif2 Chl4/Iml3-binding domain to Chl4 (***Hinshaw and Harrison, 2013***), and from the Mif2 signature motif to the Cse4 C-terminus (***Figure 1C***, ***Supplementary file 1***) (***Kato et al., 2013***) are consistent with previously described interfaces. Crosslinks between Ame1/Okp1 and Cse4 occur exclusively between Okp1 and Cse4, suggesting that Okp1 is the direct binding partner of Cse4. Furthermore, Okp1 was the only COMA subunit that crosslinked to the three canonical histones H2A, H2B and H4 with the exception of one crosslink between Ame1 and H2A. Our analysis indicated a close association between Chl4/Iml3 and all COMA subunits. A direct interaction between COMA and Chl4 was reported previously and the Ctf19/Mcm21 heterodimer was found to be required for the kinetochore localization of Chl4 and Iml3 (***Schmitzberger et al., 2017***).

The essential N-terminal domain of Cse4 is required for Okp1 binding

To further characterize the interaction between Ame1/Okp1 and Cse4-NCPs we aimed to identify the binding interface of the Ame1/Okp1:Cse4-NCP complex. Two crosslinks were detected between Okp1 and the essential Cse4 N-terminus (***Figure 1C***, ***Supplementary file 1***). A multiple sequence alignment (MSA) of Cse4$^{CENP\text{-}A}$ protein sequences (***Figure 2A***) detected a conserved region (ScCse4 aa 34–61), unique to Cse4 proteins of interrelated yeasts, which is almost identical to the so-called 'essential N-terminal domain' (END), aa 28–60, shown to be required for the essential function of the Cse4 N-terminus and for recruiting the 'Mcm21p/Ctf19p/Okp1p complex' to minichromosomes (***Keith et al., 1999***; ***Ortiz et al., 1999***; ***Chen et al., 2000***).

To assess whether the Cse4 END mediates the interaction with Ame1/Okp1 we tested binding of recombinant Ame1/Okp1 to reconstituted wild-type and deletion mutants (***Figure 2B***) of Cse4- and to H3-NCPs by SEC (***Figure 2C***). Wild-type Cse4-NCP but not H3-NCP formed a stoichiometric complex with Ame1/Okp1 (***Figure 2C***) which is consistent with our EMSA and XLMS analyses (***Figure 1A,C***). In addition, Ame1/Okp1 bound to a Cse4-NCP retained the ability to interact with the MTW1c (***Hornung et al., 2014***), forming a direct link between the KMN network and the centromeric nucleosome (***Figure 2C***). Truncation of the first 30 N-terminal residues of Cse4 neither affected its ability to bind Ame1/Okp1, nor was it essential for viability (***Figure 2C***) (***Chen et al., 2000***). However, the Cse4Δ31–60 mutant abrogated Ame1/Okp1:Cse4-NCP complex formation (***Figure 2C***). To further narrow down the interface, two deletion mutants splitting the END in half, Cse4Δ34–46 and Cse4Δ48–61 (***Figure 2B***), were tested in SEC experiments. While Cse4Δ48–61 associated with Ame1/Okp1, deletion of amino acids 34–46 completely disrupted the interaction (***Figure 2D***). All Cse4 N-terminal mutant and wild-type NCPs eluted at similar retention times from the SEC column indicating that the Cse4 N-terminal deletions did not affect Cse4 incorporation and stability of the nucleosomes (***Figure 2C,D***).

The crosslink-derived distance restraints as well as SEC analysis identified a conserved Cse4 peptide motif of amino acids 34–46 which is necessary for Ame1/Okp1 interaction. To test whether this motif is essential for cell viability, we depleted endogenous Cse4 from the nucleus using the anchor-

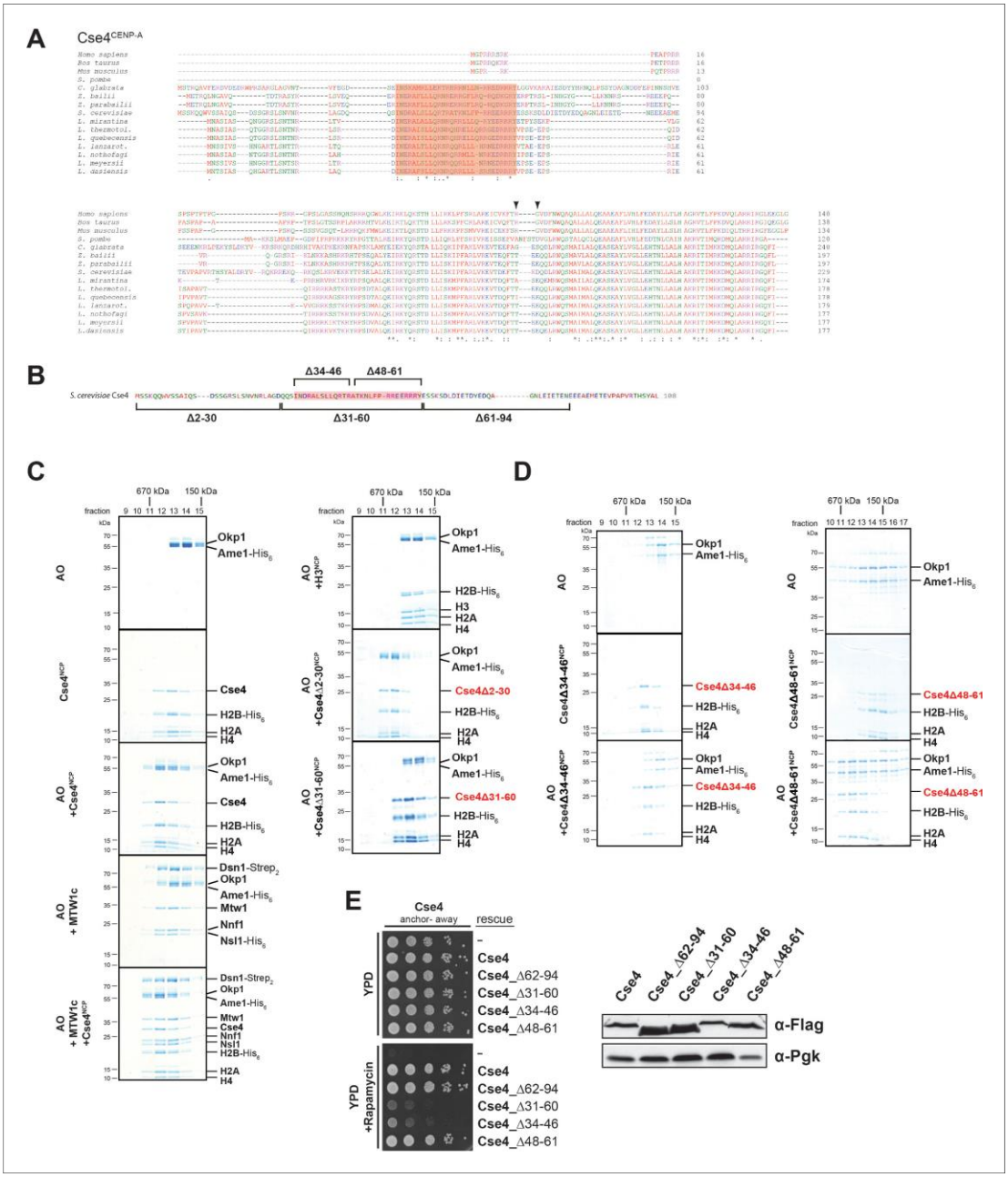

Figure 2. A short helical motif within the Cse4 N-terminus serves as Ame1/Okp1 docking site and is essential in vivo. (**A**) Multiple sequence alignment of Cse4^{CENP-A} proteins. Yeast protein sequences with the highest similarities to *S. cerevisiae* Cse4, three mammalian and the *S. pombe* homologous CENP-A protein sequences were included in the alignment. The amino acid (aa) patch, conserved in interrelated yeasts, is highlighted in pink (*S. cerevisiae* Cse4 aa 34–61). The RG motif in the mammalian sequences is indicated by arrowheads. Amino acid residues are colored and annotated

Figure 2 continued on next page

Vázquez-Novelle MD, Petronczki M. 2010. Relocation of the chromosomal passenger complex prevents mitotic checkpoint engagement at anaphase. *Current Biology* **20**:1402–1407. DOI: https://doi.org/10.1016/j.cub.2010.06.036, PMID: 20619651

Vijayachandran LS, Viola C, Garzoni F, Trowitzsch S, Bieniossek C, Chaillet M, Schaffitzel C, Busso D, Romier C, Poterszman A, Richmond TJ, Berger I. 2011. Robots, pipelines, polyproteins: enabling multiprotein expression in Prokaryotic and eukaryotic cells. *Journal of Structural Biology* **175**:198–208. DOI: https://doi.org/10.1016/j.jsb.2011.03.007, PMID: 21419851

Walzthoeni T, Claassen M, Leitner A, Herzog F, Bohn S, Förster F, Beck M, Aebersold R. 2012. False discovery rate estimation for cross-linked peptides identified by mass spectrometry. *Nature Methods* **9**:901–903. DOI: https://doi.org/10.1038/nmeth.2103, PMID: 22772729

Weir JR, Faesen AC, Klare K, Petrovic A, Basilico F, Fischböck J, Pentakota S, Keller J, Pesenti ME, Pan D, Vogt D, Wohlgemuth S, Herzog F, Musacchio A. 2016. Insights from biochemical reconstitution into the architecture of human kinetochores. *Nature* **537**:249–253. DOI: https://doi.org/10.1038/nature19333, PMID: 27580032

Weissmann F, Petzold G, VanderLinden R, Huis In 't Veld PJ, Brown NG, Lampert F, Westermann S, Stark H, Schulman BA, Peters JM. 2016. biGBac enables rapid gene assembly for the expression of large multisubunit protein complexes. *PNAS* **113**:E2564–E2569. DOI: https://doi.org/10.1073/pnas.1604935113, PMID: 27114506

Westermann S, Cheeseman IM, Anderson S, Yates JR, Drubin DG, Barnes G. 2003. Architecture of the budding yeast kinetochore reveals a conserved molecular core. *The Journal of Cell Biology* **163**:215–222. DOI: https://doi.org/10.1083/jcb.200305100, PMID: 14581449

Westermann S, Avila-Sakar A, Wang HW, Niederstrasser H, Wong J, Drubin DG, Nogales E, Barnes G. 2005. Formation of a dynamic kinetochore- microtubule interface through assembly of the Dam1 ring complex. *Molecular Cell* **17**:277–290. DOI: https://doi.org/10.1016/j.molcel.2004.12.019, PMID: 15664196

Westermann S, Schleiffer A. 2013. Family matters: structural and functional conservation of centromere-associated proteins from yeast to humans. *Trends in Cell Biology* **23**:260–269. DOI: https://doi.org/10.1016/j.tcb.2013.01.010, PMID: 23481674

Widlund PO, Lyssand JS, Anderson S, Niessen S, Yates JR, Davis TN. 2006. Phosphorylation of the chromosomal passenger protein Bir1 is required for localization of Ndc10 to the spindle during anaphase and full spindle elongation. *Molecular Biology of the Cell* **17**:1065–1074. DOI: https://doi.org/10.1091/mbc.e05-07-0640, PMID: 16381814

Xiao H, Wang F, Wisniewski J, Shaytan AK, Ghirlando R, FitzGerald PC, Huang Y, Wei D, Li S, Landsman D, Panchenko AR, Wu C. 2017. Molecular basis of CENP-C association with the CENP-A nucleosome at yeast centromeres. *Genes & Development* **31**:1958–1972. DOI: https://doi.org/10.1101/gad.304782.117, PMID: 29074736

Yue Z, Carvalho A, Xu Z, Yuan X, Cardinale S, Ribeiro S, Lai F, Ogawa H, Gudmundsdottir E, Gassmann R, Morrison CG, Ruchaud S, Earnshaw WC. 2008. Deconstructing survivin: comprehensive genetic analysis of survivin function by conditional knockout in a vertebrate cell line. *The Journal of Cell Biology* **183**:279–296. DOI: https://doi.org/10.1083/jcb.200806118, PMID: 18936249

Zhou Z, Feng H, Zhou BR, Ghirlando R, Hu K, Zwolak A, Miller Jenkins LM, Xiao H, Tjandra N, Wu C, Bai Y. 2011. Structural basis for recognition of centromere histone variant CenH3 by the chaperone Scm3. *Nature* **472**:234–237. DOI: https://doi.org/10.1038/nature09854, PMID: 21412236

Pentakota S, Zhou K, Smith C, Maffini S, Petrovic A, Morgan GP, Weir JR, Vetter IR, Musacchio A, Luger K. 2017. Decoding the centromeric nucleosome through CENP-N. *eLife* **6**:e33442. DOI: https://doi.org/10.7554/eLife.33442

Pesenti ME, Prumbaum D, Auckland P, Smith CM, Faesen AC, Petrovic A, Erent M, Maffini S, Pentakota S, Weir JR, Lin Y-C, Raunser S, McAinsh AD, Musacchio A. 2018. Reconstitution of a 26-Subunit human kinetochore reveals cooperative microtubule binding by CENP-OPQUR and NDC80. *Molecular Cell* **71**:923–939. DOI: https://doi.org/10.1016/j.molcel.2018.07.038

Pfau SJ, Amon A. 2012. Chromosomal instability and aneuploidy in cancer: from yeast to man. *EMBO Reports* **13**:515–527. DOI: https://doi.org/10.1038/embor.2012.65, PMID: 22614003

Poddar A, Roy N, Sinha P. 1999. MCM21 and MCM22, two novel genes of the yeast Saccharomyces cerevisiae are required for chromosome transmission. *Molecular Microbiology* **31**:349–360. DOI: https://doi.org/10.1046/j.1365-2958.1999.01179.x, PMID: 9987135

Przewloka MR, Venkei Z, Bolanos-Garcia VM, Debski J, Dadlez M, Glover DM. 2011. CENP-C is a structural platform for kinetochore assembly. *Current Biology* **21**:399–405. DOI: https://doi.org/10.1016/j.cub.2011.02.005, PMID: 21353555

Samejima K, Platani M, Wolny M, Ogawa H, Vargiu G, Knight PJ, Peckham M, Earnshaw WC. 2015. The inner centromere protein (INCENP) Coil is a single α-Helix (SAH) Domain that binds directly to microtubules and is important for chromosome passenger complex (CPC) Localization and function in mitosis. *Journal of Biological Chemistry* **290**:21460–21472. DOI: https://doi.org/10.1074/jbc.M115.645317, PMID: 26175154

Santaguida S, Musacchio A. 2009. The life and miracles of kinetochores. *The EMBO Journal* **28**:2511–2531. DOI: https://doi.org/10.1038/emboj.2009.173, PMID: 19629042

Schindelin J, Arganda-Carreras I, Frise E, Kaynig V, Longair M, Pietzsch T, Preibisch S, Rueden C, Saalfeld S, Schmid B, Tinevez JY, White DJ, Hartenstein V, Eliceiri K, Tomancak P, Cardona A. 2012. Fiji: an open-source platform for biological-image analysis. *Nature Methods* **9**:676–682. DOI: https://doi.org/10.1038/nmeth.2019, PMID: 22743772

Schmitzberger F, Richter MM, Gordiyenko Y, Robinson CV, Dadlez M, Westermann S. 2017. Molecular basis for inner kinetochore configuration through RWD domain-peptide interactions. *The EMBO Journal* **36**:3458–3482. DOI: https://doi.org/10.15252/embj.201796636, PMID: 29046335

Schmitzberger F, Harrison SC. 2012. RWD domain: a recurring module in kinetochore architecture shown by a Ctf19-Mcm21 complex structure. *EMBO Reports* **13**:216–222. DOI: https://doi.org/10.1038/embor.2012.1, PMID: 22322944

Screpanti E, De Antoni A, Alushin GM, Petrovic A, Melis T, Nogales E, Musacchio A. 2011. Direct binding of Cenp-C to the Mis12 complex joins the inner and outer kinetochore. *Current Biology* **21**:391–398. DOI: https://doi.org/10.1016/j.cub.2010.12.039, PMID: 21353556

Sievers F, Wilm A, Dineen D, Gibson TJ, Karplus K, Li W, Lopez R, McWilliam H, Remmert M, Söding J, Thompson JD, Higgins DG. 2011. Fast, scalable generation of high-quality protein multiple sequence alignments using clustal omega. *Molecular Systems Biology* **7**:539. DOI: https://doi.org/10.1038/msb.2011.75, PMID: 21988835

Spencer F, Gerring SL, Connelly C, Hieter P. 1990. Mitotic chromosome transmission fidelity mutants in saccharomyces cerevisiae. *Genetics* **124**:237–249. PMID: 2407610

Tachiwana H, Kagawa W, Shiga T, Osakabe A, Miya Y, Saito K, Hayashi-Takanaka Y, Oda T, Sato M, Park SY, Kimura H, Kurumizaka H. 2011. Crystal structure of the human centromeric nucleosome containing CENP-A. *Nature* **476**:232–235. DOI: https://doi.org/10.1038/nature10258, PMID: 21743476

Tanaka TU, Rachidi N, Janke C, Pereira G, Galova M, Schiebel E, Stark MJ, Nasmyth K. 2002. Evidence that the Ipl1-Sli15 (Aurora kinase-INCENP) complex promotes chromosome bi-orientation by altering kinetochore-spindle pole connections. *Cell* **108**:317–329. DOI: https://doi.org/10.1016/S0092-8674(02)00633-5, PMID: 11853667

Tanaka K, Mukae N, Dewar H, van Breugel M, James EK, Prescott AR, Antony C, Tanaka TU. 2005. Molecular mechanisms of kinetochore capture by spindle microtubules. *Nature* **434**:987–994. DOI: https://doi.org/10.1038/nature03483, PMID: 15846338

Tian T, Li X, Liu Y, Wang C, Liu X, Bi G, Zhang X, Yao X, Zhou ZH, Zang J. 2018. Molecular basis for CENP-N recognition of CENP-A nucleosome on the human kinetochore. *Cell Research* **28**:374–378. DOI: https://doi.org/10.1038/cr.2018.13, PMID: 29350209

Turco E, Gallego LD, Schneider M, Köhler A. 2015. Monoubiquitination of histone H2B is intrinsic to the Bre1 RING domain-Rad6 interaction and augmented by a second Rad6-binding site on Bre1. *Journal of Biological Chemistry* **290**:5298–5310. DOI: https://doi.org/10.1074/jbc.M114.626788, PMID: 25548288

van der Horst A, Vromans MJ, Bouwman K, van der Waal MS, Hadders MA, Lens SM. 2015. Inter-domain cooperation in INCENP promotes aurora B relocation from centromeres to microtubules. *Cell Reports* **12**:380–387. DOI: https://doi.org/10.1016/j.celrep.2015.06.038, PMID: 26166576

van Hooff JJ, Tromer E, van Wijk LM, Snel B, Kops GJ. 2017. Evolutionary dynamics of the kinetochore network in eukaryotes as revealed by comparative genomics. *EMBO Reports* **18**:1559–1571. DOI: https://doi.org/10.15252/embr.201744102, PMID: 28642229

Vázquez-Novelle MD, Sansregret L, Dick AE, Smith CA, McAinsh AD, Gerlich DW, Petronczki M. 2014. Cdk1 inactivation terminates mitotic checkpoint surveillance and stabilizes kinetochore attachments in anaphase. *Current Biology* **24**:638–645. DOI: https://doi.org/10.1016/j.cub.2014.01.034, PMID: 24583019

Hinshaw SM, Harrison SC. 2019. The structure of the Ctf19c/CCAN from budding yeast. *eLife* **8**:e44239. DOI: https://doi.org/10.7554/eLife.44239, PMID: 30762520

Hori T, Okada M, Maenaka K, Fukagawa T. 2008. CENP-O class proteins form a stable complex and are required for proper kinetochore function. *Molecular Biology of the Cell* **19**:843–854. DOI: https://doi.org/10.1091/mbc.e07-06-0556, PMID: 18094054

Hornung P, Troc P, Malvezzi F, Maier M, Demianova Z, Zimniak T, Litos G, Lampert F, Schleiffer A, Brunner M, Mechtler K, Herzog F, Marlovits TC, Westermann S. 2014. A cooperative mechanism drives budding yeast kinetochore assembly downstream of CENP-A. *The Journal of Cell Biology* **206**:509–524. DOI: https://doi.org/10.1083/jcb.201403081, PMID: 25135934

Hyland KM, Kingsbury J, Koshland D, Hieter P. 1999. Ctf19p: A novel kinetochore protein in Saccharomyces cerevisiae and a potential link between the kinetochore and mitotic spindle. *The Journal of Cell Biology* **145**:15–28. DOI: https://doi.org/10.1083/jcb.145.1.15, PMID: 10189365

Jeyaprakash AA, Klein UR, Lindner D, Ebert J, Nigg EA, Conti E. 2007. Structure of a Survivin-Borealin-INCENP core complex reveals how chromosomal passengers travel together. *Cell* **131**:271–285. DOI: https://doi.org/10.1016/j.cell.2007.07.045, PMID: 17956729

Joglekar AP, Bouck DC, Molk JN, Bloom KS, Salmon ED. 2006. Molecular architecture of a kinetochore-microtubule attachment site. *Nature Cell Biology* **8**:581–585. DOI: https://doi.org/10.1038/ncb1414, PMID: 16715078

Joglekar AP, Bloom K, Salmon ED. 2009. In vivo protein architecture of the eukaryotic kinetochore with nanometer scale accuracy. *Current Biology* **19**:694–699. DOI: https://doi.org/10.1016/j.cub.2009.02.056, PMID: 19345105

Kaitna S, Mendoza M, Jantsch-Plunger V, Glotzer M. 2000. Incenp and an aurora-like kinase form a complex essential for chromosome segregation and efficient completion of cytokinesis. *Current Biology* **10**:1172–1181. DOI: https://doi.org/10.1016/S0960-9822(00)00721-1, PMID: 11050385

Kang J, Cheeseman IM, Kallstrom G, Velmurugan S, Barnes G, Chan CS. 2001. Functional cooperation of Dam1, Ipl1, and the inner centromere protein (INCENP)-related protein Sli15 during chromosome segregation. *The Journal of Cell Biology* **155**:763–774. DOI: https://doi.org/10.1083/jcb.200105029, PMID: 11724818

Kato H, Jiang J, Zhou BR, Rozendaal M, Feng H, Ghirlando R, Xiao TS, Straight AF, Bai Y. 2013. A conserved mechanism for centromeric nucleosome recognition by centromere protein CENP-C. *Science* **340**:1110–1113. DOI: https://doi.org/10.1126/science.1235532, PMID: 23723239

Kawashima SA, Yamagishi Y, Honda T, Ishiguro K, Watanabe Y. 2010. Phosphorylation of H2A by Bub1 prevents chromosomal instability through localizing shugoshin. *Science* **327**:172–177. DOI: https://doi.org/10.1126/science.1180189, PMID: 19965387

Keith KC, Baker RE, Chen Y, Harris K, Stoler S, Fitzgerald-Hayes M. 1999. Analysis of primary structural determinants that distinguish the centromere-specific function of histone variant Cse4p from histone H3. *Molecular and Cellular Biology* **19**:6130–6139. DOI: https://doi.org/10.1128/MCB.19.9.6130, PMID: 10454560

Klein UR, Nigg EA, Gruneberg U. 2006. Centromere targeting of the chromosomal passenger complex requires a ternary subcomplex of Borealin, Survivin, and the N-terminal domain of INCENP. *Molecular Biology of the Cell* **17**:2547–2558. DOI: https://doi.org/10.1091/mbc.e05-12-1133, PMID: 16571674

Knockleby J, Vogel J. 2009. The COMA complex is required for Sli15/INCENP-mediated correction of defective kinetochore attachments. *Cell Cycle* **8**:2570–2577. DOI: https://doi.org/10.4161/cc.8.16.9267, PMID: 19597337

Krenn V, Musacchio A. 2015. The aurora B kinase in chromosome Bi-Orientation and spindle checkpoint signaling. *Frontiers in Oncology* **5**:225. DOI: https://doi.org/10.3389/fonc.2015.00225, PMID: 26528436

Lampson MA, Cheeseman IM. 2011. Sensing centromere tension: aurora B and the regulation of kinetochore function. *Trends in Cell Biology* **21**:133–140. DOI: https://doi.org/10.1016/j.tcb.2010.10.007, PMID: 21106376

Lechner J, Carbon J. 1991. A 240 kd multisubunit protein complex, CBF3, is a major component of the budding yeast centromere. *Cell* **64**:717–725. DOI: https://doi.org/10.1016/0092-8674(91)90501-O, PMID: 1997204

Liu D, Vader G, Vromans MJ, Lampson MA, Lens SM. 2009. Sensing chromosome bi-orientation by spatial separation of aurora B kinase from kinetochore substrates. *Science* **323**:1350–1353. DOI: https://doi.org/10.1126/science.1167000, PMID: 19150808

Meluh PB, Koshland D. 1997. Budding yeast centromere composition and assembly as revealed by in vivo cross-linking. *Genes & Development* **11**:3401–3412. DOI: https://doi.org/10.1101/gad.11.24.3401, PMID: 9407032

Miranda JJ, De Wulf P, Sorger PK, Harrison SC. 2005. The yeast DASH complex forms closed rings on microtubules. *Nature Structural & Molecular Biology* **12**:138–143. DOI: https://doi.org/10.1038/nsmb896, PMID: 15640796

Musacchio A, Desai A. 2017. A molecular view of kinetochore assembly and function. *Biology* **6**:5. DOI: https://doi.org/10.3390/biology6010005

Ng R, Carbon J. 1987. Mutational and in vitro protein-binding studies on centromere DNA from Saccharomyces cerevisiae. *Molecular and Cellular Biology* **7**:4522–4534. DOI: https://doi.org/10.1128/MCB.7.12.4522, PMID: 2830498

Okada M, Cheeseman IM, Hori T, Okawa K, McLeod IX, Yates JR, Desai A, Fukagawa T2006. The CENP-H-I complex is required for the efficient incorporation of newly synthesized CENP-A into centromeres. *Nature Cell Biology* **8**:446–457. DOI: https://doi.org/10.1038/ncb1396, PMID: 16622420

Ortiz J, Stemmann O, Rank S, Lechner J. 1999. A putative protein complex consisting of Ctf19, Mcm21, and Okp1 represents a missing link in the budding yeast kinetochore. *Genes & Development* **13**:1140–1155. DOI: https://doi.org/10.1101/gad.13.9.1140, PMID: 10323865

DeLuca JG, Gall WE, Ciferri C, Cimini D, Musacchio A, Salmon ED. 2006. Kinetochore microtubule dynamics and attachment stability are regulated by Hec1. *Cell* **127**:969–982. DOI: https://doi.org/10.1016/j.cell.2006.09.047, PMID: 17129782

DeLuca KF, Lens SM, DeLuca JG. 2011. Temporal changes in Hec1 phosphorylation control kinetochore-microtubule attachment stability during mitosis. *Journal of Cell Science* **124**:622–634. DOI: https://doi.org/10.1242/jcs.072629, PMID: 21266467

Dimitrova YN, Jenni S, Valverde R, Khin Y, Harrison SC. 2016. Structure of the MIND complex defines a regulatory focus for yeast kinetochore assembly. *Cell* **167**:1014–1027. DOI: https://doi.org/10.1016/j.cell.2016.10.011

Drozdetskiy A, Cole C, Procter J, Barton GJ. 2015. JPred4: a protein secondary structure prediction server. *Nucleic Acids Research* **43**:W389–W394. DOI: https://doi.org/10.1093/nar/gkv332, PMID: 25883141

Earnshaw WC, Rothfield N. 1985. Identification of a family of human centromere proteins using autoimmune sera from patients with scleroderma. *Chromosoma* **91**:313–321. DOI: https://doi.org/10.1007/BF00328227, PMID: 2579778

Fernius J, Marston AL. 2009. Establishment of cohesion at the pericentromere by the Ctf19 kinetochore subcomplex and the replication fork-associated factor, Csm3. *PLOS Genetics* **5**:e1000629. DOI: https://doi.org/10.1371/journal.pgen.1000629, PMID: 19730685

Fink S, Turnbull K, Desai A, Campbell CS. 2017. An engineered minimal chromosomal passenger complex reveals a role for INCENP/Sli15 spindle association in chromosome biorientation. *The Journal of Cell Biology* **216**:911–923. DOI: https://doi.org/10.1083/jcb.201609123, PMID: 28314741

Fitzgerald-Hayes M, Clarke L, Carbon J. 1982. Nucleotide sequence comparisons and functional analysis of yeast centromere DNAs. *Cell* **29**:235–244. DOI: https://doi.org/10.1016/0092-8674(82)90108-8, PMID: 7049398

Foley EA, Kapoor TM. 2013. Microtubule attachment and spindle assembly checkpoint signalling at the kinetochore. *Nature Reviews Molecular Cell Biology* **14**:25–37. DOI: https://doi.org/10.1038/nrm3494, PMID: 23258294

Foltz DR, Jansen LE, Black BE, Bailey AO, Yates JR, Cleveland DW. 2006. The human CENP-A centromeric nucleosome-associated complex. *Nature Cell Biology* **8**:458–469. DOI: https://doi.org/10.1038/ncb1397, PMID: 16622419

Fukagawa T, Earnshaw WC. 2014. The centromere: chromatin foundation for the kinetochore machinery. *Developmental Cell* **30**:496–508. DOI: https://doi.org/10.1016/j.devcel.2014.08.016, PMID: 25203206

García-Rodríguez LJ, Kasciukovic T, Denninger V, Tanaka TU. 2019. Aurora B-INCENP localization at centromeres/Inner kinetochores is required for chromosome Bi-orientation in budding yeast. *Current Biology* **29**:1536–1544. DOI: https://doi.org/10.1016/j.cub.2019.03.051, PMID: 31006569

Grimm M, Zimniak T, Kahraman A, Herzog F. 2015. xVis: a web server for the schematic visualization and interpretation of crosslink-derived spatial restraints. *Nucleic Acids Research* **43**:W362–W369. DOI: https://doi.org/10.1093/nar/gkv463, PMID: 25956653

Guse A, Carroll CW, Moree B, Fuller CJ, Straight AF. 2011. In vitro centromere and kinetochore assembly on defined chromatin templates. *Nature* **477**:354–358. DOI: https://doi.org/10.1038/nature10379, PMID: 21874020

Haase J, Bonner MK, Halas H, Kelly AE. 2017. Distinct roles of the chromosomal passenger complex in the detection of and response to errors in Kinetochore-Microtubule attachment. *Developmental Cell* **42**:640–654. DOI: https://doi.org/10.1016/j.devcel.2017.08.022

Haruki H, Nishikawa J, Laemmli UK. 2008. The anchor-away technique: rapid, conditional establishment of yeast mutant phenotypes. *Molecular Cell* **31**:925–932. DOI: https://doi.org/10.1016/j.molcel.2008.07.020, PMID: 18922474

Hasson D, Panchenko T, Salimian KJ, Salman MU, Sekulic N, Alonso A, Warburton PE, Black BE. 2013. The octamer is the major form of CENP-A nucleosomes at human centromeres. *Nature Structural & Molecular Biology* **20**:687–695. DOI: https://doi.org/10.1038/nsmb.2562, PMID: 23644596

Hengeveld RCC, Vromans MJM, Vleugel M, Hadders MA, Lens SMA. 2017. Inner centromere localization of the CPC maintains centromere cohesion and allows mitotic checkpoint silencing. *Nature Communications* **8**:15542. DOI: https://doi.org/10.1038/ncomms15542, PMID: 28561035

Herzog F, Kahraman A, Boehringer D, Mak R, Bracher A, Walzthoeni T, Leitner A, Beck M, Hartl FU, Ban N, Malmström L, Aebersold R. 2012. Structural probing of a protein phosphatase 2A network by chemical cross-linking and mass spectrometry. *Science* **337**:1348–1352. DOI: https://doi.org/10.1126/science.1221483, PMID: 22984071

Hieter P, Mann C, Snyder M, Davis RW. 1985. Mitotic stability of yeast chromosomes: a colony color assay that measures nondisjunction and chromosome loss. *Cell* **40**:381–392. DOI: https://doi.org/10.1016/0092-8674(85)90152-7, PMID: 3967296

Hindriksen S, Lens SMA, Hadders MA. 2017. The ins and outs of aurora B inner centromere localization. *Frontiers in Cell and Developmental Biology* **5**:112. DOI: https://doi.org/10.3389/fcell.2017.00112, PMID: 29312936

Hinshaw SM, Makrantoni V, Harrison SC, Marston AL. 2017. The kinetochore receptor for the cohesin loading complex. *Cell* **171**:72–84. DOI: https://doi.org/10.1016/j.cell.2017.08.017, PMID: 28938124

Hinshaw SM, Harrison SC. 2013. An Iml3-Chl4 heterodimer links the core centromere to factors required for accurate chromosome segregation. *Cell Reports* **5**:29–36. DOI: https://doi.org/10.1016/j.celrep.2013.08.036, PMID: 24075991

Gallego, Julie Rojas, Jessica Andreani, Alwin Köhler, Franz Herzog

References

Adams RR, Wheatley SP, Gouldsworthy AM, Kandels-Lewis SE, Carmena M, Smythe C, Gerloff DL, Earnshaw WC. 2000. INCENP binds the Aurora-related kinase AIRK2 and is required to target it to chromosomes, the central spindle and cleavage furrow. *Current Biology* **10**:1075–1078. DOI: https://doi.org/10.1016/S0960-9822(00)00673-4, PMID: 10996078

Akiyoshi B, Nelson CR, Biggins S. 2013. The aurora B kinase promotes inner and outer kinetochore interactions in budding yeast. *Genetics* **194**:785–789. DOI: https://doi.org/10.1534/genetics.113.150839, PMID: 23636741

Anedchenko EA, Samel-Pommerencke A, Tran Nguyen TM, Shahnejat-Bushehri S, Pöpsel J, Lauster D, Herrmann A, Rappsilber J, Cuomo A, Bonaldi T, Ehrenhofer-Murray AE. 2019. The kinetochore module Okp1^{CENP-Q}/Ame1^{CENP-U} is a reader for N-terminal modifications on the centromeric histone Cse4^{CENP-A}. *The EMBO Journal* **38**:e98991. DOI: https://doi.org/10.15252/embj.201898991, PMID: 30389668

Baker DJ, Chen J, van Deursen JM. 2005. The mitotic checkpoint in cancer and aging: what have mice taught Us? *Current Opinion in Cell Biology* **17**:583–589. DOI: https://doi.org/10.1016/j.ceb.2005.09.011, PMID: 16226453

Bekier ME, Mazur T, Rashid MS, Taylor WR. 2015. Borealin dimerization mediates optimal CPC checkpoint function by enhancing localization to centromeres and kinetochores. *Nature Communications* **6**:6775. DOI: https://doi.org/10.1038/ncomms7775, PMID: 25854549

Biggins S. 2013. The composition, functions, and regulation of the budding yeast kinetochore. *Genetics* **194**:817–846. DOI: https://doi.org/10.1534/genetics.112.145276, PMID: 23908374

Biggins S, Murray AW. 2001. The budding yeast protein kinase Ipl1/Aurora allows the absence of tension to activate the spindle checkpoint. *Genes & Development* **15**:3118–3129. DOI: https://doi.org/10.1101/gad.934801, PMID: 11731476

Bodor DL, Mata JF, Sergeev M, David AF, Salimian KJ, Panchenko T, Cleveland DW, Black BE, Shah JV, Jansen LE. 2014. The quantitative architecture of centromeric chromatin. *eLife* **3**:e02137. DOI: https://doi.org/10.7554/eLife.02137, PMID: 25027692

Boeckmann L, Takahashi Y, Au WC, Mishra PK, Choy JS, Dawson AR, Szeto MY, Waybright TJ, Heger C, McAndrew C, Goldsmith PK, Veenstra TD, Baker RE, Basrai MA. 2013. Phosphorylation of centromeric histone H3 variant regulates chromosome segregation in saccharomyces cerevisiae. *Molecular Biology of the Cell* **24**:2034–2044. DOI: https://doi.org/10.1091/mbc.e12-12-0893, PMID: 23637466

Camahort R, Shivaraju M, Mattingly M, Li B, Nakanishi S, Zhu D, Shilatifard A, Workman JL, Gerton JL. 2009. Cse4 is part of an octameric nucleosome in budding yeast. *Molecular Cell* **35**:794–805. DOI: https://doi.org/10.1016/j.molcel.2009.07.022, PMID: 19782029

Campbell CS, Desai A. 2013. Tension sensing by aurora B kinase is independent of survivin-based centromere localization. *Nature* **497**:118–121. DOI: https://doi.org/10.1038/nature12057, PMID: 23604256

Carmena M, Wheelock M, Funabiki H, Earnshaw WC. 2012. The chromosomal passenger complex (CPC): from easy rider to the godfather of mitosis. *Nature Reviews Molecular Cell Biology* **13**:789–803. DOI: https://doi.org/10.1038/nrm3474, PMID: 23175282

Carroll CW, Silva MC, Godek KM, Jansen LE, Straight AF. 2009. Centromere assembly requires the direct recognition of CENP-A nucleosomes by CENP-N. *Nature Cell Biology* **11**:896–902. DOI: https://doi.org/10.1038/ncb1899, PMID: 19543270

Carroll CW, Milks KJ, Straight AF. 2010. Dual recognition of CENP-A nucleosomes is required for centromere assembly. *The Journal of Cell Biology* **189**:1143–1155. DOI: https://doi.org/10.1083/jcb.201001013, PMID: 20566683

Cheeseman IM, Anderson S, Jwa M, Green EM, Kang J, Yates JR, Chan CS, Drubin DG, Barnes G. 2002. Phospho-regulation of kinetochore-microtubule attachments by the Aurora kinase Ipl1p. *Cell* **111**:163–172. DOI: https://doi.org/10.1016/S0092-8674(02)00973-X, PMID: 12408861

Cheeseman IM, Chappie JS, Wilson-Kubalek EM, Desai A. 2006. The conserved KMN network constitutes the core microtubule-binding site of the kinetochore. *Cell* **127**:983–997. DOI: https://doi.org/10.1016/j.cell.2006.09.039, PMID: 17129783

Chen Y, Baker RE, Keith KC, Harris K, Stoler S, Fitzgerald-Hayes M. 2000. The N terminus of the centromere H3-like protein Cse4p performs an essential function distinct from that of the histone fold domain. *Molecular and Cellular Biology* **20**:7037–7048. DOI: https://doi.org/10.1128/MCB.20.18.7037-7048.2000, PMID: 10958698

Chittori S, Hong J, Saunders H, Feng H, Ghirlando R, Kelly AE, Bai Y, Subramaniam S. 2018. Structural mechanisms of centromeric nucleosome recognition by the kinetochore protein CENP-N. *Science* **359**:339–343. DOI: https://doi.org/10.1126/science.aar2781, PMID: 29269420

Cho US, Harrison SC. 2011. Ndc10 is a platform for inner kinetochore assembly in budding yeast. *Nature Structural & Molecular Biology* **19**:48–55. DOI: https://doi.org/10.1038/nsmb.2178, PMID: 22139014

De Wulf P, McAinsh AD, Sorger PK. 2003. Hierarchical assembly of the budding yeast kinetochore from multiple subcomplexes. *Genes & Development* **17**:2902–2921. DOI: https://doi.org/10.1101/gad.1144403, PMID: 14633972

Author ORCIDs
Jessica Andreani https://orcid.org/0000-0003-4435-9093
Franz Herzog https://orcid.org/0000-0001-8270-1449

Decision letter and Author response
Decision letter https://doi.org/10.7554/eLife.42879.025
Author response https://doi.org/10.7554/eLife.42879.026

Additional files

Supplementary files

- Supplementary file 1. Inter- and intra-protein cross-links detected on in vitro reconstituted Cse4 containing nucleosomes interacting with the kinetochore complexes Ame1/Okp1, Ctf19/Mcm21, Mif2, Chl4/Iml3 and MTW1c.
DOI: https://doi.org/10.7554/eLife.42879.014
- Supplementary file 2. Inter- and intra-protein cross-links detected on in vitro reconstituted Sli15/Ipl1 interacting with the inner kinetochore proteins Ctf19, Okp1, Ame1 and Mcm21 (COMA).
DOI: https://doi.org/10.7554/eLife.42879.015
- Supplementary file 3. Predicted and experimentally annotated protein domains and motifs depicted in protein cross-link networks.
DOI: https://doi.org/10.7554/eLife.42879.016
- Supplementary file 4. Plasmids used in this study.
DOI: https://doi.org/10.7554/eLife.42879.017
- Supplementary file 5. Yeast strains used in this study.
DOI: https://doi.org/10.7554/eLife.42879.018
- Transparent reporting form
DOI: https://doi.org/10.7554/eLife.42879.019

Data availability

The mass spectrometry raw data was uploaded to the PRIDE Archive and is publicly available through the following identifiers: PXD011235 (COMA-Sli15/Ipl1); PXD011236 (CCAN).

The following datasets were generated:

Author(s)	Year	Dataset title	Dataset URL	Database and Identifier
Josef Fischböck-Halwachs, Sylvia Singh, Mia Potocnjak, Götz Hagemann, Victor Solis-Mezarino, Stephan Woike, Medini Ghodgaonkar-Steger, Florian Weissmann, Laura D. Gallego, Julie Rojas, Jessica Andreani, Alwin Köhler, Franz Herzog	2019	COMA-CPC	https://www.ebi.ac.uk/pride/archive/projects/PXD011235	PRIDE, PXD011235
Josef Fischböck-Halwachs, Sylvia Singh, Mia Potocnjak, Götz Hagemann, Victor Solis-Mezarino, Stephan Woike, Medini Ghodgaonkar-Steger, Florian Weissmann, Laura D.	2019	CCAN	https://www.ebi.ac.uk/pride/archive/projects/PXD011236	PRIDE, PXD011236

Supplementary Materials for

Interaction of Sli15/Ipl1 with the COMA complex is important for chromosome segregation in budding yeast

Josef Fischböck-Halwachs[1]*, Sylvia Singh[1]*, Mia Potocnjak[1]*, Götz Hagemann[1], Victor Solis-Mezarino[1], Stephan Woike[1], Medini Ghodgaonkar-Steger[1], Florian Weissmann[2], Laura D. Gallego[3], Julie Rojas[4], Jessica Andreani-Feuillet[5], Alwin Köhler[3], Franz Herzog[1]†

[1]Gene Center Munich and Department of Biochemistry, Ludwig-Maximilians-Universität München, Feodor-Lynen-Str. 25, 81377 Munich, Germany
[2]Research Institute of Molecular Pathology (IMP), Campus Vienna Biocenter (VBC) 1, 1030 Vienna, Austria
[3]Max F. Perutz Laboratories, Medical University of Vienna, Vienna Biocenter Campus, 1030 Vienna, Austria
[4]Laboratory of Chromosome Biology, Max Planck Institute of Biochemistry, Am Klopferspitz 18, 82152 Martinsried, Germany
[5]Institute for Integrative Biology of the Cell (I2BC), CEA, CNRS, Univ. Paris-Sud, Université Paris-Saclay, 91198, Gif-sur-Yvette cedex, France

* These authors contributed equally.

† Corresponding author. Email: herzog@genzentrum.lmu.de

This file includes

Supplementary figures

Figure S1

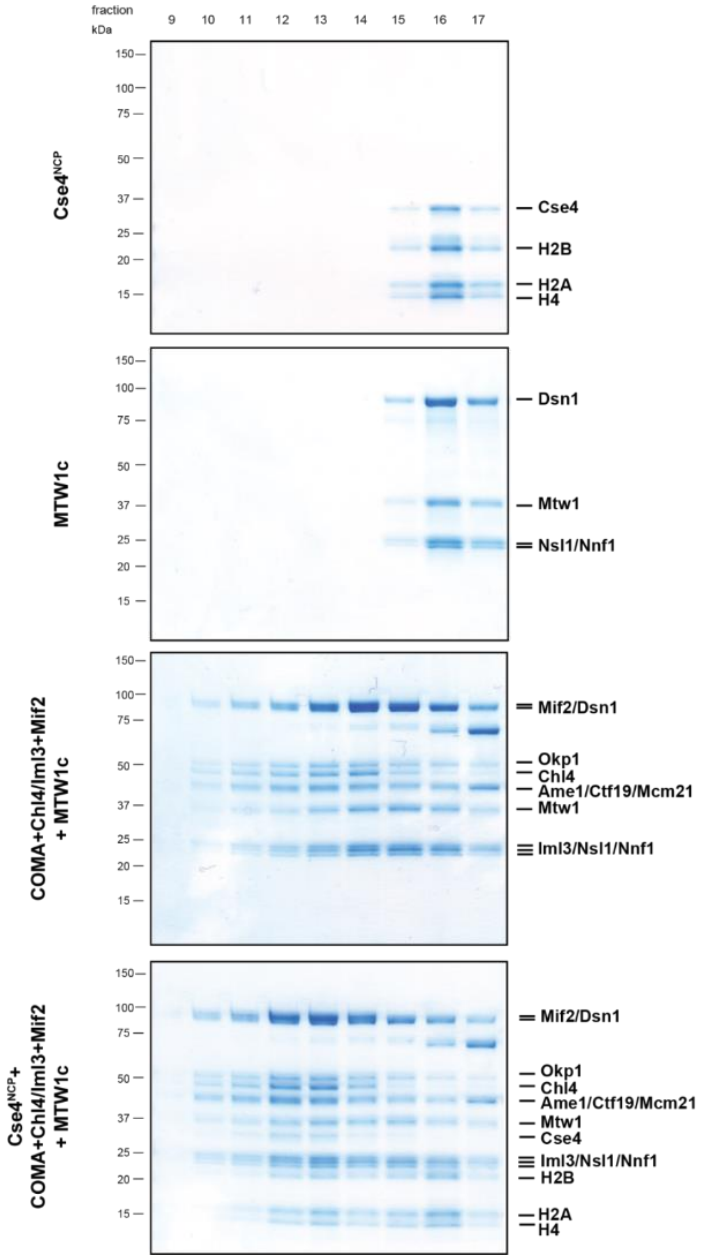

Figure S1. Size exclusion chromatography (SEC) of the *in vitro* reconstituted Ctf19/Mcm21/Ame1/Okp1 (COMA):Chl4/Iml3:Mif2:MTW1c:Cse4-NCP complex. Proteins were mixed in an equimolar ratio, incubated on ice for 1 h and run on a Superose 6 increase 3.2/300 column. Eluted proteins were visualized by SDS-PAGE and Coomassie staining. For XLMS analysis shown in Figure 1C the pre-incubated complex was cross-linked prior to SEC, then

elution fractions 12 and 13 corresponding to the non-cross-linked analysis were pooled and digested for mass spectrometric analysis.

Figure S2

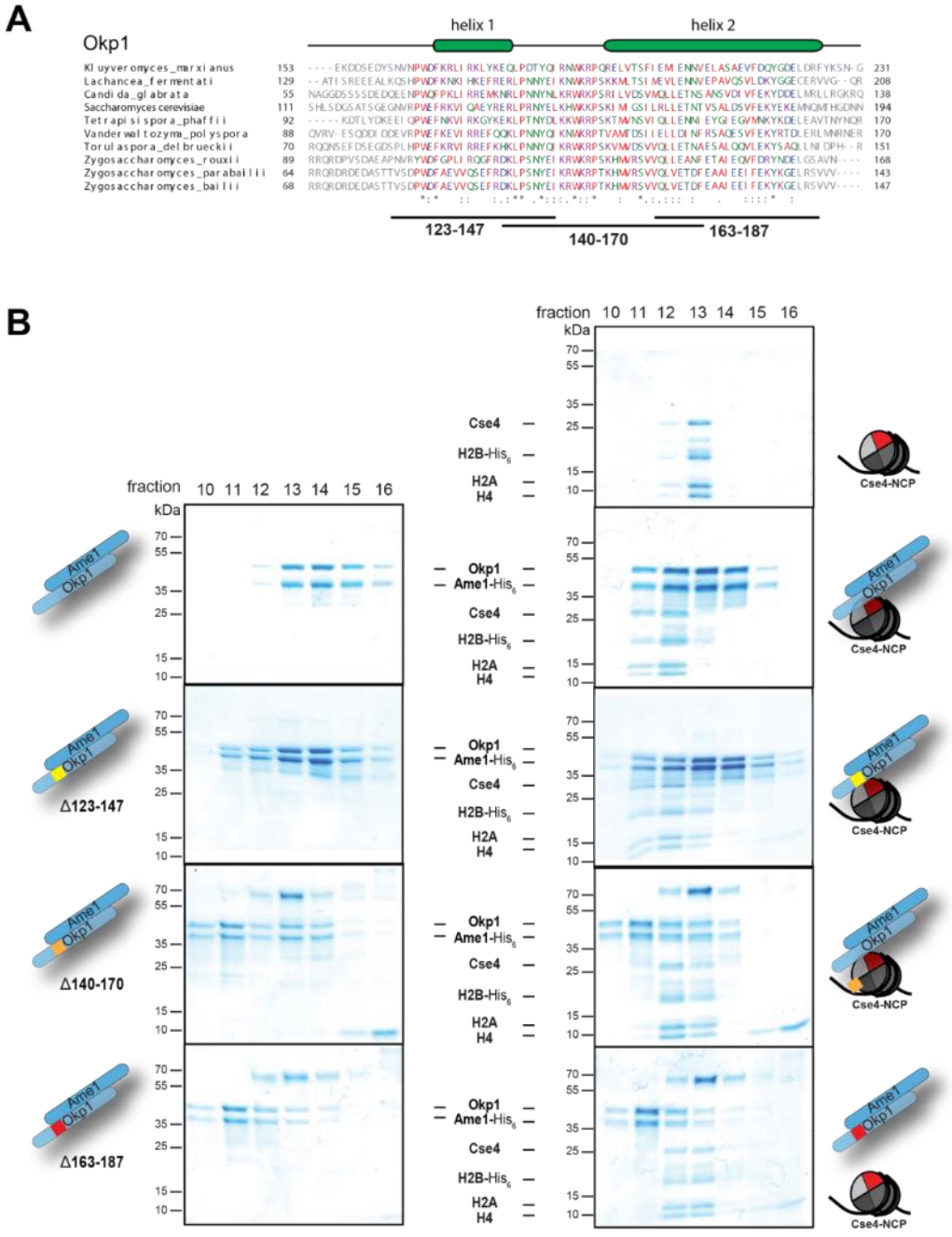

Figure S2. Identification of the Cse4 binding site on Okp1. (A) Multiple sequence alignment of Okp1 amino acid sequences from related yeast species. Amino acid residues of the conserved region are colored and annotated according to the ClustalW color and annotation codes. Green

bars above the alignment represent alpha helical regions predicted by Jpred (Drozdetskiy et al., 2015). Lines below the alignment indicate the overlapping Okp1 deletion mutants analysed in (B). **(B)** Size exclusion chromatography (SEC) analysis of equimolar mixtures of reconstituted Cse4-NCPs with recombinant wild-type Ame1/Okp1, Ame1/Okp1Δ123-147, Ame1/Okp1Δ140-170 or Ame1/Okp1Δ163-187 mutant complexes. Eluted proteins were visualized by SDS-PAGE and Coomassie staining.

Figure S3

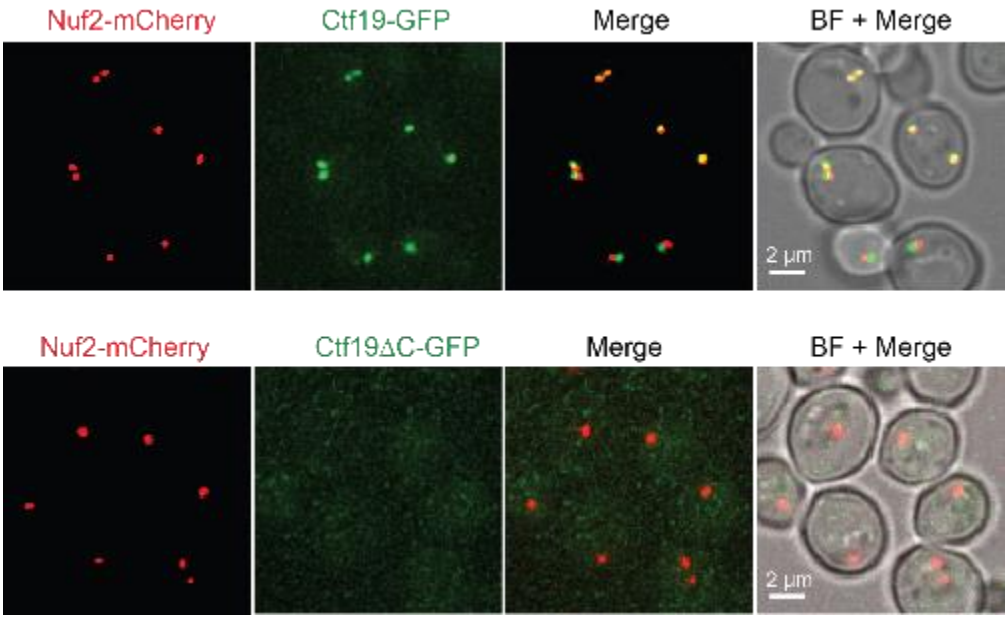

Figure S3. Ctf19ΔC-GFP did not localize to kinetochores. Live cell microscopy of non-synchronized cells grown in synthetic medium expressing either Ctf19-GFP or Ctf19ΔC-GFP and Nuf2-mCherry as kinetochore marker. Merged mCherry and GFP signals are shown on the right.BF: Brightfield.

Supplementary tables

Table S1. Plasmids used in this study

Plasmid	description	source
pST44-Cse4	pST44-6xHis-TEV-Flag-H2B-CSE4-H2A-H4	Alwin Köhler
BSW1	pST44-6xHis-TEV-Flag-H2B-CSE4Δ2-30-H2A-H4	this study
BSW2	pST44-6xHis-TEV-Flag-H2B-CSE4Δ31-60-H2A-H4	this study
BSW4	pST44-6xHis-TEV-Flag-H2B-CSE4Δ34-46-H2A-H4	this study
BSW5	pST44-6xHis-TEV-Flag-H2B-CSE4Δ48-61-H2A-H4	this study
pST44-H3	pST44-6xHis-TEV-Flag-H2B-H3-H2A-H4	Alwin Köhler
BJF6	pLIB-MIF2-6xHis-6xFlag	this study
BMP37	pETDuet-6xHis-CHL4/IML3	this study
pPH74	pST39-OKP1-AME1-6xHis	Stefan Westermann
BJF26	pST39-OKP1Δ123-147-AME1-6xHis	this study
BJF27	pST39-OKP1Δ140-170-AME1-6xHis	this study
BJF28	pST39-OKP1Δ163-187-AME1-6xHis	this study
pSW661	pST39-CTF19-MCM21-6xHis	Stefan Westermann
BJF25	pST39-CTF19ΔC270-369 -MCM21-6xHis	this study
BJF7	pBIG1-MCM21-6xHis-6xFlag/CTF19	this study
BJF50	pBIG1-AME1-6xHis-6xFlag /OKP1	this study
BMP75	pBIG1-MTW1-NNF1-NSL1-DSN1-2xStrep	this study
BJF10	pBIG-CTF3-MCM16-MCM22	this study
BMS52	pETDuet-6xHis-CNN1-WIP1-1xFlag	this study
BMS64	pETDuet-6xHis-NKP1-NKP2	this study
BMS65	pETDuet-MHF2-MHF1-1xStrep	this study
BJF1	pBIG1-SLI15-2xStrep-HA-6xHis/IPL1	this study
BSS93	pRS313-pCSE4-3xFlag-CSE4	this study
BSS94	pRS313-pCSE4-3xFlag-CSE4Δ31-60	this study
BSS95	pRS313-pCSE4-3xFlag-CSE4Δ62-94	this study
BSS96	pRS313-pCSE4-3xFlag-CSE4Δ34-46	this study
BSS97	pRS313-pCSE4-3xFlag-CSE4Δ48-61	this study
BSS134	pRS313-pCTF19-CTF19WT-SLI15Δ2-228-6xHis-7xFlag	this study
BSS146	pRS313-pAME1-AME1-SLI15Δ2-228-6xHis-7xFlag	this study
BSS142	pRS313-pOKP1-OKP1-SLI15Δ2-228-6xHis-7xFlag	this study
BSS145	pRS313-pMIF2-MIF2-SLI15Δ2-228-6xHis-7xFlag	this study
BSS143	pRS313-pCTF3-CTF3-SLI15Δ2-228-6xHis-7xFlag	this study
BSS144	pRS313-pMTW1-MTW1-SLI15Δ2-228-6xHis-7xFlag	this study
BSS141	pRS313-pDSN1-DSN1-SLI15Δ2-228-6xHis-7xFlag	this study
BSS147	pRS313-pCNN1-CNN1-SLI15Δ2-228-6xHis-7xFlag	this study
BSS1	pRS313-pSLI15-SLI15-6xHis-6xFlag	this study

Plasmid	description	source
BSS15	pRS313-pSLI15-SLI15ΔSAH-6xHis-6xFlag	this study
BSS2	pRS313-pSLI15-SLI15Δ2-228-6xHis-6xFlag	this study
BSS16	pRS313-pSLI15-SLI15Δ2-228ΔSAH-6xHis-6xFlag	this study
BSS129	pRS313-pCTF19-CTF19-6xHis-7xFlag	this study
BSS159	pRS313-pCTF19-3xMyc-CTF19Δ2-30-6xHis-7xFlag	this study
BSS76	pRS313-pAME1-AME1-6xHis-7xFlag	this study
BSS169	pRS313-pOKP1-OKP1-6xHis-6xFlag	this study
BSS172	pRS313-pOKP1-OKP1Δ123-147-6xHis-6xFlag	this study
BSS174	pRS313-pOKP1-OKP1Δ163-187-6xHis-6xFlag	this study
BSS165	pRS313-pAME1-AME1-SLI15Δ2-228-ΔINbox(626-698)-6xHis-7xFlag	this study
BSS167	pRS313-pAME1-AME1-SLI15Δ2-228-ΔSAH(516-575)-6xHis-7xFlag	this study
BSS164	pRS313-pOKP1-OKP1-SLI15Δ2-228-ΔINbox(626-698)-6xHis-7xFlag	this study
BSS166	pRS313-pOKP1-OKP1-SLI15Δ2-228-ΔSAH(516-575)-6xHis-7xFlag	this study
BSS175	pRS313-pAME1-AME1-CTF19-6xHis-7xFlag	this study
BSS176	pRS313-pAME1-AME1-CTF19ΔC270-369 -6xHis-7xFlag	this study
BSS177	pRS313-pOKP1-OKP1-CTF19-6xHis-7xFlag	this study
BSS178	pRS313-pOKP1-OKP1-CTF19ΔC270-369 -6xHis-7xFlag	this study
BSS212	pRS313-pCTF19-CTF19-OKP1-6xHis-7xFlag	this study
BSS213	pRS313-pCTF19-CTF19ΔC270-369-OKP1-6-xHis-7xFlag	this study
BSS214	pRS313-pCTF19-CTF19-OKP1-GFP	this study
BSS215	pRS313-pCTF19-CTF19ΔC270-369-OKP1-GFP	this study
pYCF1/CEN3.L	YRp14/TEL cassette (pYCF1) with a CEN3 insert	(Spencer et al. 1990)

Table S2. Yeast strains used in this study.

All strains are isogenic with the S288c background

strain	genotype
YSS225	MAT a, tor1-1, fpr1::loxP-Leu2-loxP, RPL13A-2xFKBP12::lox-TRP1-loxP, CSE4-FRB::KanMX
YSS226	MAT a, tor1-1, fpr1::loxP-Leu2-loxP, RPL13A-2xFKBP12::lox-TRP1-loxP, CSE4-FRB::KanMX, pRS313-pCSE4-3xFlag-CSE4
YSS227	MAT a, tor1-1, fpr1::loxP-Leu2-loxP, RPL13A-2xFKBP12::lox-TRP1-loxP, CSE4-FRB::KanMX, pRS313-pCSE4-3xFlag-CSE4Δ62-94
YSS228	MAT a, tor1-1, fpr1::loxP-Leu2-loxP, RPL13A-2xFKBP12::lox-TRP1-loxP, CSE4-FRB::KanMX, pRS313-pCSE4-3xFlag-CSE4Δ31-60
YSS229	MAT a, tor1-1, fpr1::loxP-Leu2-loxP, RPL13A-2xFKBP12::lox-TRP1-loxP, CSE4-FRB::KanMX, pRS313-pCSE4-3xFlag-CSE4Δ34-46
YSS230	MAT a, tor1-1, fpr1::loxP-Leu2-loxP, RPL13A-2xFKBP12::lox-TRP1-loxP, CSE4-FRB::KanMX, pRS313-pCSE4-3xFlag-CSE4Δ48-61
YSS1	MAT a, tor1-1, fpr1::loxP-Leu2-loxP, RPL13A-2xFKBP12::lox-TRP1-loxP, Sli15-FRB::KanMX
YSS69	MAT a, tor1-1, fpr1::loxP-Leu2-loxP, RPL13A-2xFKBP12::lox-TRP1-loxP, Sli15-FRB::KanMX, pRS313-pSLI15-SLI15-6xHis-6xFlag
YSS70	MAT a, tor1-1, fpr1::loxP-Leu2-loxP, RPL13A-2xFKBP12::lox-TRP1-loxP, Sli15-FRB::KanMX, pRS313-pSLI15-SLI15Δ2-228-6xHis-6xFlag
YSS81	MAT a, tor1-1, fpr1::loxP-Leu2-loxP, RPL13A-2xFKBP12::lox-TRP1-loxP, Sli15-FRB::KanMX, pRS313-pSLI15-SLI15ΔSAH-6xHis-6xFlag
YSS87	MAT a, tor1-1, fpr1::loxP-Leu2-loxP, RPL13A-2xFKBP12::lox-TRP1-loxP, Sli15-FRB::KanMX, pRS313-pSLI15-SLI15Δ2-228ΔSAH-6xHis-6xFlag
YSS213	MAT a, tor1-1, fpr1::loxP-Leu2-loxP, RPL13A-2xFKBP12::lox-TRP1-loxP, CTF19-FRB::KanMX
YSS216	MAT a, tor1-1, fpr1::loxP-Leu2-loxP, RPL13A-2xFKBP12::lox-TRP1-loxP, CTF19-FRB::KanMX, sli15Δ2-228::hphNT1
YSS321	MAT a, tor1-1, fpr1::loxP-Leu2-loxP, RPL13A-2xFKBP12::lox-TRP1-loxP, CTF19-FRB::KanMX, pRS313-pCTF19-CTF19-6xHis-7xFlag
YSS325	MAT a, tor1-1, fpr1::loxP-Leu2-loxP, RPL13A-2xFKBP12::lox-TRP1-loxP, CTF19-FRB::KanMX, sli15Δ2-228::hphNT1, pRS313-pCTF19-CTF19-6xHis-7xFlag
YSS301	MAT a, tor1-1, fpr1::loxP-Leu2-loxP, RPL13A-2xFKBP12::lox-TRP1-loxP, CTF19-FRB::KanMX, sli15Δ2-228::hphNT1, pRS313-pCTF19-CTF19WT-SLI15Δ2-228-6xHis-7xFlag
YSS348	MAT a, tor1-1, fpr1::loxP-Leu2-loxP, RPL13A-2xFKBP12::lox-TRP1-loxP, CTF19-FRB::KanMX, sli15Δ2-228::hphNT1, pRS313-pCTF19-3xMyc-CTF19Δ2-30-6xHis-7xFlag

strain	genotype
YSS334	MAT a, tor1-1, fpr1::loxP-Leu2-loxP, RPL13A-2xFKBP12::lox-TRP1-loxP, CTF19-FRB::KanMX, sli15Δ2-228::hphNT1, pRS313-pAME1-AME1-6xHis-7xFlag
YSS335	MAT a, tor1-1, fpr1::loxP-Leu2-loxP, RPL13A-2xFKBP12::lox-TRP1-loxP, CTF19-FRB::KanMX, sli15Δ2-228::hphNT1, pRS313-pAME1-AME1-SLI15Δ2-228-6xHis-7xFlag
YSS336	MAT a, tor1-1, fpr1::loxP-Leu2-loxP, RPL13A-2xFKBP12::lox-TRP1-loxP, CTF19-FRB::KanMX, sli15Δ2-228::hphNT1, pRS313-pAME1-AME1-SLI15Δ2-228-ΔINbox(626-698)-6xHis-7xFlag
YSS337	MAT a, tor1-1, fpr1::loxP-Leu2-loxP, RPL13A-2xFKBP12::lox-TRP1-loxP, CTF19-FRB::KanMX, sli15Δ2-228::hphNT1, pRS313-pAME1-AME1-SLI15Δ2-228-ΔSAH(516-575)-6xHis-7xFlag
YSS92	MAT a, tor1-1, fpr1::loxP-Leu2-loxP, RPL13A-2xFKBP12::lox-TRP1-loxP, OKP1-FRB::KanMX
YSS351	MAT a, tor1-1, fpr1::loxP-Leu2-loxP, RPL13A-2xFKBP12::lox-TRP1-loxP, OKP1-FRB::KanMX, pRS313-pOKP1-OKP1-6xHis-6xFlag
YSS394	MAT a, tor1-1, fpr1::loxP-Leu2-loxP, RPL13A-2xFKBP12::lox-TRP1-loxP, OKP1-FRB::KanMX, pRS313-pOKP1-OKP1Δ122-147-6xHis-6xFlag
YSS395	MAT a, tor1-1, fpr1::loxP-Leu2-loxP, RPL13A-2xFKBP12::lox-TRP1-loxP, OKP1-FRB::KanMX, pRS313-pOKP1-OKP1Δ163-187-6xHis-6xFlag
YSS342	MAT a, tor1-1, fpr1::loxP-Leu2-loxP, RPL13A-2xFKBP12::lox-TRP1-loxP, CTF19-FRB::KanMX, sli15Δ2-228::hphNT1, pRS313-pOKP1-OKP1-6xHis-6xFlag
YSS343	MAT a, tor1-1, fpr1::loxP-Leu2-loxP, RPL13A-2xFKBP12::lox-TRP1-loxP, CTF19-FRB::KanMX, sli15Δ2-228::hphNT1, pRS313-pOKP1-OKP1-SLI15Δ2-228-6xHis-7xFlag
YSS344	MAT a, tor1-1, fpr1::loxP-Leu2-loxP, RPL13A-2xFKBP12::lox-TRP1-loxP, CTF19-FRB::KanMX, sli15Δ2-228::hphNT1, pRS313-pOKP1-OKP1-SLI15Δ2-228-ΔINbox(626-698)-6xHis-7xFlag
YSS345	MAT a, tor1-1, fpr1::loxP-Leu2-loxP, RPL13A-2xFKBP12::lox-TRP1-loxP, CTF19-FRB::KanMX, sli15Δ2-228::hphNT1, pRS313-pOKP1-OKP1-SLI15Δ2-228-ΔSAH(516-575)-6xHis-7xFlag
YSS315	MAT a, tor1-1, fpr1::loxP-Leu2-loxP, RPL13A-2xFKBP12::lox-TRP1-loxP, CTF19-FRB::KanMX, sli15Δ2-228::hphNT1, pRS313-pMIF2-MIF2-SLI15Δ2-228-6xHis-7xFlag
YSS313	MAT a, tor1-1, fpr1::loxP-Leu2-loxP, RPL13A-2xFKBP12::lox-TRP1-loxP, CTF19-FRB::KanMX, sli15Δ2-228::hphNT1, pRS313-pCTF3-CTF3-SLI15Δ2-228-6xHis-7xFlag
YSS314	MAT a, tor1-1, fpr1::loxP-Leu2-loxP, RPL13A-2xFKBP12::lox-TRP1-loxP, CTF19-FRB::KanMX, sli15Δ2-228::hphNT1, pRS313-pMTW1-MTW1-SLI15Δ2-228-6xHis-7xFlag

strain	genotype
YSS311	MAT a, tor1-1, fpr1::loxP-Leu2-loxP, RPL13A-2xFKBP12::lox-TRP1-loxP, CTF19-FRB::KanMX, sli15Δ2-228::hphNT1, pRS313-pDSN1-DSN1-SLI15Δ2-228-6xHis-7xFlag
YSS317	MAT a, tor1-1, fpr1::loxP-Leu2-loxP, RPL13A-2xFKBP12::lox-TRP1-loxP, CTF19-FRB::KanMX, sli15Δ2-228::hphNT1, pRS313-pCNN1-CNN1-SLI15Δ2-228-6xHis-7xFlag
YSS366	MAT a, tor1-1, fpr1::loxP-Leu2-loxP, RPL13A-2xFKBP12::lox-TRP1-loxP, CTF19-FRB::KanMX, sli15Δ2-228::hphNT1, pRS313-pSLI15-SLI15Δ2-228-6xHis-6xFlag
YSS399	MAT a, tor1-1, fpr1::loxP-Leu2-loxP, RPL13A-2xFKBP12::lox-TRP1-loxP, CTF19-FRB::KanMX, sli15Δ2-228::hphNT1, pRS313-pAME1-AME1-CTF19-6xHis-7xFlag
YSS400	MAT a, tor1-1, fpr1::loxP-Leu2-loxP, RPL13A-2xFKBP12::lox-TRP1-loxP, CTF19-FRB::KanMX, sli15Δ2-228::hphNT1, pRS313-pAME1-AME1-CTF19ΔC270-369-6xHis-7xFlag
YSS405	MAT a, tor1-1, fpr1::loxP-Leu2-loxP, RPL13A-2xFKBP12::lox-TRP1-loxP, CTF19-FRB::KanMX, pRS313-pOKP1-OKP1-CTF19-6xHis-7xFlag
YSS406	MAT a, tor1-1, fpr1::loxP-Leu2-loxP, RPL13A-2xFKBP12::lox-TRP1-loxP, CTF19-FRB::KanMX, pRS313-pOKP1-OKP1-CTF19ΔC270-369-6xHis-7xFlag
YSS401	MAT a, tor1-1, fpr1::loxP-Leu2-loxP, RPL13A-2xFKBP12::lox-TRP1-loxP, CTF19-FRB::KanMX, sli15Δ2-228::hphNT1, pRS313-pOKP1-OKP1-CTF19-6xHis-7xFlag
YSS402	MAT a, tor1-1, fpr1::loxP-Leu2-loxP, RPL13A-2xFKBP12::lox-TRP1-loxP, CTF19-FRB::KanMX, sli15Δ2-228::hphNT1, pRS313-pOKP1-OKP1-CTF19ΔC270-369-6xHis-7xFlag
YSS511	MAT a, tor1-1, fpr1::loxP-Leu2-loxP, RPL13A-2xFKBP12::lox-TRP1-loxP, CTF19-FRB::KanMX, pRS313-pCTF19-CTF19-Okp1-6xHis-7xFlag
YSS512	MAT a, tor1-1, fpr1::loxP-Leu2-loxP, RPL13A-2xFKBP12::lox-TRP1-loxP, CTF19-FRB::KanMX, pRS313-pCTF19-CTF19ΔC270-369-Okp1-6xHis-7xFlag
YSS513	MAT a, tor1-1, fpr1::loxP-Leu2-loxP, RPL13A-2xFKBP12::lox-TRP1-loxP, CTF19-FRB::KanMX, sli15Δ2-228::hphNT1, pRS313-pCTF19-CTF19-Okp1-6xHis-7xFlag
SS514	MAT a, tor1-1, fpr1::loxP-Leu2-loxP, RPL13A-2xFKBP12::lox-TRP1-loxP, CTF19-FRB::KanMX, sli15Δ2-228::hphNT1, pRS313-pCTF19-CTF19ΔC270-369-Okp1-6xHis-7xFlag
YSS515	MAT a, tor1-1, fpr1::loxP-Leu2-loxP, RPL13A-2xFKBP12::lox-TRP1-loxP, CTF19-FRB::KanMX, NDC80-mCherry::natNT2, pRS313-pCTF19-CTF19-Okp1-GFP

strain	genotype
YSS516	MAT a, tor1-1, fpr1::loxP-Leu2-loxP, RPL13A-2xFKBP12::lox-TRP1-loxP, CTF19-FRB::KanMX, NDC80-mCherry::natNT2, pRS313-pCTF19-CTF19ΔC270-369-OKP1-GFP
YSS255	MAT a, tor1-1, fpr1::loxP-Leu2-loxP, RPL13A-2xFKBP12::lox-TRP1-loxP, NDC80-mCherry::natNT2, CTF19-GFP::HIS
YSS256	MAT a, tor1-1, fpr1::loxP-Leu2-loxP, RPL13A-2xFKBP12::lox-TRP1-loxP, NDC80-mCherry::natNT2, CTF19ΔC270-369-GFP::HIS

Table S3. Inter- and intra-protein cross-links detected on *in vitro* reconstituted Cse4 containing nucleosomes interacting with the kinetochore complexes Ame1/Okp1, Ctf19/Mcm21, Mif2, Chl4/Iml3 and MTW1c. Ctf19/Mcm21, Mif2 and MTW1 complexes were recombinantly expressed in insect cells and affinity-purified via Mcm21-6xFLAG-6xHis, Mif2-6xFLAG-6xHis, or Dsn1-6xFLAG-6xHis, respectively. Ame1/Okp1, Chl4/Iml3 and Cse4 nucleosomes were expressed in *E. coli* and *in vitro* reconstituted as described (see materials and methods). A nearly stoichiometric supramolecular complex of Ame1/Okp1:Ctf19/Mcm21:Chl4/Iml3:Mif2:MTW1c and Cse4-NCPs was generated *in vitro* (see Figure S1) and chemical cross-links introduced by BS3 were identified as described (see materials and methods). In total, 349 inter-protein (marked in dark blue) and 395 intra-protein (marked in light blue) cross-links were detected on the recombinant complex (for a graphical representation of the cross-link network see Figure 1C).

https://doi.org/10.7554/eLife.42879.014

Table S4. Inter- and intra-protein cross-links detected on *in vitro* reconstituted Sli15/Ipl1 interacting with the inner kinetochore proteins Ctf19, Okp1, Ame1 and Mcm21 (COMA). COMA and Sli15/Ipl1 complexes were recombinantly expressed in insect cells and affinity-purified via Ame1-6xFLAG-6xHis, Mcm21-6xFLAG-6xHis, or Sli15-2xStrep, respectively. A nearly stoichiometric supramolecular complex of COMA and Sli15/Ipl1 was generated *in vitro* and chemical cross-links introduced by BS3 were identified as described (see materials and methods). In total, 98 inter-protein (marked in dark blue) and 69 intra-protein (marked in light blue) cross-links were detected on the recombinant complex (for a graphical representation of the cross-link network see Figure 4A).

https://doi.org/10.7554/eLife.42879.015

Table S5. Predicted and experimentally annotated protein domains and motifs depicted in protein cross-link networks.

Native or *in vitro* reconstituted recombinant protein complexes were prepared and cross-linked as described in materials and methods. The identified inter- and intra-protein cross-links are visualized as protein network representations in Figure 1C and Figure 4A and are listed in Tables S3 and S4.

Protein	Domain/Motif	Start	End	Reference
AME1	MIND binding	1	15	(Hornung et al., 2014)
AME1	coiled coil	177	272	MARCOIL prediction
AME1	Okp1 binding	129	247	(Schmitzberger et al., 2017)
AME1	Nkp1-Nkp2 binding	268	292	(Schmitzberger et al., 2017)
CENPA/ CSE4	histone core	113	227	(Zhou et al., 2011)
CENPA/ CSE4	CATD	166	201	(Zhou et al., 2011)
CHL4	IML3 binding	361	458	(Hinshaw and Harrison, 2013)
CTF19	RWD	134	361	Sequence alignment model /Psipred strcuture prediction
H2A	histone core	14	90	(Wang et al., 2013)
H2B	histone core	34	105	(Wang et al., 2013)
H3	histone core	63	132	(Wang et al., 2013)
H4	histone core	24	96	(Wang et al., 2013)
IML3	dimerization	169	198	(Hinshaw and Harrison, 2013)
IPL1	kinase domain	104	355	Sequence alignment model
MCM21	RWD	156	368	Sequence alignment model /Psipred strcuture prediction
MIF2	MTW1C binding	1	35	(Hornung et al., 2014)
MIF2	signature motif	238	312	(Hornung et al., 2014)
MIF2	IML3/CHL4 binding	256	549	(Hinshaw and Harrison, 2013)
MIF2	cupin fold	439	526	(Hornung et al., 2014)
OKP1	core domain	166	211	(Schmitzberger et al., 2017)
OKP1	coiled coil	183	290	MARCOIL prediction
OKP1	Ame1 binding	234	264	(Schmitzberger et al., 2017)
OKP1	Ctf19-Mcm21 binding „segment1“	321	329	(Schmitzberger et al., 2017)
OKP1	coiled coil	346	381	MARCOIL prediction
OKP1	Nkp1-Nkp2	357	375	(Schmitzberger et al., 2017)
SLI15	CEN targeting	1	227	(Campbell and Desai, 2013)
SLI15	MT binding	229	565	(Fink et al., 2017)
SLI15	SAH	517	565	(Fink et al., 2017)
SLI15	IPL1 binding IN-box	630	681	(Adams et al., 2000, Kang et al., 2001)

References

ADAMS, R. R., WHEATLEY, S. P., GOULDSWORTHY, A. M., KANDELS-LEWIS, S. E., CARMENA, M., SMYTHE, C., GERLOFF, D. L. & EARNSHAW, W. C. 2000. INCENP binds the Aurora-related kinase AIRK2 and is required to target it to chromosomes, the central spindle and cleavage furrow. *Curr Biol,* 10**,** 1075-8.

CAMPBELL, C. S. & DESAI, A. 2013. Tension sensing by Aurora B kinase is independent of survivin-based centromere localization. *Nature,* 497**,** 118-21.

COX, J. & MANN, M. 2008. MaxQuant enables high peptide identification rates, individualized p.p.b.-range mass accuracies and proteome-wide protein quantification. *Nat Biotechnol,* 26**,** 1367-72.

DROZDETSKIY, A., COLE, C., PROCTER, J. & BARTON, G. J. 2015. JPred4: a protein secondary structure prediction server. *Nucleic Acids Res,* 43**,** W389-94.

FINK, S., TURNBULL, K., DESAI, A. & CAMPBELL, C. S. 2017. An engineered minimal chromosomal passenger complex reveals a role for INCENP/Sli15 spindle association in chromosome biorientation. *J Cell Biol,* 216**,** 911-923.

HINSHAW, S. M. & HARRISON, S. C. 2013. An Iml3-Chl4 heterodimer links the core centromere to factors required for accurate chromosome segregation. *Cell Rep,* 5**,** 29-36.

HORNUNG, P., TROC, P., MALVEZZI, F., MAIER, M., DEMIANOVA, Z., ZIMNIAK, T., LITOS, G., LAMPERT, F., SCHLEIFFER, A., BRUNNER, M., MECHTLER, K., HERZOG, F., MARLOVITS, T. C. & WESTERMANN, S. 2014. A cooperative mechanism drives budding yeast kinetochore assembly downstream of CENP-A. *J Cell Biol,* 206**,** 509-24.

KANG, J., CHEESEMAN, I. M., KALLSTROM, G., VELMURUGAN, S., BARNES, G. & CHAN, C. S. 2001. Functional cooperation of Dam1, Ipl1, and the inner centromere protein (INCENP)-related protein Sli15 during chromosome segregation. *J Cell Biol,* 155**,** 763-74.

SCHMITZBERGER, F., RICHTER, M. M., GORDIYENKO, Y., ROBINSON, C. V., DADLEZ, M. & WESTERMANN, S. 2017. Molecular basis for inner kinetochore configuration through RWD domain-peptide interactions. *EMBO J*.

WANG, F., LI, G., ALTAF, M., LU, C., CURRIE, M. A., JOHNSON, A. & MOAZED, D. 2013. Heterochromatin protein Sir3 induces contacts between the amino terminus of histone H4 and nucleosomal DNA. *Proc Natl Acad Sci U S A,* 110**,** 8495-500.

ZHOU, Z., FENG, H., ZHOU, B. R., GHIRLANDO, R., HU, K., ZWOLAK, A., MILLER JENKINS, L. M., XIAO, H., TJANDRA, N., WU, C. & BAI, Y. 2011. Structural basis for recognition of centromere histone variant CenH3 by the chaperone Scm3. *Nature,* 472**,** 234-7.

SPENCER, F., GERRING, S. L., CONNELLY, C. & HIETER, P. 1990. Mitotic chromosome transmission fidelity mutants in Saccharomyces cerevisiae. *Genetics,* 124**,** 237-49.

3.2 Ndc10 recruits the outer kinetochore MTW1 complex through its N terminus in mitosis

Potocnjak M, Singh S, Speljko T, Kumar CN, Brandstetter K, Harz H, Leonhardt H, Herzog F. Ndc10 recruits the outer kinetochore MTW1 complex through its N terminus in mitosis. Manuscript in preparation.

Budding yeast Ndc10 recruits the outer kinetochore MTW1 complex through its N-terminus in mitosis

Mia Potocnjak[1], Sylvia Singh[1], Tea Speljko[1], Chandni Natalia Kumar[1], Katharina Brandstetter[2], Hartmann Harz[2], Heinrich Leonhardt[2] & Franz Herzog[1†]

[1]Gene Center Munich and Department of Biochemistry, Ludwig-Maximilians-Universität München, Feodor-Lynen-Str. 25, 81377 Munich, Germany

[2]Department of Biology II, Ludwig-Maximilians-Universität München, Butenandtstr. 1, 81377 Munich, Germany

[†]Correspondence should be addressed to FH (herzog@genzentrum.lmu.de)

ABSTRACT

Kinetochores are macromolecular protein assemblies at centromeric chromatin that mediate the accurate segregation of chromosomes during cell division. Kinetochores link the centromeric DNA, wrapped around Cse4^{CENP-A} containing nucleosomes, to spindle microtubules. The budding yeast CBF3 complex binds to a specific centromere defining DNA element and is essential for kinetochore assembly in budding yeast. Here, we show that the Ndc10 subunit of the CBF3 complex recruits the outer kinetochore in mitosis through direct interaction of its N-terminus with the MTW1 complex. The Ndc10 interaction site at the Mtw1 head domain is close to residues that mediate the binding of Mif2 and Ame1. Our findings indicate that the Ndc10 interaction is strongly enhanced upon Ipl1$^{Aurora-B}$ phosphorylation of Dsn1 *in vitro,* which is consistent with co-purification of the MTW1 complex and Ndc10 selectively from mitotic cells. Moreover, MTW1 complex binding by Ndc10 was found to be important once recruitment through Mif2 is impaired. Our results suggest that Ndc10 represents a third pathway of the point centromere kinetochore architecture that directly links the centromeric nucleosome to a single microtubule.

INTRODUCTION

The kinetochore is a multi-protein structure that mediates the interaction between eukaryotic chromosomes and spindle microtubules enabling accurate distribution of the genetic material during cell division. Kinetochores assemble on a chromosomal locus of specialised chromatin called the centromere. The point centromere of budding yeasts represents the minimal system required for faithful segregation of sister chromatids linking only a single $Cse4^{CENP-A}$ containing nucleosome to a single microtubule. In contrast, the human regional centromere contains about 100 CENP-A containing nucleosomes linking roughly 30-40 spindle microtubules (Pluta et al. 1995, Clarke and Baum 1990, Fitzgerald-Hayes, Clarke and Carbon 1982, Willard 1990).

The *S. cerevisiae* centromere is defined by a conserved ~125 bp long centromeric DNA segment (CEN) that consists of three distinct centromere defining elements (CDE), the 8 bp long CDEI, the 78-86 bp AT rich CDEII and the 25 bp CDEIII sequence (Hegemann and Fleig 1993). CDEII wraps the $Cse4^{CENP-A}$ containing nucleosome, flanked by the CDEI bound Cbf1 protein and the CDEIII bound CBF3 complex (CBF3C) (Mellor et al. 1991, Goh and Kilmartin 1993, Lechner and Carbon 1991). All kinetochore proteins apart from Cbf1 require the CBF3C for their recruitment. CBF3C consists of the four subunit CBF3 core complex which refers to Skp1:Ctf13:(Cep3)2 subassembly and Ndc10 homodimer (Doheny et al. 1993, Goh and Kilmartin 1993, Russell et al. 1999, Strunnikov et al. 1995, Jiang et al. 1993, Yan et al. 2019, Leber et al. 2018). The function of Skp1 and Ctf13 in the kinetochore context has not been clarified, but they appear to have a regulatory function within the CBF3c (Lingelbach and Kaplan 2004, Rodrigo-Brenni et al. 2004, Russell et al. 1999). Skp1 promotes Ctf13 phosphorylation, as demonstrated in insect cells, and activates CBF3c to bind CEN DNA *in vitro* (Kaplan et al. 1997). Assembly of the CBF3 complex is highly regulated by posttranslational modifications (Stemmann and Lechner 1996, Kaplan et al. 1997, Kitagawa et al. 1999). Cep3 and Ndc10 components, along with Ctf13 directly interact with DNA (Yan et al. 2018). The Cep3 homodimer has an N-terminal Gal4-like zinc cluster domain that displays specificity for CCG triplets in the CDEIII region of centromeric DNA (Bellizzi et al. 2007, Purvis and Singleton 2008). Furthermore, it contains an αMN helix that binds a conserved TGT motif essential for CBF3 binding (Russell et al. 1999). CEN DNA specificity of the CBF3c relies solely on the Cep3 protein as Ndc10 and Ctf13 also bind non-centromeric DNA, however they might increase overall

affinity of the CBF3c for CEN DNA binding (Perriches and Singleton 2012). Ndc10 also associates with the centromeric histone chaperone Scm3^{HJURP} responsible for Cse4 deposition (Camahort et al. 2007). Ndc10 was initially described as a part of the CBF3 complex and the molecular details of this interaction as well as its interaction with the DNA are thoroughly investigated (Cho and Harrison 2011, Lee et al. 2019, Zhang et al. 2019, Yan et al. 2018). However, it was shown that Ndc10 also displays functions not related directly to the centromere such as interaction with the chromosomal passenger complex through Bir1^{Survivin} (Bouck and Bloom 2005, Yoon and Carbon 1999).

Cse4^{CENP-A} containing nucleosomes specifically recruit inner kinetochore members of the constitutive centromere associated network (CCAN) or CTF19 complex (CTF19c) in budding yeast (Hori et al. 2008, Foltz et al. 2006). This creates a hub for the recruitment of the outer kinetochore responsible for microtubule binding (Cheeseman et al. 2006, Cheeseman and Desai 2008). The inner kinetochore proteins Mif2^{CENP-C} and Ame1/Okp1 are the only known link between the Cse4 nucleosome and the outer kinetochore KMN complex comprised of the SPC105^{KNL1}, MTW1c^{MIS12} and NDC80c^{NDC80} complexes (Anedchenko et al. 2019, Fischbock-Halwachs et al. 2019, Westermann et al. 2003, Killinger et al. 2020, Dimitrova et al. 2016, Przewloka et al. 2011). The Mif2 and Ame1 N-terminal motifs directly interact with the Mtw1/Nnf1 heterodimer of the four subunit MTW1 complex (Mtw1/Dsn1/Nsl1/Nnf1). This interaction is enhanced through Ip1$^{Aurora-B}$ phosphorylation of Dsn1 on amino acids S240 and S250 which in turn releases the interaction of Dsn1/Nnf1 (head II) to Mtw1/Nnf1 (head I). This results in the exposure of a head I binding site that can further be occupied by Mif2 or Ame1 (Dimitrova et al. 2016, Akiyoshi et al. 2013a). Mif2 and Ame1/Okp1 are the only essential components of the CTF19c. Interestingly the Mif2 interaction with MTW1c is not essential, while the deletion of the N-terminal Mtw1 binding motif of Ame1 (Ame1Δ2-14) results in a lethal phenotype (Hornung et al. 2014).

Here we show that in budding yeast Ndc10 protein, besides Mif2 and Ame1/Okp1, establishes a third direct link to the outer kinetochore MTW1 complex during mitosis. The CBF3c subunit Ndc10 displays a stable interaction with the MTW1c. With its N-terminal region Ndc10 contacts head I of the Mtw1/Nnf1 heterodimer in an Ipl1$^{Aurora-B}$ phosphorylation dependent manner. Using biochemical and cell viability assays, we demonstrate that Ndc10 N-terminal mutants are impaired in Mtw1 interaction and display benomyl and temperature hypersensitivity. Importantly binding of Mtw1 by Ndc10 becomes crucial if the Mif2 pathway is impaired.

Furthermore, we demonstrate that the interaction profile differs throughout the cell cycle peaking in early mitosis. We also characterize the binding interdependencies between the three links Ndc10, Mif2 and Ame1/Okp1 pinpointing the interaction site and phosphorylation conditions between Ndc10 and Mif2 proteins.

How the budding yeast point centromere, attaching a single Cse4 nucleosome to only a single microtubule, supports the tension during chromosome segregation is not yet understood. As opposed to the human kinetochore, the budding yeast kinetochore is assembled throughout the cell cycle and maintains attachment with the microtubule (Biggins 2013, Hara and Fukagawa 2020). Our findings show important contacts within the budding yeast kinetochore offering insights into the assembly of the kinetochore backbone as well as the higher order kinetochore organization.

RESULTS

Cell cycle dependent binding of Ndc10 and Mtw1

To identify kinetochore components associated with the CBF3 complex, we employed native Ndc10-6xHis-6xFlag pull-downs from G1 or G2/M arrested *S. cerevisiae* cells using alpha factor or galactose induced overexpression of Mps1, respectively. Under both conditions, besides CBF3 complex and histone protein subunits, the Mtw1/Nnf1 heterodimer co-precipitated as the most prominent interactor (Figure 1A). Strikingly, in pull-down samples from cells arrested in G2/M phase, Ndc10 co-precipitated 4x more Mtw1/Nnf1 than in pull-downs from cells arrested in G1 phase, whereas similar levels of CBF3complex components were recovered in both conditions (**Figure 1A**). This indicates that the Ndc10 – Mtw1 interaction is cell cycle dependent and occurs in mitosis.

Connectivity of the inner kinetochore receptors and MTW1c

Using crosslinking mass spectrometry on a preassembled $Ndc10^{1-551}$, Mif2, Ame1/Okp1 and MTW1c complex we aimed to determine the interaction sites between Ndc10 and the MTW1c in the presence of the two known Mtw1 receptors Ame1 and Mif2 (**Figure 1B**). The crosslinks between $Ndc10^{1-551}$ and Mtw1/Nnf1 predominantly emanate from their N-terminal domains and are mainly formed between Ndc10 and Mtw1, whereas only one crosslink connects $Ndc10^{1-551}$ and Nnf1. Furthermore, we also found two crosslinks between $Ndc10^{1-551}$ and Mif2.

$Ndc10^{1-551}$, Mif2, Ame1/Okp1 and MTW1c were able to form a stable complex without obvious competition between the subcomplexes, as demonstrated by size-exclusion chromatography (SEC) (**Figure S1**).

The CBF3 complex subunit Ndc10 binds the outer kinetochore MTW1 complex and the binding is enhanced by $Dsn1^{S240/S250}$ phosphorylation

In order to confirm and further investigate the observed interaction between Ndc10 and the MTW1c, *in vitro* purified MTW1c and the N-terminal domain of $Ndc10^{1-551}$ were analysed using analytical SEC. Combining MTW1c and $Ndc10^{1-551}$ in a 1:1 molar ratio and subsequent SEC analysis resulted in a larger shift in the SEC chromatogram, compared to the elution profiles of the single proteins, indicating a stable association (**Figure 1C**).

The MTW1c exhibits an extended Y shaped structure formed by the Dsn1/Nsl1 and Mtw1/Nnf1 heterodimers, where the N-terminal globular modules remain accessible for interactions. As previously reported, the inner kinetochore proteins Ame1 and Mif2 (Dimitrova et al. 2016, Hornung et al. 2011) create a direct link between the centromeric nucleosome and the Mtw1c by interacting with its N-terminus. Upon phosphorylation of Dsn1 on S240 and S250 by Ipl1 kinase, the N-terminal modules of the Mtw1C are driven apart allowing for a stronger binding of Ame1 and Mif2. Accordingly, we investigated whether Ndc10 binding is enhanced in a similar manner. We performed *in vitro* binding assays using immobilised, dephosphorylated wildtype Mtw1C or phosphomimic $Mtw1C^{S240D/S250D}$ complexes as bait and incubated with Mif2, Ame1/Okp1 or $Ndc10^{1-551}$, respectively (**Figure 1D**). We observed a 4-fold increase in Ndc10 binding to phosphomimic $MTW1C^{S240D/S250D}$ compared to the wildtype complex (**Figure 1E**). No obvious increase in binding affinity for Mif2 or Ame1/Okp1 was observed in all four independently set up replicates.

Ndc10 binds the Mtw1/Nnf1 head I domain and its binding mode differs from that of Ame1 and Mif2

This finding led us to investigate whether Ndc10 binds in the same region of the Mtw1/Nnf1 head I domain as Ame1 and Mif2 (Hornung et al. 2011, Dimitrova et al. 2016). We separately expressed Dsn1/Nsl1 and Mtw1/Nnf1 as stable heterodimers and carried out *in vitro* binding assays with $Ndc10^{1-551}$. Consistent with our *in vivo* pull-down and crosslinking results, Ndc10 demonstrated selective interaction with the Mtw1/Nnf1 heterodimer (**Figure 2A**).

Furthermore, we narrowed down the interaction site to aa 25-90 on the Mtw1 protein which is the same helix-loop-helix region involved in Ame1 and Mif2 interaction (**Figure 2B, F**). Pairwise point mutations to alanine in this region (V24/I27, I28/V31, N32/Y36, E73/D77, D81/E84, L85/L88) as well as deletion of the loop region (aa 41-69) did not abrogate Ndc10 binding (**Figure S2A, Figure 2F).** In contrast, deletion of the same loop (aa 41-69) led to the complete loss of Mif2 and Ame1/Okp1 binding, despite no reported immediate contacts with the Mtw1 protein in this region (**Figure S2B**).

Next, to find out whether Mtw1 helix 1 (aa 24-40), helix 2 (aa 70-90), or both helices of the helix-loop-helix region are involved in Ndc10 binding, we performed binding assays with the corresponding Mtw1 helix peptides (**Figure 2F**). $Ndc10^{1-551}$ preferably binds helix 1, while the overall binding is enhanced in the presence of both helices (**Figure 2C, D and E**). Although all of the Mtw1 binding sites were available for interaction, no binding to Mif2 or Ame1/Okp1 was detected, even with both helices combined (**Figure 2E**). However, the lack of binding might be attributed to the fact that Nnf1 binding sites are missing (Dimitrova et al. 2016). The finding that $Ndc10^{1-551}$ preferably binds helix 1 and does not require Nnf1 for binding, suggests, that the Ndc10-Mtw1 binding mechanism is more robust and presumably less affected by small perturbations.

In addition, in order to confirm the differential binding mechanism, we also created a set of mutants ($Mtw1^{N32A/Y36A}$, $Mtw1^{N32A/Y36A/E73A/D77A}$, $Mtw1^{D25A/D81A/E84A}$) known to disrupt the interaction with Mif2 or Ame1/Okp1 (Dimitrova et al. 2016, Killinger et al. 2020) and tested their effect on Ndc10 binding. All of the mutants abrogated the binding to Mif2 and Ame1/Okp1, however did not perturb Ndc10 binding which further corroborates that the Ndc10 binding mode is different from that of Mif2 or Ame1/Okp1 (**Figure 2F and 2G**).

The N-terminus of Ndc10 is required for MTW1 complex binding

Based on previous findings that the N-termini of Ame1 and Mif2 interact with the Mtw1/Nnf1 head I domain (Hornung et al. 2011, Dimitrova et al. 2016), we designed $Ndc10^{1-551}$ N-terminal deletion mutants, as well as mutants of conserved sites based on a multiple sequence alignment of interrelated yeast species (**Figure 3A**). Deletion of the first 11, 36 or 63 amino acids (Ndc10Δ11, -Δ36, -Δ63), led to the loss of Mtw1/Nnf1 binding (**Figure 3B**). However, to evaluate the importance of this interaction and ensure that only the Ndc10-Mtw1 interaction was affected, we tested Ndc10 point mutations in the most conserved region (Y52A, I53A,

Q54Aand W55A) in an *in vitro* binding assay, and found that Ndc10$^{1-551}$-Y52A was sufficient to abrogate the interaction with Mtw1/Nnf1 (Figure 3C).

In order to evaluate this finding *in vivo*, we used the anchor-away technique, where the endogenous Ndc10-FRB protein is anchored away from the nucleus upon addition of rapamycin, and tested whether the lethal phenotype is rescued by ectopic expression of the Ndc10 wild-type or mutant proteins, respectively. All the mutants were able to rescue the lethal phenotype at 30 °C, however Ndc10-Y52A showed benomyl sensitivity and a lethal phenotype at 37 °C, indicating a chromosome segregation defect (Figure 3D). To test whether kinetochore localisation is affected, we carried out live cell imaging of wild-type Ndc10-GFP and the two mutants that displayed a temperature sensitive phenotype (Ndc10-Y52A-GFP and Ndc10-W55A-GFP). After overnight treatment with rapamycin both mutants displayed proper kinetochore localization which was indistinguishable from that of wild-type Ndc10-GFP (Figure 3E).

MTW1c binding by Ndc10 becomes essential when the Mif2 pathway is impaired

It is plausible that the mutation of only one amino acid is not sufficient to completely abrogate the interaction *in vivo*. Ndc10-Y52A is not the only interaction site between Ndc10$^{1-551}$ and Mtw1, since Ndc10-Δ11 also led to a loss of interaction. We therefore tested the impact of Ndc10-Δ11 as well as Ndc10-Δ11-Y52A on cell viability, yet, both mutants had no further impact on the phenotype observed with the Ndc10-Y52A point mutant (Figure S3A). As the minimal mutation of Ndc10 displays a similar growth phenotype as Mif2-Δ35 ('ΔNT') (Hornung et al. 2014) we conclude that, similar to Mif2, Ndc10 plays a functionally less important role than Ame1. Since Mif2 and Ndc10 are equally redundant, we next asked whether disrupting the Mif2 and Ndc10 pathways conferred a synthetic effect. Indeed, expression of Ndc10-Y52A and Ndc10-Δ11-Y52A in a Mif2-Δ35 background resulted in severely impaired growth or lethality, although protein levels similar to wild-type levels were detected by western blot analysis (Figure 3F and 3G). Taken together we conclude that the Ndc10 and Mif2 pathways become essential once either of them is compromised.

Mif2 binds Ndc10$^{1-551}$ in a phosphorylation dependent manner

Further, we investigated binding dependencies between Mif2, Ame1/Okp1 and Ndc10$^{1-551}$ within the inner kinetochore. Since Mif2 formed a stable complex with Ndc10$^{1-551}$ in *in vitro*

binding assays, we tested Mif2 mutants carrying either a deletion between the Mtw1 binding N-terminus and the CENP-C motif, responsible for Cse4 binding (Mif2Δ35-237), or a smaller and a larger deletion of the CENP-C motif alone (Mif2Δ238-312 and Mif2 Δ238-370), to pinpoint the binding site on Mif2. Only the deletion of aa 35-237 led to a loss of binding, suggesting that the CENP-C motif is not involved (Figure 4B and 4C).

We found that insect cell-purified Mif2 binds $Ndc10^{1-551}$, however upon dephosphorylation with λ phosphatase the binding was lost, indicating that Mif2 - $Ndc10^{1-551}$ binding is phosphorylation-dependent. Re-phosphorylation by known kinetochore kinases Sli15/$Ipl1^{Aurora\ B}$, $Cdc5^{PLK1}$ and $Cdc28^{CDK1}$ restored binding upon $Cdc5^{PLK1}$ phosphorylation which was even further enhanced in combination with $Cdc28^{CDK1}$ phosphorylation. In contrast, Sli15/$Ipl1^{Aurora\ B}$ kinase did not have any effect on the Mif2 - $Ndc10^{1-551}$ binding (Figure 4D and 4E). To delimit the binding site on Mif2, we created a series of deletion and phospho-ablative mutants by converting serines or threonines to alanines. Testing this mutant panel in *in vitro* binding assays with Ndc10, we were able to narrow down the binding interface to Mif2 amino acids 221-240, a serine-rich region containing 8 phosphorylation sites (Figure 4A, 4F and 4G). We conclude that Mif2 binds $Ndc10^{1-551}$ in the region of aa 221-240 in a phosphorylation dependent manner. Moreover, we did not find any evidence that the N-terminal domain of Ndc10 interacts with Ame1/Okp1 using SEC experiments (Figure S4).

The Ndc10 N-terminus interacts with Mif2

Probing our $Ndc10^{1-551}$ mutant panel, we found, that the minimal deletion of the first 11 amino acids (Ndc10-Δ11) already abrogated Mif2 binding (Figure 5A). Along the same lines, Mif2 binding was also impaired with Ndc10-Y52A and Ndc10-W55A. We could also observe that Mif2 occupies a wider region on Ndc10 than Mtw1. Specifically, whereas only the Ndc10-Y52A/W55A double mutant was able to abrogate Mtw1 and Mif2 binding, mutation of Y45A/Y48A and L132A/L135A affected only Mif2 binding (Figure S5A and S5B). Overlapping Ndc10 sites for Mif2 and Mtw1 suggests a certain hierarchy of Ndc10 binding, or competition between Mtw1 and Mif2. To discern between the two possibilities, we took advantage of the Mif2-Δ170 mutant lacking the Mtw1-, but preserving the Ndc10-binding site. Incubation of Mtw1/Nnf1 with $Ndc10^{1-551}$ and either wild-type Mif2 or the Mif2-Δ170 version resulted in alterations in Ndc10 binding. Mif2-Δ170 was able to compete off Ndc10 from Mtw1/Nnf1 resulting in an almost 50% reduction of Mtw1/Nnf1-bound Ndc10 (Figure 5C and 5D).

As we could show that in G2/M phase Mtw1/Nnf1 copurification with Ndc10 is enhanced and we did not find enrichment of Mif2 (**Figure 1A**), suggests that Mif2 does not bind Ndc10 during mitosis leaving Ndc10 available for recruitment of the KMN network. We found that Mif2 binding of Chl4/Iml3 reduced Ndc10 levels bound by Mif2. This apart from phosphorylation could be one way of regulating the hierarchy and orderly binding of the budding yeast kinetochore (**Figure 5E and 5F**).

DISCUSSION

Using biochemical and genetic approaches we have discovered a new link required for the proper function of the budding yeast kinetochore. The budding yeast kinetochore with its point centromere represents a minimal structure required for chromosome segregation. Assembly of the entire kinetochore occurs on a single Cse4^{CENP-A} nucleosome and provides the connection to a single microtubule, sufficient for accurate separation of the genetic material. In human cells equal distribution of the genetic material occurs through regional centromeres, where kinetochores assemble on ~100 CENP-A nucleosomes and link 30-40 microtubules. A substantial tension created through the pulling forces of the depolymerizing microtubules in anaphase must be supported by the kinetochore architecture. The minimal structure of the budding yeast point centromere might be required to sustain even more tension which is exerted by a single microtubule. The critical and only essential inner kinetochore subunits that support this assembly are the Cse4 nucleosome binding Mif2^{CENP-C} and Ame1/Okp1 proteins responsible for recruitment of the KMN network. The N-termini of Mif2 and Ame1 create specific recruitment sites for the MTW1C which is tethered via the Mtw1 helix-loop-helix region in the Mtw1/Nnf1 head I domain (Hornung et al. 2014, Dimitrova et al. 2016). This interaction is regulated and augmented by Ipl1$^{Aurora-B}$ activity on MTW1C, where Mif2 binding depends on Dsn1$^{S240/S250}$ phosphorylation, while the Ame1 interaction is only minorly strengthened (Hamilton et al. 2020).

We have now identified a yet unknown function of the Ndc10 protein, a member of the centromere binding CBF3 complex, by providing another recruitment site for the Mtw1c. We used biochemical assays to study the differences and similarities between the two known MTW1c receptors Mif2 and Ame1 and the Ndc10 protein. MTW1c binding by Ndc10 is

mediated by a binding mechanism comparable to that of Mif2 and Ame1, and which is also strengthened upon Dsn1 phosphorylation. This finding implicated the same helix-loop-helix region as MTW1c binding domain which we were able to show. However, distinct Mif2 and Ame1 binding sites in this domain are sensitive to any perturbation in this region, even if the amino acids required for the binding are preserved (Dimitrova et al. 2016). Incubation with helix 1 (aa 24-40) and helix 2 (aa70-90) peptides, or deletion of the loop region (aa 41-69), which was considered not to be relevant for the binding, did not support the association. This indicates, that besides the annotated Mif2 and Ame1 contact sites the distance between the two helices also has a role in proper Mif2 and Ame1 binding. Conversely, the Ndc10 interaction remained unaffected by such perturbations, most likely because the Ndc10 binding site resides predominantly on helix 1.

The binding site of Mtw1c on Ndc10 also lies in the very N-terminus as is the case for Mif2 and Ame1. We were able to pinpoint several sites responsible for the binding which allowed us to assess the relevance of this interaction *in vivo*. Expression of Ndc10 point or deletion mutants in yeast after anchoring-away endogenous Ndc10 - apart from benomyl or temperature sensitivity - had no major effect on yeast cell growth. A similar mild phenotype was observed for the Mif2-ΔNT mutant while expression of Ame1-ΔN caused lethality (Hornung et al. 2014). However, the simultaneous disruption of both redundant pathways (Ndc10 and Mif2) led to severe growth defects or even synthetic lethality. Based on this finding we speculate that although the Ame1 pathway is essential, the cell does not solely rely on this interaction. Hence, the Ndc10 and Mif2 pathways become vital once one of them is impaired (Figure 6G).

As previously reported, Mif2 and Ame1/Okp1 form a stable complex *in vitro* (Hornung et al. 2014) thus, we aimed to further elucidate the binding interdependencies of the three Mtw1 receptors. We did not find convincing evidence of $Ndc10^{1-551}$ binding to Ame1/Okp1, but we cannot exclude that they could form a complex under different conditions. However, $Ndc10^{1-551}$ associated with Mif2 into a stable complex and we mapped the binding domain to the region between the Mtw1 binding N-terminus and the Cse4 binding CENP-C motif. Moreover, the interaction seems to be regulated by phosphorylation. As the budding yeast kinetochore remains assembled during the cell cycle (Biggins 2013, Hara and Fukagawa 2020), additional factors such as cell cycle kinases might be responsible for the timely regulation of kinetochore function. When Mif2 is phosphorylated it interacts with the same, albeit slightly larger, N-terminal domain of Ndc10 as Mtw1, raising the question whether there is a competition in

binding. The Mif2-Δ170 mutant, lacking the Mtw1C binding domain, binds Ndc10, but impairs association of Ndc10 and Mtw1. This might be especially important in recruitment of the inner kinetochore proteins to the Cse4 nucleosome, preventing premature recruitment of the KMN network. Using immunoprecipitation and mass spectrometry from synchronized yeast cells we were able to show that Ndc10 binds Mtw1c in a cell cycle-dependent manner with a 4x increase in enrichment of Mtw1/Nnf1 in mitosis. We therefore speculate that Ndc10 and Mif2 association is required, but not crucial in the initial step of kinetochore assembly. Subsequent binding of additional factors to Mif2, such as Chl4/Iml3, could release the binding of Ndc10, which then becomes available to interact with the Mtw1c in mitosis. Our research raises new questions about the complex kinetochore binding hierarchy and its posttranslational regulation and can provide a stepping stone for exciting experiments in the future.

MATERIALS AND METHODS

Plasmid construction

Respective DNA was amplified from yeast genomic DNA using Phusion High Fidelity DNA Polymerase or Q5® High-Fidelity DNA Polymerase (New England Biolabs). $Ndc10^{1-551}$ was amplified from yeast genomic DNA and cloned into pet28 a (+) vector (Addgene), using *Nde*I and *Bam*HI sites, in frame with an N-terminal 6xHis tag and a Thrombin cleavage site. The individual mutants were generated using the Q5 site-directed mutagenesis kit based on the recommended protocol (New England Biolabs). 1xStrep-Clb2 was cloned into pet28 a (+) vector (Addgene) using the Gibson assembly method.

For insect cell expression, open reading frames of *Mif2-6xHis-6xFlag*, *MTW1c* (*Dsn1-6xHis-2xStrep*, *Mtw1*, *Nnf1*, and *Nsl1*), *6xHis-Cdc5*, *Cdc28*, *Cks1* and *Sli15-2xStrep-1xHA-6xHis* and *Ipl1* were amplified from yeast genomic DNA and cloned into the pLIB or pBIG1 vectors according to the biGBac system (Weissmann et al. 2016). The constructs for insect cell expression were transformed into DH10Bac *E. coli* cells (ThermoFisher Scientific) for Bacmid generation. Viruses were generated and amplified in Sf21 cells (ThermoFisher Scientific) and the proteins were expressed in High Five cells (ThermoFisher Scientific). All plasmids used in this study are listed in Table S1.

Expression and purification of proteins from *E. coli* cells

Ame1-6xHis-Okp1, Mtw1/Nnf1-6xHis, 1xStrep-Mtw1/Nnf1-6xHis, 6xHis-thrombin-Ndc10 constructs and the corresponding mutants (Table S1) were expressed *in E. coli* Rosetta 2 cells (Merck). Cells were grown at 37 ˚C until OD600 0.6 followed by induction with 0.5 mM IPTG at 18 ˚C, overnight. Cells were harvested by centrifugation for 10 min, 3500 x g, at 4 °C.

Ame1-6xHis/Okp1 protein expression and purification from *E. coli* was performed as described previously (Hornung et al. 2011).

Chl4/Iml3 protein expression and purification was performed as described (Fischbock-Halwachs et al. 2019).

Mtw1/Nnf1-6xHis, 1xStrep-Mtw1/Nnf1-6xHis and 6xHis-thrombin-Ndc10 were lysed in lysis buffer (50 mM HEPES pH 7.5, 300 mM NaCl, 3% glycerol, 1 mM $MgCl_2$, 0.01% Tween20, cOmplete ULTRA EDTA-free Protease Inhibitor Cocktail (Roche)) using an M110L Microfluidizer (Microfluidics). Cell lysates were treated with 25 U/ml benzonase (Merck), prior to centrifugation at 48000 x g for 25 min at 4 °C. Mtw1/Nnf1-6xHis and 6xHis-thrombin-Ndc10 were bound to Ni-NTA agarose (Qiagen) for 1 h at 4 °C, washed in wash buffer (50 mM HEPES pH 7.5, 400 mM NaCl, 30 mM imidazole, 3% glycerol, 0.01% Tween20) and eluted in 50 mM HEPES pH 7.5, 150 mM NaCl, 250 mM imidazole, 5% glycerol.

1xStrep-Mtw1/Nnf1-6xHis was bound to Strep-Tactin Superflow agarose (Qiagen) for 1 h at 4 °C washed with a buffer containing 50 mM HEPES pH 7.5, 400 mM NaCl, 3% glycerol, 0.01% Tween20 and eluted in 50 mM HEPES pH 7.5, 150 mM NaCl, 8 mM biotin, 5% glycerol. All proteins were buffer exchanged into a buffer containing 50 mM HEPES pH 7.5, 120 mM NaCl, 10% glycerol using a PD10 desalting column (GE Healthcare)

Expression and purification of proteins from insect cells

Mif2-6xHis-6xFlag, MTW1c (Dsn1-6xHis-2xStrep/Mtw1/Nnf1/Nsl1), 6xHis-Cdc5, Sli15-2xStrep-1xHA-6xHis/Ipl1 and the corresponding mutants thereof (Table S1) were expressed in High Five insect cell suspension culture (ThermoFisher Scientific) using Express Five medium supplemented with 1% v/v Gibco L-glutamine (ThermoFisher Scientific) and 1% v/v pluronic (Invitrogen). 1 l of $1x10^6$/ml High Five cells was infected with 10 ml of the virus and incubated at 95 rpm, 27.5 °C for three days.

Suspension cell cultures were harvested for 10 min, 1000 x g at 4 °C. Cells were resuspended in lysis buffer (50 mM HEPES pH 7.5, 150 mM NaCl, 3% glycerol, 1mM $MgCl_2$, 0.01% Tween20, cOmplete ULTRA EDTA-free Protease Inhibitor Cocktail (Roche)). Insect cells were lysed by dounce homogenization (Wheaton douncer) with 15 strokes on ice and cell lysates were treated with 25 U/ml benzonase (Merck) prior to centrifugation at 48000 x g, 25 min at 4 °C. Mif2-6xHis-6xFlag or 6xHis-Cdc5 containing cleared lysates were incubated with Ni-NTA agarose (Qiagen) for 1 h at 4 °C, washed with 50 mM HEPES pH 7.5, 400 mM NaCl, 30 mM imidazole, 3% glycerol, 0.01% Tween20 and eluted in 50 mM HEPES pH 7.5, 150 mM NaCl, 250 mM imidazole, 5% glycerol.

For Dsn1-2xStrep/Mtw1/Nsl1/Nnf1, 1xStrep-Mps1 and Sli15-2xStrep-HA-6xHis/Ipl1 purification, the cleared lysates were incubated with Strep-Tactin Superflow agarose (Qiagen) for 1 h at 4 °C washed with 50 mM HEPES pH 7.5, 400 mM NaCl, 3% glycerol, 0.01% Tween20 and eluted in 50 mM HEPES pH 7.5, 150 mM NaCl, 8 mM biotin, 5% glycerol.

Peak elution fractions of all the recombinant proteins were buffer exchanged using a PD10 column (GE Healthcare) in a desalting buffer (50 mM HEPES pH 7.5, 120 mM NaCl, 10% glycerol).

Purification of the $CDC28^{Cdk1}$ complex

For the reconstitution of the Cdc28-Clb2-Cks1 complex, 1xStrep-Clb2 was expressed and purified from *E. coli* followed by incubation with insect cell lysate containing expressed Cdc28 and Cks1. 1xStrep-Clb2 was expressed and harvested as described for the *E. coli* protocol. Cells were lysed by sonication in a buffer containing 50 mM HEPES pH 7.5, 150 mM KCl, 5% glycerol, 0.01% Tween, 1.5 mM $MgCl_2$, 1 mM DTT and complete EDTA-free protease inhibitor (Roche). Cleared lysate was incubated with Strep-Tactin Superflow resin (Qiagen) for 1 h at 4 °C. Beads were washed in a wash buffer containing 50 mM HEPES pH 7.5, 150 mM KCl, 5% glycerol, 1 mM DTT and incubated with the cleared insect cell lysates (expressed and harvested as previously described), containing recombinant Cdc28 and Cks1, for one hour at 4°C. Beads were washed with wash buffer and eluted in elution buffer (50 mM HEPES pH 7.5, 300 mM KCl, 5% glycerol, 1 mM DTT, 10 mM biotin). The eluate was dialyzed in 50 mM HEPES pH 7.5, 150 mM KCl, 10% glycerol) and flash-frozen aliquots were stored at -80 °C.

In vitro binding assays

For binding assays using the Mtw1 complex (Dsn1 wild-type or Dsn1$^{S240D/S250D}$-6xHis-2xStrep/Mtw1/Nsl1/Nnf1) or the 1xStrep-Mtw1/Nnf1-6xHis heterodimer as a bait, the protein complexes, along with the respective wild-type or mutant candidate binding proteins/protein complexes, were mixed in a 1:2 molar ratio and incubated on ice for 30 min. The volumes were adjusted with low salt buffer (30 mM HEPES pH 7.5, 150 mM NaCl, 3% glycerol, 0.01% Tween20). The sample mixture was further immobilised on a Strep-Tactin Superflow resin (Qiagen) for 1 h at 4 °C, 1200 rpm using a thermomixer (Eppendorf) and washed two times with high salt buffer (30 mM HEPES pH 7.5, 300 mM NaCl, 3% glycerol, 0.02% Tween20) and one time with low salt buffer. Samples were eluted in a buffer containing 30 mM HEPES pH 7.5, 150 mM NaCl, 3% glycerol and 8 mM biotin for 20 min at 4 °C and 1200 rpm using a thermomixer (Eppendorf).

Binding assays with Mif2-6xHis-6xFlag and 1xFlag-thrombin-Ndc10$^{1-551}$ were performed in the same manner with two exceptions: 1) the proteins were immobilised on M2 anti-FLAG agarose beads (Sigma-Aldrich) and 2) elution was performed in a buffer containing 30 mM HEPES pH 7.5, 150 mM NaCl, 3% glycerol and 1mg/ml Flag peptide. Proteins were resolved on 4-20% gradient SDS-PAGE gels (Bio-Rad) and visualised by Coomassie staining (Roth). Protein band intensities were quantified using ImageJ and the standard deviation was calculated from 2-4 biological replicates.

Immunoblotting of Mif2-FLAG (Fig 1 D) was performed by separating input or eluate fractions on 10% SDS-PAGE gels. Proteins were transferred to PVDF membrane and Western blot analysis was performed by incubating the membrane for 1 h in a 1:10000 dilution of a mouse monoclonal ANTI-FLAG® M2 primary antibody (Sigma-Aldrich) and using HRP-conjugated rabbit anti-mouse IgG (abcam) as secondary antibody.

Analytical size exclusion chromatography

Analytical SEC experiments were performed on a Superdex 200 Increase 3.2/300 or a Superose 6 Increase 3.2/300 column (GE Healthcare). Proteins were mixed in equimolar ratios and incubated on ice for 1 h prior to injection. Samples were eluted under isocratic conditions at 4 °C in a buffer containing 50 mM HEPES pH 7.5, 180 mM NaCl, 3% glycerol. Elution of proteins

was monitored by absorbance at 280 nm. 100 µl fractions were collected and analysed by SDS-PAGE and Coomassie staining.

Yeast growth assay

The anchor-away strains (Table S2) were created by endogenously tagging the *Ndc10* locus with the FRB domain in a strain expressing the ribosomal RPL13-FKB12 anchor. The endogenous protein can be anchored away by addition of 1 µg/ml rapamycin to the growth medium. For the rescue experiment wild-type or mutant *Ndc10* coding sequences were cloned into the pRS313 vector along with the corresponding 200 bp promoter region and a C terminal 6xHis--6xFlag tag (Table S1). Point mutations were made using the Q5® Site-Directed Mutagenesis Kit (NEB). The rescue constructs were transformed into a Ndc10-FRB strain and the cell growth was tested by spotting 2.5 µl of five 10-fold serial dilutions starting at OD600 = 0.5 on YPD plates in the presence or absence of rapamycin (1 µg/ml). To test benomyl sensitivity, dilutions were plated on YPD + rapamycin + benomyl (15 µg/ml) plates. Plates were incubated at 30 °C or 37 °C for 2-3 days.

Immunoprecipitation to evaluate Ndc10 expression levels in the anchor-away strains using western blot analysis

Ndc10 anchor-away strains BTS2, BTS5, BSS313 and BSS325 (Table S1) ectopically expressing Ndc10 wild-type and mutant proteins were grown in 50 ml SD(-)His medium at 30 °C to an OD600 of 1-1.5. An equivalent of 50 OD of cells was harvested by centrifugation (5 min, 3140 x g, 4 °C) and the pellet was resuspended in lysis buffer (25 mM HEPES pH 8, 150 mM KCl, 5% glycerol, 2 mM MgCl2, 0.08% NP40, 0.1 mM EDTA, 0.5 mM EGTA and complete EDTA-free protease inhibitor (Roche)) and lysed by intermittent vortexing using 500 µl glass beads (0.5 mm diameter, Microspec). Lysates were cleared at 21000 x g, 4 °C for 30 minutes. The lysate was further incubated with 20 µl of anti-FLAG M2 agarose (Sigma-Aldrich) at 4 °C for one hour. Beads were washed twice with lysis buffer and eluted in the same buffer containing 0.5 mg/ml 3xFLAG peptide. Samples were analysed using 10% SDS-PAGE gels followed by immunoblotting using anti-FLAG M2 (1:5000, Sigma-Aldrich) or anti-Pgk1 (1:10000, Invitrogen) antibodies, and visualized by the HRP-conjugated anti mouse secondary antibody (1:15000, Santa Cruz).

Co-Immunoprecipitation of Ndc10 from yeast cell extracts and mass spectrometric analysis

A yeast strain expressing endogenously tagged Ndc10-6xHis-6xFlag and equipped with galactose inducible 1xmyc-Mps1 (pGAL-1xmyc-Mps1) (Table S2) was used for synchronized (G1- or G2/M-phase) immunoprecipitation experiments. 1 l YPD medium was set to OD600 0.2 and grown at 30 °C, 180 rpm until OD600 0.5. The cells were pelleted and the medium was exchanged with YPD medium and alpha factor (10 mg/l for G1 phase arrest) or with YEP medium + 2% galactose + 2% raffinose (for G2/M phase arrest) and grown for 3.5 h until the cells were uniformly synchronized. Cells were harvested by centrifugation for 10 min at 3500 x g, 4 °C and resuspended in lysis buffer (25 mM HEPES pH 8.0, 150 mM KCl, 2 mM $MgCl_2$, 15% glycerol, 0,1% NP40, 0.1 mM EDTA, 0.5 mM EGTA, 2 mM DTT, cOmplete ULTRA EDTA-free Protease Inhibitor Cocktail (Roche), 1x Halt Phosphatase Inhibitor Cocktail (ThermoFisher Scientific). The cells were lysed using an M110L Microfluidizer (Microfluidics) followed by benzonase (25 U/ml) treatment (Merck) for 30 min on a rotation wheel at 4 °C. The lysate was cleared by centrifugation (48000 x g, 25 min, 4 °C) and protein was bound to M2 anti-FLAG agarose (Sigma-Aldrich) for 2 h on a rotation wheel at 4 °C. The beads were washed in a buffer containing 25 mM HEPES pH 8.0, 150 mM KCl, 15% glycerol, 0.1% NP40 and the protein was eluted in the same buffer with addition of 1 mg/ml 3xFLAG peptide. The eluate was rebound to Ni-NTA agarose (Qiagen) for 30 min at 4 °C in a thermomixer with 1200 rpm shaking. The beads were washed two times in a buffer containing 25 mM HEPES pH 8.0, 150 mM KCl, 15% glycerol. The beads were digested by addition of 2 sample volumes of 8 M urea, reduced with 5 mM TCEP (ThermoFisher Scientific) for 15 min and alkylated with 10 mM iodoacetamide (Sigma-Aldrich) for 30 min. Peptides were released from the beads by sequential digestion with lysyl endopeptidase (1:50 w/w, Wako) for 2 h followed by trypsin treatment at 35 °C overnight, 1200 rpm (1:50 ratio w/w, Promega). The reaction was stopped with 1% (v/v) trifluoroacetic acid and the peptides were purified using C18 cartridges (Sep-Pak, Waters). Samples were analysed by LC-MS/MS using an Orbitrap Elite instrument (Thermo Fisher Scientific). Protein intensities of two biological replicates were obtained using the MaxQuant software (Cox and Mann 2008). Raw IBAQ intensities were normalized to the Ndc10 bait.

Live cell microscopy

For live cell microscopy of Ndc10-GFP, Ndc10-Y52A-GFP or Ndc10-W55A-GFP localization, the Ndc10 anchor-away strain expressing endogenously tagged Okp1-mCherry as kinetochore marker was transformed with the corresponding constructs (pRS313-Ndc10-GFP, pRS313-Ndc10-Y52A or pRS313-Ndc10-W55A-GFP, Table S1). Transformed yeast cells were grown in selective medium (–His/-Trp) in the presence of 1 mg/ml rapamycin at 30 °C until OD600 ~0.5. Cells were immobilized on concanavalin-A (Sigma-Aldrich) coated slides (Ibidi) and imaged in an environmental chamber maintained at 30 °C (Oko Labs). Live cell imaging was carried out on a Nikon TiE microscope equipped with a Yokogawa CSU-W1 spinning disk confocal unit (50 µm pinhole size), an Andor Borealis illumination unit, Andor ALC600 laser beam combiner (405 nm / 488 nm / 561 nm / 640 nm), and Andor IXON 888 Ultra EMCCD camera. The microscope was controlled by software from Nikon (NIS Elements, ver. 5.02.00). Tiled images (5x5 with 5% overlap) were acquired for each condition with a pixel size of 130 nm using a Nikon PlanApo 100x/1.45 NA oil immersion objective and a Perfect Focus System (Nikon). GFP and mCherry were excited for 500 ms using the 488 and 561 nm laser lines, respectively. The emission of GFP and mCherry was captured by using a 525/50 nm and a 600/50 nm filter, respectively. In addition, differential interference contrast (DIC) images were acquired.

Crosslinking mass spectrometry

Recombinant Mif2:Ame1/Okp1:Ndc10:MTW1c$^{Dsn1\ S240/250D}$ complex was crosslinked using a zero-length crosslinker DMTMM (4-(4,6-dimethoxy-1,3,5-triazin-2-yl)-4-methylmorpholinium chloride, Sigma Aldrich) for 6 min at 10 °C and 1200 rpm at a final concentration of 40 mM. The reaction was quenched using a desalting column (ThermoFisher Scientific), followed by addition of ammonium bicarbonate at a final concentration of 100 mM. The crosslinked samples were subjected to tryptic digestion as described in the protocol above. After reversed phase chromatography, peptides were further enriched on a Superdex Peptide PC 3.2/30 column (300×3.2 mm). Collected fractions were analysed by liquid chromatography coupled to tandem mass spectrometry using an LTQ Orbitrap Elite (ThermoFisher Scientific) instrument (Herzog et al. 2012) and the crosslinked peptides were identified using xQuest software (Walzthoeni et al. 2012). The results were filtered with an MS1 tolerance window of −4 to 4 ppm and score ≥ 22 followed by manual validation.

Amino acid sequence alignment

Multiple sequence alignment of Mif2 and Ndc10 protein sequences from interrelated budding yeast species was conducted with Clustal Omega (Sievers et al. 2011). Protein sequences with the highest similarity were determined by protein BLAST and included in the Clustal Omega alignment.

Data availability

The mass spectrometry raw data was uploaded to the PRIDE Archive. The access information is for the recombinant Mif2:Ame1/Okp1:Ndc10:Mtw1C$^{Dsn1\ S240/250D}$ XLMS data: Project accession: PXD022043, Username: reviewer_pxd022043@ebi.ac.uk, and Password: LYn3YmQk.

Acknowledgements

M.P. was funded by the Graduate School (Quantitative Biosciences Munich) of the German Research Foundation (DFG). C.K. und F.H. was supported by the Research Training Center (GRK1721) of th DFG. F.H. was supported European Research Council (ERC-StG no. 638218), the Human Frontier Science Program (RGP0008/2015), by the Bavarian Research Center of Molecular Biosystems and by an LMU excellent junior grant.

Author contributions

M.P. conceived the study, designed and executed the experiments. S.S and T.S performed *in vivo* experiments. C.K. helped with cloning. K.B and H.H. performed microscopy. M.P. and F.H. wrote the manuscript.

Conflict of interest

The authors declare that they have no conflict of interest.

REFERENCES:

Akiyoshi B, Nelson CR, Biggins S (2013) The aurora B kinase promotes inner and outer kinetochore interactions in budding yeast. *Genetics* 194: 785-9

Anedchenko EA, Samel-Pommerencke A, Tran Nguyen TM, Shahnejat-Bushehri S, Popsel J, Lauster D, Herrmann A, Rappsilber J, Cuomo A, Bonaldi T, Ehrenhofer-Murray AE (2019) The kinetochore module Okp1(CENP-Q)/Ame1(CENP-U) is a reader for N-terminal modifications on the centromeric histone Cse4(CENP-A). *The EMBO journal* 38
Bellizzi JJ, 3rd, Sorger PK, Harrison SC (2007) Crystal structure of the yeast inner kinetochore subunit Cep3p. *Structure* 15: 1422-30
Biggins S (2013) The composition, functions, and regulation of the budding yeast kinetochore. *Genetics* 194: 817-46
Bouck DC, Bloom KS (2005) The kinetochore protein Ndc10p is required for spindle stability and cytokinesis in yeast. *Proceedings of the National Academy of Sciences of the United States of America* 102: 5408-13
Camahort R, Li B, Florens L, Swanson SK, Washburn MP, Gerton JL (2007) Scm3 is essential to recruit the histone h3 variant cse4 to centromeres and to maintain a functional kinetochore. *Molecular cell* 26: 853-65
Cheeseman IM, Chappie JS, Wilson-Kubalek EM, Desai A (2006) The conserved KMN network constitutes the core microtubule-binding site of the kinetochore. *Cell* 127: 983-97
Cheeseman IM, Desai A (2008) Molecular architecture of the kinetochore-microtubule interface. *Nat Rev Mol Cell Biol* 9: 33-46
Cho US, Harrison SC (2011) Ndc10 is a platform for inner kinetochore assembly in budding yeast. *Nat Struct Mol Biol* 19: 48-55
Clarke L, Baum MP (1990) Functional analysis of a centromere from fission yeast: a role for centromere-specific repeated DNA sequences. *Mol Cell Biol* 10: 1863-72
Cox, J. & M. Mann (2008) MaxQuant enables high peptide identification rates, individualized p.p.b.-range mass accuracies and proteome-wide protein quantification. Nat Biotechnol, 26, 1367-72.
Dimitrova YN, Jenni S, Valverde R, Khin Y, Harrison SC (2016) Structure of the MIND Complex Defines a Regulatory Focus for Yeast Kinetochore Assembly. *Cell* 167: 1014-1027 e12
Doheny KF, Sorger PK, Hyman AA, Tugendreich S, Spencer F, Hieter P (1993) Identification of essential components of the S. cerevisiae kinetochore. *Cell* 73: 761-74
Fischbock-Halwachs J, Singh S, Potocnjak M, Hagemann G, Solis-Mezarino V, Woike S, Ghodgaonkar-Steger M, Weissmann F, Gallego LD, Rojas J, Andreani J, Kohler A, Herzog F (2019) The COMA complex interacts with Cse4 and positions Sli15/Ipl1 at the budding yeast inner kinetochore. *Elife* 8
Fitzgerald-Hayes M, Clarke L, Carbon J (1982) Nucleotide sequence comparisons and functional analysis of yeast centromere DNAs. *Cell* 29: 235-44
Foltz DR, Jansen LE, Black BE, Bailey AO, Yates JR, 3rd, Cleveland DW (2006) The human CENP-A centromeric nucleosome-associated complex. *Nat Cell Biol* 8: 458-69
Goh PY, Kilmartin JV (1993) NDC10: a gene involved in chromosome segregation in Saccharomyces cerevisiae. *The Journal of cell biology* 121: 503-12
Hamilton GE, Helgeson LA, Noland CL, Asbury CL, Dimitrova YN, Davis TN (2020) Reconstitution reveals two paths of force transmission through the kinetochore. *eLife* 9
Hara M, Fukagawa T (2020) Dynamics of kinetochore structure and its regulations during mitotic progression. *Cell Mol Life Sci* 77: 2981-2995
Hegemann JH, Fleig UN (1993) The centromere of budding yeast. *Bioessays* 15: 451-60
Herzog F, Kahraman A, Boehringer D, Mak R, Bracher A, Walzthoeni T, Leitner A, Beck M, Hartl FU, Ban N, Malmstrom L, Aebersold R (2012) Structural probing of a protein phosphatase 2A network by chemical cross-linking and mass spectrometry. *Science* 337: 1348-52
Hori T, Amano M, Suzuki A, Backer CB, Welburn JP, Dong Y, McEwen BF, Shang WH, Suzuki E, Okawa K, Cheeseman IM, Fukagawa T (2008) CCAN makes multiple contacts with centromeric DNA to provide distinct pathways to the outer kinetochore. *Cell* 135: 1039-52
Hornung P, Maier M, Alushin GM, Lander GC, Nogales E, Westermann S (2011) Molecular architecture and connectivity of the budding yeast Mtw1 kinetochore complex. *J Mol Biol* 405: 548-59

Hornung P, Troc P, Malvezzi F, Maier M, Demianova Z, Zimniak T, Litos G, Lampert F, Schleiffer A, Brunner M, Mechtler K, Herzog F, Marlovits TC, Westermann S (2014) A cooperative mechanism drives budding yeast kinetochore assembly downstream of CENP-A. *J Cell Biol* 206: 509-24
Jiang W, Lechner J, Carbon J (1993) Isolation and characterization of a gene (CBF2) specifying a protein component of the budding yeast kinetochore. *The Journal of cell biology* 121: 513-9
Kaplan KB, Hyman AA, Sorger PK (1997) Regulating the yeast kinetochore by ubiquitin-dependent degradation and Skp1p-mediated phosphorylation. *Cell* 91: 491-500
Killinger K, Böhm M, Steinbach P, Hagemann G, Blüggel M, Jänen K, Hohoff S, Bayer P, Herzog F, Westermann S (2020) Auto-inhibition of Mif2/CENP-C ensures centromere-dependent kinetochore assembly in budding yeast. *The EMBO journal* 39: e102938
Kitagawa K, Skowyra D, Elledge SJ, Harper JW, Hieter P (1999) SGT1 encodes an essential component of the yeast kinetochore assembly pathway and a novel subunit of the SCF ubiquitin ligase complex. *Molecular cell* 4: 21-33
Leber V, Nans A, Singleton MR (2018) Structural basis for assembly of the CBF3 kinetochore complex. *The EMBO journal* 37: 269-281
Lechner J, Carbon J (1991) A 240 kd multisubunit protein complex, CBF3, is a major component of the budding yeast centromere. *Cell* 64: 717-25
Lee PD, Wei H, Tan D, Harrison SC (2019) Structure of the Centromere Binding Factor 3 Complex from Kluyveromyces lactis. *J Mol Biol* 431: 4444-4454
Lingelbach LB, Kaplan KB (2004) The interaction between Sgt1p and Skp1p is regulated by HSP90 chaperones and is required for proper CBF3 assembly. *Mol Cell Biol* 24: 8938-50
Mellor J, Rathjen J, Jiang W, Barnes CA, Dowell SJ (1991) DNA binding of CPF1 is required for optimal centromere function but not for maintaining methionine prototrophy in yeast. *Nucleic acids research* 19: 2961-9
Perriches T, Singleton MR (2012) Structure of yeast kinetochore Ndc10 DNA-binding domain reveals unexpected evolutionary relationship to tyrosine recombinases. *J Biol Chem* 287: 5173-9
Pluta AF, Mackay AM, Ainsztein AM, Goldberg IG, Earnshaw WC (1995) The centromere: hub of chromosomal activities. *Science* 270: 1591-4
Przewloka MR, Venkei Z, Bolanos-Garcia VM, Debski J, Dadlez M, Glover DM (2011) CENP-C is a structural platform for kinetochore assembly. *Current biology : CB* 21: 399-405
Purvis A, Singleton MR (2008) Insights into kinetochore-DNA interactions from the structure of Cep3Delta. *EMBO Rep* 9: 56-62
Rodrigo-Brenni MC, Thomas S, Bouck DC, Kaplan KB (2004) Sgt1p and Skp1p modulate the assembly and turnover of CBF3 complexes required for proper kinetochore function. *Mol Biol Cell* 15: 3366-78
Russell ID, Grancell AS, Sorger PK (1999) The unstable F-box protein p58-Ctf13 forms the structural core of the CBF3 kinetochore complex. *The Journal of cell biology* 145: 933-50
Sievers, F., A. Wilm, D. Dineen, T. J. Gibson, K. Karplus, W. Li, R. Lopez, H. McWilliam, M. Remmert, J. Söding, J. D. Thompson & D. G. Higgins (2011) Fast, scalable generation of high-quality protein multiple sequence alignments using Clustal Omega. Mol Syst Biol, 7, 539.
Stemmann O, Lechner J (1996) The Saccharomyces cerevisiae kinetochore contains a cyclin-CDK complexing homologue, as identified by in vitro reconstitution. *The EMBO journal* 15: 3611-20
Strunnikov AV, Kingsbury J, Koshland D (1995) CEP3 encodes a centromere protein of Saccharomyces cerevisiae. *The Journal of cell biology* 128: 749-60
Walzthoeni T, Claassen M, Leitner A, Herzog F, Bohn S, Forster F, Beck M, Aebersold R (2012) False discovery rate estimation for cross-linked peptides identified by mass spectrometry. *Nature methods* 9: 901-3
Weissmann F, Petzold G, VanderLinden R, Huis In 't Veld PJ, Brown NG, Lampert F, Westermann S, Stark H, Schulman BA, Peters JM (2016) biGBac enables rapid gene assembly for the expression of large multisubunit protein complexes. *Proc Natl Acad Sci U S A* 113: E2564-9
Westermann S, Cheeseman IM, Anderson S, Yates JR, 3rd, Drubin DG, Barnes G (2003) Architecture of the budding yeast kinetochore reveals a conserved molecular core. *J Cell Biol* 163: 215-22

Willard HF (1990) Centromeres of mammalian chromosomes. *Trends Genet* 6: 410-6
Yan K, Yang J, Zhang Z, McLaughlin SH, Chang L, Fasci D, Ehrenhofer-Murray AE, Heck AJR, Barford D (2019) Structure of the inner kinetochore CCAN complex assembled onto a centromeric nucleosome. *Nature* 574: 278-282
Yan K, Zhang Z, Yang J, McLaughlin SH, Barford D (2018) Architecture of the CBF3-centromere complex of the budding yeast kinetochore. *Nature structural & molecular biology* 25: 1103-1110
Yoon HJ, Carbon J (1999) Participation of Bir1p, a member of the inhibitor of apoptosis family, in yeast chromosome segregation events. *Proceedings of the National Academy of Sciences of the United States of America* 96: 13208-13
Zhang W, Lukoyanova N, Miah S, Lucas J, Vaughan CK (2019) Insights into Centromere DNA Bending Revealed by the Cryo-EM Structure of the Core Centromere Binding Factor 3 with Ndc10. *Cell reports* 26: 1070

FIGURES

Figure 1

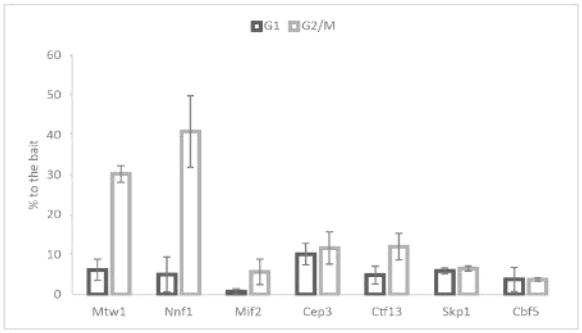

G1	IBAQ
Ndc10	100.0
Cep3	12.8
Nnf1	9.4
Mtw1	8.8
H3	7.6
Ctf13	7.1
Cbf5	6.8
Skp1	5.1
H2B2	3.3
H2BZ	3.3
H2A2	3.1
H4	1.6
Nkp1	0.4
Spc25	0.3
Cbf1	0.3

G2/M	IBAQ
Ndc10	100.0
H2B2	37.2
Mtw1	32.3
Nnf1	31.9
Cep3	15.7
Ctf13	15.3
H4	13.7
H2AZ	9.1
Skp1	7.2
H2A2	4.8
H3	4.3
Cbf5	4.2
Mif2	2.5
Nsl1	1.3
Cdc5	0.7
Cbf1	0.4
Okp1	0.4
Spc25	0.3
Mps1	0.1

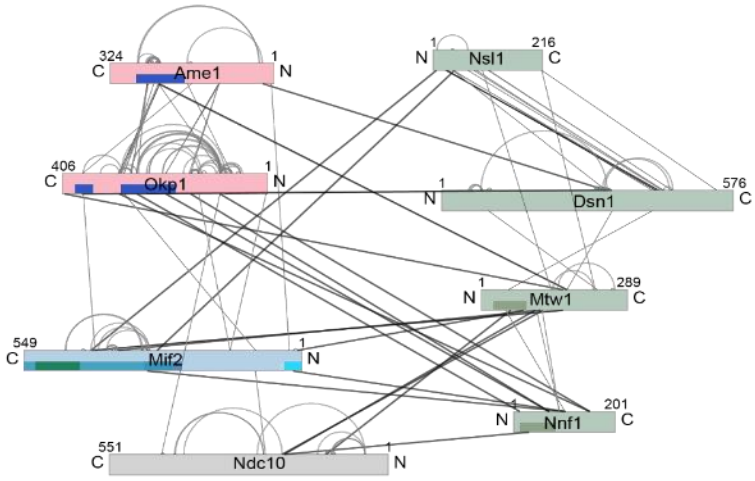

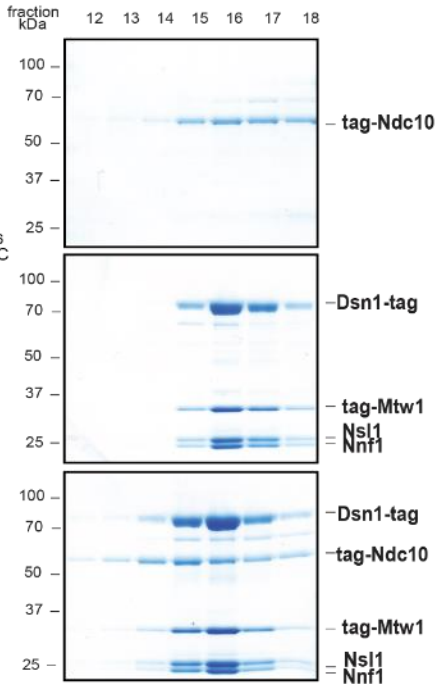

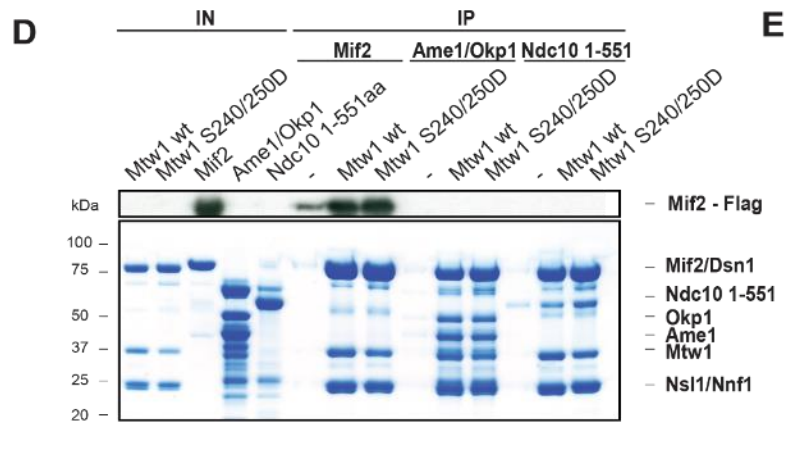

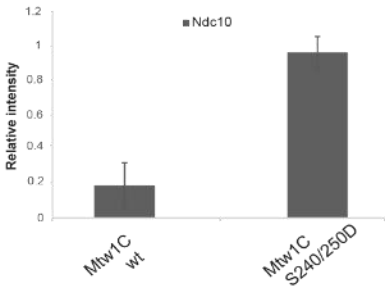

Figure 1. Ndc10 binding to the MTW1 complex is cell cycle and phosphorylation dependent

(A) Relative abundances of proteins that coprecipitated with the endogenously tagged full length Ndc10-6xHis-6xFlag. Cells were synchronized in G1 or G2/M phase using alpha factor or galactose induced Mps1 overexpression, respectively. Pull-down samples were analysed by mass spectrometry and the raw IBAQ intensities were normalised to the bait. (B) Crosslinking mass spectrometry analysis of the recombinant Mif2:Ame1/Okp1:Ndc10:Mtw1C$^{Dsn1\ S240/250D}$ complex (Table S4). Proteins are indicated as bars with the known domains indicated (Table S5). Subunits of the same complex are shown in the same color. Inter-protein crosslinks are depicted in black or dark gray and intra-protein crosslinks in light gray. (C) The interaction between Ndc10 and the MTW1 complex was analysed by size exclusion chromatography. Proteins were mixed in equimolar ratio and run on a Superose 6 Increase 3.2/300 column. The peak fractions were visualised by SDS-PAGE and Coomassie staining. (D) *In vitro* binding assay probing the interaction of immobilised wild-type Mtw1c or Mtw1c$^{Dsn1\ S240/250D}$ with Mif2, Ame1/Okp1 and Ndc10. Bound proteins were analysed by SDS-PAGE and Coomassie staining. Levels of Mif2 protein are visualized by Western blot as it overlaps with Dsn1 protein. IN: input sample, IP: immunoprecipitated sample. (E) Quantification of bound Ndc10$^{1-551}$ protein levels shown in (D). Protein band intensities were quantified using ImageJ. Bars represent the average of four experiments with error bars indicating the standard deviation.

Figure 2

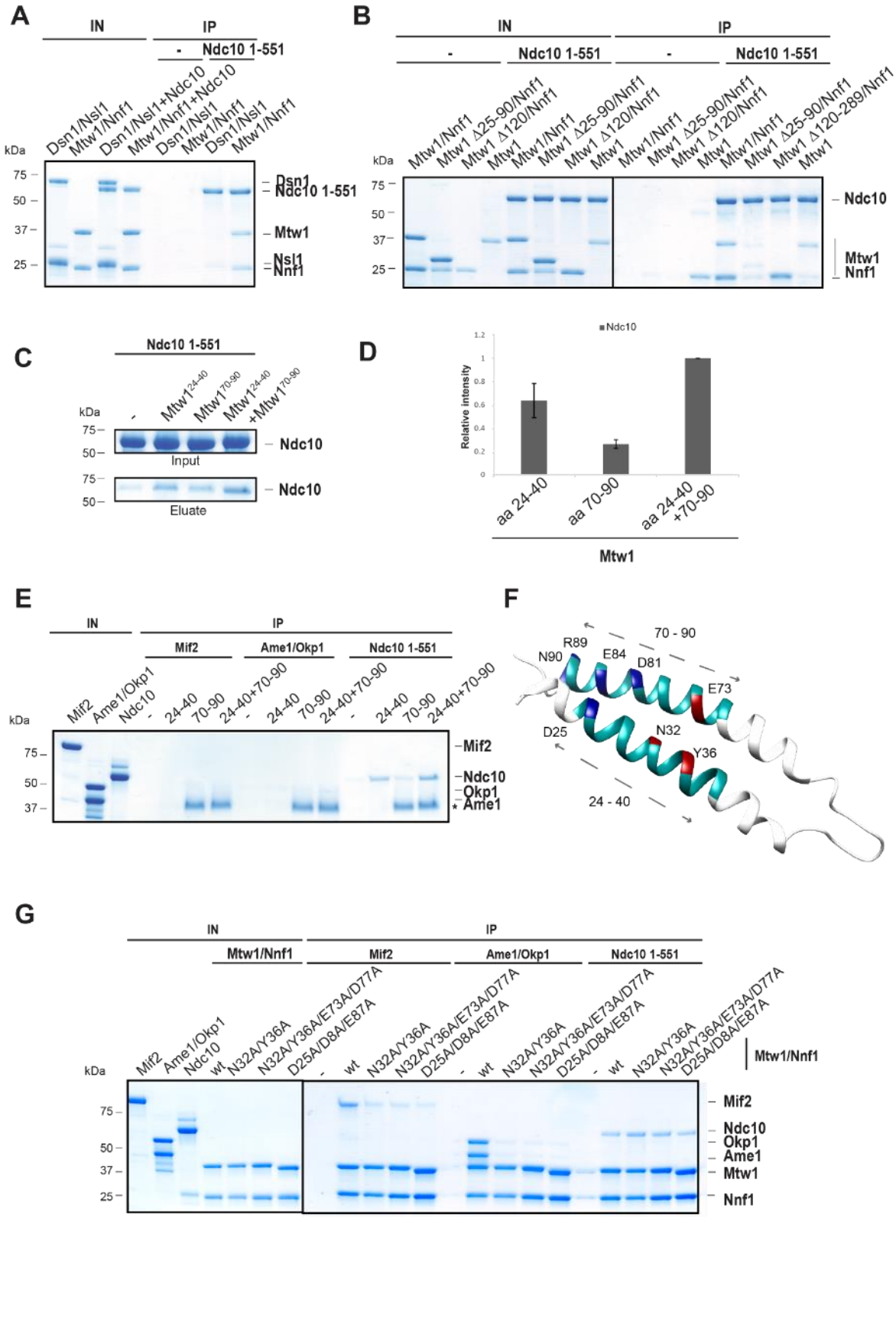
A
IN
IP
- Ndc10 1-551
Dsn1/Nsl1
Mtw1/Nnf1
Dsn1/Nsl1+Ndc10
Mtw1/Nnf1+Ndc10
kDa
75
50
37
25
Dsn1
Ndc10 1-551
Mtw1
Nsl1
Nnf1
B
IN
IP
- Ndc10 1-551 - Ndc10 1-551
Mtw1/Nnf1
Mtw1 Δ25-90/Nnf1
Mtw1 Δ120/Nnf1
Mtw1
Mtw1 Δ120-289/Nnf1
kDa
75
50
37
25
Ndc10
Mtw1
Nnf1
C
Ndc10 1-551
kDa
-
Mtw1 24-40
Mtw1 70-90
Mtw1 24-40 +Mtw1 70-90
75
50
Input
Ndc10
Eluate
Ndc10
D
Ndc10
Relative intensity
1.2
1
0.8
0.6
0.4
0.2
0
aa 24-40
aa 70-90
aa 24-40 +70-90
Mtw1
E
IN
IP
Mif2
Ame1/Okp1
Ndc10 1-551
Mif2
Ame1/Okp1
Ndc10
-
24-40
70-90
24-40+70-90
kDa
75
50
37
Mif2
Ndc10
Okp1
Ame1
F
70 - 90
R89
N90
E84
D81
E73
D25
N32
Y36
24 - 40
G
IN
IP
Mtw1/Nnf1
Mif2
Ame1/Okp1
Ndc10 1-551
Mif2
Ame1/Okp1
Ndc10
wt
N32A/Y36A
N32A/Y36A/E73A/D77A
D25A/D8A/E87A
-
kDa
75
50
37
25
Mtw1/Nnf1
Mif2
Ndc10
Okp1
Ame1
Mtw1
Nnf1

Figure 2. The Mtw1$^{24-40}$ helix is responsible for Ndc10 binding

(A) The role of the Dsn1/Nsl1 or Mtw1/Nnf1 heterodimer in Ndc10$^{1-551}$ binding was assessed *in vitro*. Heterodimers were separately expressed, purified from *E. coli* and binding to immobilised 1xFlag-Ndc10$^{1-551}$ was tested *in vitro*. (B) To further narrow down the Ndc10$^{1-551}$ binding site on the Mtw1/Nnf1 heterodimer, 1xFlag-Ndc10$^{1-551}$ was immobilised and incubated with wild-type Mtw1/Nnf1 Mtw1$^{\Delta 25-90}$/Nnf1, Mtw1$^{\Delta 120-289}$/Nnf1 or monomeric Mtw1. (C) *In vitro* binding assay of Mtw1$^{24-40}$, Mtw1$^{70-90}$ or their combination to Ndc10$^{1-551}$. 1×Strep-tagged peptides (Table S3) were incubated with recombinant Ndc10$^{1-551}$ at a molar ratio of 2:1. (D) Ndc10$^{1-551}$ levels bound to the respective peptides shown in (C) were quantified with ImageJ. Each bar represents the average of three experiments and the highest intensity (Mtw1$^{24-40}$+Mtw1$^{70-90}$) was set to 1 with error bars indicating the standard deviation. (E) Experiment as described in (C) was performed using Mif2, Ame1/Okp1 and Ndc10 as prey. *asterisk indicates contaminant band. (F) Model of the Mtw1 helix-loop-helix region is displayed based on the crystal structure (PDB entry 5T58) (Dimitrova et al. 2016). The region used to design the helix 1 (aa 24-40) and helix 2 (aa 70-90) peptides is indicated in green and by dashed arrows. The Mif2 and Ame1 binding sites constituted by the corresponding critical binding residues are shown in dark blue and red, respectively (Dimitrova et al. 2016). (G) Empty Strep beads or immobilised 1xStrep-Mtw1/Nnf1 wild-type or the respective point mutants (depicted in (F)) responsible for breaking the interaction with either Mif2 of Ame1 (Dimitrova et al. 2016) were incubated with Mif2, Ame1/Okp1 or Ndc10$^{1-551}$. Eluates were analysed by SDS-PAGE and Coomassie staining.

Figure 3

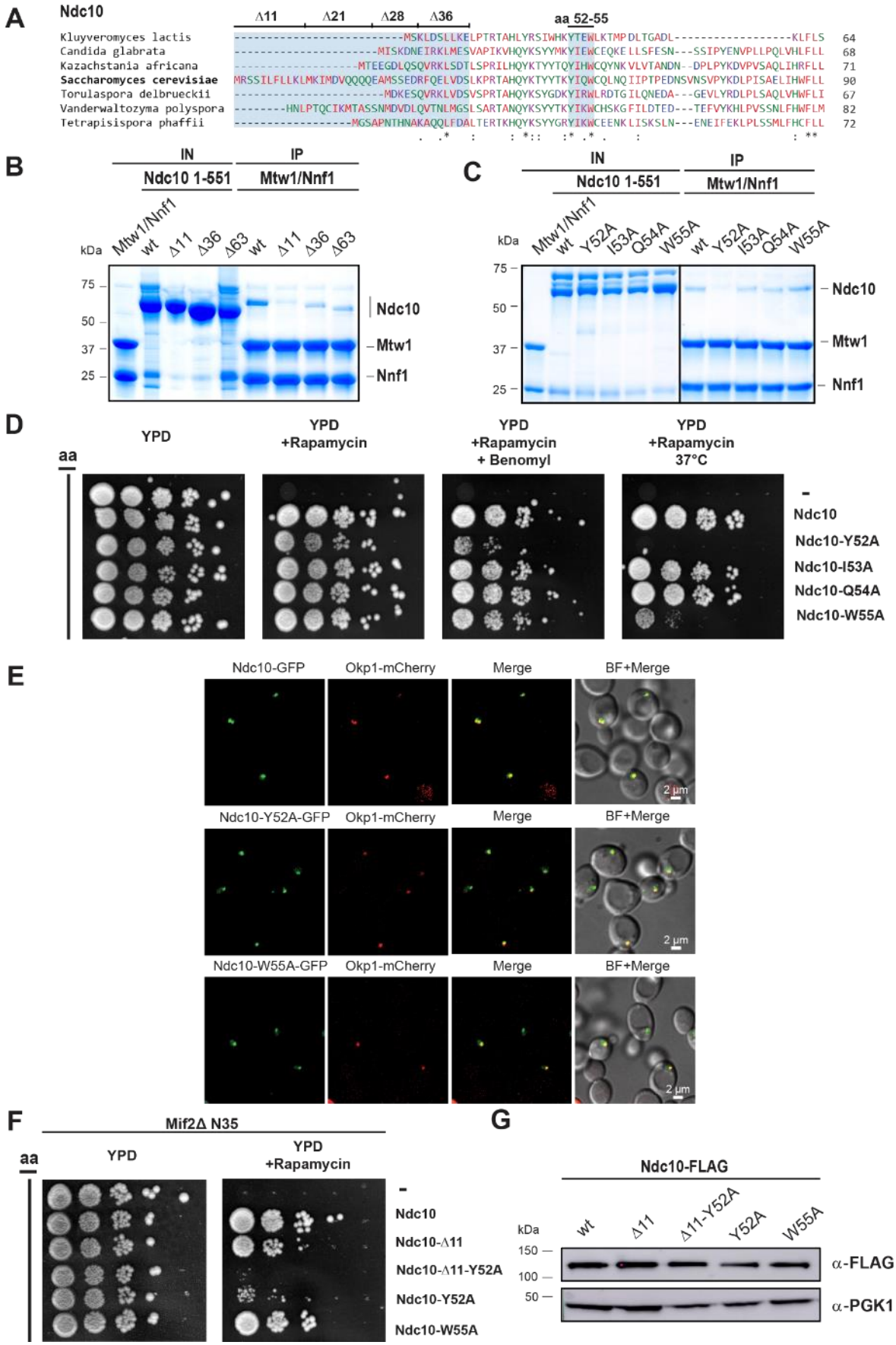
A
Ndc10
Δ11
Δ21
Δ28
Δ36
aa 52-55
Kluyveromyces lactis
Candida glabrata
Kazachstania africana
Saccharomyces cerevisiae
Torulaspora delbrueckii
Vanderwaltozyma polyspora
Tetrapisispora phaffii
B
IN
IP
Ndc10 1-551
Mtw1/Nnf1
kDa
Mtw1/Nnf1
wt
Δ11
Δ36
Δ63
75
50
37
25
Ndc10
Mtw1
Nnf1
C
IN
IP
Ndc10 1-551
Mtw1/Nnf1
Y52A
I53A
Q54A
W55A
D
aa
YPD
YPD +Rapamycin
YPD +Rapamycin + Benomyl
YPD +Rapamycin 37°C
-
Ndc10
Ndc10-Y52A
Ndc10-I53A
Ndc10-Q54A
Ndc10-W55A
E
Ndc10-GFP
Okp1-mCherry
Merge
BF+Merge
Ndc10-Y52A-GFP
Ndc10-W55A-GFP
2 µm
F
Mif2Δ N35
aa
YPD
YPD +Rapamycin
-
Ndc10
Ndc10-Δ11
Ndc10-Δ11-Y52A
Ndc10-Y52A
Ndc10-W55A
G
Ndc10-FLAG
kDa
wt
Δ11
Δ11-Y52A
Y52A
W55A
150
100
50
α-FLAG
α-PGK1

Figure 3. The conserved N-terminal Ndc10 residue Y52 is important for Mtw1 interaction and essential for cell viability at restrictive temperature

(A) Amino acid sequence alignment of the $Ndc10^{1-173}$ N-terminal region from interrelated yeast species with the highest similarities to *S. cerevisiae.* The region used for N-terminal deletion analysis and the conserved region used for point mutational analysis are indicated and shaded in light blue. Amino acids are colored according to the Clustal Omega color scheme. Residues that are identical among aligned protein sequences (*), conserved substitutions (:), and semiconserved substitutions (.) are indicated. (B) *In vitro* binding assay analysing the interaction of Ndc10 N-terminal deletion mutants with Mtw1/Nnf1. 1xStrep-Mtw1/Nnf1 was immobilised and incubated with $Ndc10^{1-551}$ wild-type or deletion mutants ($Ndc10^{\Delta 11}$, $Ndc10^{\Delta 36}$, $Ndc10^{\Delta 63}$). (C) Mtw1 interaction with $Ndc10^{1-551}$ point mutants ($Ndc10^{Y52A}$, $Ndc10^{I53A}$, $Ndc10^{Q54A}$, $Ndc10^{W55A}$) was tested as described in (B) (D) Cell viability assay of Ndc10 point mutants using the anchor-away technique. Ndc10-FRB strains transformed with the indicated Ndc10 rescue alleles were spotted in serial dilutions on YPD plates with or without addition of rapamycin (1 µg/ml) and benomyl (15 µg/ml) and incubated at 30 °C or restrictive temperature (37 °C), respectively. (E) Live cell microscopy showing the localization of ectopically expressed wild-type Ndc10-GFP and Ndc10-Y52A-GFP, Ndc-W55A-GFP mutant proteins analyzed in a Ndc10 anchor-away strain. Strains were grown and analyzed in the presence of 1 µg/ml rapamycin. Okp1-mCherry was used as kinetochore marker. BF: brightfield image. (F) Cell viability assay of Ndc10 wild-type, Ndc10-Δ11, the Ndc10-Y52A point mutant or the combination of both Ndc10-Δ11-Y52A analysed in a*Ndc10-FRB/mif2-Δ35* background. (G) Western blot analysis of ectopically expressed Ndc10 wild-type and mutant protein levels from the experiment shown in (F). Ndc10 proteins are visualized using anti-Flag antibody, Pgk1 levels are shown as a loading control.

Figure 4

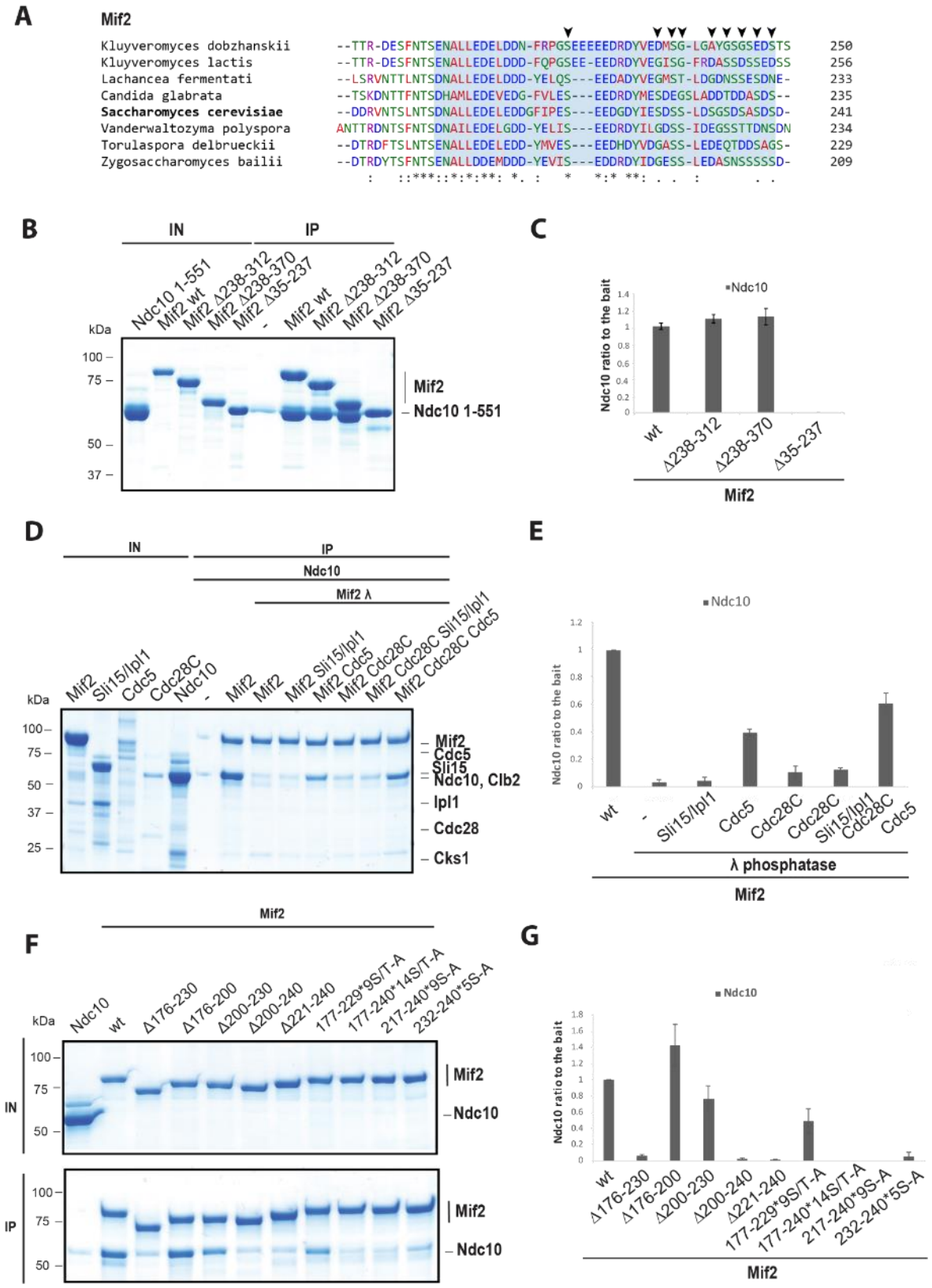
A
Mif2
Kluyveromyces dobzhanskii --TTR-DESFNTSENALLEDELDDN-FRPGSEEEEEDRDYVEDMSG-LGAYGSGSEDSTS 250
Kluyveromyces lactis --TTR-DESFNTSENALLEDELDDD-FQPGSEE-EEDRDYVEGISG-FRDASSDSSEDSS 256
Lachancea fermentati --LSRVNTTLNTSDNALLEDELDDD-YELQS---EEDADYVEGMST-LDGDNSSESDNE- 233
Candida glabrata --TSKDNTTFNTSDHAMLEDEVEDG-FVLES---EEDRDYMESDEGSLADDTDDASDS-- 235
Saccharomyces cerevisiae --DDRVNTSLNTSDNALLEDELEDDGFIPES---EEDGDYIESDSS-LDSGSDSASDSD- 241
Vanderwaltozyma polyspora ANTTRDNTSFNTSDNAILEDELGDD-YELIS---EEDRDYILGDSS-IDEGSSTTDNSDN 234
Torulaspora delbrueckii --DTRDFTSLNTSENALLEDELEDD-YMVES---EEDHDYVDGASS-LEDEQTDDSAGS- 229
Zygosaccharomyces bailii --DTRDYTSFNTSENALLDDEMDDD-YEVIS---EDDRDYIDGESS-LEDASNSSSSSD- 209
B
IN
IP
Ndc10 1-551
Mif2 wt
Mif2 Δ238-312
Mif2 Δ238-370
Mif2 Δ35-237
kDa
100
75
50
37
Mif2
Ndc10 1-551
C
Ndc10
Ndc10 ratio to the bait
wt
Δ238-312
Δ238-370
Δ35-237
Mif2
D
IN
IP
Ndc10
Mif2 λ
Mif2
Sli15/Ipl1
Cdc5
Cdc28C
Ndc10
Mif2 Sli15/Ipl1
Mif2 Cdc5
Mif2 Cdc28C
Mif2 Cdc28C Sli15/Ipl1
Mif2 Cdc28C Cdc5
kDa
100
75
50
37
25
Mif2
Cdc5
Sli15
Ndc10, Clb2
Ipl1
Cdc28
Cks1
E
Ndc10
Ndc10 ratio to the bait
wt
Sli15/Ipl1
Cdc5
Cdc28C
Cdc28C
Sli15/Ipl1
Cdc28C
Cdc5
λ phosphatase
Mif2
F
Mif2
Ndc10
wt
Δ176-230
Δ176-200
Δ200-230
Δ200-240
Δ221-240
177-229*9S/T-A
177-240*14S/T-A
217-240*9S-A
232-240*5S-A
kDa
IN
IP
100
75
50
Mif2
Ndc10
G
Ndc10
Ndc10 ratio to the bait
wt
Δ176-230
Δ176-200
Δ200-230
Δ200-240
Δ221-240
177-229*9S/T-A
177-240*14S/T-A
217-240*9S-A
232-240*5S-A
Mif2

Figure 4. Ndc10 binds to a serine-rich region in Mif2 (aa 220-240)

(A) Amino acid sequence alignment of the Mif2$^{189-241}$ region from interrelated yeast species with the highest similarities to *S. cerevisiae*. The region spanning *Sc*Mif2-200-240 is shaded in light blue. Phosphorylation sites used for mutational analysis are indicated by arrowheads. Residues that are identical among aligned protein sequences (*), conserved substitutions (:), and semiconserved substitutions (.) are indicated accordingly. **(B)** Ndc10$^{1-551}$ interaction with Mif2 was tested by immobilising Mif2-6xHis-6xFlag wild-type or mutant proteins (Mif2$^{\Delta 238-312}$, Mif2$^{\Delta 238-370}$, Mif2$^{\Delta 35-237}$) and incubating with Ndc10$^{1-551}$. **(C)** Bound Ndc10$^{1-551}$ levels were quantified using ImageJ and Ndc10 ratio to the bait Mif2 is shown (n=2). **(D)** The effect of Mif2 phosphorylation on Ndc10$^{1-551}$ binding was tested in an *in vitro* binding assay. Insect cell-expressed Mif2-6xHis-6xFlag was dephosphorylated using λ phosphatase and re-phosphorylated with the known kinetochore kinases (Sli15ΔN228/Ipl1$^{\text{Aurora B}}$, Cdc5$^{\text{Plk1}}$, Cdc28$^{\text{Cdk1}}$) in a buffer containing 1 mM ATP and 2.5 mM $MgCl_2$. **(E)** Quantification of the experiment shown in (D) as described in (C). **(F)** *In vitro* binding assay to delimit the Ndc10 binding site on Mif2. Indicated Mif2-6xHis-6xFlag deletions or phosphorylation-site mutants were immobilised and binding to Ndc10$^{1-551}$ was analysed. **(G)** Bound Ndc10 levels from the experiment shown in (F) were quantified as described in (C).

Figure 5

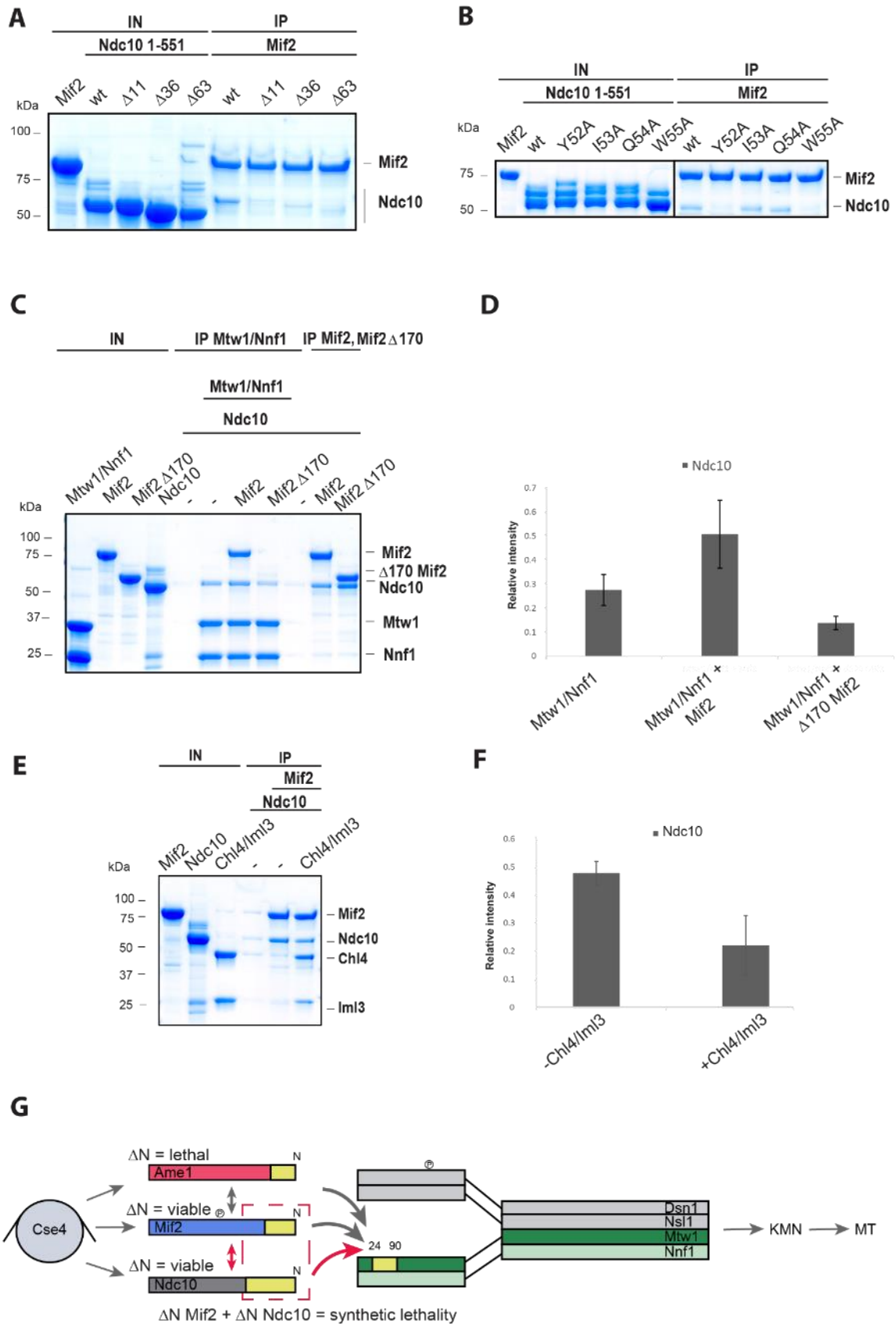
A
IN
IP
Ndc10 1-551
Mif2
kDa
Mif2
wt
Δ11
Δ36
Δ63
wt
Δ11
Δ36
Δ63
100
75
50
Mif2
Ndc10
B
IN
IP
Ndc10 1-551
Mif2
kDa
Mif2
wt
Y52A
I53A
Q54A
W55A
wt
Y52A
I53A
Q54A
W55A
75
50
Mif2
Ndc10
C
IN
IP Mtw1/Nnf1
IP Mif2, Mif2Δ170
Mtw1/Nnf1
Ndc10
Mtw1/Nnf1
Mif2
Mif2Δ170
Ndc10
Mif2
Mif2Δ170
Mif2
Mif2Δ170
kDa
100
75
50
37
25
Mif2
Δ170 Mif2
Ndc10
Mtw1
Nnf1
D
Ndc10
Relative intensity
0.7
0.6
0.5
0.4
0.3
0.2
0.1
0
Mtw1/Nnf1
Mtw1/Nnf1 + Mif2
Mtw1/Nnf1 + Δ170 Mif2
E
IN
IP
Mif2
Ndc10
kDa
Mif2
Ndc10
Chl4/Iml3
Chl4/Iml3
100
75
50
37
25
Mif2
Ndc10
Chl4
Iml3
F
Ndc10
Relative intensity
0.6
0.5
0.4
0.3
0.2
0.1
0
-Chl4/Iml3
+Chl4/Iml3
G
ΔN = lethal
Ame1
N
ΔN = viable
Mif2
N
ΔN = viable
Ndc10
N
Cse4
24
90
Dsn1
Nsl1
Mtw1
Nnf1
KMN
MT
ΔN Mif2 + ΔN Ndc10 = synthetic lethality

Figure 5. Mif2 binding to Ndc10$^{1-551}$ occurs via the same N-terminal region as Mtw1 binding

(A) Mif2-6xHis-6xFlag was immobilised and incubated with Ndc10$^{1-551}$ wild-type or the indicated deletion mutants in a 1:1 molar ratio. **(B)** Immobilised Mif2-6xHis-6xFlag was incubated with Ndc10$^{1-551}$ point mutants (Ndc10^{Y52A}, Ndc10^{I53A}, Ndc10^{Q54A}, Ndc10^{W55A}). **(C)** Competition between Mtw1 and Mif2 was tested using the Mif2-Δ170 mutant lacking the Mtw1 binding domain. 1xStrep-Mtw1/Nnf1 was immobilised and incubated with Ndc10$^{1-551}$, Ndc10$^{1-551}$ and Mif2 or Ndc10$^{1-551}$ and Mif2-Δ170. The interaction between Ndc10 and Mif2 wild-type or Mif2-Δ170 was tested by immobilising the corresponding proteins and incubating with Ndc10$^{1-551}$. **(D)** Quantification of the Ndc10 levels retained by Mtw1/Nnf1 as shown in (C). Protein levels were quantified using ImageJ with bars depicting the relative intensity and with error bars indicating the standard deviation (n=2). **(E)** Competition between Chl4/Iml3 and Ndc10$^{1-551}$ for Mif2 binding was tested by immobilising Mif2-6xHis-6xFlag and incubating with the indicated proteins. **(F)** The experiment shown in (E) was quantified as described in (D). **(G)** Model summarising the phosphorylation dependent recruitment of Mtw1/Nnf1 (green) via the three inner kinetochore receptors Ame1 (red), Mif2 (blue) and Ndc10 (grey) through their N terminal domains. While the N terminal deletion of Ame1 is lethal and crucial for cell viability, perturbations in both, the N terminal regions of Mif2 and Ndc10 cause synthetic lethality.

Supplemental information

Supplemental Figures

Figure S1

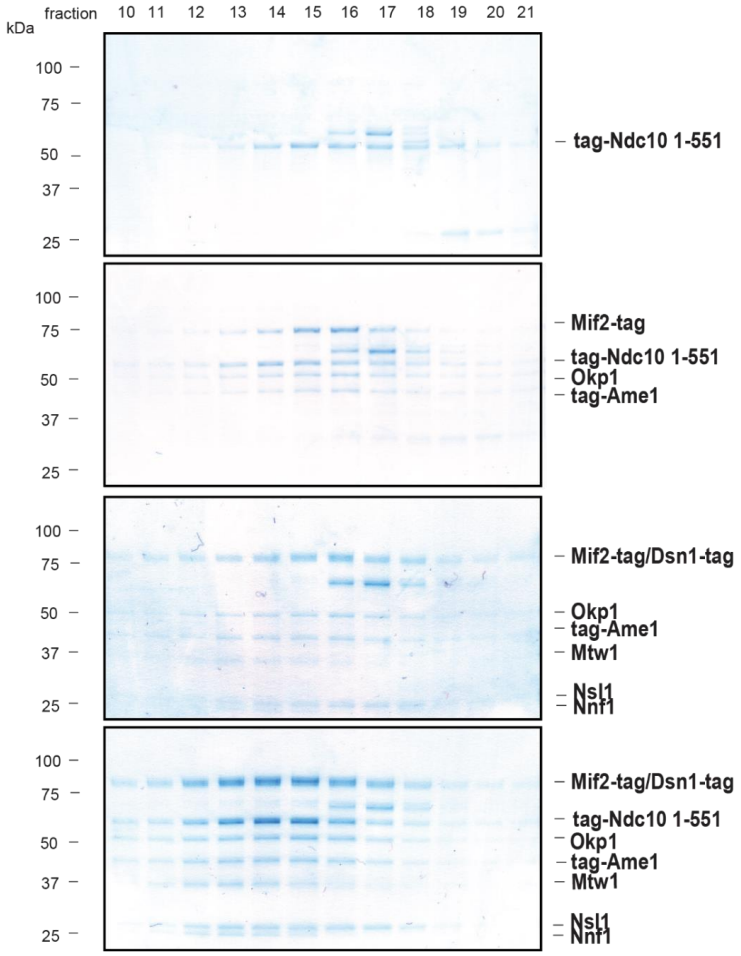

Figure S1. Analysis of Ndc10$^{1-551}$, Mif2, Ame1/Okp1 and Mtw1C complex formation by size exclusion chromatography. The interaction between 6xHis-Ndc10$^{1-551}$, Mif2-6xHis-6xFlag, 6xHis-Ame1/Okp1 and Mtw1c (Mtw1/Nnf1/Dsn1-6xHis-6xFlag/Nsl1) was analyzed using size exclusion chromatography. Protein complexes were mixed in an equimolar ratio and incubated on ice for 1 h. The samples were run on a Superose 6 Increase 3.2/300 column and analyzed by SDS-PAGE and Coomassie staining. The shift in fraction 11 and 12 indicates association of the larger complex.

Figure S2

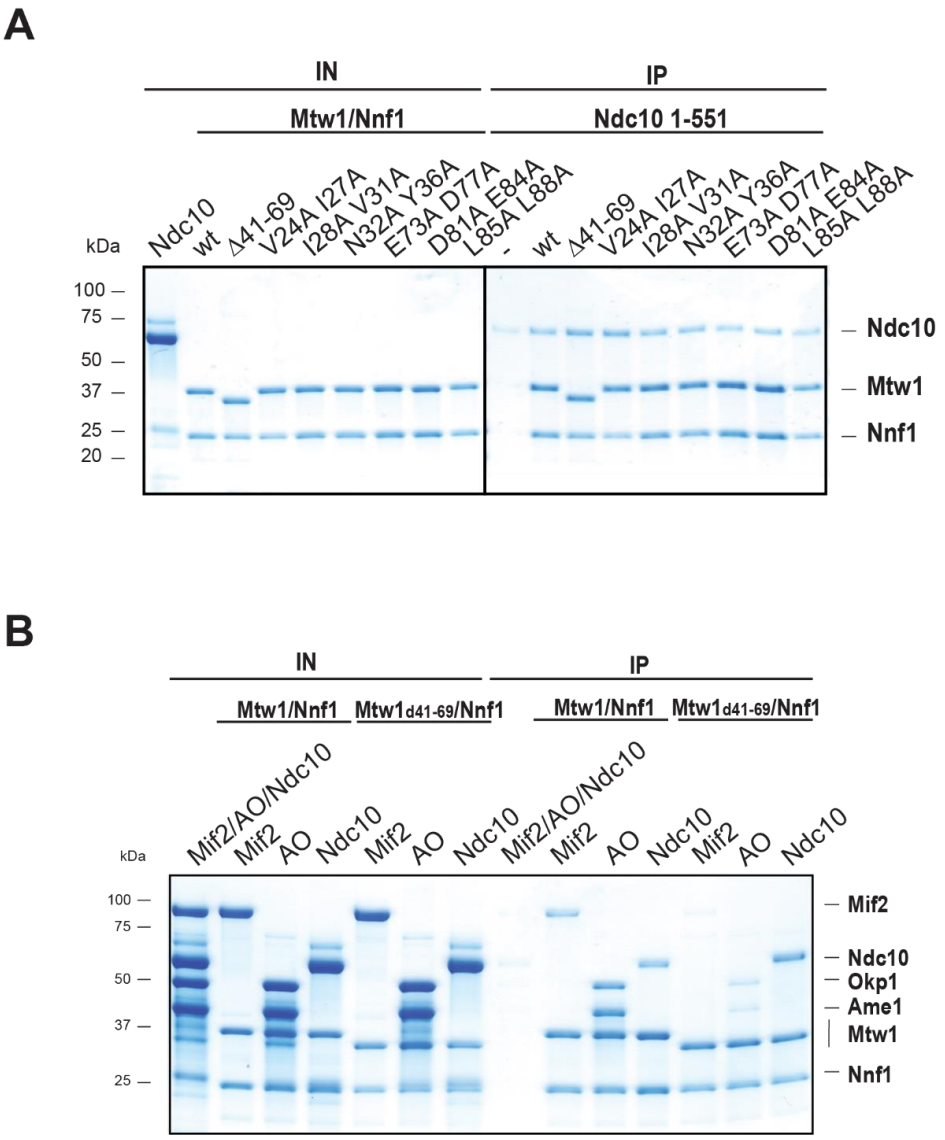

Figure S2. Ndc10$^{1-551}$displays more robust binding comparing to Mif2 and Ame1/Okp1

(A) *In vitro* binding assay was performed by immobilizing 1xStrep-Mtw1/Nnf1 wild-type or the indicated Mtw1 deletion or double-point mutants and incubating with 6xHis-Ndc10$^{1-551}$. (B) *In vitro* binding assay to estimate the effect of the Mtw1$^{41-69}$ loop deletion on Mif2-6xHis-6xFlag, 6xHis-Ame1/Okp1 or 6xHis-Ndc10$^{1-551}$ binding. The eluted protein complexes were visualized by SDS-PAGE and Coomassie staining. IN: input sample, IP: immunoprecipitated sample.

Figure S3

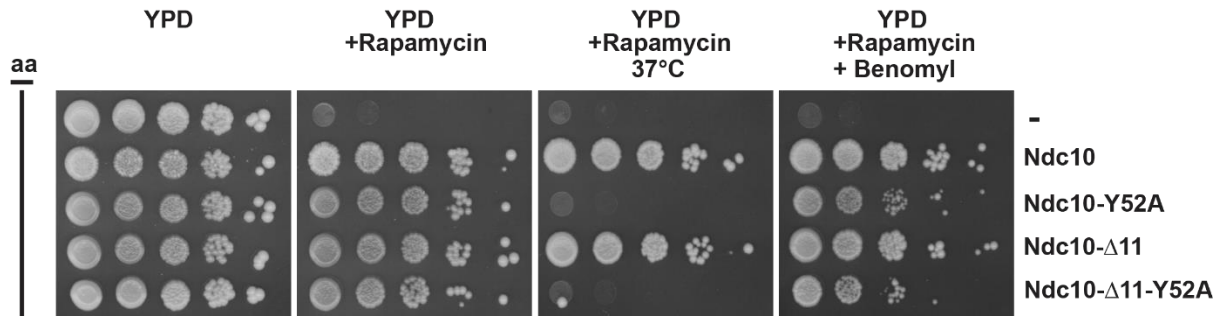

Figure S3. *In vivo* effect of mutating Ndc10 – Mtw1 binding sites

In vivo analysis of Ndc10 mutants using the anchor-away technique. Yeast cell growth of a Ndc10-FRB strain was tested in serial dilutions either untransformed (-) or transformed with the indicated Ndc10 rescue constructs on YPD medium in the absence or presence of 1 µg/ml rapamycin and/or 15 ug/ml benomyl at permissive (30 °C) or restrictive temperature (37 °C).

Figure S4

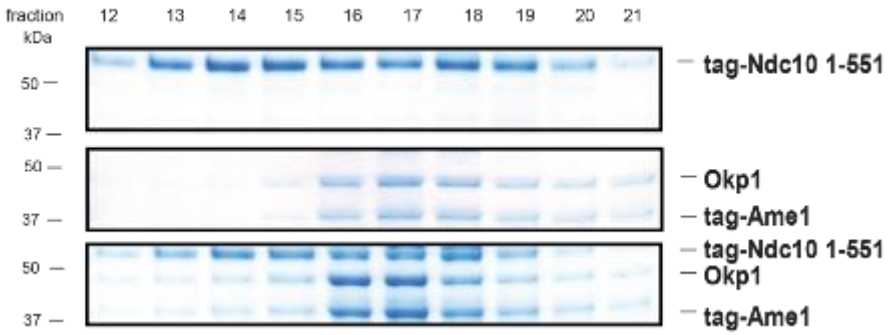

Figure S4. Ame1/Okp1 does not form a stable complex with Ndc10$^{1-551}$ in size exclusion chromatography analysis.

The interaction between 6xHis-Ndc10$^{1-551}$ and 6xHis-Ame1/Okp1 was analyzed using size exclusion chromatography. Protein complexes were mixed in an equimolar ratio, incubated on ice for 1 h prior to injection and run on a Superose 6 Increase 3.2/300 column. Collected peak fractions were analyzed by SDS-PAGE and Coomassie staining.

Figure S5

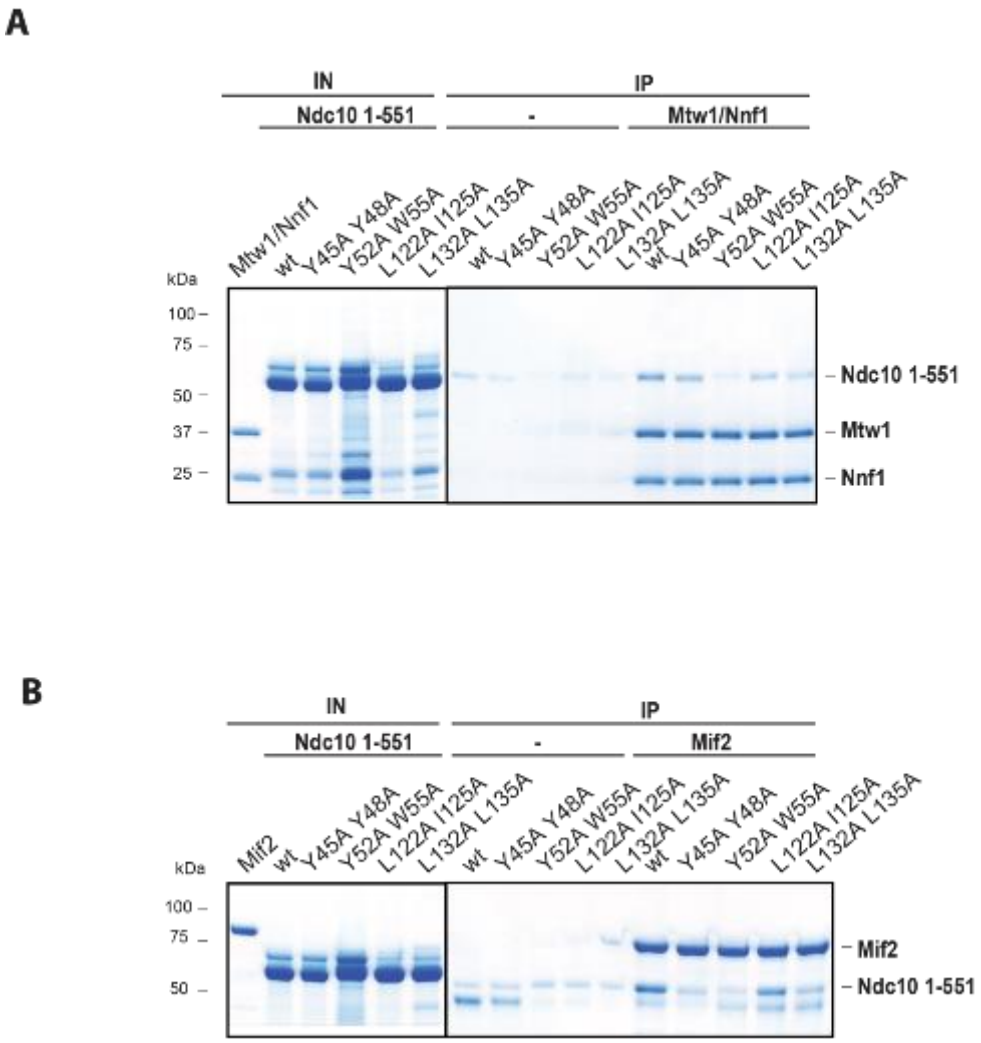

Figure S5. Mif2 occupies a larger binding site on Ndc10 than Mtw1

(A) *In vitro* binding assay to estimate the effect of conserved Ndc10 residues based on a multiple sequence alignment from interrelated yeast species on Mtw1/Nnf1 binding. 1xStrep-Mtw1/Nnf1 was immobilized and probed by incubation with indicated 6xHis-Ndc10$^{1-551}$ mutants. (B) Binding assay to access the influence of mutation in the conserved areas of Ndc10 on Mif2 binding. Mif2-6xHis-6xFlag was immobilized and probed with the indicated 6xHis-Ndc10$^{1-551}$ mutants. Eluted proteins were visualized by SDS-PAGE and Coomassie staining.

Supplemental Tables

Table S1. Plasmids used in this study.

Number	Plasmid	Source
BMP82	pET28 6xHis-Thrombin-Ndc10$^{1-551}$	This study
BMP131	pET28 6xHis-Thrombin-Ndc10$^{63-551}$ (Δ63)	This study
BMP83	pET28 6xHis-Thrombin-Ndc10$^{1-107,139-551}$ (Δ107-139)	This study
BMP132	pET28 6xHis-Thrombin-Ndc10$^{139-551}$ (Δ139)	This study
BMP142	pET28 6xHis-Thrombin-Ndc10$^{1-551}$ Y45AY48A	This study
BMP143	pET28 6xHis-Thrombin-Ndc10$^{1-551}$ Y52AW55A	This study
BMP155	pET28 6xHis-Thrombin-Ndc10$^{1-551}$ L122A L125A	This study
BMP156	pET28 6xHis-Thrombin-Ndc10$^{1-551}$ L132A L135A	This study
BMP197	pET28 6xHis-Thrombin-Ndc10$^{1-551}$ Y52A	This study
BMP198	pET28 6xHis-Thrombin-Ndc10$^{1-551}$ I53A	This study
BMP199	pET28 6xHis-Thrombin-Ndc10$^{1-551}$ Q54A	This study
BMP200	pET28 6xHis-Thrombin-Ndc10$^{1-551}$ W55A	This study
BMP102	pETDuet-1 Mtw1/Nnf1-6xHis	This study
BMP62	pST39 Dsn1/Nsl1-6xHis/Mtw1	Stefan Westermann
BMP181	pETDuet-1 1xStrep-Mtw1/Nnf1-6xHis	This study
BMP136	pETDuet-1 1xStrep-Mtw1$^{\Delta 25-90}$/Nnf1-6xHis	This study
BMP135	pETDuet-1 1xStrep-Mtw1$^{\Delta 120-289}$/Nnf1-6xHis	This study
BMS20	pET28 1xStrep-Mtw1	This study
BMP75	pBIG1 Dsn1-2xStrep/Mtw1/Nsl1/Nnf1	(Fischbock-Halwachs et al. 2019)
BTS16	pBIG1 Dsn1$^{S240D/S250D}$-6xHis-2xStrep /Mtw1/Nsl1/Nnf1	This study
BMP123	pST39 Okp1-6xHis/Ame1	Stefan Westermann
BJF6	pLib-Mif2-6xHis-6xFlag	(Fischbock-Halwachs et al. 2019)
BMP201	pLib-Mif2$^{\Delta 35-237}$-6xHis-6xFlag	This study

BMP202	pLib-Mif2$^{\Delta 238-312}$-6xHis-6xFlag	This study
BMP203	pLib-Mif2$^{\Delta 238-370}$-6xHis-6xFlag	This study
BSS227	pLib-Mif2$^{\Delta 176-230}$-6xHis-6xFlag	This study
BSS230	pLib-Mif2$^{\Delta 176-200}$-6xHis-6xFlag	This study
BSS231	pLib-Mif2$^{\Delta 200-230}$-6xHis-6xFlag	This study
BSS290	pLib-Mif2$^{\Delta 200-240}$-6xHis-6xFlag	This study
BSS292	pLib-Mif2$^{\Delta 221-240}$-6xHis-6xFlag	This study
BSS327	pLib-Mif2$^{\Delta N2-170}$-6xHis-6xFlag	This study
BSS280	pLib-Mif2-S177A-T194A-S195A-S198A-S199A-S217A-S226A-S228A-S229A-6xHis-6xFlag	This study
BSS285	pLib-Mif2-S177A-T194A-S195A-S198A-S199A-S217A-S226A-S228A-S229A-S232A-S234A-S236A-S238A-S240A-6xHis-6xFlag	This study
BSS287	pLib-Mif2-S217A-S226A-S228A-S229A-S232A-S234A-S236A-S238A-S240A-6xHis-6xFlag	This study
BSS294	pLib-Mif2-S232A-S234A-S236A-S238A-S240A-6xHis-6xFlag	This study
BJF1	pBIG1-SLI15-2xStrep-HA-6xHis/IPL1	(Fischbock-Halwachs et al. 2019)
BCK44	pET28-1xStrep-Clb2	This study
BSS25	pLib-Cdc28	This study
BSS26	pLib-Cks1	This study
BSS75	pLib-6xHis-Cdc5	This study
BMP37	pETDuet-1-6-His-Chl4/Iml3	(Fischbock-Halwachs et al. 2019)
BTS1	pRS313-200 5'UTR Ndc10-6xHis-FLAG	This study
BTS2	pRS313-200 5'UTR Ndc10^{Y52A}-6xHis-6xFLAG	This study
BTS3	pRS313-200 5'UTR Ndc10^{I53A}-6xHis-6xFLAG	This study
BTS4	pRS313-200 5'UTR Ndc10^{Q54A}-6xHis-6xFLAG	This study
BTS5	pRS313-200 5'UTR Ndc10^{W55A}-6xHis-6xFLAG	This study
BSS313	pRS313-200 5'UTR Ndc10$^{\Delta N2-11}$-6xHis-6xFLAG	This study
BSS325	pRS313-200 5'UTR Ndc10$^{\Delta N2-11-Y52A}$-6xHis-6xFLAG	This study

BSS340	pRS313-200 5'UTR Ndc10$^{\Delta N2-21}$-6xHis-6xFLAG	This study
BSS341	pRS313-200 5'UTR Ndc10$^{\Delta N2-28}$-6xHis-6xFLAG	This study
BSS339	pRS313-200 5'UTR Ndc10$^{\Delta N2-36}$-6xHis-6xFLAG	This study
BSS260	pRS313-200 5'UTR Ndc10-GFP	This study
BSS306	pRS313-200 5'UTR Ndc10^{Y52A}-GFP	This study
BSS329	pRS313-200 5'UTR Ndc10^{W55A}-GFP	This study

Table S2. Yeast strains used in this study.

Number	Genotype
YTS35	MAT a, tor1-1, fpr1::loxP-Leu2-loxP, RPL13A-2xFKBP12::lox-TRP1-loxP, Ndc10-FRB::KanMX, pRS313-NDC10-6xHis6xFLAG::HIS
YTS37	MAT a, tor1-1, fpr1::loxP-Leu2-loxP, RPL13A-2xFKBP12::lox-TRP1-loxP, Ndc10-FRB::KanMX, pRS313-NDC10^{Y52A}-6xHis6xFLAG::HIS
YTS39	MAT a, tor1-1, fpr1::loxP-Leu2-loxP, RPL13A-2xFKBP12::lox-TRP1-loxP, Ndc10-FRB::KanMX, pRS313-NDC10^{I53A}-6xHis6xFLAG::HIS
YTS41	MAT a, tor1-1, fpr1::loxP-Leu2-loxP, RPL13A-2xFKBP12::lox-TRP1-loxP, Ndc10-FRB::KanMX, pRS313-NDC10^{Q54A}-6xHis6xFLAG::HIS
YTS43	MAT a, tor1-1, fpr1::loxP-Leu2-loxP, RPL13A-2xFKBP12::lox-TRP1-loxP, Ndc10-FRB::KanMX, pRS313-NDC10^{W55A}-6xHis6xFLAG::HIS
YSS699	MAT a, tor1-1, fpr1::loxP-Leu2-loxP, RPL13A-2xFKBP12::lox-TRP1-loxP, Ndc10-FRB::KanMX, pRS313-NDC10$^{\Delta N2-11}$-6xHis6xFLAG::HIS
YSS667	MAT a, tor1-1, fpr1::loxP-Leu2-loxP, RPL13A-2xFKBP12::lox-TRP1-loxP, Ndc10 FRB::KanMX, pRS313-NDC10$^{\Delta N2-11-Y52A}$-6xHis6xFLAG::HIS
YSS712	MAT a, tor1-1, fpr1::loxP-Leu2-loxP, RPL13A-2xFKBP12::lox-TRP1-loxP, Ndc10-FRB::KanMX, pRS313-NDC10$^{\Delta N2-21}$-6xHis6xFLAG::HIS
YSS713	MAT a, tor1-1, fpr1::loxP-Leu2-loxP, RPL13A-2xFKBP12::lox-TRP1-loxP, Ndc10-FRB::KanMX, pRS313-NDC10$^{\Delta N2-28}$-6xHis6xFLAG::HIS
YSS702	MAT a, tor1-1, fpr1::loxP-Leu2-loxP, RPL13A-2xFKBP12::lox-TRP1-loxP, Ndc10-FRB::KanMX, pRS313-NDC10$^{\Delta N2-36}$-6xHis6xFLAG::HIS
YSS691	MAT a, tor1-1, fpr1::loxP-Leu2-loxP, RPL13A-2xFKBP12::lox-TRP1-loxP, Ndc10-FRB::KanMX, mif2ΔN2-35::hphNT1
YSS704	MAT a, tor1-1, fpr1::loxP-Leu2-loxP, RPL13A-2xFKBP12::lox-TRP1-loxP, Ndc10-FRB::KanMX, mif2ΔN2-35::hphNT1, pRS313-NDC10-6xHis6xFLAG::HIS
YSS705	MAT a, tor1-1, fpr1::loxP-Leu2-loxP, RPL13A-2xFKBP12::lox-TRP1-loxP, Ndc10-FRB::KanMX, mif2ΔN2-35::hphNT1. pRS313-NDC10$^{\Delta N2-11}$-6xHis6xFLAG::HIS
YSS706	MAT a, tor1-1, fpr1::loxP-Leu2-loxP, RPL13A-2xFKBP12::lox-TRP1-loxP, Ndc10-FRB::KanMX, mif2ΔN2-35::hphNT1. pRS313-NDC10$^{\Delta N2-11-Y52A}$-6xHis6xFLAG::HIS
YSS696	MAT a, tor1-1, fpr1::loxP-Leu2-loxP, RPL13A-2xFKBP12::lox-TRP1-loxP, Ndc10-

YSS697	FRB::KanMX, mif2ΔN2-35::hphNT1. pRS313-NDC10^{Y52A}-6xHis6xFLAG::HIS
YSS709	MAT a, tor1-1, fpr1::loxP-Leu2-loxP, RPL13A-2xFKBP12::lox-TRP1-loxP, Ndc10-FRB::KanMX, mif2ΔN2-35::hphNT1. pRS313-NDC10^{W55A}-6xHis6xFLAG::HIS
YSS710	MAT a, tor1-1, fpr1::loxP-Leu2-loxP, RPL13A-2xFKBP12::lox-TRP1-loxP, Ndc10-FRB::KanMX, mif2ΔN2-35::hphNT1. pRS313-NDC10$^{\Delta N2-21}$-6xHis6xFLAG::HIS
YSS711	MAT a, tor1-1, fpr1::loxP-Leu2-loxP, RPL13A-2xFKBP12::lox-TRP1-loxP, Ndc10-FRB::KanMX, mif2ΔN2-35::hphNT1. pRS313-NDC10$^{\Delta N2-28}$-6xHis6xFLAG::HIS
YSS663	MAT a, tor1-1, fpr1::loxP-Leu2-loxP, RPL13A-2xFKBP12::lox-TRP1-loxP, Ndc10-FRB::KanMX, mif2ΔN2-35::hphNT1. pRS313-NDC10$^{\Delta N2-36}$-6xHis6xFLAG::HIS
YSS665	MAT a, tor1-1, fpr1::loxP-Leu2-loxP, RPL13A-2xFKBP12::lox-TRP1-loxP, Ndc10-FRB::KanMX, Okp1-mCherry::natNT2, pRS313-NDC10-GFP
YSS675	MAT a, tor1-1, fpr1::loxP-Leu2-loxP, RPL13A-2xFKBP12::lox-TRP1-loxP, Ndc10-FRB::KanMX, Okp1-mCherry::natNT2, pRS313-NDC10^{Y52A}-GFP
YTZ50	MAT a, tor1-1, fpr1::loxP-Leu2-loxP, RPL13A-2xFKBP12::lox-TRP1-loxP, Ndc10-FRB::KanMX, Okp1-mCherry::natNT2, pRS313-NDC10^{W55A}-GFP
	pGAL-1myc-MPS1, Ndc10-6xHis-6xFLAG

Table S3.

Peptides were preceded with a Strep tag and a short linker (SAWSHPQFEKGG*SA*).

Number Protein ID	Sequence
PA0123 Mtw1$^{24-40}$	SAWSHPQFEKGG*SA*VDDIINAVNEIMYKCTA
PA0124 Mtw1$^{70-90}$	SAWSHPQFEKGG*SA*SLLENSVDKNFDKLELYVLRN

Table S4. Inter- and intra-protein crosslinks on recombinant Mif2:Ame1/Okp1:Ndc10$^{1-551}$:Mtw1c$^{Dsn1\ S240/250D}$ complex used in Figure 7B

Mif2 and Mtw1c were recombinantly expressed in insect cells while Ndc10$^{1-551}$ and Ame1/Okp1 were expressed and purified from *E. coli*. The complex was assembled and incubated on ice prior to cross linking. In total, 96 inter-protein (dark green) and 170 intra-protein (light green) crosslinks were detected on the recombinant complex depicted in Figure 1B.

Submitted to PRIDE Archive with project accession code: PXD022043.

Table S5. Predicted and published domains depicted in the crosslink network

The crosslink network on the recombinant Ndc10$^{1-551}$:Mif2:Ame1/Okp1:Mtw1c complex from Table S4 was depicted in Figure 1B with addition of previously identified protein domains.

Protein	Domain/Motif	Start	End	Reference
Ame1	coiled coil	177	272	MARCOIL prediction
Mif2	MTW1C binding	1	35	(Hornung et al. 2014)
Mif2	signature motif	238	312	(Hornung et al. 2014)
Mif2	IML3/CHL4 binding	256	549	(Hinshaw and Harrison 2013)
Mif2	cupin fold	439	526	(Hornung et al. 2014)
Okp1	coiled coil	183	290	MARCOIL prediction
Okp1	coiled coil	346	381	MARCOIL prediction
Mtw1	Mif2 and Ame1 binding domain	25	90	(Dimitrova et al. 2016)
Nnf1	Mif2 and Ame1 binding domain	13	83	(Dimitrova et al. 2016)

References:

Dimitrova YN, Jenni S, Valverde R, Khin Y, Harrison SC (2016) Structure of the MIND Complex Defines a Regulatory Focus for Yeast Kinetochore Assembly. *Cell* 167: 1014-1027 e1012

Fischbock-Halwachs J, Singh S, Potocnjak M, Hagemann G, Solis-Mezarino V, Woike S, Ghodgaonkar-Steger M, Weissmann F, Gallego LD, Rojas J *et al* (2019) The COMA complex interacts with Cse4 and positions Sli15/Ipl1 at the budding yeast inner kinetochore. *eLife* 8

Hinshaw SM, Harrison SC (2013) An Iml3-Chl4 heterodimer links the core centromere to factors required for accurate chromosome segregation. *Cell reports* 5: 29-36

Hornung P, Troc P, Malvezzi F, Maier M, Demianova Z, Zimniak T, Litos G, Lampert F, Schleiffer A, Brunner M *et al* (2014) A cooperative mechanism drives budding yeast kinetochore assembly downstream of CENP-A. *The Journal of cell biology* 206: 509-524

3.3 C-Terminal Motifs of the MTW1 Complex Cooperatively Stabilize Outer Kinetochore Assembly in Budding Yeast

Ghodgaonkar-Steger M*, **Potocnjak M***, Zimniak T, Fischböck-Halwachs J, Solis-Mezarino V, Singh S, Speljko T, Hagemann G, Drexler DJ, Witte G, Herzog F. C-Terminal Motifs of the MTW1 Complex Cooperatively Stabilize Outer Kinetochore Assembly in Budding Yeast. Cell Reports. 2020; 32, 108190. doi: 10.1016/j.celrep.2020.108190. (*equal contribution)

Cell Reports

Article

C-Terminal Motifs of the MTW1 Complex Cooperatively Stabilize Outer Kinetochore Assembly in Budding Yeast

Graphical Abstract

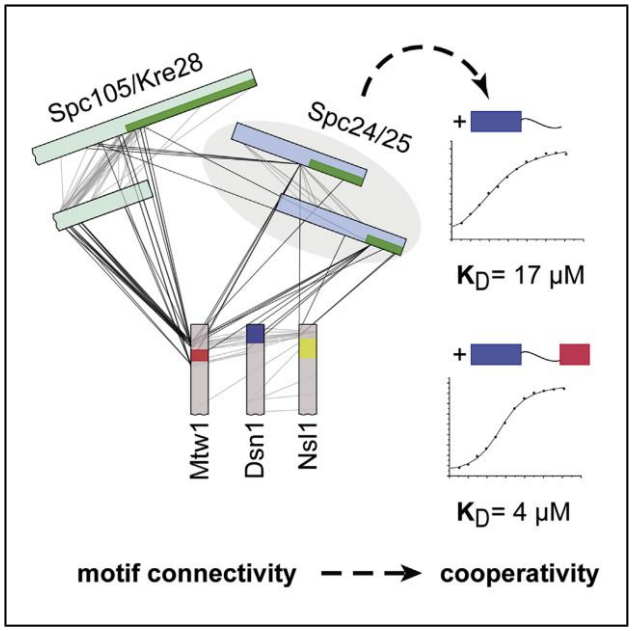

Authors

Medini Ghodgaonkar-Steger, Mia Potocnjak, Tomasz Zimniak, ..., David Jan Drexler, Gregor Witte, Franz Herzog

Correspondence

herzog@genzentrum.lmu.de

In Brief

The kinetochore links chromosomes to spindle microtubules and has to withstand the pulling forces of depolymerizing microtubules to segregate chromosomes during cell division. Using chemical crosslinking and mass spectrometry, Ghodgaonkar-Steger et al. identify the protein motifs that cooperatively stabilize the 10-subunit outer kinetochore network that forms the microtubule binding site.

Highlights

- XL-MS of native kinetochore complexes identifies KMN subunit connectivity in yeast
- Two C-terminal MTW1 subunit motifs recruit SPC105 complex through Kre28
- C-terminal MTW1 motifs cooperatively stabilize the KMN network
- Cooperative assembly of the KMN network is enhanced by NDC80-SPC105 association

Ghodgaonkar-Steger et al., 2020, Cell Reports *32*, 108190
September 29, 2020
https://doi.org/10.1016/j.celrep.2020.108190

Cell Reports

CellPress
OPEN ACCESS

Article

C-Terminal Motifs of the MTW1 Complex Cooperatively Stabilize Outer Kinetochore Assembly in Budding Yeast

Medini Ghodgaonkar-Steger,[1,2] Mia Potocnjak,[1,2] Tomasz Zimniak,[1] Josef Fischböck-Halwachs,[1] Victor Solis-Mezarino,[1] Sylvia Singh,[1] Tea Speljko,[1] Götz Hagemann,[1] David Jan Drexler,[1] Gregor Witte,[1] and Franz Herzog[1,3,*]

[1]Gene Center Munich and Department of Biochemistry, Ludwig-Maximilians-Universität München, Feodor-Lynen-Str. 25, 81377 Munich, Germany
[2]These authors contributed equally
[3]Lead Contact
*Correspondence: herzog@genzentrum.lmu.de
https://doi.org/10.1016/j.celrep.2020.108190

SUMMARY

Kinetochores are macromolecular protein assemblies at centromeres that mediate accurate chromosome segregation during cell division. The outer kinetochore KNL1^{SPC105}, MIS12^{MTW1}, and NDC80^{NDC80} complexes assemble the KMN network, which harbors the sites of microtubule binding and spindle assembly checkpoint signaling. The buildup of the KMN network that transmits microtubule pulling forces to budding yeast point centromeres is poorly understood. Here, we identify 225 inter-protein crosslinks by mass spectrometry on KMN complexes isolated from *Saccharomyces cerevisiae* that delineate the KMN subunit connectivity for outer kinetochore assembly. C-Terminal motifs of Nsl1 and Mtw1 recruit the SPC105 complex through Kre28, and both motifs aid tethering of the NDC80 complex by the previously reported Dsn1 C terminus. We show that a hub of three C-terminal MTW1 subunit motifs mediates the cooperative stabilization of the KMN network, which is augmented by a direct NDC80-SPC105 association.

INTRODUCTION

In eukaryotes, the kinetochore mediates the faithful distribution of the genetic material to daughter cells during each cell division. The kinetochore is a macromolecular protein complex that assembles at specialized chromatin regions called centromeres and connects chromosomes to spindle microtubules. In budding yeast, the kinetochore is built on point centromeres, a specific DNA sequence of ~125 bp wrapped around a single Cse4-containing nucleosome, the budding yeast ortholog of the human histone H3 variant CENP-A (the human orthologs are superscripted if appropriate). By contrast, the human kinetochore is assembled on regional centromeres that span over megabases of DNA containing ~200 CENP-A nucleosomes (Bodor et al., 2014; Pluta et al., 1995). The core structure and function of the kinetochore are largely conserved between budding yeast and humans but differ in terms of complexity and size (Cheeseman and Desai, 2008; Joglekar et al., 2009; Santaguida and Musacchio, 2009; van Hooff et al., 2017). The kinetochore architecture can be subdivided into the outer kinetochore that constitutes the microtubule binding interface and the inner kinetochore that is assembled at centromeric chromatin by the constitutive centromere-associated network (CCAN) or CTF19 complex (CTF19c) in budding yeast (Cheeseman and Desai, 2008).

The essential inner kinetochore proteins Mif2^{CENP-C} and Ame1/Okp1 bind to the C- and N-terminal domains of Cse4^{CENP-A} (Anedchenko et al., 2019; Fischboeck et al., 2018; Westermann et al., 2003; Xiao et al., 2017), respectively, and to the MTW1^{MIS12} complex (Dimitrova et al., 2016; Przewloka et al., 2011; Screpanti et al., 2011), serving as direct links between the outer kinetochore and the centromeric nucleosome.

In all eukaryotes, the outer kinetochore is built up by the 10-subunit KMN network that is assembled by three distinct subcomplexes: the SPC105^{KNL1} complex including the subunits Spc105^{KNL1} and Kre28^{ZWINT}; the MTW1^{MIS12} complex (MTW1c^{MIS12c}) comprising the subunits Mtw1^{MIS12}, Dsn1^{DSN1}, Nsl1^{NSL1}, and Nnf1^{PMF1}; and the NDC80^{NDC80} complex composed of Ndc80^{NDC80}, Nuf2^{NUF2}, Spc24^{SPC24}, and Spc25^{SPC25}.

The NDC80c contributes the essential microtubule binding activity of the KMN network (Cheeseman et al., 2006; Ciferri et al., 2008; Wei et al., 2007) constituted by two calponin homology domains in Ndc80 and Nuf2 and the basic Ndc80 N-terminal tail (Guimaraes et al., 2008; Miller et al., 2008). At the opposite end, RWD (RING finger- and WD-repeat-containing proteins and DEAD-like helicases) domains within the Spc24/25 dimer mediate kinetochore targeting of the microtubule-binding subunits through their interaction with the MTW1c^{MIS12c} (Malvezzi et al., 2013; Petrovic et al., 2010). Ndc80 also binds the yeast-specific DASH/Dam1 complex, which is an essential microtubule-binding complex in budding yeasts (Cheeseman et al., 2001; De Wulf et al., 2003; Westermann et al., 2006; Lampert et al., 2013).

Crystal structures of human (Petrovic et al., 2016) and *Kluyveromyces lactis* (Dimitrova et al., 2016) MTW1^{MIS12} complexes show that its four subunits are assembled as two heterodimers whose C and N termini are organized at opposite ends. The N-terminal head domain formed by Mtw1^{MIS12} and Nnf1^{PMF1} interacts with the N termini of Mif2^{CENP-C} (Petrovic et al., 2016; Przewloka et al., 2011; Screpanti et al., 2011) and Ame1 (Dimitrova et al., 2016; Hornung et al., 2011). Biochemical data showed that the C terminus of Dsn1 is required for recruiting the NDC80c (Dimitrova et al., 2016; Kudalkar et al., 2015; Malvezzi et al., 2013) in budding yeasts and that the C termini of Mtw1 and Nsl1 aid in stabilizing this interaction (Kudalkar et al., 2015). Crystal structures of the Dsn1 peptide or a Cnn1 helical peptide in complex with the globular Spc24/25 RWD domains revealed the same binding mode of these two NDC80c recruiters (Bock et al., 2012; Dimitrova et al., 2016; Malvezzi et al., 2013; Schleiffer et al., 2012; Wei et al., 2006). Similarly, the human ortholog of Cnn1, CENP-T, has been identified as docking site for the NDC80c (Gascoigne et al., 2011; Nishino et al., 2013). The role of Cnn1 in bridging NDC80c to the centromere becomes crucial in cells where the MTW1c function is compromised (Hornung et al., 2014; Lang et al., 2018; Rago et al., 2015).

A comparison of the reported protein contacts linking the subcomplexes of the KMN network in humans and budding yeast indicates similarities and differences in assembly that are largely based on the varying length and sequences of the C-terminal tails extending from the coiled-coil (CC) shaft of the orthologous MTW1c^{MIS12c} subunits (Dimitrova et al., 2016; Petrovic et al., 2010, 2014, 2016). In humans, two motifs within the C-terminal NSL1 tail, which are not conserved in budding yeast, are required for binding the NDC80c and KNL1c. The C-terminal NSL1$^{258–281}$ motif was sufficient to establish a tight interaction with the homodimeric RWD domains of KNL1 (Petrovic et al., 2010, 2014) in the absence of its binding partner ZWINT, whereas the PVIHL motif (NSL1$^{209–213}$) is necessary for binding NDC80c, but a high-affinity MIS12c-NDC80c interaction likely requires additional contacts (Petrovic et al., 2010).

The Spc105^{KNL1} N terminus serves as an assembly platform for spindle checkpoint proteins (London et al., 2012; Shepperd et al., 2012; Yamagishi et al., 2012), but how the SPC105c is recruited to the KMN network in *Saccharomyces cerevisiae* has not yet been addressed.

The inability to capture flexible and disordered regions and the difficulty to analyze full-length assemblies larger than individual subcomplexes have limited a comprehensive description of the kinetochore architecture. The mass spectrometric identification of chemical crosslinks (XL-MS) has been developed to study the protein connectivity of native or *in vitro*-reconstituted protein complexes (Herzog et al., 2012; Walzthoeni et al., 2012).

We present a comprehensive protein connectivity map of the native budding yeast outer kinetochore. The detection of several crosslinks to the Mtw1 C terminus indicates the importance of this region and identifies a predicted helical motif. We show that the C-terminal helical motifs of Mtw1 and Nsl1 synergistically interact with the Spc105/Kre28 complex, whereas the Spc24/25 heterodimer is recruited through association with the Dsn1, Nsl1, and Mtw1 C termini. Moreover, we demonstrate *in vitro* that, in contrast to humans, the C-terminal homodimeric RWD domains of Spc105 are dispensable for the recruitment of the SPC105c to the KMN network and that this interaction is mediated, in part, through the predicted CC domain of Kre28. Our *in vitro* reconstitution assays identify the molecular basis of the cooperative assembly of the SPC105c and NDC80c onto the MTW1c C termini that is further stabilized by a weak SPC105c-NDC80c association.

RESULTS

A Protein Connectivity Map of the KMN Network

To obtain a complete map of protein-protein contacts of the budding yeast outer kinetochore, we performed large-scale purifications of endogenously 6xHis-6xFLAG-tagged kinetochore proteins from *S. cerevisiae* (Figure 1A; Table S1). The quantitative mass spectrometric analysis of the Dsn1 purification yielded a nearly stoichiometric 10-subunit KMN network (Akiyoshi et al., 2010), low abundant CTF19 subcomplexes such as COMA (Ctf19/Okp1/Mcm21/Ame1) (Hornung et al., 2014), and subunits of the DASH/Dam1 complex. Isolation of Cnn1 and Wip1 coprecipitated Mcm16/Ctf3/Mcm21, Chl4/Iml3, and COMA complexes, whereas the KMN subunits were predominantly low abundant (Figure 1A). In reciprocal purifications of Mcm16 and Ctf3, the CTF19 subcomplexes Cnn1/Wip1, COMA, and Chl4/Iml3 were enriched over the KMN proteins, in agreement with previous studies indicating that direct interaction with Mcm16/Ctf3/Mcm21$^{CENP-H/I/K}$ anchors Cnn1/Wip1$^{CENP-T/W}$ through Chl4/Iml3$^{CENP-N/L}$ at the inner kinetochore and that Mcm16/Ctf3/Mcm21$^{CENP-H/I/K}$ has a direct role in recruiting NDC80c in a Cnn1^{CENP-T}-dependent manner (Basilico et al., 2014; Kim and Yu, 2015; Pekgöz Altunkaya et al., 2016).

In order to map the protein connectivity, we performed XL-MS analysis of the purified native kinetochore complexes. In total, we identified 225 inter-protein and 237 intra-protein crosslinks on the KMN network and its associated CTF19c subunits (Figure 1B; Tables S4 and S5). The majority of the detected crosslinks in our native kinetochore network is in agreement with previous studies (Hornung et al., 2011, 2014; Kudalkar et al., 2015; Maskell et al., 2010). Crosslinks between Mcm16/Ctf3/Mcm21 and Cnn1 correspond to crosslinks recently reported on *in vitro*-reconstituted complexes (Pekgöz Altunkaya et al., 2016) and are consistent with the structure of the Spc24/25 RWD dimer bound to the Cnn1$^{60–84}$ N-terminal peptide (Lang et al., 2018; Malvezzi et al., 2013; Schleiffer et al., 2012). The crosslink-derived restraints are also in agreement with the crystal structure of the *K. lactis* MTW1c (Dimitrova et al., 2016) and indicate that the C termini of Mtw1, Nsl1, and Dsn1 are in close proximity, forming a hub of tightly aligned helical motifs (Figures 1B and 2A). In particular, our connectivity map pinpointed the Mtw1 C terminus as the central site for building up the KMN network. Several crosslinks in the Mtw1 C terminus indicated that Spc105/Kre28 is recruited through the C-terminal part of Spc105 and the predicted CC of Kre28 and that NDC80c is bound through the RWD domains of Spc24/25 (Kudalkar et al., 2015) (Figure 1B; Tables S4 and S5).

Furthermore, we recombinantly expressed the 10-subunit KMN network from a single baculovirus in insect cells (Weissmann et al., 2016) and purified a stoichiometric KMN super-complex to homogeneity (Figure S1A). The XL-MS analysis of the

CellPress
OPEN ACCESS

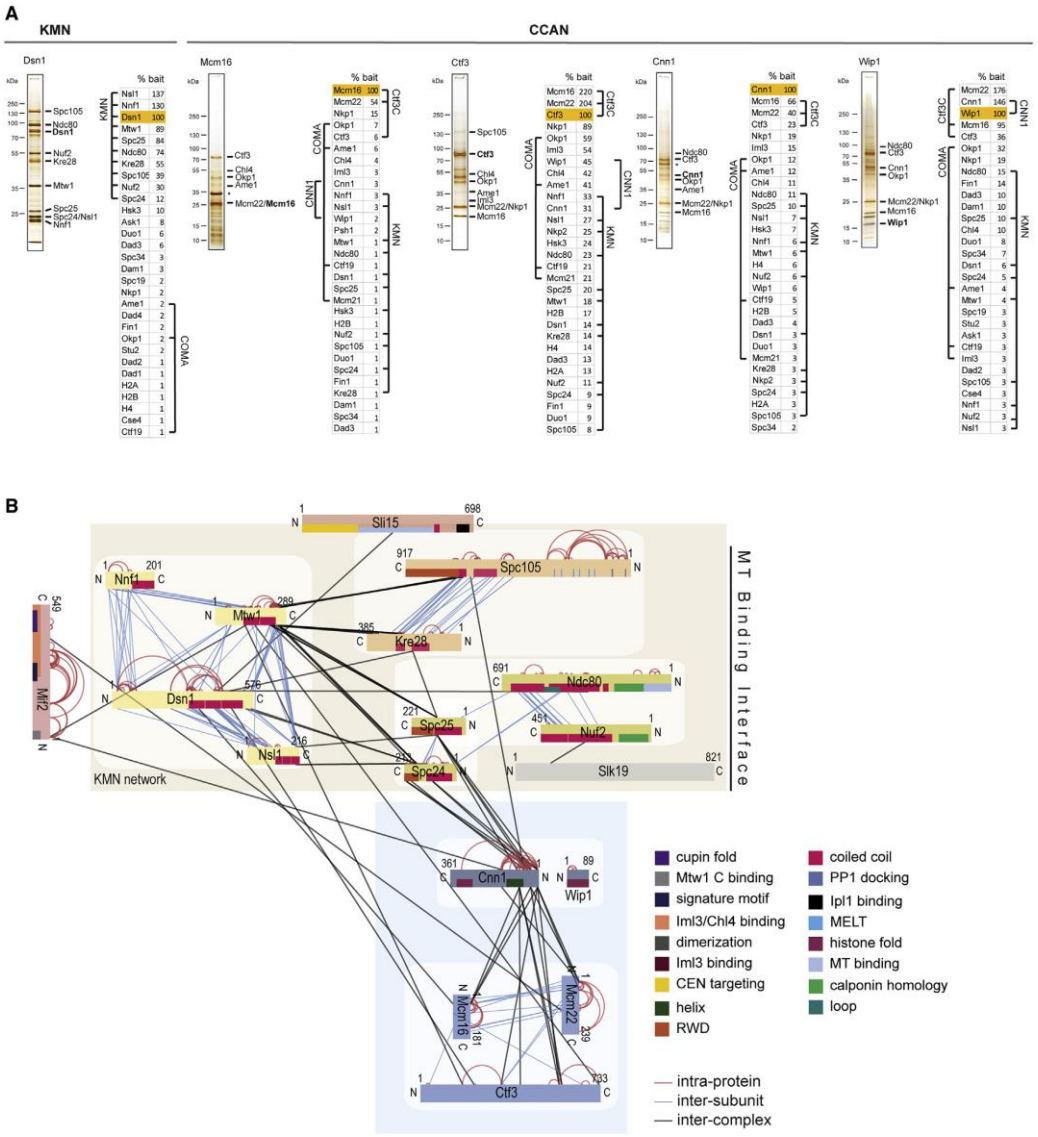

Figure 1. Subunit Connectivity of the Native Budding Yeast Outer Kinetochore Based on Crosslink-Derived Spatial Restraints

(A) The indicated kinetochore proteins were endogenously 6xHis-6xFLAG tagged and affinity purified using anti-FLAG magnetic beads from yeast cell extracts. The eluted proteins were visualized by SDS-PAGE and silver staining and subjected to mass spectrometric analysis before and after crosslinking. Protein intensities detected by mass spectrometry were normalized to the bait, and their relative abundance to the bait is indicated. Proteins were annotated on the SDS-PAGE, with asterisk (*) indicating contaminants.

(B) Schematic representation of 225 inter-protein and 238 intra-protein crosslinks (Table S4) identified on 5 different kinetochore subcomplexes (shown in A) delineated the protein connectivity of the KMN network and its interactors. Proteins are represented as bars indicating annotated domains according to a color scheme (Table S5), and subunits of a complex are shown in the same color. Protein lengths and crosslink sites are scaled to the amino acid sequence.

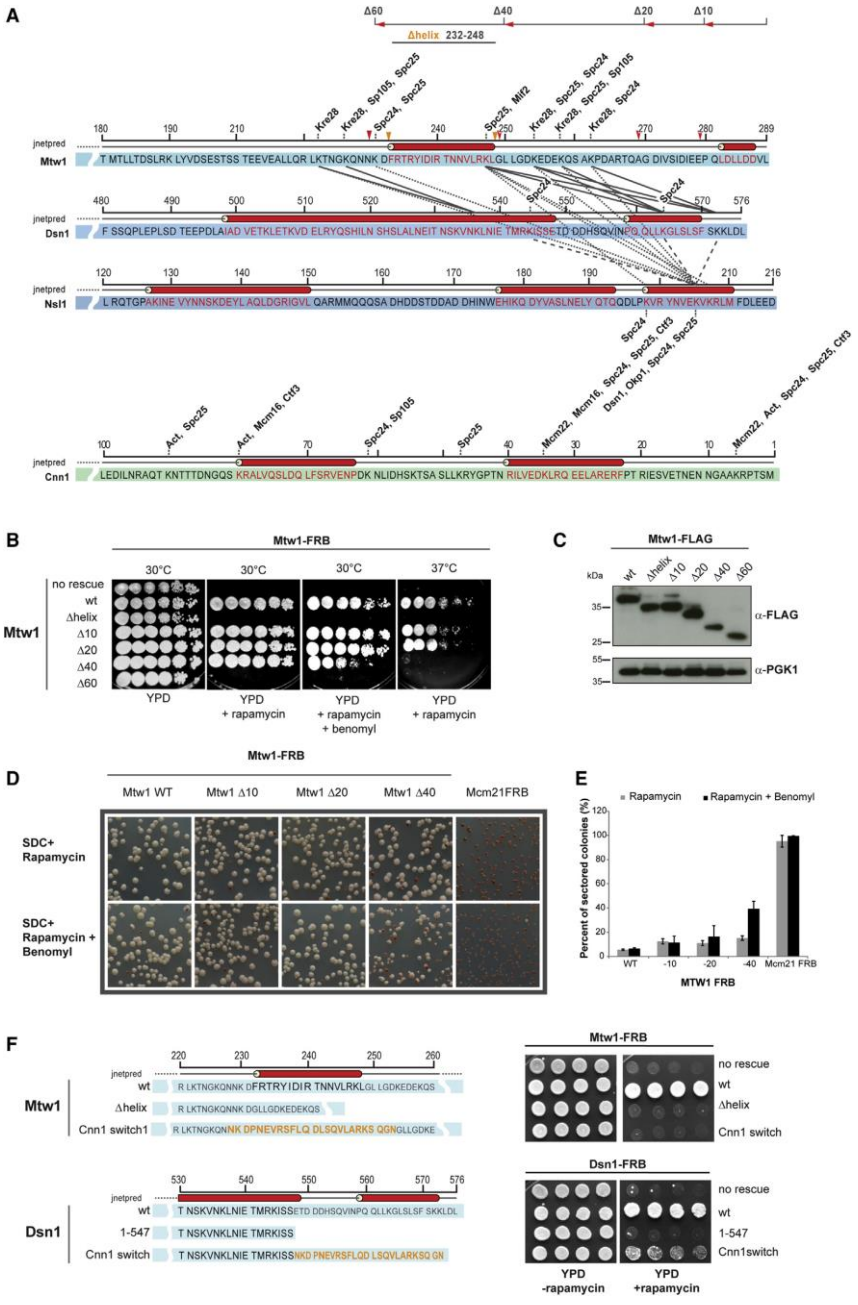

(legend on next page)

recombinant KMN network identified 191 inter-protein crosslinks (Figure S1B; Table S6) that confirmed the crosslinks on the native KMN network preparations but showed additional restraints connecting the C-terminal CC domain of Spc105 to the CCs of Ndc80 and Spc24/25.

Multiple C Termini of the MTW1 Complex Create a Hub for the KMN Network Assembly

Inter-protein crosslinks between the C termini of Mtw1, Dsn1, and Nsl1 are collinear, suggesting that the tails are aligned and protrude from one end of the MTW1c CC shaft (Dimitrova et al., 2016) (Figure 2A). Consistent with previous reports, we observed crosslinks from the C termini of Dsn1 and Nsl1 to lysine residues in the globular heads and the following CC extensions of Spc24/25. Crosslinks from Dsn1 and Nsl1 as well as from Spc24/25 and Spc105/Kre28 intersected close to a region of Mtw1 (residues 232–248) predicted to be a short helix (Figure 2A; Figure S2A). The flanking sequences of this putative Mtw1 helix were crosslinked to lysine residues within the CC domains of Spc105/Kre28 and Spc24/25 (Figures 1B and 2A; Table S4). The SPC105c was not crosslinked to the Nsl1 C terminus, which has been previously shown to tether KNL1c to the human KMN network (Petrovic et al., 2010, 2014). Nine crosslinks between the Cnn1 N terminus and Spc24/25 were validated by previous studies showing that Cnn1 competes with Dsn1 for Spc24/25 binding (Bock et al., 2012; Malvezzi et al., 2013; Schleiffer et al., 2012) and is the major site of Spc24/25 interaction (Figure 2A). Notably, a crosslink between the Cnn1 N terminus and the Spc105 CC region (residues 551–711) indicated a putative association of Cnn1 with the SPC105c.

Our XL-MS data suggest that helical motifs within the C termini of Mtw1, Dsn1, and Nsl1 are tightly aligned, providing a hub for interactions in order to cooperatively stabilize the KMN assembly.

The Short Helical Motif in the Mtw1 C Terminus Is Essential for Cell Survival

To address whether Mtw1 has a unique role in KMN assembly, we generated Mtw1 mutants lacking the helical motif (Mtw1-Δhelix or Mtw1Δ232–248) or the C-terminal 20, 40, or 60 amino acids (aa; Mtw1Δ20, Mtw1Δ40, or Mtw1Δ60, respectively). As the deletion of Mtw1 is lethal in budding yeast (Goshima and Yanagida, 2000), we used the anchor-away technique to conditionally remove the endogenous Mtw1-FRB from the nucleus by addition of rapamycin (Haruki et al., 2008) and ectopically express Mtw1 wild-type or mutant rescue alleles. The lethal phenotype could be rescued by expression of Mtw1 wild type (Figure 2B), and C-terminal truncations lacking up to 40 amino acids (Mtw1Δ10, Mtw1Δ20, and Mtw1Δ40) did not affect cell growth at 30°C. However, the expression of Mtw1Δ60 and Mtw1Δhelix did not rescue the lethal phenotype, indicating that the helical motif Mtw1$^{232–248}$ is essential for cell viability (Figures 2B and 2C). The Mtw1Δ40 mutant showed benomyl sensitivity and a temperature-sensitive growth defect at 37°C. To further corroborate the phenotype of the Mtw1Δ40 mutant, we performed a minichromosome loss assay (Figures 2B and 2D) (Hieter et al., 1985) by transforming an Mtw1 anchor-away strain with various Mtw1 rescue constructs and a centromeric plasmid carrying the SUP11 gene as a marker, which indicates minichromosome loss through red pigmentation. Whereas the Mtw1Δ10, Mtw1Δ20, and Mtw1Δ40 mutants showed only a minor increase in segregation defects compared with the wild-type Mtw1 on normal growth medium, the rate of missegregation was increased 5-fold for Mtw1Δ40 on benomyl-containing plates (Figures 2D and 2E). This indicated the functional relevance of amino acids 250–269 for the Mtw1 C terminus.

Dsn1 and Cnn1 have been shown to compete for the same binding site on the heterodimeric RWD domains of Spc24/25 (Bock et al., 2012; Malvezzi et al., 2013; Schleiffer et al., 2012). The short helices of Dsn1$^{560–571}$ and Cnn1$^{65–79}$ (Figure S2A) insert into the same hydrophobic cleft of the Spc24/25 RWD dimer (Dimitrova et al., 2016; Malvezzi et al., 2013). Moreover, a helix-switch assay substituting the last 29 amino acids of Dsn1 with the Cnn1$^{65–84}$ helical motif rescued cell death upon deletion of the Dsn1 C terminus (Dsn1$^{1–547}$) (Malvezzi et al., 2013). Similarly, we investigated whether substitution of the Mtw1$^{232–248}$ helix with the Cnn1$^{60–84}$ peptide rescued lethality of the Mtw1Δhelix mutant (Figure 2F). Replacing the Mtw1 residues 229–248 with Cnn1$^{60–84}$ did not rescue the growth defect, whereas the C-terminal fusion of Cnn1$^{60–84}$ to Dsn1$^{1–547}$ could partially rescue the lethal phenotype of Dsn1$^{1–547}$ (Figure 2F) (Malvezzi et al., 2013). This result indicated that the Mtw1 and Dsn1 helices execute non-redundant functions. The fact that substitution of the Mtw1$^{232–248}$ helix by Cnn1$^{60–84}$ was lethal suggested that the binding partner or site is different to that of the Dsn1 and Cnn1 helical peptides.

Deletion of the Mtw1$^{232–248}$ Helix Affects the Assembly of the Outer and Inner Kinetochore

Our XL-MS and *in vivo* experiments suggested that the Mtw1$^{232–248}$ helix mediated association of the NDC80c and SPC105c. To address the contribution of the Mtw1$^{232–248}$ helix to kinetochore assembly in the cell, we affinity purified

Figure 2. C-Terminal Motifs of the MTW1c Establish a Hub for the KMN Network Assembly

(A) Schematic representation of inter-protein crosslinks detected on the C-terminal tails of Mtw1, Dsn1, and Nsl1 and N-terminal tail of Cnn1. Predicted helical motifs are shown as red cylinders. Crosslinks from Dsn1 to Mtw1, from Nsl1 to Mtw1, or from Dsn1 to Nsl1 are indicated by bold, dotted, or dashed lines, respectively. Crosslinks from MTW1c subunits to other kinetochore proteins are indicated by black dotted vertical lines.

(B) Analysis of Mtw1 C-terminal deletion mutants in cell viability assays using the anchor-away technique. Mtw1-FRB strains harboring the indicated rescue alleles were spotted in serial dilutions on YPD, YPD + rapamycin, or YPD + rapamycin + benomyl plates and incubated at 30°C or 37°C.

(C) Western blot analysis of immunoprecipitated Mtw1-1xFLAG showed expression levels of the wild-type and mutant proteins. Pgk1 served as a loading control.

(D) Analysis of chromosomal segregation defect using a sectoring assay. MTW1 anchor-away strains were plated on synthetic defined complete media (SDC) + rapamycin or SDC + rapamycin + benomyl and grown at 30°C. A Mcm21-FRB strain served as a positive control.

(E) Quantification of the segregation assay performed in (D) displayed as mean ± standard deviation (SD) of 3 replicates.

(F) Growth assay analyzing the phenotype of the Mtw1/Cnn1 switch mutant where the Mtw1$^{232–248}$ helix was replaced by the Cnn1$^{60–84}$ helix in comparison with the previously published Dsn1 switch mutant (Malvezzi et al., 2013).

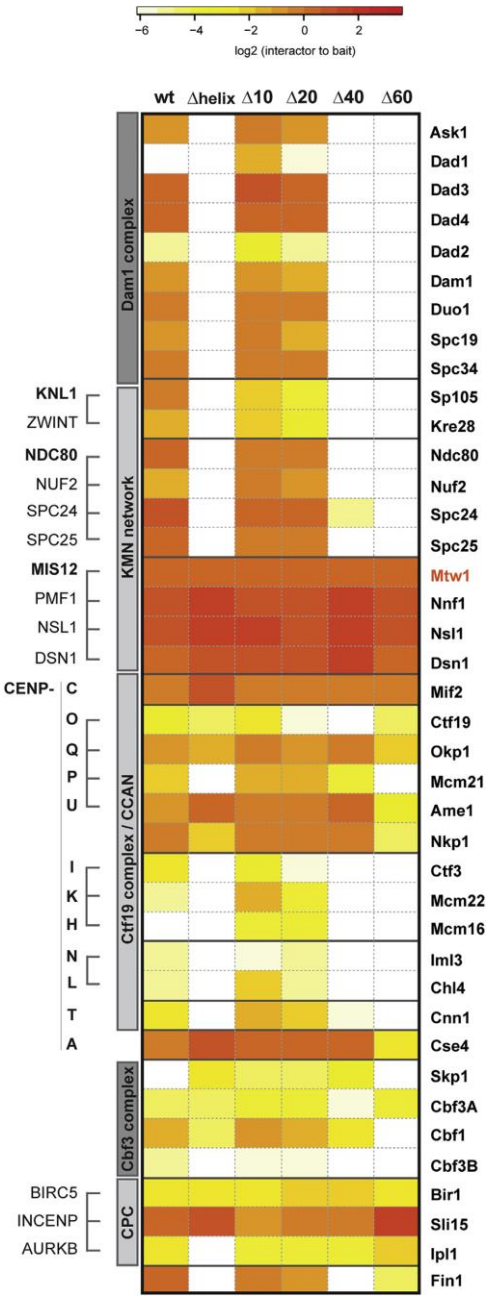

Figure 3. The Mtw1 C-Terminal Helix Is Critical for Outer Kinetochore Assembly

The heatmap summarizes the relative abundances of kinetochore proteins that copurified with the Mtw1 full-length (Kudalkar et al., 2015), the C-terminally truncated Mtw1 (Δ10, Δ20, Δ40, and Δ60), and the Mtw1Δhelix (Δ232–248) mutants. The 1xFLAG-tagged Mtw1 proteins were ectopically expressed in the Mtw1-FRB anchor-away background and purified from exponentially grown cells. Copurifying protein complexes were analyzed by mass spectrometry, and protein raw intensities were $\log_2$ transformed and normalized to the Mtw1 wild-type intensity. The mean of these ratios from 4 biological replicates is displayed according to the color scale.

ectopically expressed 1xFLAG-tagged Mtw1 wild-type and mutant (Mtw1Δ10, Mtw1Δ20, Mtw1Δ40, Mtw1Δ60, and Mtw1-Δhelix$^{232–248}$) proteins from whole-cell extracts and analyzed the complex composition by quantitative mass spectrometry (Figure 3). The Mtw1 mutant proteins did not affect formation of the tetrameric MTW1c and copurified similar levels of Mif2, Cse4, and subunits of the COMA complex. Truncation of the C-terminal 10 or 20 amino acids did not alter association of Mtw1 with kinetochore proteins. By contrast, the Mtw1-Δhelix$^{232–248}$, Mtw1Δ40, and Mtw1Δ60 mutants abrogated the interactions with the SPC105, NDC80, and DASH/Dam1 complexes and also affected the levels of the coprecipitated Mcm16/Ctf3/Mcm22 and Chl4/Iml3 complexes and of Cnn1. This is consistent with the finding that loss of NDC80c might destabilize Mcm16/Ctf3/Mcm22 and consequently affect the levels of associated Chl4/Iml3 and Cnn1 at the kinetochore (Basilico et al., 2014; Hinshaw and Harrison, 2019; Kim and Yu, 2015; Pekgöz Altunkaya et al., 2016). Although the helix$^{232–248}$ was present in the Mtw1Δ40 protein, the deletion of flanking C-terminal residues might compromise its integrity or weaken the interaction of NDC80c and SPC105c; thus, only residual levels of Spc24 were retained under the purification conditions. In summary, the Mtw1$^{232–248}$ helix is essential for the endogenous assembly of the KMN network and consequently may contribute to the cooperative stabilization of CTF19c subcomplexes at the kinetochore.

The Mtw1$^{232–248}$ Helical Peptide Is Required for the Interaction with the NDC80 and SPC105 Complexes

The crosslinking data identified several contacts between the Mtw1 C terminus and Spc105/Kre28 (Figures 1B and 2A), suggesting that it might be involved in recruiting Spc105/Kre28 to the KMN network. We performed peptide binding assays using a panel of Strep-tagged Cnn1$^{60–84}$, Mtw1$^{228–252}$, Dsn1$^{548–576}$, Nsl1$^{163–192}$, and Nsl1$^{183–216}$ helical peptides (Table S3) as baits in pull-down assays with recombinant Spc24/25 or Spc105/Kre28 complexes (Figure 4). Spc24/25 interacted with the Cnn1$^{60–84}$, Mtw1$^{228–252}$, and Dsn1$^{548–576}$ peptides. The Cnn1$^{60–84}$ peptide retained the highest levels of Spc24/25, which were significantly reduced for the Dsn1$^{548–576}$ and Mtw1$^{228–252}$ peptides. The two Nsl1 peptides Nsl1$^{163–192}$ and Nsl1$^{183–216}$ included the two C-terminal helical motifs of Nsl1 (Figure S2A). In our *in vitro* binding assay neither of the two Nsl1 peptides showed detectable binding of the Spc24/25 complex. An equimolar mixture of the Mtw1$^{228–252}$ and Dsn1$^{548–576}$ peptides retained higher levels of the Spc24/25 complex than achieved

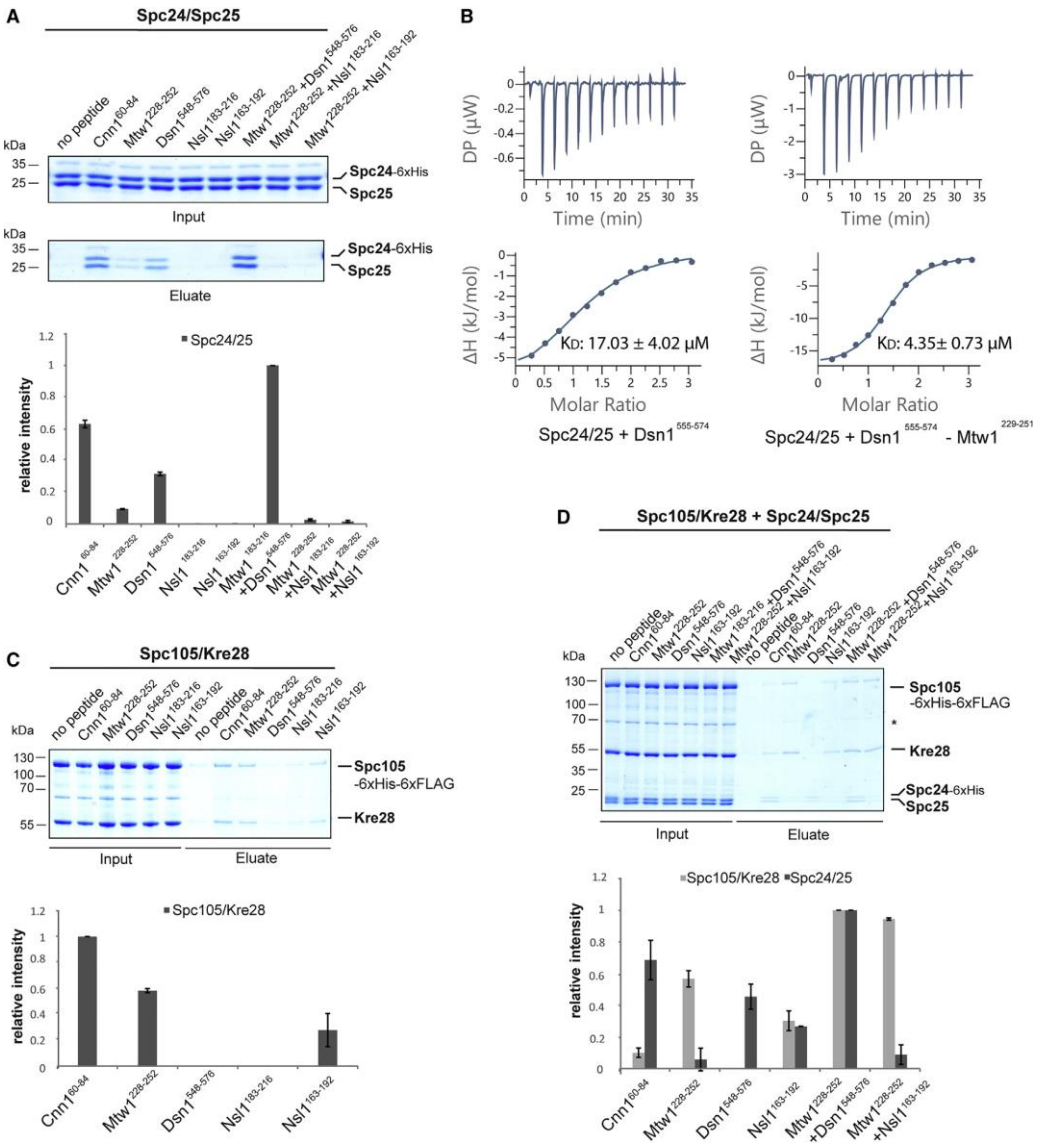

Figure 4. Motifs within the Mtw1, Dsn1, and Nsl1 C Termini and the Cnn1 N Terminus Show Different Relative Binding Affinities to Spc24/25 and Spc105/Kre28 Complexes *in Vitro*

(A) *In vitro* binding assay of Mtw1$^{228–252}$, Cnn1$^{60–84}$, Dsn1$^{548–576}$, Nsl1$^{183–216}$, or Nsl1$^{163–192}$ peptides to the Spc24/25 heterodimer. The 1xStrep-tagged peptides (Table S3) were incubated with recombinant Spc24/25 or Spc105/Kre28 at a molar ratio of 25:1. Bound complexes were isolated and eluted proteins were visualized by SDS-PAGE and Coomassie staining, respectively.

(B) Isothermal titration calorimetry with 51 μM Spc24-His/25 and 800 μM Dsn1$^{555–574}$ or Dsn1$^{555–574}$-Mtw1$^{229–251}$ peptide (Table S3).

(C) *In vitro* binding assay of Mtw1$^{228–252}$, Cnn1$^{60–84}$, Dsn1$^{548–576}$, Nsl1$^{183–216}$, or Nsl1$^{163–192}$ peptides to the Spc105/Kre28 complex analyzed as described in (A).

(legend continued on next page)

with the Dsn1$^{548–576}$ peptide alone, indicating an additive effect of Mtw1$^{228–252}$ and Dsn1$^{548–576}$ on the Spc24/25 interaction (Figure 4A). Accordingly, isothermal titration calorimetry (ITC) experiments of the Spc24/25 complex with the Dsn1$^{555–574}$ peptide alone or fused to the Mtw1$^{229–251}$ peptide (Table S3) resulted in an apparent dissociation constant (K_D) of 17.03 and 4.35 μM (Figure 4B), respectively. This confirmed the synergistic effect of both motifs on recruiting the NDC80c and is consistent with the observation that Cnn1 inhibits this interaction (Bock et al., 2012), as Cnn1$^{60–84}$ and Cnn1$^{1–270}$ showed a K_D value of 3.50 and 0.016 μM with Spc24/25, respectively (Malvezzi et al., 2013).

Recombinant Spc105/Kre28 was pulled down by the Cnn1$^{60–84}$ and Mtw1$^{228–252}$ peptides and was retained by the Nsl1$^{163–192}$ peptide to just above background levels (Figure 4C). In the presence of both Spc24/25 and Spc105/Kre28, Cnn1$^{60–84}$ exhibited higher relative affinity to Spc24/25, while Mtw1$^{228–252}$ preferentially bound Spc105/Kre28 (Figure 4D). Dsn1$^{548–576}$ exclusively isolated the Spc24/25 complex, and the equimolar mixture of Mtw1$^{228–252}$ and Dsn1$^{548–576}$ retained a nearly stoichiometric super-complex of Spc24/25 and Spc105/Kre28 at levels higher than pulled down by the individual peptides, suggesting a cooperative stabilization induced by the presence of the Mtw1$^{228–252}$ and Dsn1$^{548–576}$ peptides.

The Nsl1$^{163–192}$ peptide selectively bound Spc105/Kre28 and the mixture of Nsl1$^{163–192}$ and Mtw1$^{228–252}$ showed an increased relative affinity toward Spc105/Kre28, suggesting that Nsl1$^{163–192}$ cooperatively stabilized the Mtw1$^{228–252}$-Spc105/Kre28 interaction. This peptide binding assay indicated that the Mtw1$^{228–252}$ helical motif cooperatively stabilized the interactions of Dsn1$^{548–576}$ with the NDC80c and of Nsl1$^{163–192}$ with the SPC105c, which suggested that the Mtw1$^{228–252}$ helix is part of the interfaces for tethering NDC80c and SPC105c and that even at the level of isolated motifs the Mtw1$^{228–252}$ helix induces cooperative stabilization of the KMN network.

Cooperativity of Intra- and Inter-subcomplex Contacts Stabilizes the KMN Network

To investigate the recruitment of the NDC80c and SPC105c in the context of the full-length tetrameric MTW1c, we purified wild-type MTW1c composed of Mtw1, Nnf1, Nsl1, and 6xHis-1xStrep-Dsn1$^{171–576}$ (Hornung et al., 2011) and three mutant MTW1 complexes, including Mtw1Δhelix$^{232–248}$, Mtw1Δ60, and Dsn1$^{171–547}$, lacking the C-terminal 20 amino acids required for its interaction with Spc24/25 (Malvezzi et al., 2013). The recombinant MTW1 complexes were immobilized on streptavidin beads and incubated either with Spc24/25 or Spc105/Kre28, or both (Figure 5A). In agreement with the peptide binding assay, only the Mtw1 wild-type complex interacted with Spc24/25 (Figures 4A and 4C and 5A) (Dimitrova et al., 2016; Malvezzi et al., 2013). Notably, the Mtw1 helix motif was necessary for the interaction, as its deletion also abrogated Spc24/25 binding. Next, we addressed the requirement of the Mtw1 C terminus or Dsn1 C terminus for Spc105/Kre28 binding. Deletion of the Mtw1$^{232–248}$ helix reduced the isolated Spc105/Kre28 levels by more than half (Figures 5A and 5B), and truncation of the C-terminal 60 amino acids reduced Spc105/Kre28 to background levels.

In competitive binding assays in the presence of both Spc24/25 and Spc105/Kre28, we consistently observed a 2-fold increase in the bound Spc105/Kre28 levels (Figures 5A and 5B). Whether SPC105c and NDC80c interact in the absence of the MTW1c is unknown. We detected a crosslink between lysine-118 of Spc25 and lysine-199 of Kre28 in the native KMN network (Figure 1B; Table S4) and two and three crosslinks from recombinant Spc24 and Spc25, respectively, to Spc105 (Figure S1B; Table S6), which connected the CCs flanking the C-terminal RWD domains (Figure S2B) (Petrovic et al., 2014). Together with the two crosslinks between the CC regions of Ndc80 and Spc105 (Figure S1B; Table S6), these restraints suggested a direct association of the CC in Spc105/Kre28 and NDC80c. SEC and *in vitro* binding experiments indicated a weak Spc105/Kre28-Spc24/25 interaction by a shift of the Spc24/25 peak fraction in the presence of the Spc105/Kre28 complex (Figures S3A and S3B).

The *in vitro* binding assays using the wild-type and mutant MTW1c were in agreement with the peptide binding experiments and demonstrated the requirement of the putative Mtw1$^{232–248}$ helix for recruiting NDC80c and SPC105c and indicated cooperative stabilization of the KMN network through direct binding of NDC80c to SPC105c.

The Mtw1 Helix Residues 244–248 Mediate the Interaction with Spc24/25

To further narrow down the binding site of Spc105/Kre28 and Spc24/25 on the Mtw1$^{232–248}$ helix, we performed a multiple sequence alignment of the helix region from interrelated budding yeasts (Figure 5C). Based on this analysis, we generated point mutants of residues in either half of the helix (MTW1cMtw1$^{F232D/Y236D}$, MTW1cMtw1$^{R233D/Y236D}$, MTW1cMtw1$^{V244D/L248D}$) (Figures 5C–5F). In *in vitro* binding assays, the MTW1cMtw1$^{F232D/Y236D}$ mutant still bound Spc24/25 but showed reduced levels of associated Spc105/Kre28 (Figures 5D and 5E). In comparison, MTW1cMtw1$^{R233D/Y236D}$ retained similar levels of Spc105/Kre28 but showed further reduction of the bound Spc24/25 complex. Both the Mtw1Δhelix (Figures 5A and 5B) and the helix double point mutations showed more than 60% reduction in the Spc105/Kre28 binding compared with wild-type MTW1c, indicating that additional contacts may contribute to the cooperative stabilization. Notably, the two point mutations in the second helix half, Mtw1$^{V244D/L248D}$, abrogated Spc24/25 binding beyond the detection limit despite the presence of full-length Dsn1 (Figure 5D). In cell viability assays using the anchor-away method, Mtw1$^{F232D/Y236D}$ and Mtw1$^{R233D/Y236D}$, which displayed reduced levels of Spc24/25 binding, showed normal growth with a slight sensitivity to benomyl, whereas the expression of Mtw1$^{V244D/L248D}$ was lethal (Figures 5F and 5G). Taken together, the lethality caused upon mutation of the Mtw1 residues valine-244 and leucine-248

(D) *In vitro* competition assay of Spc105/Kre28 and Spc24/25 complexes for binding to the indicated peptides. Equimolar ratios of Spc105/Kre28 and Spc24/25 complexes were incubated with the immobilized peptides, and bound proteins were analyzed as described in (A). The bar charts in (A), (C), and (D) show the relative intensities of the bound proteins quantified by ImageJ (Schneider et al., 2012) and normalized to the most intense signal displayed as mean ± SD (n = 2).

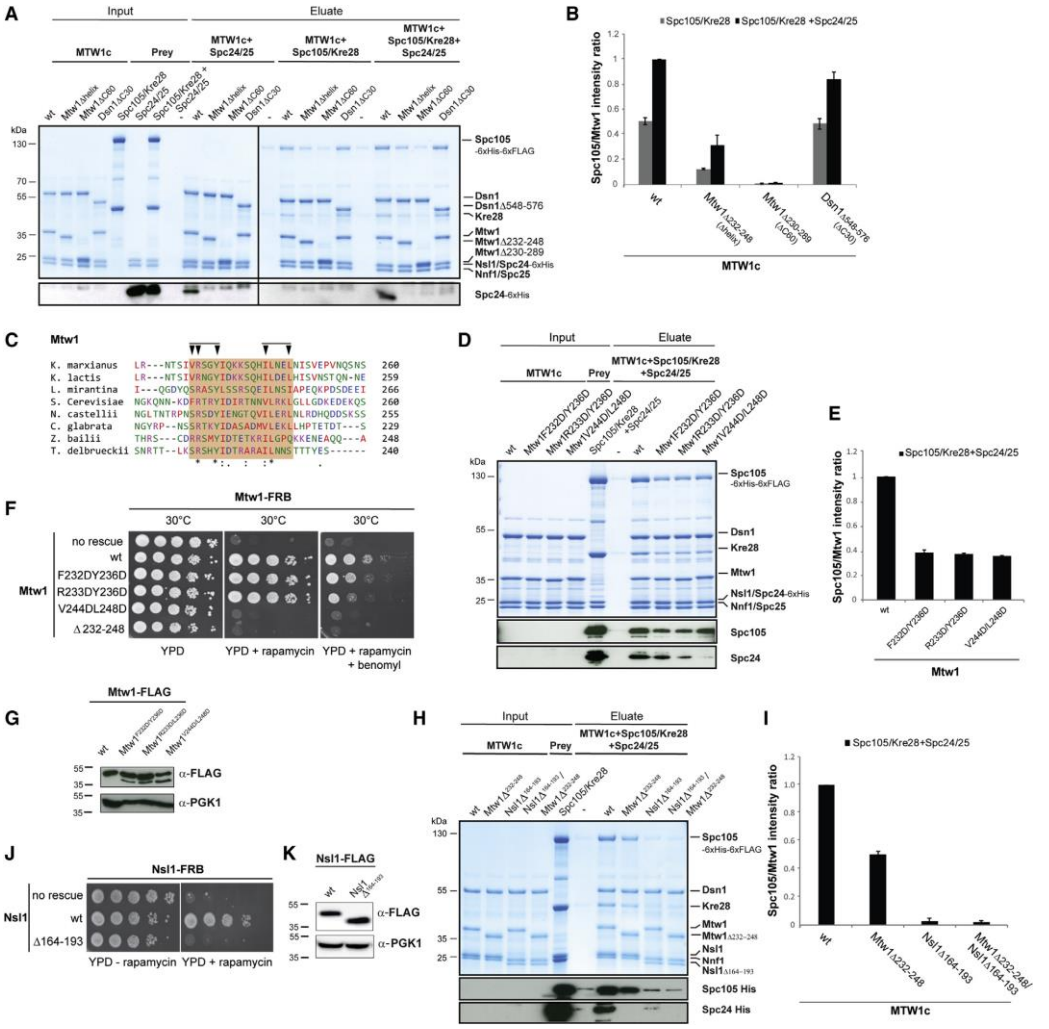

Figure 5. Cooperative Interactions between MTW1c C-Terminal Motifs and Spc24/25 and Spc105/Kre28 Complexes Stabilize the KMN Network

(A) The interaction of the Spc24/25 and/or Spc105/Kre28 complexes with C-terminal motifs of the MTW1c was assessed *in vitro*. Immobilized MTW1 wild-type and mutant complexes were incubated with either Spc24/25, Spc105/Kre28, or both. Bound complexes were eluted and analyzed by SDS-PAGE and Coomassie staining. Western blotting using anti-His antibody was performed to visualize the Spc24-6xHis levels.

(B) Quantification of bound Spc105 levels of the experiments described in (A) by measuring band intensities with ImageJ. The ratio of Spc105 to Mtw1 protein intensities was calculated as mean ± SD of 3 replicates.

(C) Amino acid sequence alignment of the Mtw1 helix$^{232–248}$ region from various budding yeast species. The predicted helical region of residues 232–248 in budding yeast is highlighted in pink. Amino acid residues are colored and annotated according to the Clustal Omega (Sievers et al., 2011) color and annotation codes. Arrowheads indicate the positions of the double mutations shown in (D) and (E).

(D) Double mutants of the Mtw1 helix$^{232–248}$ showed distinct effects on recruiting Spc24/25 or Spc105/Kre28 to the MTW1 complex *in vitro*. Mtw1 wild-type or Mtw1 mutant-containing complexes were incubated with Spc105/Kre28 and Spc24/25 at a molar ratio of 1:3, and experiments were analyzed as described in (A). The levels of Spc105-6xHis and Spc24-6xHis bound to the MTW1c were visualized by western blotting using the anti-His antibody.

(E) Quantification of the bound Spc105 levels relative to Mtw1 of the experiments in (D) (n = 2) as described in (B).

(legend continued on next page)

correlated with the loss of NDC80c binding *in vitro*, indicating that amino acids 244–248 of Mtw1 are necessary for Spc24/25 binding.

The Nsl1$^{163–192}$ Helical Motif Is Required for Recruiting the SPC105 and NDC80 Complexes

The peptide binding assay identified the Nsl1$^{163–192}$ motif to interact with Spc105/Kre28 (Figures 4C and 4D). We tested whether deletion of the Nsl1$^{164–193}$ helix in the recombinant MTW1c would affect binding of Spc105/Kre28 (Figures 5H and 5I). Deletion of the Nsl1$^{164–193}$ motif reduced Spc105/Kre28 levels associated with MTW1c to background levels and thus had a larger effect on Spc105/Kre28 binding than deletion of the Mtw1$^{233–248}$ helix. Consistent with the previous assay (Figure 5A), the deletion of the Mtw1$^{233–248}$ helix abrogated association with Spc24/25, but the MTW1cNsl1Δhelix$^{164–193}$ mutant retained minor Spc24/25 levels. As a direct interaction between the Nsl1$^{163–192}$ peptide and Spc24/25 was not detected (Figure 4A), its significant contribution to the recruitment of Spc24/25 to MTW1c may be a consequence of the lost cooperative stabilization through Spc105/Kre28 or may indicate a role in organizing the hub of C-terminal MTW1c motifs. Moreover, the Nsl1$^{163–192}$ motif was essential for cell viability (Figures 5J and 5K), which underscored its importance for the buildup of the KMN network.

A Kre28 CC Region Mediates Recruitment of Spc105/Kre28 to the MTW1 Complex

Our crosslink-derived subunit connectivity map of the native KMN network showed 4 and 12 crosslinks from the Mtw1 C terminus to Spc105 and Kre28 (Figure 1B), respectively. The majority of these crosslinks were detected at the transition of the C-terminal RWD domains to the flanking CC in Spc105 and close to the predicted C-terminal CC region in Kre28 (Figures 1B and 6A; Tables S4 and S5). In order to map the binding interface of MTW1c at the Spc105/Kre28 complex, we first deleted the Spc105 CC region (Δ551–711 "ΔCC") or the C terminus including the CC and RWD domains of Spc105 (Δ551–917 "ΔC") (Figure 6A). Both mutants did not support binding to the MTW1c (Figure 6B). Notably, these mutants also copurified significantly reduced levels of Kre28, which is in agreement with studies in higher eukaryotes (Kiyomitsu et al., 2011; Petrovic et al., 2010) and with inter-protein crosslinks connecting the CC regions of Spc105 and Kre28 (Figure 1B). This observation prompted us to test whether Kre28 itself is required for the interaction. We found that full-length Spc105 in the absence of Kre28 did not interact with the MTW1c, suggesting that Kre28 is required for recruiting Spc105/Kre28 to the MTW1c (Figure 6B).

The two predicted CCs of Kre28, Kre28$^{128–169}$ (CC1) and Kre28$^{229–259}$ (CC2) (Figure 6A), are connected by 20 crosslinks to the Spc105 CC region, Spc105$^{551–711}$ (Figure 1B; Tables S3 and S4), and 12 restraints linked Kre28$^{229–259}$ to the Mtw1 C terminus. We designed a series of double point mutants within CC1, Kre28$^{V136D/L139D}$ and Kre28$^{I143D/V146D}$, and CC2, Kre28$^{L231D/L234D}$, Kre28$^{L241D/L245D}$, and Kre28$^{M248D/V251D}$ (Figure 6C), which were copurified as stoichiometric complexes with Spc105 (Figures 6D and 6E). Mutations in CC1 did not affect interaction with MTW1c, whereas CC2 mutants retained either significantly reduced (Kre28$^{L231D/L234D}$) MTW1c levels or completely abrogated MTW1c binding (Kre28$^{L241D/L245D}$ and Kre28$^{M248D/V251D}$) (Figures 6D and 6E), suggesting that the predicted CC2 of Kre28 contributes to the recruitment of Spc105/Kre28 to the MTW1c.

To assess whether the Kre28 double point mutations were critical for the assembly of the KMN network *in vivo*, we ectopically expressed wild-type and mutant Kre28 proteins in *Kre28-FRB* anchor-away strains (Figures 6F and 6G). At 30°C, the Kre28 CC mutants showed wild-type growth, but at higher temperature mutations in CC1 abolished cell viability. This suggested that the CC1 and the CC2 were functionally distinct and indicated that the CC2 residues, which established the interaction between Spc105/Kre28 and MTW1c *in vitro*, were not essential *in vivo*. In order to perturb the integrity of the outer kinetochore, we deleted the non-essential CTF19c subunit Cnn1 (Bock et al., 2012; Pekgöz Altunkaya et al., 2016; Schleiffer et al., 2012). In a *Kre28-FRB/cnn1Δ* background, ectopic expression of the mutant Kre28 alleles showed only minor effects on cell growth at normal temperature. At higher temperature, the CC2 mutants, Kre28$^{L241D/L245D}$ and Kre28$^{M248D/V251D}$, which completely abrogated MTW1c binding *in vitro*, in contrast to Kre28$^{L231D/L234D}$ (Figures 6D and 6E), resulted in a severe growth defect (Figure 6F), indicating that these residues contribute to some extent to the stabilization of Spc105/Kre28 in the KMN network.

DISCUSSION

Our connectivity maps of the native and recombinant KMN network confirmed many known interactions that are required for recruiting the NDC80c to the CCAN (Figure 1B) and highlighted the recently described mode of NDC80c binding in humans and budding yeast through the Cnn1^{CENP-T}-Mcm16/Ctf3/Mcm22$^{CENP-H/I/K}$ pathway (Basilico et al., 2014; Bock et al., 2012; Huis In 't Veld et al., 2016; Lang et al., 2018; Pekgöz Altunkaya et al., 2016; Schleiffer et al., 2012).

Similar elongated structures were determined for the yeast and human MTW1^{MIS12} complexes (Dimitrova et al., 2016; Petrovic et al., 2016) with the N and C termini organized at opposite ends. The C termini were not proteolytically stable and thus not resolved in the structures (Dimitrova et al., 2016), indicating that

(F) Cell viability assay of the Mtw1 helix$^{232–248}$ double mutations using the anchor-away technique. Mtw1-FRB strains harboring the indicated rescue alleles were spotted in serial dilutions on YPD, YPD + rapamycin, or YPD + rapamycin + benomyl plates and incubated at 30°C or 37°C.
(G) Levels of the ectopically expressed Mtw1 proteins described in (E) are shown by western blotting.
(H) *In vitro* binding assay to investigate the interaction of the Spc105/Kre28 and Spc24/25 complexes with the MTW1c containing the Nsl1$^{Δ163–194}$ and Mtw1$^{Δ232–248}$ mutants. Experiments were performed as described in (A).
(I) Quantification of the bound Spc105 levels of the experiments in (H) (n = 2) as described in (B).
(J) Cell growth assay of the Nsl1$^{Δ163–194}$ mutant yeast cells. The Nsl1 wild-type and mutant proteins were ectopically expressed in a Nsl1-FRB strain, and cell growth was monitored by plating 1:10 serial dilutions on YPD medium at 30°C in the absence or presence of rapamycin.
(K) Levels of the ectopically expressed Nsl1 proteins described in (J) shown by western blotting.

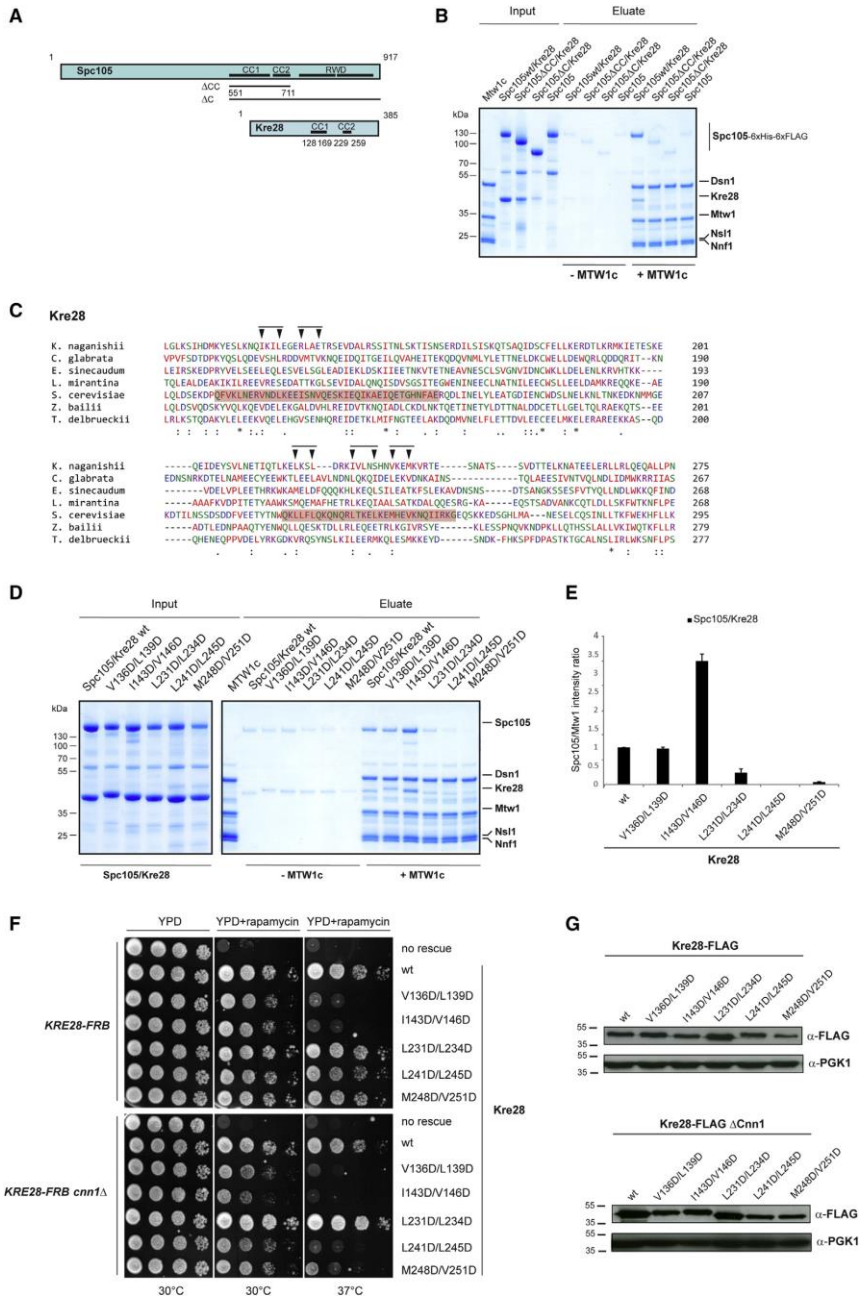

(legend on next page)

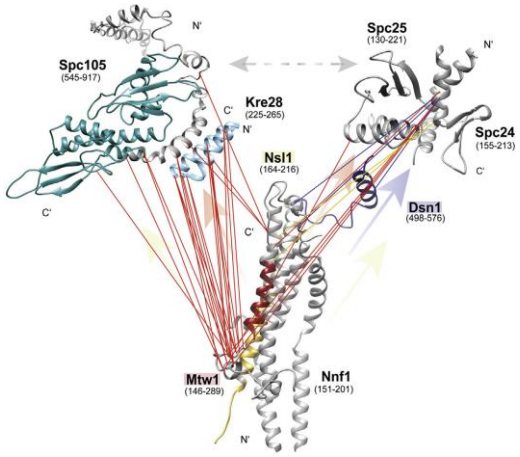

Figure 7. Crosslink Map Summarizing the Connectivity of the MTW1c C-Terminal Peptide Motifs with the Spc105/Kre28 and Spc24/25 Complexes

Models of Spc105/Kre28 and MTW1c were prepared using I-Tasser and Chimera, and the Spc24 and Spc25 C-terminal RWDs are represented by the crystal structure (PDB: 4GEQ) (Malvezzi et al., 2013). RWD domains of Spc105 (amino acids 545–917) are highlighted in cyan, and CC2 of Kre28 (amino acids 225–265) is shown in light blue. The partial model of MTW1c depicts the Mtw1 helix amino acids 232–248 (red), Nsl1 helix amino acids 164–193 (dark gold), and Dsn1 helix amino acids 547–576 (dark blue), with the accordingly colored crosslinks to Spc24/25 and Spc105/Kre28. The accordingly colored arrows indicate the binding dependencies detected in *in vitro* binding assays.

they are possibly stabilized upon binding to other KMN proteins. XL-MS analysis of the purified endogenous (Figure 1B) or the full-length recombinant KMN (Figure S1B) network showed that the crosslinks between the C termini of Mtw1, Dsn1, and Nsl1 are collinear (Figure 2A), suggesting that the tails are aligned in the KMN complex and create a hub for the interaction with the NDC80c and SPC105c.

Previous studies in yeast and humans identified the C-terminal tails of the MTW1c^{MIS12c} subunits as binding sites for the NDC80^{NDC80} and SPC105^{KNL1} complexes (Kudalkar et al., 2015; Malvezzi et al., 2013; Petrovic et al., 2010, 2014). In budding yeast, the NDC80c was shown to be recruited by the Dsn1 C terminus (Dimitrova et al., 2016; Malvezzi et al., 2013) and through interactions with the Mtw1 and Nsl1 C termini (Kudalkar et al., 2015). We found additional motifs and a hitherto underestimated role of Mtw1 and Nsl1 in KMN assembly (Figure 7). We identified a 17-amino acid helical motif (amino acids 232–248) in the Mtw1 C terminus required for binding to the Spc105/Kre28 complex and to the Spc24/25 heterodimer of the Ndc80 complex. Mutations of only two Mtw1 residues (V244D/L248D) in the tetrameric MTW1c, which did not affect association with Spc105/Kre28, resulted in loss of Spc24/25 binding and cell death (Figures 5D and 5F). Moreover, our findings *in vitro* and *in vivo* suggested that Mtw1$^{232–248}$ and Dsn1$^{548–576}$ cooperate in order to recruit NDC80c: (1) the binding of the MTW1 complex is completely abrogated by the Mtw1-Δhelix mutant despite the presence of a full-length Dsn1 protein, (2) Mtw1$^{232–248}$ and Dsn1$^{548–576}$ peptides synergistically increased the relative affinity to Spc24/25 (Figures 4A and 4B) in peptide binding assays and ITC experiments, and (3) the lethal phenotype observed upon deletion of the Mtw1 helix was not rescued by substituting the Mtw1 helix with the Cnn1$^{60–84}$ helix as it has been demonstrated by replacing the Dsn1$^{548–576}$ helix with Cnn1$^{60–84}$ (Figure 2D) (Malvezzi et al., 2013). Although Spc24/25 did not bind to the Nsl1$^{163–192}$ and Nsl1$^{183–216}$ peptides (Figure 4A), deletion of Nsl1$^{164–193}$ was lethal (Figure 5J) and abrogated binding of Spc24/25 to the MTW1c, suggesting that this Nsl1 motif might indirectly facilitate the Spc24/25 interaction (Figures 5H and 5I).

Apart from anchoring the outer kinetochore to the inner kinetochore through MTW1c^{MIS12c} and providing the microtubule binding site on NDC80c^{NDC80c}, the SPC105c^{KNL1c} of the KMN network serves as docking site for proteins of the spindle assembly checkpoint (Musacchio, 2015). In humans, the NSL1 C-terminal residues (258–281) interact with the homodimeric RWD domains of KNL1. The binding of NSL1 to KNL1 is only modestly enhanced by other members of the MIS12 complex, and the Kre28 ortholog ZWINT is dispensable for the interaction of KNL1c with MIS12c (Petrovic et al., 2010, 2014). Our results indicated that the recruitment of the Spc105/Kre28 complex in budding yeast differs from that of the human KMN network. First, the Mtw1$^{228–252}$ and the Nsl1$^{163–192}$ peptide bound Spc105/Kre28 *in vitro* (Figure 4C) and deletion of the individual motifs in the MTW1c severely affected the interaction (Figures 5A, 5B, 5H, and 5I), indicating that both motifs are required for stably tethering Spc105/Kre28. Second, the Spc105/Kre28 complex was recruited through Kre28 to the MTW1c. Moreover, the CC2 of Kre28 contributes to MTW1c binding, whereas CC1 is dispensable for this interaction (Figures 6D and 6E) and might be also functionally distinct from CC2 (Figure 6F). The role of

Figure 6. Recruitment of the Spc105/Kre28 Complex to the MTW1 Complex Is Mediated through Kre28

(A) Schematic representation of Spc105 and Kre28 deletion mutants studied in (B). ΔCC, delta coiled-coils (CC1 and CC2); ΔC, C-terminal truncation of amino acid residues 552–917.

(B) *In vitro* binding assay to study the interaction of the MTW1c with the indicated wild-type and mutant Spc105/Kre28 complexes including the various Kre28 mutants depicted in (A).

(C) Scheme of Kre28 double point mutants (arrowheads) in the CC1 (V136D/L139D, I143D/V146D) and CC2 (L231D/L234D, L241D/L245D, M248D/V251D) regions (highlighted in red orange).

(D) *In vitro* assay to investigate the binding of the MTW1c to the Spc105/Kre28 complexes carrying the Kre28 double point mutations shown in (C).

(E) Quantification of the Spc105 levels relative to Mtw1 of the experiments in (D) is displayed as mean ± SD (n = 2).

(F) Cell viability assay to test the Kre28 double point mutations applying the anchor-away technique. Cells ectopically expressing Kre28 wild-type and mutant proteins in the *KRE28-FRB* or *KRE28-FRB cnn1Δ* background were grown on YPD medium at 30°C or 37°C in the absence or presence or rapamycin.

(G) Western blot analysis of the Kre28 expression levels of the experiments shown in (F).

Kre28 has not been studied in detail, but its deletion is lethal in budding yeast (Pagliuca et al., 2009). Notably, Spc105/Kre28 bound the Cnn1$^{60–84}$ peptide *in vitro* (Figure 4C), which was also connected by a crosslink to the CC region of Spc105 (Figure 1B) in the endogenous KMN network. Whether this interaction is functionally relevant and contributes to outer kinetochore stabilization remains to be addressed.

Our peptide binding assays showed that equimolar mixtures of Mtw1$^{228–252}$ and Dsn1$^{548–576}$ or Mtw1$^{228–252}$ and Nsl1$^{163–192}$ cooperatively stabilized the association of Spc24/25 and Spc105/Kre28, respectively (Figures 4A and 4D). Although the individual Mtw1$^{228–252}$ and Dsn1$^{548–576}$ peptides, when simultaneously incubated with Spc105/Kre28 and Spc24/25, showed relatively weak affinity to Spc105/Kre28 and Spc24/25, respectively, the mixture of Mtw1$^{228–252}$ and Dsn1$^{548–576}$ peptides enriched a nearly stoichiometric super-complex of Spc105/Kre28 and Spc24/25 (Figure 4D). Similarly, the incubation of wild-type and mutant MTW1c with a mixture of Spc105/Kre28 and Spc24/25 increased the bound Spc105/Kre28 levels by 2-fold compared with incubation with Spc105/Kre28 alone (Figures 5A and 5B). These observations are consistent with a weak interaction of Spc105/Kre28 and Spc24/25 detected by SEC (Figure S3A) or by *in vitro* binding assay (Figure S3B). In humans, KNL1c and NDC80c independently interact with the MIS12c (Petrovic et al., 2010, 2014), whereas in *C. elegans* KNL1c is required for establishing a tight NDC80c-MIS12c interaction (Cheeseman et al., 2006). Whether the lack of cooperative stabilization of KNL1c and NDC80c on MIS12c is specific to the human KMN network, or whether this is the result of assays using truncated protein complexes, is unclear.

Using crosslink guided *in vitro* reconstitution (Figure 7), we identified distinct binding interfaces that cooperate in the stabilization of the NDC80c and SPC105c at the budding yeast KMN network, which may reflect the geometrical requirements of a kinetochore unit that transmits the tensile forces of a depolymerizing microtubule onto a single centromeric nucleosome. Whether cooperativity is established by similar subunit contacts within the human kinetochore, which is assembled at regional centromeres, and how post-translational modifications contribute to the formation of a high-affinity link between spindle microtubules and chromosomes will be exciting subjects of future research.

STAR★METHODS

Detailed methods are provided in the online version of this paper and include the following:

SUPPLEMENTAL INFORMATION

Supplemental Information can be found online at https://doi.org/10.1016/j.celrep.2020.108190.

ACKNOWLEDGMENTS

We thank Stefan Westermann for sharing reagents. J.F.-H., G.H., G.W., and F.H. were funded by the Research Training Group (GRK 1721), and M.P. and V.S.-M. were funded by the Graduate School (Quantitative Biosciences Munich) of the German Research Foundation (DFG). F.H. was supported by the European Research Council (ERC)-StG (638218), the Human Frontier Science Program (RGP0008/2015), the Bavarian Research Center of Molecular Biosystems, and an LMU excellent junior grant.

AUTHOR CONTRIBUTIONS

F.H. conceived the study. M.G.-S., M.P., T.Z., and J.F.-H. designed and executed the experiments with input from F.H. V.S.-M. helped with data analysis and bioinformatics. S.S. and T.S. cloned and provided recombinant proteins. G.H. assisted with data presentation. D.D. and G.W. performed the ITC experiments. M.G.-S., M.P., and F.H. wrote the manuscript.

DECLARATION OF INTERESTS

The authors declare no competing interests.

Received: February 12, 2020
Revised: July 18, 2020
Accepted: September 1, 2020
Published: September 29, 2020

REFERENCES

Akiyoshi, B., Sarangapani, K.K., Powers, A.F., Nelson, C.R., Reichow, S.L., Arellano-Santoyo, H., Gonen, T., Ranish, J.A., Asbury, C.L., and Biggins, S. (2010). Tension directly stabilizes reconstituted kinetochore-microtubule attachments. Nature *468*, 576–579.

Anedchenko, E.A., Samel-Pommerencke, A., Tran Nguyen, T.M., Shahnejat-Bushehri, S., Pöpsel, J., Lauster, D., Herrmann, A., Rappsilber, J., Cuomo, A., Bonaldi, T., and Ehrenhofer-Murray, A.E. (2019). The kinetochore module Okp1^{CENP-Q}/Ame1^{CENP-U} is a reader for N-terminal modifications on the centromeric histone Cse4^{CENP-A}. EMBO J. *38*, e98991.

Basilico, F., Maffini, S., Weir, J.R., Prumbaum, D., Rojas, A.M., Zimniak, T., De Antoni, A., Jeganathan, S., Voss, B., van Gerwen, S., et al. (2014). The pseudo GTPase CENP-M drives human kinetochore assembly. eLife *3*, e02978.

Bock, L.J., Pagliuca, C., Kobayashi, N., Grove, R.A., Oku, Y., Shrestha, K., Alfieri, C., Golfieri, C., Oldani, A., Dal Maschio, M., et al. (2012). Cnn1 inhibits the interactions between the KMN complexes of the yeast kinetochore. Nat. Cell Biol. *14*, 614–624.

Bodor, D.L., Mata, J.F., Sergeev, M., David, A.F., Salimian, K.J., Panchenko, T., Cleveland, D.W., Black, B.E., Shah, J.V., and Jansen, L.E. (2014). The quantitative architecture of centromeric chromatin. eLife *3*, e02137.

Cheeseman, I.M., and Desai, A. (2008). Molecular architecture of the kinetochore-microtubule interface. Nat. Rev. Mol. Cell Biol. *9*, 33–46.

Cheeseman, I.M., Enquist-Newman, M., Müller-Reichert, T., Drubin, D.G., and Barnes, G. (2001). Mitotic spindle integrity and kinetochore function linked by the Duo1p/Dam1p complex. J. Cell Biol. *152*, 197–212.

Cheeseman, I.M., Chappie, J.S., Wilson-Kubalek, E.M., and Desai, A. (2006). The conserved KMN network constitutes the core microtubule-binding site of the kinetochore. Cell *127*, 983–997.

Ciferri, C., Pasqualato, S., Screpanti, E., Varetti, G., Santaguida, S., Dos Reis, G., Maiolica, A., Polka, J., De Luca, J.G., De Wulf, P., et al. (2008). Implications for kinetochore-microtubule attachment from the structure of an engineered Ndc80 complex. Cell *133*, 427–439.

Cox, J., and Mann, M. (2008). MaxQuant enables high peptide identification rates, individualized p.p.b.-range mass accuracies and proteome-wide protein quantification. Nat. Biotechnol. *26*, 1367–1372.

De Wulf, P., McAinsh, A.D., and Sorger, P.K. (2003). Hierarchical assembly of the budding yeast kinetochore from multiple subcomplexes. Genes Dev. *17*, 2902–2921.

Dimitrova, Y.N., Jenni, S., Valverde, R., Khin, Y., and Harrison, S.C. (2016). Structure of the MIND Complex Defines a Regulatory Focus for Yeast Kinetochore Assembly. Cell *167*, 1014–1027.

Fischboeck, J., Singh, S., Potocnjak, M., Hagemann, G., Solis, V., Woike, S., Ghodgaonkar, M., Andreani, J., and Herzog, F. (2018). The COMA complex is required for positioning Ipl1 activity proximal to Cse4 nucleosomes in budding yeast. bioRxiv. https://doi.org/10.1101/444570.

Gascoigne, K.E., Takeuchi, K., Suzuki, A., Hori, T., Fukagawa, T., and Cheeseman, I.M. (2011). Induced ectopic kinetochore assembly bypasses the requirement for CENP-A nucleosomes. Cell *145*, 410–422.

Goshima, G., and Yanagida, M. (2000). Establishing biorientation occurs with precocious separation of the sister kinetochores, but not the arms, in the early spindle of budding yeast. Cell *100*, 619–633.

Grimm, M., Zimniak, T., Kahraman, A., and Herzog, F. (2015). xVis: a web server for the schematic visualization and interpretation of crosslink-derived spatial restraints. Nucleic Acids Res. *43* (*W1*), W362–W369.

Guimaraes, G.J., Dong, Y., McEwen, B.F., and Deluca, J.G. (2008). Kinetochore-microtubule attachment relies on the disordered N-terminal tail domain of Hec1. Curr. Biol. *18*, 1778–1784.

Haruki, H., Nishikawa, J., and Laemmli, U.K. (2008). The anchor-away technique: rapid, conditional establishment of yeast mutant phenotypes. Mol. Cell *31*, 925–932.

Herzog, F., Kahraman, A., Boehringer, D., Mak, R., Bracher, A., Walzthoeni, T., Leitner, A., Beck, M., Hartl, F.U., Ban, N., et al. (2012). Structural probing of a protein phosphatase 2A network by chemical cross-linking and mass spectrometry. Science *337*, 1348–1352.

Hieter, P., Mann, C., Snyder, M., and Davis, R.W. (1985). Mitotic stability of yeast chromosomes: a colony color assay that measures nondisjunction and chromosome loss. Cell *40*, 381–392.

Hinshaw, S.M., and Harrison, S.C. (2019). The structure of the Ctf19c/CCAN from budding yeast. eLife *8*, e44239.

Hornung, P., Maier, M., Alushin, G.M., Lander, G.C., Nogales, E., and Westermann, S. (2011). Molecular architecture and connectivity of the budding yeast Mtw1 kinetochore complex. J. Mol. Biol. *405*, 548–559.

Hornung, P., Troc, P., Malvezzi, F., Maier, M., Demianova, Z., Zimniak, T., Litos, G., Lampert, F., Schleiffer, A., Brunner, M., et al. (2014). A cooperative mechanism drives budding yeast kinetochore assembly downstream of CENP-A. J. Cell Biol. *206*, 509–524.

Huis In 't Veld, P.J., Jeganathan, S., Petrovic, A., Singh, P., John, J., Krenn, V., Weissmann, F., Bange, T., and Musacchio, A. (2016). Molecular basis of outer kinetochore assembly on CENP-T. eLife *5*, 5.

Janke, C., Magiera, M.M., Rathfelder, N., Taxis, C., Reber, S., Maekawa, H., Moreno-Borchart, A., Doenges, G., Schwob, E., Schiebel, E., and Knop, M. (2004). A versatile toolbox for PCR-based tagging of yeast genes: new fluorescent proteins, more markers and promoter substitution cassettes. Yeast *21*, 947–962.

Joglekar, A.P., Bloom, K., and Salmon, E.D. (2009). In vivo protein architecture of the eukaryotic kinetochore with nanometer scale accuracy. Curr. Biol. *19*, 694–699.

Jones, D.T. (1999). Protein secondary structure prediction based on position-specific scoring matrices. J. Mol. Biol. *292*, 195–202.

Kim, S., and Yu, H. (2015). Multiple assembly mechanisms anchor the KMN spindle checkpoint platform at human mitotic kinetochores. J. Cell Biol. *208*, 181–196.

Kiyomitsu, T., Murakami, H., and Yanagida, M. (2011). Protein interaction domain mapping of human kinetochore protein Blinkin reveals a consensus motif for binding of spindle assembly checkpoint proteins Bub1 and BubR1. Mol. Cell. Biol. *31*, 998–1011.

Kudalkar, E.M., Scarborough, E.A., Umbreit, N.T., Zelter, A., Gestaut, D.R., Riffle, M., Johnson, R.S., MacCoss, M.J., Asbury, C.L., and Davis, T.N. (2015). Regulation of outer kinetochore Ndc80 complex-based microtubule attachments by the central kinetochore Mis12/MIND complex. Proc. Natl. Acad. Sci. USA *112*, E5583–E5589.

Lampert, F., Mieck, C., Alushin, G.M., Nogales, E., and Westermann, S. (2013). Molecular requirements for the formation of a kinetochore-microtubule interface by Dam1 and Ndc80 complexes. J. Cell Biol. *200*, 21–30.

Lang, J., Barber, A., and Biggins, S. (2018). An assay for de novo kinetochore assembly reveals a key role for the CENP-T pathway in budding yeast. eLife *7*, e37819.

London, N., Ceto, S., Ranish, J.A., and Biggins, S. (2012). Phosphoregulation of Spc105 by Mps1 and PP1 regulates Bub1 localization to kinetochores. Curr. Biol. *22*, 900–906.

Malvezzi, F., Litos, G., Schleiffer, A., Heuck, A., Mechtler, K., Clausen, T., and Westermann, S. (2013). A structural basis for kinetochore recruitment of the Ndc80 complex via two distinct centromere receptors. EMBO J. *32*, 409–423.

Maskell, D.P., Hu, X.W., and Singleton, M.R. (2010). Molecular architecture and assembly of the yeast kinetochore MIND complex. J. Cell Biol. *190*, 823–834.

Miller, S.A., Johnson, M.L., and Stukenberg, P.T. (2008). Kinetochore attachments require an interaction between unstructured tails on microtubules and Ndc80(Hec1). Curr. Biol. *18*, 1785–1791.

Musacchio, A. (2015). The Molecular Biology of Spindle Assembly Checkpoint Signaling Dynamics. Curr. Biol. *25*, R1002–R1018.

Nishino, T., Rago, F., Hori, T., Tomii, K., Cheeseman, I.M., and Fukagawa, T. (2013). CENP-T provides a structural platform for outer kinetochore assembly. EMBO J. *32*, 424–436.

Pagliuca, C., Draviam, V.M., Marco, E., Sorger, P.K., and De Wulf, P. (2009). Roles for the conserved spc105p/kre28p complex in kinetochore-microtubule binding and the spindle assembly checkpoint. PLoS ONE *4*, e7640.

Pekgöz Altunkaya, G., Malvezzi, F., Demianova, Z., Zimniak, T., Litos, G., Weissmann, F., Mechtler, K., Herzog, F., and Westermann, S. (2016). CCAN Assembly Configures Composite Binding Interfaces to Promote Cross-Linking of Ndc80 Complexes at the Kinetochore. Curr. Biol. *26*, 2370–2378.

Petrovic, A., Pasqualato, S., Dube, P., Krenn, V., Santaguida, S., Cittaro, D., Monzani, S., Massimiliano, L., Keller, J., Tarricone, A., et al. (2010). The MIS12 complex is a protein interaction hub for outer kinetochore assembly. J. Cell Biol. *190*, 835–852.

Petrovic, A., Mosalaganti, S., Keller, J., Mattiuzzo, M., Overlack, K., Krenn, V., De Antoni, A., Wohlgemuth, S., Cecatiello, V., Pasqualato, S., et al. (2014). Modular assembly of RWD domains on the Mis12 complex underlies outer kinetochore organization. Mol. Cell *53*, 591–605.

Perez-Riverol, Y., Csordas, A., Bai, J., Bernal-Llinares, M., Hewapathirana, S., Kundu, D.J., Inuganti, A., Griss, J., Mayer, G., Eisenacher, M., et al. (2019). The

PRIDE database and related tools and resources in 2019: improving support for quantification data. Nucleic. Acids Res. *47*, 442–450.

Petrovic, A., Keller, J., Liu, Y., Overlack, K., John, J., Dimitrova, Y.N., Jenni, S., van Gerwen, S., Stege, P., Wohlgemuth, S., et al. (2016). Structure of the MIS12 Complex and Molecular Basis of Its Interaction with CENP-C at Human Kinetochores. Cell *167*, 1028–1040.

Pettersen, E.F., Goddard, T.D., Huang, C.C., Couch, G.S., Greenblatt, D.M., Meng, E.C., and Ferrin, T.E. (2004). UCSF Chimera–a visualization system for exploratory research and analysis. J. Comput. Chem. *25*, 1605–1612.

Pluta, A.F., Mackay, A.M., Ainsztein, A.M., Goldberg, I.G., and Earnshaw, W.C. (1995). The centromere: hub of chromosomal activities. Science *270*, 1591–1594.

Przewloka, M.R., Venkei, Z., Bolanos-Garcia, V.M., Debski, J., Dadlez, M., and Glover, D.M. (2011). CENP-C is a structural platform for kinetochore assembly. Curr. Biol. *21*, 399–405.

Rago, F., Gascoigne, K.E., and Cheeseman, I.M. (2015). Distinct organization and regulation of the outer kinetochore KMN network downstream of CENP-C and CENP-T. Curr. Biol. *25*, 671–677.

Santaguida, S., and Musacchio, A. (2009). The life and miracles of kinetochores. EMBO J. *28*, 2511–2531.

Schindelin, J., Arganda-Carreras, I., Frise, E., Kaynig, V., Longair, M., Pietzsch, T., Preibisch, S., Rueden, C., Saalfeld, S., Schmid, B., et al. (2012). Fiji: an open-source platform for biological-image analysis. Nat. Methods *9*, 676–682.

Schleiffer, A., Maier, M., Litos, G., Lampert, F., Hornung, P., Mechtler, K., and Westermann, S. (2012). CENP-T proteins are conserved centromere receptors of the Ndc80 complex. Nat. Cell Biol. *14*, 604–613.

Schneider, C.A., Rasband, W.S., and Eliceiri, K.W. (2012). NIH Image to ImageJ: 25 years of image analysis. Nat. Methods *9*, 671–675.

Screpanti, E., De Antoni, A., Alushin, G.M., Petrovic, A., Melis, T., Nogales, E., and Musacchio, A. (2011). Direct binding of Cenp-C to the Mis12 complex joins the inner and outer kinetochore. Curr. Biol. *21*, 391–398.

Shepperd, L.A., Meadows, J.C., Sochaj, A.M., Lancaster, T.C., Zou, J., Buttrick, G.J., Rappsilber, J., Hardwick, K.G., and Millar, J.B. (2012). Phosphodependent recruitment of Bub1 and Bub3 to Spc7/KNL1 by Mph1 kinase maintains the spindle checkpoint. Curr. Biol. *22*, 891–899.

Sievers, F., Wilm, A., Dineen, D., Gibson, T.J., Karplus, K., Li, W., Lopez, R., McWilliam, H., Remmert, M., Söding, J., et al. (2011). Fast, scalable generation of high-quality protein multiple sequence alignments using Clustal Omega. Mol. Syst. Biol. *7*, 539.

Spencer, F., Gerring, S.L., Connelly, C., and Hieter, P. (1990). Mitotic chromosome transmission fidelity mutants in Saccharomyces cerevisiae. Genetics *124*, 237–249.

van Hooff, J.J., Tromer, E., van Wijk, L.M., Snel, B., and Kops, G.J. (2017). Evolutionary dynamics of the kinetochore network in eukaryotes as revealed by comparative genomics. EMBO Rep. *18*, 1559–1571.

Walzthoeni, T., Claassen, M., Leitner, A., Herzog, F., Bohn, S., Förster, F., Beck, M., and Aebersold, R. (2012). False discovery rate estimation for cross-linked peptides identified by mass spectrometry. Nat. Methods *9*, 901–903.

Wei, R.R., Schnell, J.R., Larsen, N.A., Sorger, P.K., Chou, J.J., and Harrison, S.C. (2006). Structure of a central component of the yeast kinetochore: the Spc24p/Spc25p globular domain. Structure *14*, 1003–1009.

Wei, R.R., Al-Bassam, J., and Harrison, S.C. (2007). The Ndc80/HEC1 complex is a contact point for kinetochore-microtubule attachment. Nat. Struct. Mol. Biol. *14*, 54–59.

Weissmann, F., Petzold, G., VanderLinden, R., Huis In 't Veld, P.J., Brown, N.G., Lampert, F., Westermann, S., Stark, H., Schulman, B.A., and Peters, J.M. (2016). biGBac enables rapid gene assembly for the expression of large multisubunit protein complexes. Proc. Natl. Acad. Sci. USA *113*, E2564–E2569.

Westermann, S., Cheeseman, I.M., Anderson, S., Yates, J.R., 3rd, Drubin, D.G., and Barnes, G. (2003). Architecture of the budding yeast kinetochore reveals a conserved molecular core. J. Cell Biol. *163*, 215–222.

Westermann, S., Wang, H.W., Avila-Sakar, A., Drubin, D.G., Nogales, E., and Barnes, G. (2006). The Dam1 kinetochore ring complex moves processively on depolymerizing microtubule ends. Nature *440*, 565–569.

Xiao, H., Wang, F., Wisniewski, J., Shaytan, A.K., Ghirlando, R., FitzGerald, P.C., Huang, Y., Wei, D., Li, S., Landsman, D., et al. (2017). Molecular basis of CENP-C association with the CENP-A nucleosome at yeast centromeres. Genes Dev. *31*, 1958–1972.

Yamagishi, Y., Yang, C.H., Tanno, Y., and Watanabe, Y. (2012). MPS1/Mph1 phosphorylates the kinetochore protein KNL1/Spc7 to recruit SAC components. Nat. Cell Biol. *14*, 746–752.

Yang, J., Yan, R., Roy, A., Xu, D., Poisson, J., and Zhang, Y. (2015). The I-TASSER Suite: protein structure and function prediction. Nat. Methods *12*, 7–8.

Zimmermann, L., Stephens, A., Nam, S.Z., Rau, D., Kübler, J., Lozajic, M., Gabler, F., Söding, J., Lupas, A.N., and Alva, V. (2018). A Completely Reimplemented MPI Bioinformatics Toolkit with a New HHpred Server at its Core. J. Mol. Biol. *430*, 2237–2243.

STAR★METHODS

KEY RESOURCES TABLE

REAGENT or RESOURCE	SOURCE	IDENTIFIER
Antibodies		
Mouse monoclonal anti-6xHis tag	ABCAM	Cat# ab18184; RRID:AB_444306
Mouse monoclonal anti-FLAG M2	Sigma-Aldrich	Cat# F1804; RRID:AB_262044
Mouse monoclonal anti-Pgk1	Invitrogen	Cat# 459250; RRID:AB_2532235
Goat anti-mouse IgG-HRP	Santa Cruz Biotechnology	Cat# sc-2005; RRID:AB_631736
Bacterial and Virus Strains		
E. coli: BL21 (DE3)	New England Biolabs	Cat#C2527
E. coli: DH10Bac	ThermoFisher	Cat#10361012
Chemicals, Peptides, and Recombinant Proteins		
BS3-H12/D12 crosslinker	Creative Molecules	Cat#001SS
TCEP	ThermoFisher	Cat#20490
Iodoacetamide	Sigma-Aldrich	Cat#I6125
Lysyl Endopeptidase	FUJIFILM Wako Pure Chemical Corporation	Cat#125–05061
Trypsin Sequencing Grade Modified	Promega	Cat#V5111
Rapamycin	Invitrogen	Cat#PHZ1235
Benomyl	Sigma-Aldrich	Cat#381586
FuGENE HD Transfection Reagent	Sigma-Aldrich	Cat#E2311
cOmplete ULTRA EDTA-free Protease Inhibitor Cocktail	Roche	Cat#5892953001
Ni-NTA Agarose	QIAGEN	Cat#30210
Strep-Tactin Superflow Plus Agarose	QIAGEN	Cat#30004
anti-FLAG M2 agarose	Sigma-Aldrich	Cat#A2220
Peptides listed in Table S3	Ontores	N/A
Mtw1 complex	this paper	N/A
Spc24/25	this paper	N/A
Spc105/Kre28	this paper	N/A
KMN complex	this paper	N/A
Critical Commercial Assays		
Q5 Site-Directed Mutagenesis Kit	New England Biolabs	Cat#E0552S
Mini-prep kit	QIAGEN	Cat#27104
Deposited Data		
PRIDE, *in vivo* network	Perez-Riverol et al., 2019	PXD011774
PRIDE, *in vitro* reconstituted KMN	Perez-Riverol et al., 2019	PXD011775
Experimental Models: Cell Lines		
S. frugiperda: SF21	ThermoFisher	Cat#11497013
Trichoplusia ni: High five	ThermoFisher	Cat#B85502
Experimental Models: Organisms/Strains		
E. coli: BL21 (DE3)	New England Biolabs	Cat#C2527
E. coli: DH10Bac	ThermoFisher	Cat#10361012
S. cerevisiae: S288c listed in Table S1		N/A
Recombinant DNA		
pETDuet-1 vector	Novagen	Cat#71146-3
pETDuet-1 Spc24-6xHis-Spc25	this paper	N/A

(*Continued on next page*)

Continued

REAGENT or RESOURCE	SOURCE	IDENTIFIER
pKP-29	Gift from Hopfner Lab	N/A
pKP29-6xHis-1xStrep-Dsn1Δ2-171-Nsl1-Nnf1-Mtw1 (mutants listed in Table S2)	this paper	N/A
pLIB	Weissmann et al., 2016	Addgene #80610
Spc105-6xFlag-6xHis-Kre28 (mutants listed in Table S2)	this paper	N/A
pBIG2ABC	Weissmann et al., 2016	Addgene # 80617
pBIG2ABC Ndc18-Nuf2-Spc24-Spc25-Mtw1-Nnf1-Nsl1-Dsn1-Spc105-6xHis6xFlag-Kre28	this paper	N/A
pYCF1/ CEN3.L	Nasmyth Lab	N/A
Software and Algorithms		
xQuest	Walzthoeni et al., 2012	
xVis	Grimm et al., 2015	https://xvis.genzentrum.lmu.de/login.php
MaxQuant	Cox and Mann, 2008	https://www.maxquant.org/
Clustal Omega	Sievers et al., 2011	https://www.ebi.ac.uk/Tools/msa/clustalo/
BLAST	NCBI	https://blast.ncbi.nlm.nih.gov/Blast.cgi
I-Tasser	Yang et al., 2015	https://zhanglab.ccmb.med.umich.edu/I-TASSER/
UCSF Chimera	Pettersen et al., 2004	http://www.cgl.ucsf.edu/; Pettersen et al., 2004
PSIPRED	Jones, 1999	http://bioinf.cs.ucl.ac.uk/psipred/
HHpred	Zimmermann et al., 2018	https://toolkit.tuebingen.mpg.de/tools/hhpred
ImageJ	Schindelin et al., 2012	https://imagej.nih.gov/ij/
Other		
Sep-Pak tC18 cartridges	Waters	Cat#WAT054960
PD-10 Desalting Columns	GE Healthcare	Cat#17085101

RESOURCE AVAILABILITY

Lead Contact

Further information and requests for resources and reagents should be directed to and will be fulfilled by the Lead Contact, Franz Herzog (herzog@genzentrum.lmu.de).

Materials Availability

All unique/stable reagents generated in this study are available from the Lead Contact on request.

Data and Code Availability

The mass spectrometry data reported in this paper have been deposited to the ProteomeXchange Consortium via the PRIDE partner repository. The accession number for the endogenous KMN XL-MS data is PRIDE: PXD011774 and for the recombinant KMN XL-MS data is PRIDE: PXD011775.

EXPERIMENTAL MODEL AND SUBJECT DETAILS

Genes used for expression of recombinants proteins were PCR amplified from *S. cerevisiae* gDNA. *E. coli* BL21 (DE3) cells were grown in LB media on 18°C or 37°C. Yeast strains were grown in yeast extract/peptone or synthetic media [without Histidine (SD - His), without Uracil (SD - Ura), or both (SD - His - Ura) and with all amino acids but low (6 μg/ml) adenine (SD complete)]. Cells were typically incubated at 30°C unless otherwise indicated

METHOD DETAILS

Plasmids and yeast strains

All plasmids and yeast strains used in this study are listed in Tables S1 and S2, respectively. For protein expression in *E. coli*, cDNAs of Spc24 and Spc25 were cloned into pETDuet-1 (Novagen) using NcoI/BamHI in sequence with the C-terminal 6xHis tag and NdcI/KpnI, respectively. 6xHis1xStrepDsn1$^{\Delta 2\text{-}171}$/Nsl1/Nnf1/Mtw1 genes were sequentially cloned with AscI/AarI sites into the pKP-29 polycistronic vector cut with AscI/NotI (Table S2). Open reading frames (ORFs) encoding the Spc105-6xHis6xFLAG and Kre28 subunits were amplified from yeast genomic DNA and cloned into the pBIG1 vector according to the biGBac system (Weissmann et al., 2016). Similarly, Dsn1/Nsl1/Nnf1/Mtw1 and Ndc80/Nuf2/Spc24/25 ORFs were amplified and subsequently cloned into pBIG1 plasmids. The KMN network complex was assembled in a pBIG2 vector. Mtw1, Nsl1 and Kre28 mutants were generated using the Q5 mutagenesis kit (New England Biolabs). Constructs were sequence verified.

Yeast strains were created in the S288C background (Table S1). Epitope tags were inserted at the 3′ ends of genes at their native loci by a PCR based tagging standard approach (Janke et al., 2004). The anchor-away technique of Mtw1 mutants (Mtw1-FRB) was performed by endogenously tagging the FRB domain to the Mtw1 in a strain expressing the ribosomal RPL13-FKBP12 anchor. The Mcm21-FRB strain was created similarly (Haruki et al., 2008). For Mtw1 anchor away and rescue experiments, we cloned the 5′ UTR region (200 bp) with the Mtw1-1xFLAG into the pRS313 vector. C-terminal gene truncations were made with the Q5® Site-Directed Mutagenesis Kit (NEB). The sectoring assay plasmid (2886) used in this study was pYCF1/ CEN3. The Mtw1 rescue and sectoring assay plasmids were co-transformed into the Mtw1 anchor-away strain and selected on SD – His – Ura plates. Anchor-away rescue experiments for *Dsn1-1xFLAG* or *Kre28-1xFLAG* were performed in the same manner. The cell growth was tested on YPD plates in the absence or presence of rapamycin.

Yeast growth assays

To test the temperature and benomyl sensitivity of anchor-away strains ectopically expressing wild-type and mutant proteins, cells were grown overnight in YPD broth at 30°C. 2.5 μL of five 10-fold serial dilutions starting at OD_{600} = 0.5 were spotted on YPD plates, YPD + rapamycin (1 μg/ml, Invitrogen) and YPD + rapamycin + benomyl (15 μg/ml,Merck) plates. Plates were incubated at 30°C or 37°C for 3-5 days.

Minichromosome loss assay

The sectoring assay was performed as described (Spencer et al., 1990), ensuring that the cultures were first grown overnight in SD – His – Ura media that selected for SUP11 plasmid and Mtw1 mutant constructs. An aliquot (OD600 0.5) was harvested and the pellet was resuspended in 100 μl aqua dest. 200 μl of a 1:10000 dilution was plated on SD complete low Ade, SD complete low Ade + rapamycin (1 μg/ml) and SD complete low Ade + rapamycin + benomyl (15 μg/ml) plates. The plates were incubated at 30°C for 3 days. The percent of red or sectored versus completely white colonies was scored. A Mcm21-FRB strain served as a positive control. The experiments were performed at least three times and an average with the standard deviation was calculated for each strain.

Purification of recombinant Spc24/25 and MTW1c

For Spc24-6xHis/Spc-25 or MTW1c (6xHis-1xStrep-Dsn1$^{\Delta 2\text{-}171}$/Nsl1/Nnf1/Mtw1 or mutants thereof listed in Table S2) expression, bacteria were grown to an OD_{600} of 0.6 at 37°C and protein expression was induced with 0.2 mM (Spc24-6xHis/25) or 0.5 mM (MTW1c) IPTG overnight at 18°C. Cells were lysed in lysis buffer (30 mM HEPES, pH 7.5, 300 mM NaCl, 5% glycerol, 30 mM imidazole, 0.02% Tween, 5% glycerol, Complete EDTA-free protease inhibitors [Roche]) using a M-110L Microfluidizer (Microfluidics). The cleared lysate was incubated with Ni-NTA agarose beads (QIAGEN). The protein complexes were eluted with buffer containing 30 mM HEPES (pH 7.5), 150 mM NaCl, 0.01% Tween, 3% glycerol and 250 mM imidazole. The Spc24/25 complex was further purified on a Superdex 200 HiLoad 16/60 column (GE Healthcare) in a buffer containing 30 mM HEPES (pH 7.5), 150 mM NaCl and 3% glycerol.

Purification of Spc105/Kre28 and KMN complexes

Viruses were generated by transfection of Sf21 insect cells (Thermo Scientific) with the recombinant baculoviral genome using FuGENE HD transfection reagent (Promega). Protein complexes were expressed in High Five (Thermo Scientific) insect cell suspension cultures.

For purification of Spc105/Kre28 and KMN complexes, insect cells were lysed in lysis buffer (50 mM Tris, pH 7.5, 150 mM NaCl, 5% glycerol, Complete EDTA-free protease inhibitors [Roche]) using a Dounce homogenizer. Cleared extracts were incubated with M2 anti-FLAG agarose (Sigma-Aldrich) for 1 h, washed 3x with lysis buffer and eluted in lysis buffer containing 1 mg/ml 3xFLAG peptide and 10% glycerol.

In vitro binding assays

For peptide binding analysis recombinant Spc24/25 or Spc105/Kre28 complexes were incubated with a 25-fold molar excess of 1xStrep-tagged peptides (Table S3) in binding buffer (30 mM HEPES pH 8, 150 or 300 mM NaCl, 5% glycerol and 0.02% NP40) and incubated at 25°C/1000 rpm for 30 minutes using a thermomixer (Eppendorf). The protein complexes were bound to Strep-Tactin

Superflow agarose (QIAGEN) at 1000 rpm and room temperature for 30 min. The immobilized protein complexes were washed twice with binding buffer and eluted in 30 mM HEPES (pH 8), 500 mM NaCl, 5% glycerol, 0.02% NP40 and 8 mM biotin.

For binding assays using Mtw1 protein complexes, Mtw1 complex purified via 6xHis tag and eluted in imidazole (described above) was concentrated on Strep-Tactin Superflow agarose (QIAGEN) and washed with Strep-wash buffer (30 mM HEPES pH 7.5, 150 mM NaCl, 5% glycerol, 0.01% Tween 20). The immobilized MTW1c was incubated with the various protein complexes in a 1:3 ratio for 30 minutes in a thermomixer (Eppendorf) at 1200 rpm and 4°C and washed with Strep-high salt wash buffer (30 mM HEPES pH 7.5, 300 mM NaCl, 5% glycerol, 0.02% Tween 20). The complexes were eluted in 30 mM HEPES pH 8.0, 150 mM NaCl, 5% glycerol and 8 mM biotin. Proteins were resolved on 10%–15% gradient SDS-PAGE gels and stained with Coomassie Brilliant Blue G250 (Roth). Immunoblotting for Spc24-6xHis was performed using mouse anti-6xHis tag (1:1000, ABCAM) and visualized with goat anti-mouse HRP -conjugated secondary antibody (1:15000, Santa Cruz).

Analytical size exclusion chromatography

Analytical size exclusion chromatography was performed on a Superose 6 Increase 3.2/300 column (GE Healthcare). Proteins were mixed in an equimolar ratio and incubated for 1 h on ice. Samples were eluted under isocratic conditions at 4°C in a buffer containing 50 mM HEPES pH 7.5, 180 mM NaCl, 3% glycerol. Elution of proteins was monitored by absorbance at 280 nm. 100 µl fractions were collected and analyzed by SDS-PAGE and Silver staining.

Isothermal titration calorimetry

ITC experiments were performed using a PEAQ-ITC system (Malvern) with 51 µM of Spc24-6xHis/25 in 30 mM HEPES (pH 7.5), 150 mM NaCl and 5% glycerol in the cell. 800 µM of Dsn1$^{555-574}$ or Dsn1$^{555-574}$-Mtw1$^{229-251}$ peptide (Table S3) were titrated into the cell in 13 individual injections of 3 µl, spaced 150 s apart at 25°C. Data evaluation was performed with the Malvern software package. Experiments were performed in triplicates to confirm the robustness of the assay.

Sample preparation for native crosslinking analysis

A PCR-based approach was used for tagging Dsn1, Mcm16, Ctf3, Cnn1, and Wip1 with 6xHis-6xFLAG at the endogenous loci in a DDY1810 (protease deficient) background. Cells were grown in YPD medium in 5 l flasks for initial tests or in a 300 l fermenter (Bioengineering) for preparative kinetochore purifications. Cell pellets were resuspended in lysis buffer (25 mM HEPES pH 8, 150 mM KCl, 5% glycerol, 2 mM $MgCl_2$, 0.02% NP-40) and droplets of yeast cell suspension were flash-frozen in liquid nitrogen and subsequently grinded into powder by a SPEX SamplePrep 970EFM freezer mill (C3 Prozess- und Analysentechnik GmbH). For protein complex purification 200 g of frozen cell powder were dissolved in 90 mL lysis buffer supplemented with phosphatase (Thermo Fisher Scientific) and protease inhibitors (Protease Inhibitors Cocktail Mix IV, Merck). Whole cell lysates were incubated with 120 U/ml benzonase (Sigma-Aldrich) for 30 min at room temperature and centrifuged at 65000 x g for 30 min. Tagged kinetochore subunits were immunoprecipitated by incubating cleared lysates with Protein A Dynabeads (Life Technologies) coupled to anti-FLAG M2 antibody (Sigma-Aldrich). Beads were washed once with 50 mL and once with 25 mL lysis buffer. Bound protein complexes were eluted from the magnetic beads using 0.15 mg/ml 2xStrep-6xFLAG peptide. Excess of peptide was removed by passing the eluate over a Strep-Tactin column (QIAGEN). For chemical crosslinking the eluted complexes were re-isolated on a Ni-NTA (QIAGEN) matrix.

Chemical crosslinking and mass spectrometry

Purified native and *in vitro* reconstituted kinetochore complexes were crosslinked by resuspending protein bound beads in an equimolar mixture of isotopically light (hydrogen) and heavy (deuterium) labeled bis[sulfosuccinimidyl]suberate (BS3, H_{12}/D_{12}) (Creative Molecules) at a final concentration of 0.25 - 0.5 mM at 30°C for 30 min. The crosslinking reaction was quenched by adding ammonium bicarbonate to a final concentration of 100 mM for 20 min at 30°C. The chemical crosslinks on native kinetochore complexes were identified by mass spectrometry as previously described (Walzthoeni et al., 2012). Briefly, crosslinked complexes were reduced with 5 mM TCEP (Thermo Fisher Scientific) at 35°C for 15 min and alkylated with 10 mM iodoacetamide (Sigma-Aldrich) at room temperature for 30 min in the dark. Proteins were digested with Lys-C (1:50 (w/w), Wako Pure Chemical Industries) at 35°C for 3 h, diluted with 50 mM ammonium bicarbonate to 1 M urea, and digested with trypsin (1:50 (w/w), Promega) overnight. Peptides were acidified with trifluoroacetic acid (TFA) at a final concentration of 1% and purified by reversed phase chromatography using C18 cartridges (Sep-Pak, Waters). Crosslinked peptides were enriched on a Superdex Peptide PC 3.2/30 column using water/acetonitrile/TFA (75/25/0.1, v/v/v) as mobile phase at a flow rate of 50 µl/min and were analyzed by liquid chromatography coupled to tandem mass spectrometry (LC-MS/MS) using an Orbitrap Elite instrument (Thermo Fisher Scientific). Fragment ion spectra were searched and crosslinks were identified by the dedicated software *xQuest* (Walzthoeni et al., 2012). The results were filtered according to the following parameters: Δ score $\leq$ 0.85, MS1 tolerance window of -4 to 4 ppm and score $\geq$ 22. The quality of all crosslink spectra passing the filter was manually validated and crosslinks were visualized as network plots using the webserver *xVis* (Grimm et al., 2015). The mass spectrometry proteomics data have been deposited to the ProteomeXchange Consortium via the PRIDE (Perez-Riverol et al., 2019) partner repository with the dataset identifier PXD011774 (in vivo network) and PXD011775 (*in vitro* reconstituted KMN).

Immunoprecipitation of the *in vivo* Mtw1 complex

Mtw1 anchor-away strains YTZ83-YTZ88 (Table S1) ectopically expressing Mtw1 wild-type and mutant proteins from rescue plasmids were grown at 30°C in 50 mL SD(-)His + 2% dextrose medium to an OD_{600} of 1-1.5. The cell density was normalized to the same OD_{600} and cells were pelleted and frozen as droplets in liquid N_2 and homogenized using a freezer mill.

For immunoprecipitation assays, 0.25-1 g of yeast powder were resuspended in IP buffer with protease inhibitors (25 mM HEPES pH 7.5, 150 mM KCl, 0.08% NP-40, 1 mM EDTA, 5 mM EGTA, 2 mM $MgCl_2$, 1.5x protease- [Calbiochem] and HALT phosphatase inhibitor cocktail [Thermo Fisher Scientific]) and lysed by intermittent vortexing and incubation on ice using 500 µL glass beads (0.5 mm diameter, Microspec). Lysates were cleared at 21000 x g for 30 minutes. 20 µL of anti-FLAG M2 agarose (Sigma-Aldrich) were incubated with the lysate at 4°C for one hour. Beads were washed once with 1 mL of IP buffer and once with wash buffer (25 mM HEPES pH 7.5, 150 mM KCl, 0.008% NP-40, 1 mM EDTA, 5 mM EGTA, 2 mM $MgCl_2$). Mtw1 proteins were eluted in wash buffer containing 0.5 mg/ml 3xFLAG peptide. Samples were analyzed using 4%–20% gradient SDS-PAGE gels (Mini-PROTEAN TGX, BioRad), immunoblotted using anti-FLAG M2 (1:5000, Sigma-Aldrich) and anti-Pgk1 (1:10000, Invitrogenantibodies, and visualized by the HRP-conjugated anti mouse secondary antibody (1:10000, Santa Cruz).

For mass spectrometric analysis, 5-20 g of yeast powder was lysed and Mtw1-1xFLAG purification was performed as described above. The eluates were subjected to tryptic digestion using the protocol described in the section above, and the tryptic peptides were separated from the 3xFLAG peptide by size exclusion chromatography. Samples were analyzed by LC-MS/MS using an Orbitrap Elite instrument (Thermo Fisher Scientific).

Protein intensities obtained by the software suite MaxQuant (Cox and Mann, 2008) of 5 biological replicates were extracted and merged by protein name. The least correlated replicate was removed and thus, 4 replicates per Mtw1 variant were analyzed. Proteins detected in a single replicate were eliminated and single peptide identifications present in at least 3 replicates were included. Protein raw intensities were normalized to the peptide count and log2-transformed. To penalize the lack of reproducibility, not detected protein intensity values in replicates were set to the minimum abundance in the matrix minus an offset. The average ratios of interactor to bait intensities were calculated and displayed by a color scale.

Amino acid sequence alignment

Interrelated budding yeast species with the highest similarity to *S. cerevisiae* Mtw1 or Kre28 protein were determined by a protein BLAST search. Multiple sequence alignments of Mtw1 and Kre28 protein sequences were conducted using Clustal Omega (Sievers et al., 2011).

Structural model prediction of KMN

Individual models were predicted using I-Tasser (Yang et al., 2015). The template for the MTW1c C-terminal region was specified without alignment using crystallized *K. lactis* MTW1c (PDB entry 5T58) (Dimitrova et al., 2016). The alignment of individual proteins was performed in UCSF Chimera (Pettersen et al., 2004) applying the match maker tool. Spc105 was modeled using the crystal structure of human Knl1 (PDB entry 4NF9) (Petrovic et al., 2014). The Kre28 model was obtained without a template.

QUANTIFICATION AND STATISTICAL ANALYSIS

Statistical analyses are described in the Figure legends and the Method Details.

Cell Reports, Volume *32*

Supplemental Information

C-Terminal Motifs of the MTW1 Complex Cooperatively Stabilize Outer Kinetochore Assembly in Budding Yeast

Medini Ghodgaonkar-Steger, Mia Potocnjak, Tomasz Zimniak, Josef Fischböck-Halwachs, Victor Solis-Mezarino, Sylvia Singh, Tea Speljko, Götz Hagemann, David Jan Drexler, Gregor Witte, and Franz Herzog

Supplemental Information

Supplemental Figures

Figure S1

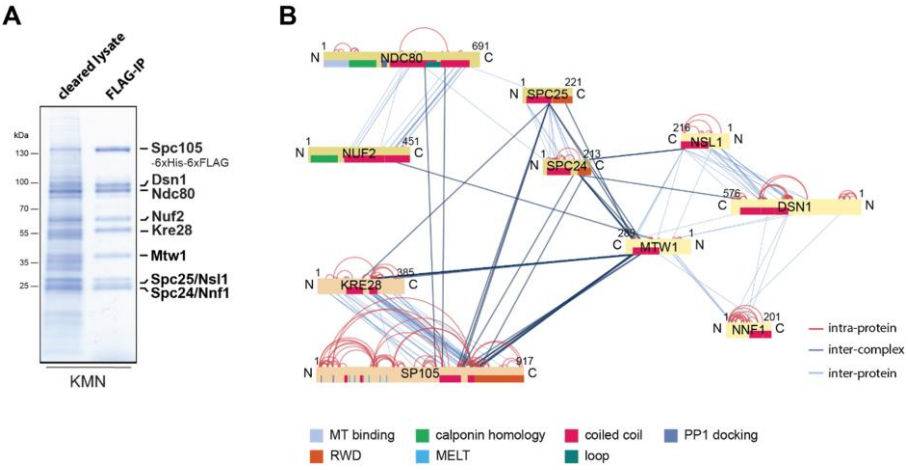

Figure S1. Crosslink-derived subunit connectivity map of the recombinant KMN network. Related to Figure 1, Figure 2 and Figure 7. (**A**) The recombinant KMN network complex was purified by a single-step FLAG immunoprecipitation from insect cells expressing the 10 subunits from a single baculovirus. The FLAG peptide eluate was analysed by SDS-PAGE and Coomassie staining. (**B**) KMN was crosslinked with BS3. A topological map of the KMN complex was generated based on identified inter- and intra-protein cross-links (Table S6). Proteins are represented as bars and the protein lengths and linkage sites correspond to the amino acid sequence.

Figure S2

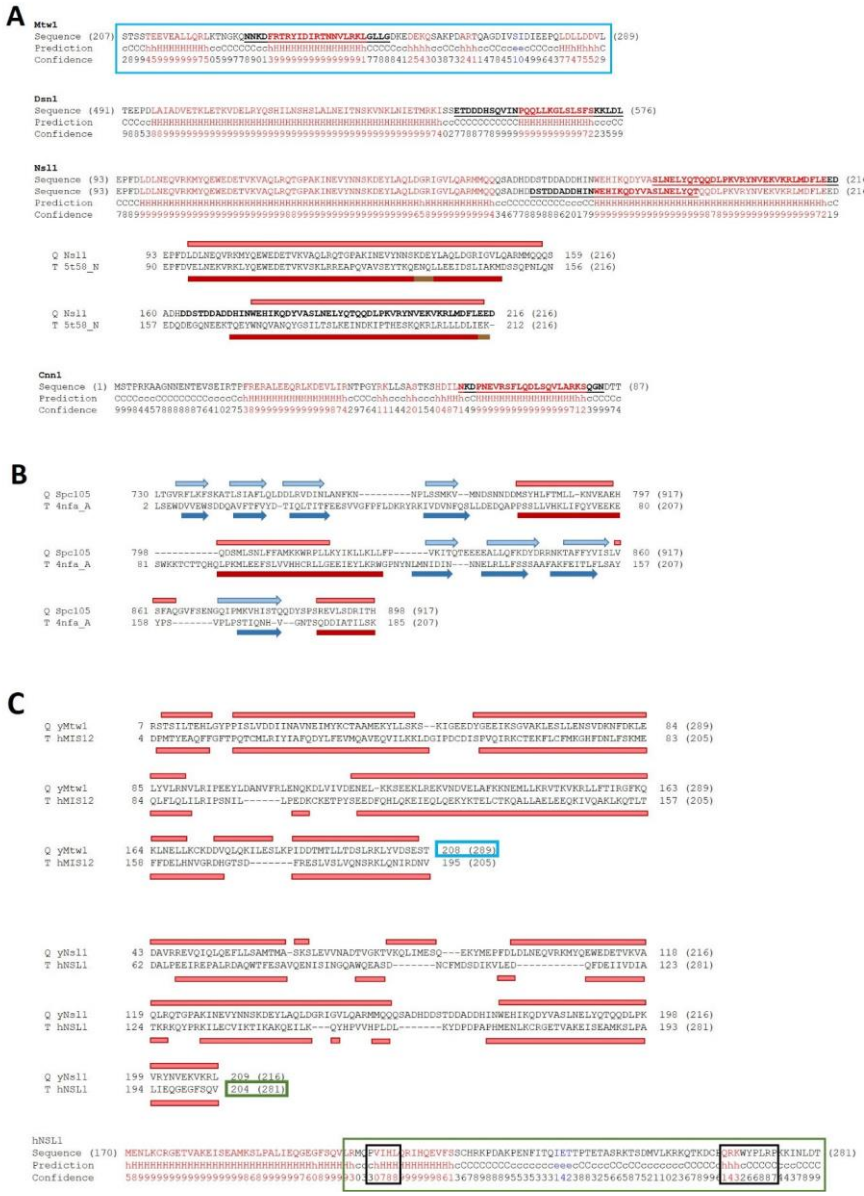

Figure S2. Bioinformatic sequence and secondary structure analysis of helical motifs interacting with dimeric RWD domains of the KMN network. Related to Figure 2. (**A**) Secondary structure predictions of the C-terminal regions of Mtw1, Dsn1 and Nsl1 and the N-terminal part of Cnn1 were obtained using PSIPRED. H (red), E (blue) and C (black) denote residues in predicted helices, β-strands or coils, respectively. Confidence values are ranging from 0 to 9 with uppercase letters for high confidence (6-9) and lowercase letters for low confidence (0-5). The peptide sequences used in peptide binding assays (table S3) are shown in bold and underlined. The query sequence of Nsl1 was also matched against *Kluyveromyces lactis* Nsl1 represented by PDB ID 5t58, chain N (Dimitrova et al., 2016) using the HHpred server and the alignment was displayed below the predicted secondary structure for Nsl1. The high confidence of the query-template match was indicated by HHpred true positive probability: 100.00, E-value=3.3e-52 and score=345.36. The secondary structure elements predicted by PSIPRED are displayed above the alignment of Nsl1 (light red rectangles: predicted helices) and the DSSP-assigned secondary structure elements (Kabsch and Sander, 1983) are displayed below the alignment (dark red rectangles: helices, brown rectangles: turns). The sequence alignment of human Mis12 and *Saccharomyces cerevisiae* Mtw1, depicted in (C), showed the extended C-terminal tail (light blue box) of Mtw1. (**B**) The C-terminus of Spc105 is predicted to adopt a dimeric RWD domain fold. The query sequence of Spc105 was matched and aligned with the template RWD dimer of human KNL1 represented by PDB ID 4nfa, chain A (Petrovic et al., 2014) using the HHpred server. The high confidence of the query-template match was indicated by HHpred true positive probability: 98.83, E-value=7.3e-08 and score=99.88. The secondary structure elements predicted by PSIPRED are displayed above the alignment of Spc105 (light blue arrows: predicted β-strands, light red rectangles: predicted helices) and the DSSP-assigned secondary structure elements (Kabsch and Sander, 1983) are displayed below the alignment (dark blue arrows: β-strands, dark red rectangles: helices). (**C**) Comparison of yeast to human sequences of Mtw1 to MIS12 and of Nsl1 to NSL1, respectively. Aligned regions were matched by HHpred with true positive probability: 99.98 for Mtw1 to MIS12 and 97.66 for Nsl1 to NSL1. Unmatched regions include the C-terminal Mtw1 amino acids 209-289 (light blue box) and the human NSL1 residues 205-281 (green box). The unmatched NSL1 region contains the PVIHL motif involved in interacting with HP1-α and Spc24/Spc25 (Petrovic et al., 2010) and the QRKWYPLRP flexible peptide which was co-crystallized with KNL1 (2131-2337) in PDB ID 4nf9 (Petrovic et al., 2014).

Figure S3

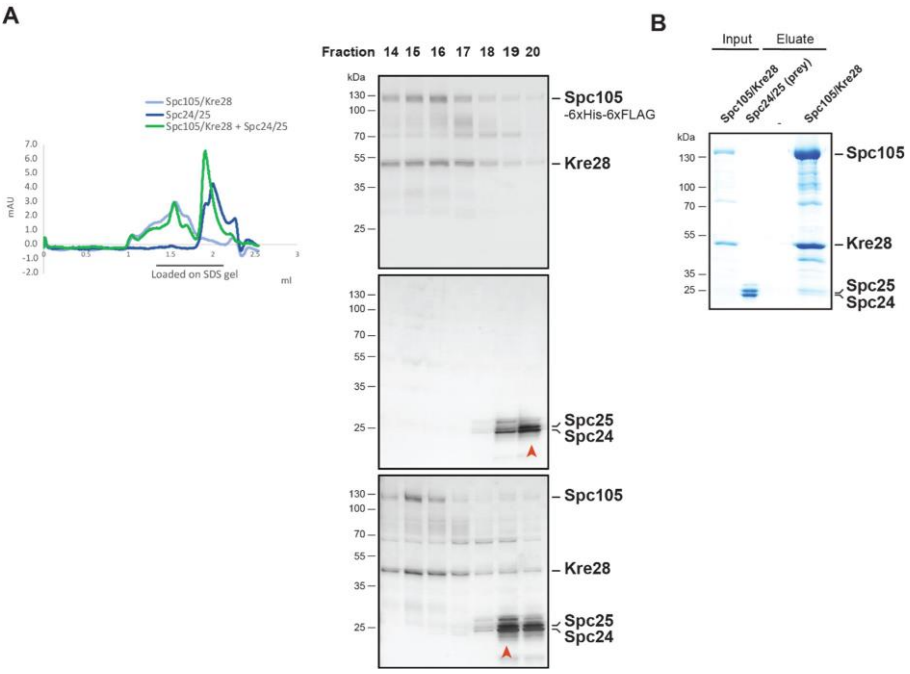

Figure S3. Analysis of the Spc105/Kre28 and Spc24/25 interaction by size exclusion chromatography. Related to Figure 5. (A) The interaction between Spc105/Kre28 and Spc24/25 complexes in the absence of MTW1c was analyzed using size exclusion chromatography. Protein complexes were mixed in an equimolar ratio, incubated on ice for 1 h and run on a Superose 6 Increase 3.2/300 column. The separated fractions were analyzed by SDS-PAGE and silver staining. The shift of the Spc24/25 peak fraction in the presence of Spc105/Kre28 indicated association of the complexes. **(B)** The *in vitro* binding assay was performed by immobilizing recombinant Spc105/Kre28 on anti-FLAG beads which were incubated with Spc24/25. The eluted protein complexes were visualized by SDS-PAGE and Coomassie staining.

Supplemental Tables

Table S1. Yeast strains used in this study. Related to Figure 1, Figure 2, Figure 3, Figure 5, Figure 6.

All strains are isogenic and unless specified with the S288C background.

Submitted as Excel file.

Table S2. Plasmids used in this study. Related to Figure 2, Figure 3, Figure 4, Figure 5, Figure 6.

Number	Plasmid
2886	pYCF1/ CEN3.L
BTZ51	pRS313-200 5'UTR Mtw1 ORF ^{WT}-1xFLAG
BTZ52	pRS313-200 5'UTR Mtw1 ORF$^{aa1-279}$-1xFLAG
BTZ53	pRS313-200 5'UTR Mtw1 ORF$^{aa\ 1-269}$-1xFLAG
BTZ54	pRS313-200 5'UTR Mtw1 ORF$^{aa\ 1-249}$-1xFLAG
BTZ55	pRS313-200 5'UTR Mtw1 ORF$^{aa\ 1-229}$-1xFLAG
BTZ60	pRS313-200 5'UTR Mtw1 ORF$^{\Delta Helix\ residues\ 232-248}$-1xFLAG
BMS5a	pRS313-200 5'UTR Mtw1 ORF$^{\Delta Helix\ replaced\ by\ CNN1\ residues\ 63-84}$-1xFLAG
BMS7a	pRS313-200 5' UTR Dsn1 ORF ^{WT} -1xFLAG
BMS8a	pRS313-Dsn1$^{aa1-574}$-1xFLAG
BMS9a	pRS313-Dsn1$^{aa1-574\ fused\ to\ CNN1\ residues\ 63-84}$-1xFLAG
BMS16	pDuet-Spc24-6xHis-Spc25
BMS 66	pRS313-200 5'UTR Mtw1 ORF^{F232DY236D}-1xFLAG
BMS 67	pRS313-200 5'UTR Mtw1 ORF^{V244DL248D}-1xFLAG
BMS68	pRS313-200 5'UTR Mtw1 ORF^{R233DY326D}-1xFLAG
BMP11	pKP29-6xHis-1xStrep-Dsn1$^{\Delta 2-171}$-Nsl1-Nnf1-Mtw1
BMP12	pKp29-6xHis-1xStrep-Dsn1$^{\Delta 2-171}$-Nsl1-Nnf1-Mtw1$^{\Delta 60}$

BMP13	pKP29-6xHis-1xStrep-Dsn1$^{\Delta 2\text{-}171}$-Nsl1-Nnf1-Mtw1$^{\Delta 232\text{-}248}$
BMP16	pKP29-6xHis-1xStrep-Dsn1$^{\Delta 2\text{-}171}$-Nsl1-Nnf1-Mtw1$^{\Delta 547\text{-}576}$
BMP58	pKp29-6xHis-1xStrep-Dsn1$^{\Delta 2\text{-}171}$-Nsl1-Nnf1-Mtw1 $^{F232D\ Y236D}$
BMP59	pKP29-6xHis-1xStrep-Dsn1$^{\Delta 2\text{-}171}$-Nsl1-Nnf1-Mtw1 $^{V244D\ L248D}$
BMP67	pKP29-6xHis-1xStrep-Dsn1$^{\Delta 2\text{-}171}$-Nsl1-Nnf1-Mtw1 $^{R233D\ Y236D}$
BMP69	Spc105-6xFlag-6xHis-Kre28
BMP70	Spc105-6xFlag-6xHis-Kre28 $^{M248D\ V251D}$
BMP71	Spc105-6xFlag-6xHis-Kre28 $^{L241D\ L245D}$
BMP72	Spc105-6xFlag-6xHis-Kre28 $^{L231D\ L234D}$
BMP73	Spc105-6xFlag-6xHis-Kre28 $^{V136D\ L139D}$
BMP74	Spc105-6xFlag-6xHis-Kre28 $^{I143D\ V146D}$
BMP91	pKP29-6xHis-1xStrep-Dsn1$^{\Delta 2\text{-}171}$-Nsl1$^{\Delta 164\text{-}193}$-Nnf1-Mtw1
BMP93	pKP29-6xHis-1xStrep-Dsn1$^{\Delta 2\text{-}171}$-Nsl1$^{\Delta 164\text{-}193}$-Nnf1-Mtw1 $^{\Delta 232\text{-}248}$
BMP109	pBIG2ABC Ndc18-Nuf2-Spc24-Spc25-Mtw1-Nnf1-Nsl1-Dsn1-Spc105-6xHis6xFlag-Kre28
BMS69	pRS313-200 5'UTR Nsl11-1xFLAG
BMS70	pRS313-200 5'UTR Nsl1 ORF$^{\Delta 164\text{-}193}$-1xFLAG
BMS71	pRS313-200 5'UTR Kre28 ORF ^{WT}-1xFLAG
BMS72	pRS313-200 5'UTR Kre28 ORFM ^{248DV251D}-1xFLAG
BMS73	pRS313-200 5'UTR Kre28 ORFL^{241DL245D}-1xFLAG
BMS74	pRS313-200 5'UTR Kre28 ORF^{L231DL234D}-1xFLAG
BMS75	pRS313-200 5'UTR Kre28 ORF^{V136DL139D}-1xFLAG
BMS76	pRS313-200 5'UTR Kre28 ORF^{I143DV146D}-1xFLAG

Table S3. Peptides related to Figure 4.

Peptides 1-14 (underlined) were preceded with a Strep tag and a short linker (SAWSHPQFEK*GGSA*).

Number Protein ID	Sequence
MSP1 Cnn1$^{60-84}$	SAWSHPQFEK*GGSA*NKDPNEVRSFLQDLSQVLARKSQGN
MSP5 Mtw1$^{228-252}$	SAWSHPQFEK*GGSA*NNKDFRTRYIDIRTNNVLRKLGLLG
MSP9 Dsn1$^{548-576}$	SAWSHPQFEK*GGSA*ETDDDHSQVINPQQLLKGLSLSFSKKLDL
MSP13 Nsl1-1$^{183-216}$	SAWSHPQFEK*GGSA*DSTDDADDHINWEHIKQDYVASLNELYQT
MSP14 Nsl1-2$^{163-192}$	SAWSHPQFEK*GGSA*SLNELYQTQQDLPKVRYNVEKVKRLMDFLEED
MSP15 Dsn1$^{555-574}$-linker	QVINPQQLLKGLSLSFSKKLGGGSGGGSGGSGGSA
MSP16 Dsn1$^{555-574}$-linker-Mtw1$^{229-251}$	QVINPQQLLKGLSLSFSKKLGGGSGGGSGGSGGSANKDFRTRYIDIRTNNVLRKLGLL

Table S4. Inter- and intra-protein crosslinks identified on native affinity-purified kinetochore complexes. Related to Figure 1.

Kinetochore complexes were affinity-purified through the 6×His-6×FLAG-tag on 5 subunits from lysates of exponentially grown budding yeast cells using an anti-FLAG antibody and were chemically crosslinked by BS3 (Materials and methods). In total 225 inter-protein (dark blue) and 237 intra-protein (light blue) crosslinks on the kinetochore structure which are visualized in Figure 1B. In addition, 10 inter-protein (dark green) and 20 intra-protein (light green) crosslinks were detected on kinetochore associated complexes like the Dam1 complex which are not displayed in Figure 1B for simplicity purpose.

The listed crosslinks are sorted alphabetically according to Protein1 and to the Id.score. (No – Crosslink identifier; Bait – UniProt entry name of bait protein; Topology – amino acid sequences of peptides indicating the relative position of the linked lysines; Protein1, Protein2– UniProt name of crosslinked proteins; AbsPos1, AbsPos2 – absolute amino acid position of linked lysines; m/z – mass to charge ratio; z – charge; Error – mass deviation from the monoisotopic precursor mass in ppm; mions, number of fragment ions per crosslink; Nseen – number of fragment ion spectra assigned to the crosslink in entire dataset; Nexp – number of experiments identifying the crosslink; Id.Score – xQuest identification score)

Submitted as Excel file.

Table S5. Predicted and experimentally annotated protein domains and motifs depicted in protein crosslink networks. Related to Figure 1 and S1.

Protein name along with known or predicted domains with residue numbers are indicated. Where appropriate domain functions are mentioned.

Protein	Domain/Motif	Start	End	Reference
Mif2	MTW1C binding	1	35	(Hornung et al., 2014)
Mif2	signature motif	238	312	(Hornung et al., 2014)
Mif2	IML3/CHL4 binding	256	549	(Hinshaw and Harrison, 2013)
Mif2	cupin fold	439	526	(Hornung et al., 2014)
Mtw1	coiled coil	116	168	(Dimitrova et al., 2016)
Mtw1	coiled coil	169	233	(Dimitrova et al., 2016)
Dsn1	coiled coil	363	395	(Dimitrova et al., 2016)
Dsn1	coiled coil	396	424	(Dimitrova et al., 2016)
Dsn1	coiled coil	425	479	(Dimitrova et al., 2016)
Nsl1	coiled coil	97	150	(Dimitrova et al., 2016)
Nsl1	coiled coil	151	168	(Dimitrova et al., 2016)
Nsl1	coiled coil	169	216	(Dimitrova et al., 2016)
Nnf1	coiled coil	121	179	(Dimitrova et al., 2016)
Nnf1	coiled coil	180	205	(Dimitrova et al., 2016)
Cnn1	histone fold	271	335	(Schleiffer et al., 2012)
Cnn1	coiled coil Spc24/25 binding	61	79	(Malvezzi et al., 2013)
Wip1	histone fold	1	89	Sequence alignment model
Ndc80	MT binding	1	113	(Lampert et al., 2013)
Ndc80	calponin homology	114	233	(Wei et al., 2007)
Ndc80	coiled coil	258	279	MARCOIL prediction
Ndc80	coiled coil	294	499	MARCOIL prediction
Ndc80	loop	453	520	(Maure et al., 2011)
Ndc80	coiled coil	519	645	MARCOIL prediction
Nuf2	calponin homology	13	132	(Ciferri et al., 2008)
Nuf2	coiled coil	161	338	MARCOIL prediction
Nuf2	coiled coil	341	450	MARCOIL prediction
Spc24	coiled coil	19	123	MARCOIL prediction
Spc24	RWD	155	213	(Wei et al., 2006)
Spc25	coiled coil	18	129	MARCOIL prediction
Spc25	RWD	133	221	(Wei et al., 2006)
Spc105	PP1 docking	21	24	(Rosenberg et al., 2011)
Spc105	PP1 docking	74	78	(Rosenberg et al., 2011)
Spc105	coiled coil	125	138	MARCOIL prediction
Spc105	MELT	146	149	(London et al., 2012)
Spc105	MELT	169	172	(London et al., 2012)
Spc105	coiled coil	194	206	MARCOIL prediction
Spc105	MELT	208	211	(London et al., 2012)
Spc105	MELT	232	235	(London et al., 2012)
Spc105	MELT	281	284	(London et al., 2012)
Spc105	MELT	310	313	(London et al., 2012)
Spc105	coiled coil	551	638	(Lupas et al., 1991)
Spc105	coiled coil	670	708	(Lupas et al., 1991)
Spc105	RWD	714	865	JPred4
Kre28	coiled coil	128	169	MARCOIL prediction
Kre28	coiled coil	229	259	MARCOIL prediction
Mtw1	Coiled coil	232	248	JPred4
Dsn1	Coiled coil	388	399	JPred4

Protein	Domain/Motif	Start	End	Reference
Nsl1	Coiled coil	176	192	JPred4
Nsl1	Coiled coil	199	210	JPred4

Table S6. Inter- and intra-protein crosslinks identified on the recombinant KMN network complex. Related to Figure 7 and Figure S1.

The 10 outer kinetochore subunits were coexpressed in insect cells from a single multigene baculovirus. A stoichiometric KMN complex was purified through Spc105-6xFLAG-6xHis and chemical crosslinks introduced by BS3 were identified as described (Materials and Methods). In total, 191 inter-protein (dark blue) and 253 (light blue) intra-protein crosslinks were detected on the recombinant complex and are visualized in Figure S1. The crosslinks and parameters of identification are displayed as described (Table S3).

Submitted as Excel file.

Supplemental References

Ciferri, C., Pasqualato, S., Screpanti, E., Varetti, G., Santaguida, S., Dos Reis, G., Maiolica, A., Polka, J., De Luca, J.G., De Wulf, P., *et al.* (2008). Implications for kinetochore-microtubule attachment from the structure of an engineered Ndc80 complex. Cell *133*, 427-439.

Dimitrova, Y.N., Jenni, S., Valverde, R., Khin, Y., and Harrison, S.C. (2016). Structure of the MIND Complex Defines a Regulatory Focus for Yeast Kinetochore Assembly. Cell *167*, 1014-1027 e1012.

Hinshaw, S.M., and Harrison, S.C. (2013). An Iml3-Chl4 heterodimer links the core centromere to factors required for accurate chromosome segregation. Cell reports *5*, 29-36.

Hornung, P., Troc, P., Malvezzi, F., Maier, M., Demianova, Z., Zimniak, T., Litos, G., Lampert, F., Schleiffer, A., Brunner, M., *et al.* (2014). A cooperative mechanism drives budding yeast kinetochore assembly downstream of CENP-A. The Journal of cell biology *206*, 509-524.

Kabsch, W., and Sander, C. (1983). Dictionary of protein secondary structure: pattern recognition of hydrogen-bonded and geometrical features. Biopolymers *22*, 2577-2637.

Lampert, F., Mieck, C., Alushin, G.M., Nogales, E., and Westermann, S. (2013). Molecular requirements for the formation of a kinetochore-microtubule interface by Dam1 and Ndc80 complexes. J Cell Biol *200*, 21-30.

London, N., Ceto, S., Ranish, J.A., and Biggins, S. (2012). Phosphoregulation of Spc105 by Mps1 and PP1 regulates Bub1 localization to kinetochores. Current biology : CB *22*, 900-906.

Lupas, A., Van Dyke, M., and Stock, J. (1991). Predicting coiled coils from protein sequences. Science *252*, 1162-1164.

Malvezzi, F., Litos, G., Schleiffer, A., Heuck, A., Mechtler, K., Clausen, T., and Westermann, S. (2013). A structural basis for kinetochore recruitment of the Ndc80 complex via two distinct centromere receptors. The EMBO journal *32*, 409-423.

Maure, J.F., Komoto, S., Oku, Y., Mino, A., Pasqualato, S., Natsume, K., Clayton, L., Musacchio, A., and Tanaka, T.U. (2011). The Ndc80 loop region facilitates formation of kinetochore attachment to the dynamic microtubule plus end. Current biology : CB *21*, 207-213.

Petrovic, A., Mosalaganti, S., Keller, J., Mattiuzzo, M., Overlack, K., Krenn, V., De Antoni, A., Wohlgemuth, S., Cecatiello, V., Pasqualato, S., *et al.* (2014). Modular assembly of RWD domains on the Mis12 complex underlies outer kinetochore organization. Molecular cell *53*, 591-605.

Petrovic, A., Pasqualato, S., Dube, P., Krenn, V., Santaguida, S., Cittaro, D., Monzani, S., Massimiliano, L., Keller, J., Tarricone, A., *et al.* (2010). The MIS12 complex is a protein interaction hub for outer kinetochore assembly. The Journal of cell biology *190*, 835-852.

Rosenberg, J.S., Cross, F.R., and Funabiki, H. (2011). KNL1/Spc105 recruits PP1 to silence the spindle assembly checkpoint. Current biology : CB *21*, 942-947.

Schleiffer, A., Maier, M., Litos, G., Lampert, F., Hornung, P., Mechtler, K., and Westermann, S. (2012). CENP-T proteins are conserved centromere receptors of the Ndc80 complex. Nat Cell Biol *14*, 604-613.

Wei, R.R., Al-Bassam, J., and Harrison, S.C. (2007). The Ndc80/HEC1 complex is a contact point for kinetochore-microtubule attachment. Nat Struct Mol Biol *14*, 54-59.

Wei, R.R., Schnell, J.R., Larsen, N.A., Sorger, P.K., Chou, J.J., and Harrison, S.C. (2006). Structure of a central component of the yeast kinetochore: the Spc24p/Spc25p globular domain. Structure *14*, 1003-1009.

4 Discussion

The initial goal of this thesis was to characterise essential kinetochore complexes associated with the centromeric nucleosome in budding yeast, which bridge the centromeric DNA and the microtubule binding KMN network at the outer kinetochore. The budding yeast kinetochore assembled on a point centromere is thought to represent the simplest kinetochore unit. It links a single Cse4^{CENP-A} containing nucleosome to a single microtubule. The human kinetochore has been proposed to be built up by several such units. Roughly 100 CENP-A nucleosomes give rise to a human kinetochore that attaches 20-30 microtubules (Verdaasdonk and Bloom 2011). Before the start of my work the only known interactor of the Cse4^{CENP-A} nucleosome was Mif2^{CENP-C} (Kato et al. 2013). Using biochemical reconstitution, co-immunoprecipitation and crosslinking combined with mass spectrometry we have identified two additional kinetochore components – Ame1/Okp1 and Ndc10, which connect the outer kinetochore to the centromeric nucleosome. Furthermore, we have identified previously unknown interactions within the inner and outer kinetochore that are crucial for the cooperative stabilization of the kinetochore architecture and its function.

4.1 Mif2 and Ame1/Okp1 are direct and selective interactors of the Cse4 containing nucleosome

In order to screen for direct interactors of the budding yeast centromeric nucleosome we reconstituted the individual CTF19c^{CCAN} subcomplexes, Mif2, Ame1/Okp1, Ctf19/Mcm21, Chl4/Iml3, Mcm16/Ctf3/Mcm22, Cnn1/Wip1, Nkp1/Nkp2, Mhf1/Mhf2, and Cse4 or H3 containing nucleosomes *in vitro*. As Mif2 was previously identified to bind the C-terminal tail of Cse4 it served as a positive control. Applying the electrophoretic mobility shift assay (EMSA) I have identified Ame1/Okp1 as another selective binding partner of the Cse4 nucleosome (Figure 7A and B). The interaction does not rely on the AT-rich centromeric DNA as proposed by (Hornung et al. 2014) since we reconstituted the nucleosomes using the Widom 601 nucleosome-positioning DNA sequence. All of the other members of the CTF19c^{CCAN} did not form stable complexes with either Cse4 or H3 nucleosomes.

Furthermore, I have performed crosslinking analysis on a complex assembled on Cse4 nucleosomes by Mif2, Ame1/Okp1, Ctf19/Mcm21 and obtained a connectivity map of 349 inter-protein crosslinks. The network confirms several known interactions such as the binding of Mif2 and Ame1 to the MTW1c as well as the interaction between Mif2 and Ame1/Okp1 (Przewloka et al. 2011, Screpanti et al. 2011, Hornung et al. 2014, Dimitrova et al. 2016). Inter-protein crosslinks confirm the interaction between Mif2 and Chl4/Iml3 within the annotated Chl4/Iml3 binding domain and the formation of a complex between Ame1/Okp1, Ctf19/Mcm21 and Chl4/Iml3 (Hinshaw and Harrison 2013, Schmitzberger et al. 2017). The Mif2 signature domain uses the C-terminus of Cse4 protein as docking site (Kato et al. 2013), however we were able to identify that Ame1/Okp1 docks onto the N-terminus of Cse4 (Anedchenko et al. 2019, Fischbock-Halwachs et al. 2019). Deletion of amino acids 34-46 in the N-terminal region of Cse4 leads to the loss of interaction with Ame1/Okp1. We also showed that this region is important for cell viability using the anchor-away assay. The crosslinks pinpointed a helical region in Okp1 as the binding site of the Cse4 N-terminus which I further confirmed using deletion mutants and size exclusion chromatography. Deletion of helix2 (aa 163-187) of Okp1 prevents complex formation with Cse4 nucleosomes in EMSA or size exclusion chromatography experiments. Deletion of this region *in vivo* results in a lethal phenotype indicating that the interaction between Ame1/Okp1 and Cse4 is essential for cell viability.

The human orthologue of Chl4/Iml3, CENP-N/L, was shown to interact with the CENP-A nucleosome (Pentakota et al. 2017, Tian et al. 2018, Chittori et al. 2018), but we could not reproduce this interaction with the budding yeast orthologous proteins using EMSA or crosslinking analysis. Furthermore, the human orthologue of the CTF3 complex, CENP-HIK, binds equally well to Cse4 and H3 nucleosomes (Weir et al. 2016), however the budding yeast orthologues did not show this interaction. In summary, our results suggest that the architecture of the budding yeast inner kinetochore is distinct from the human kinetochore, which could be a consequence of assembling the kinetochore structure on highly divergent centromeres. In contrast to the regional centromeres in humans, the geometrical constraints of the budding yeast point centromere might require a specific Cse4CENP-A binding structure in order to build a high-affinity link of one Cse4 containing nucleosome to a single microtubule that facilitates the transmission of the microtubule tensile forces for biorientation and accurate chromosome segregation.

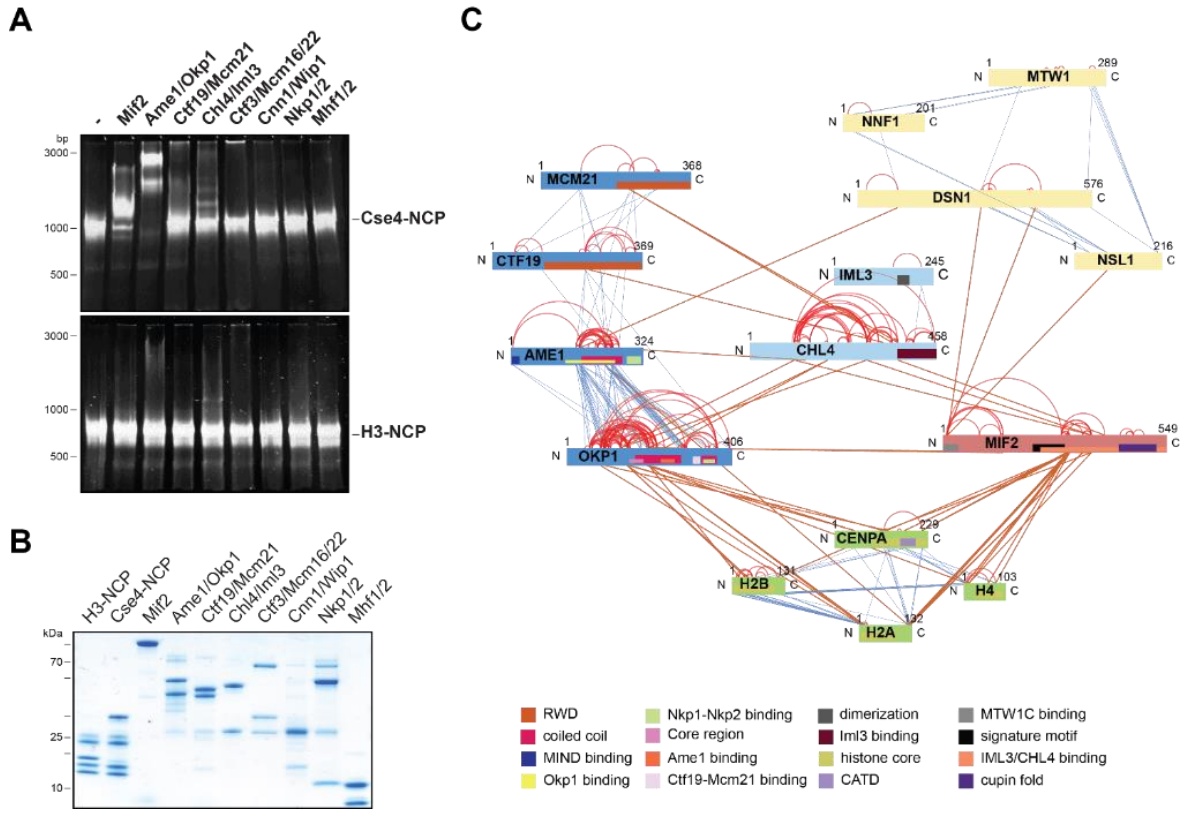

Figure 7 **The heterodimeric Ame1/Okp1 complex directly and selectively binds the Cse4 nucleosomal core particle.**

(A) Electrophoretic mobility shift assays of the indicated CTF19c^{CCAN} subunits and subcomplexes mixed in a 2:1 molar ratio with either Cse4- or H3-NCPs. DNA/protein complexes were separated on a 6% native polyacrylamide gel. The DNA is visualized by SYBR Gold staining. (B) Coomassie stained gel of the individual inner kinetochore components, recombinantly purified from *E. coli*, used in the EMSA in (A). **(C)** XLMS analysis of the *in vitro* reconstituted Cse4-NCP:Mif2:COMA:Chl4/ Iml3:MTW1c complex. Proteins are represented as bars indicating annotated domains (Supplementary file 3) according to the color scheme in the legend. Subunits of a complex are represented in the same color and protein lengths and cross-link sites are scaled to the amino acid sequence. (Figure and description from (Fischbock-Halwachs et al. 2019))

4.2 The Ndc10 N-terminus recruits MTW1c in mitosis

In addition to Ame1/Okp1 as a link between the Cse4 nucleosomes and the outer kinetochore MTW1c, I have identified Ndc10, a subunit of the CBF3 complex, as another centromeric link

within the kinetochore architecture. The CBF3 complex has been previously identified as a direct binder of Cse4 nucleosomes which displays CEN DNA specificity and is required for the recruitment of other kinetochore proteins. The CBF3c represents the assembly of Skp1:Ctf13:(Cep3)2:(Ndc10)2 with Ndc10 loosely interacting with the CBF3 core complex *in vitro* (Doheny et al. 1993, Goh and Kilmartin 1993, Russell et al. 1999, Strunnikov et al. 1995, Jiang et al. 1993, Yan et al. 2019, Leber et al. 2018). Using pull-down experiments of endogenously tagged Ndc10 from synchronized cell lines I found a previously unknown interaction with the outer kinetochore MTW1c. Interestingly, the co-precipitated levels of Mtw1/Nnf1 were 4 times higher in mitotically arrested cells compared to cells synchronized in G1 indicating that this pathway specifically recruits the outer kinetochore in mitosis. This is particularly intriguing for budding yeast where, unlike the human kinetochore, the kinetochore is fully assembled and bound to the microtubule throughout the cell cycle (Biggins 2013, Hara and Fukagawa 2020).

I have investigated this finding using biochemical and genetic experiments and compared it to the previously identified pathways which recruit the outer kinetochore via interactions with Mif2 and Ame1/Okp1. Interestingly, the Ndc10 binding mode of MTW1c is similar to the other two MTW1c recruiters. Notably, it binds to the same loop-helix-loop region (amino acids 24-90) of the Mtw1 head I domain (Dimitrova et al. 2016) with the difference that it predominantly binds helix 24-40. Mif2 and Ame1/Okp1 require the full helix-loop-helix formation for the interaction with a higher sensitivity to perturbations or even single mutations. Thus, Ndc10 might represent a more robust Mtw1 binder that does not require Nnf1 for the interaction. In comparison to Mif2 and Ame1/Okp1, the interaction of Ndc10 is even more enhanced by $Dsn1^{S240/250}$ phosphorylation through $Ipl1^{Aurora\text{-}B}$ kinase which renders the Mtw1/Nnf1 head I accessible for binding by Ndc10, Mif2 or Ame1. The Ndc10 region associating with Mtw1 lies in its N-terminus (amino acids 1-55), similar to the MTW1c binding sites of Mif2 and Ame1/Okp1. This suggests that Ndc10 is a third link required for the recruitment of an additional microtubule binding unit, and thus further stabilizes microtubule attachment in mitosis. I have identified the first 11 amino acids and residue Y52 to be required for the interaction with Mtw1 as deletion or substitution mutants cause loss of binding *in vitro*. Analysis of the corresponding mutants in cell viability assays using the anchor-away assay, suggested that the Ndc10 – Mtw1 interaction is not essential. However, expression of the Ndc10-Y52A mutant in a Mif2Δ35 mutant background resulted in severe growth defects and

synthetic lethality. This indicates that the Ndc10 pathway is redundant with the Mif2-mediated MTW1c interaction and the cell cannot solely rely on the Ame1/Okp1 link to the outer kinetochore. We do not yet fully understand the molecular details of how the three different proteins organize recruitment of the KMN network and whether there is a binding hierarchy that is potentially controlled by posttranslational modifications. This will require *in vitro* reconstitution studies of a minimal kinetochore containing the CBF3c, Mif2, Ame1/Okp1 and the outer kinetochore MTW1c.

4.3 Mif2 interacts with the Ndc10 N-terminus in a phosphorylation-dependent manner and competes with Mtw1 binding

Interaction of the two MTW1c receptors Ame1/Okp1 with Mif2 was investigated and confirmed previously (Hornung et al. 2014), we therefore aimed to map the binding interdependencies between Ndc10, Ame1/Okp1 and Mif2. Although it was reported that the COMA complex (Ctf19/Okp1/Mcm21/Ame1) interacts with the CBF3 complex (Ortiz et al. 1999) we did not find convincing evidence that this interaction occurs through Ame1/Okp1 (purified from *E. coli* or insect cells) and the N-terminal $Ndc10^{1-551}$ region, but we cannot exclude the possibility that additional factors in a cellular environment might support this interaction. In contrast, Mif2 and $Ndc10^{1-551}$ forms a stable complex *in vitro*. I have found that *in vitro* Mif2 binding occurs only upon phosphorylation of a serine-rich region (aa 217-240), predominantly by $Cdc5^{PLK1}$ kinase. Interestingly, the same region of Mif2 also binds Ame1/Okp1 in a phosphorylation-dependent manner (Hagemann *et al.* manuscript submitted). How this interaction is regulated and whether there is a competition of Ndc10 and Ame1/Okp1 for the binding site at Mif2 remains to be investigated.

Using biochemical experiments, I have determined that the binding domain of Mif2 maps to the same, albeit slightly larger region of Ndc10, as that of Mtw1. An N-terminal deletion (Ndc10-Δ11) or a single site mutation of the conserved residue Y52 to alanine abrogates both interactions of Mif2 and Mtw1 in vitro. Thus, I wanted to determine whether there is a competition between Mif2 and Mtw1 for the Ndc10 binding site. Mif2-Δ170 was unable to bind Mtw1 although its Ndc10 binding site remains preserved. Upon competition in the binding assay Mif2-Δ170 was able to reduce bound Ndc10 levels from the Ndc10-Mtw1 complex by 50%. This indicates that phosphorylated Mif2 competes off Ndc10 from the Mtw1 protein. As

I determined by *in vivo* pull-down assays, that Ndc10 predominantly co-precipitates Mtw1 and to a lesser extent Mif2 in mitosis we hypothesised that in a certain condition Mtw1 has a binding advantage over Mif2. Using binding assays, I found that Mif2 bound by its known binding partner Chl4/Iml3 (Hinshaw and Harrison 2013) has 50% reduced ability of Ndc10 binding compared to free Mif2. Apart from the de-phosphorylated state of Mif2 this might be another mechanism to enable Mtw1 to preferentially access Ndc10 in mitosis. We speculate that binding of Mif2 and Ndc10 occurs during the initial step of kinetochore assembly followed by the binding of additional factors to Mif2 such as Chl4/Iml3. This improves the accessibility of Ndc10 for Mtw1 binding and facilitates stabilization of the outer kinetochore in mitosis.

4.4 The C-terminus of the MTW1c is the centrepiece of outer kinetochore assembly

The advances in crystallography and cryo-electron microscopy over the recent years yielded high resolution structures of kinetochore proteins and sub-complexes providing the foundation for studying the kinetochore architecture (Dimitrova et al. 2016, Yan et al. 2019). The structures are predominantly limited to structured and rigid areas and thus, crosslinking and mass spectrometry has proven a useful tool to integrate the structural information on the unstructured and flexible parts which are frequently implicated in establishing the interactions between kinetochore subcomplexes. We employed large-scale purifications of endogenously tagged budding yeast kinetochore proteins in order to obtain a comprehensive network of interactions and elucidate binding dependencies in the outer kinetochore. We identified 225 inter-protein and 237 intra-protein crosslinks on the inner and outer kinetochore subunits confirming most of the known interactions (Kudalkar et al. 2015, Malvezzi et al. 2013, Pekgoz Altunkaya et al. 2016a, Schleiffer et al. 2012, Hornung et al. 2014). We observed a majority of crosslinks connecting the C-termini of the MTW1c to the other KMN subcomplexes, Spc105/Kre28 and the NDC80c. In our previous work we have shown that the N-terminus of MTW1c is a crucial link to the CCAN by connecting to Ame1/Okp1, Mif2 and Ndc10 proteins, while its C-terminal region serves as a central hub for outer kinetochore recruitment. The C-terminus of MTW1c is proteolytically unstable and flexible which is the reason why it was not possible to observe its features in the published structures (Dimitrova et al. 2016).

Crosslinks specifically indicated several regions in the C-termini of Mtw1, Dsn1 and Nsl1 described or predicted as helices. The interaction between MTW1c and Spc24/25 through the

Dsn1 helix was previously described (Kudalkar et al. 2015, Malvezzi et al. 2013). Cnn1, a CTF19c protein, binds to the same site on Spc24/25 as Dsn1, but with a higher affinity and thus, was used to compare the relative affinities of MTW1c interactions. Cnn1 levels peak in anaphase and it is believed to compete with MTW1c upon Cnn1 dephosphorylation during mitotic exit (Malvezzi et al. 2013, Bock et al. 2012).

How the budding yeast Spc105/Kre28 is recruited to the KMN network was shown at the time. In humans, motifs NSL1$^{209–213}$ and NSL1$^{258–281}$ are sufficient to recruit SPC24/25 and KNL1, respectively (Petrovic et al. 2010, Petrovic et al. 2014). These motifs, however, are not conserved in budding yeasts. Using *in vitro* binding assays with the predicted helical peptides of the MTW1c C-termini, we identified Dsn1 and Mtw1 as predominant interactors of the Spc24/25 complex. Together, Dsn1 and Mtw1 peptides synergistically increased the binding affinity to Spc24/25 indicating that multiple C-terminal motifs cooperatively stabilize KMN network assembly. Mtw1 and Nsl1 motifs showed preferential binding of the SPC105c. In order to evaluate the impact of different helices on recruiting SPC105c and Spc24/25 in the context of the full-length MTW1c I have recombinantly expressed MTW1c mutants carrying deletion or point mutations within the Mtw1, Dsn1 or Nsl1 helices. Deletion of either of the individual helices led to the loss of Spc24/25 binding, indicating that the binding is very sensitive to perturbations and that Ndc80C is cooperatively stabilized at the KMN network in order to attach the microtubules to the kinetochore.

In order to evaluate the importance of the Mtw1 helical motif we performed a series of pull-down assays from *S. cerevisiae* using different C-terminal deletion mutants and identified the associated proteins by mass spectrometry. Deletion of the Mtw1$^{232–248}$ helix resulted in loss of SPC105c and NDC80c recruitment and led to lethality in the cell growth assays. This indicates that the predicted Mtw1 helix is crucial for KMN assembly in budding yeast. Moreover, we were able to identify single amino acids within the Mtw1 helix required for Spc24/25, but not SPC105c interaction. The Mtw1$^{V244D/L248D}$ mutant that abrogated Spc24/25 binding *in vitro*, was not viable which implies that the Mtw1-Spc24/25 interaction is important for cell viability. Helix mutants within the full-length MTW1c complex showed the importance of the Nsl1 helix for Spc24/25 binding in vitro which could not be determined by the peptide binding assays. Together, our experiments indicate that the C-terminal motifs of Nsl1 and Mtw1 recruit SPC105c and support the recruitment of Spc24/25 by the Dsn1 C terminus (**Figure 8**).

4.5 The Spc105/Kre28 recruitment depends on the Kre28 coiled-coil 2 domain

In order to determine how Spc105/Kre28 is recruited to the MTW1c we created a series of deletion mutants based on the crosslink information obtained from analysis of the recombinant and endogenous KMN network. Deletion of the coiled-coil domains of Spc105 abrogated MTW1c binding and at the same time, prevented complex formation with Kre28. We therefore, expressed full-length Spc105 without Kre28 to exclude the possibility that the loss of Kre28 might have interfered with the binding, however Spc105 alone was not able to bind MTW1c. This indicates that unlike in humans where Zwint-1 is dispensable for the interaction, Kre28 is responsible for the recruitment of SPC105c to the MTW1c C-terminus. Based on the multiple sequence alignment of Kre28 from interrelated yeast species I have generated double point mutants within the two coiled-coils to determine the binding site of MTW1c on Kre28. Mutations within coiled-coil 2 impaired MTW1c binding whereas coiled-coil 1 mutants had no effect on the interaction. Notably, mutants of the coiled-coil 2 are viable as are the mutants of the Mtw1 helix showing a reduction of bound SPC105c levels indicating that this interaction might be further stabilized through phosphorylation or other protein interactions that we have not detected.

The outer kinetochore KMN network displays high levels of cooperativity. As within the MTW1c the combination of the Mtw1 and Dsn1 helical peptides increases overall affinity for the recruitment of the NDC80c, it is likely that the network has to satisfy a certain degree of protein association to withstand the pulling forces of the depolymerizing microtubules. Furthermore, binding of the full KMN super complex displays a 50 % stronger binding of SPC105c when Spc24/25 is present together with MTW1c, likely through the weak interactions between SPC105c and Spc24/25. Overall, the KMN network creates a strong and stable microtubule receptor sensitive to potential shortcomings within the system in order to prevent that chromosome segregation errors are passed on to future generations.

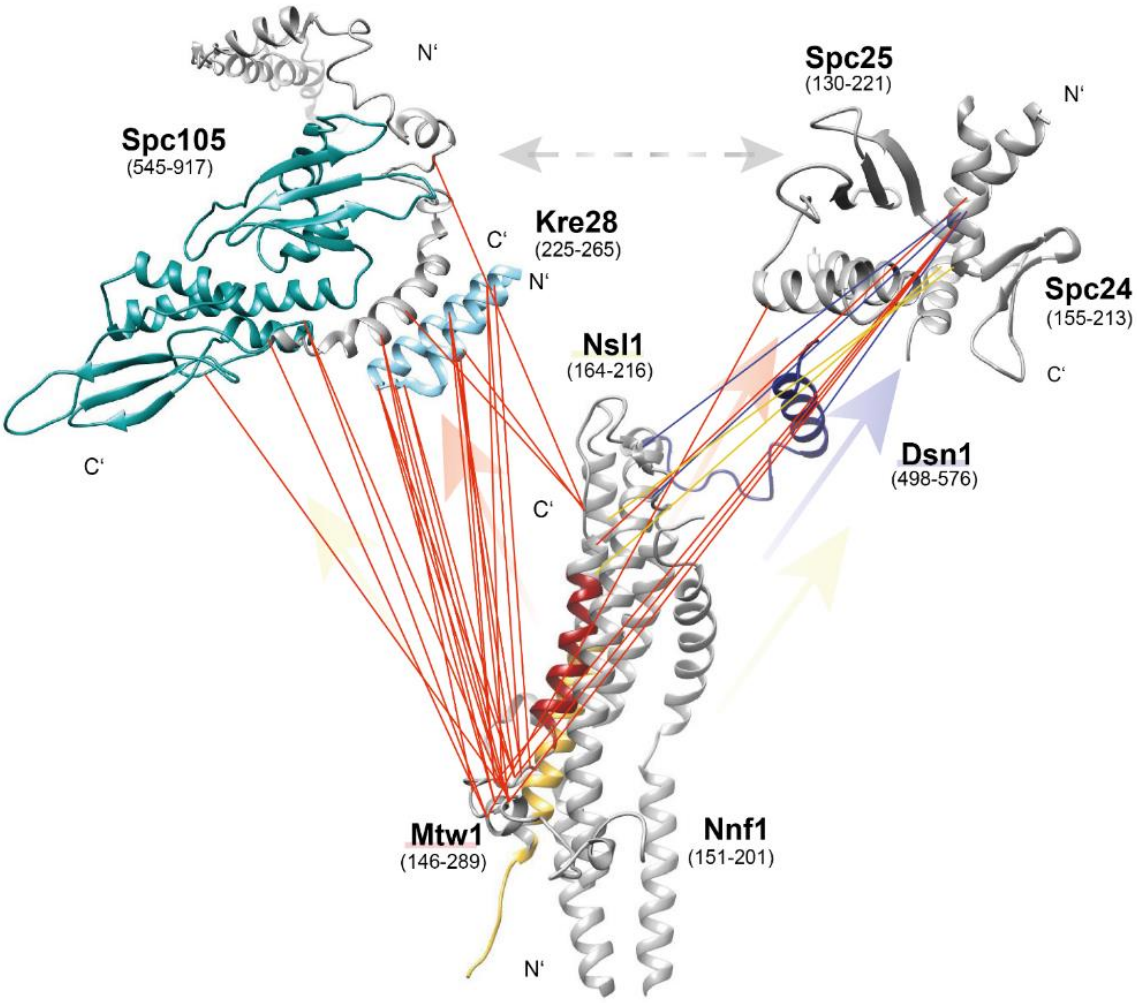

Figure 8 Crosslink Map Summarizing the Connectivity of the MTW1c C-Terminal Peptide Motifs with the Spc105/Kre28 and Spc24/25 Complexes

Models of Spc105/Kre28 and MTW1c were prepared using I-Tasser and Chimera, and the Spc24 and Spc25 C-terminal RWDs are represented by the crystal structure (PDB: 4GEQ) (Malvezzi et al. 2013). RWD domains of Spc105 (amino acids 545–917) are highlighted in cyan, and CC2 of Kre28 (amino acids 225–265) is shown in light blue. The partial model of MTW1c depicts the Mtw1 helix amino acids 232–248 (red), Nsl1 helix amino acids 164–193 (dark gold), and Dsn1 helix amino acids 547–576 (dark blue), with the accordingly colored crosslinks to Spc24/25 and Spc105/Kre28. The accordingly colored arrows indicate the binding dependencies detected in in vitro binding assays. (Figure and description from (Ghodgaonkar-Steger et al. 2020))

5 References

Akiyoshi, B., C. R. Nelson & S. Biggins (2013a) The aurora B kinase promotes inner and outer kinetochore interactions in budding yeast. *Genetics,* 194**,** 785-9.

Akiyoshi, B., C. R. Nelson, N. Duggan, S. Ceto, J. A. Ranish & S. Biggins (2013b) The Mub1/Ubr2 ubiquitin ligase complex regulates the conserved Dsn1 kinetochore protein. *PLoS Genet,* 9**,** e1003216.

Ali-Ahmad, A., S. Bilokapić, I. B. Schäfer, M. Halić & N. Sekulić (2019) CENP-C unwraps the human CENP-A nucleosome through the H2A C-terminal tail. *EMBO Rep,* 20**,** e48913.

Alushin, G. M., V. H. Ramey, S. Pasqualato, D. A. Ball, N. Grigorieff, A. Musacchio & E. Nogales (2010) The Ndc80 kinetochore complex forms oligomeric arrays along microtubules. *Nature,* 467**,** 805-10.

Amano, M., A. Suzuki, T. Hori, C. Backer, K. Okawa, I. M. Cheeseman & T. Fukagawa (2009) The CENP-S complex is essential for the stable assembly of outer kinetochore structure. *J Cell Biol,* 186**,** 173-82.

Anedchenko, E. A., A. Samel-Pommerencke, T. M. Tran Nguyen, S. Shahnejat-Bushehri, J. Pöpsel, D. Lauster, A. Herrmann, J. Rappsilber, A. Cuomo, T. Bonaldi & A. E. Ehrenhofer-Murray (2019) The kinetochore module Okp1(CENP-Q)/Ame1(CENP-U) is a reader for N-terminal modifications on the centromeric histone Cse4(CENP-A). *Embo j,* 38.

Arimura, Y., K. Shirayama, N. Horikoshi, R. Fujita, H. Taguchi, W. Kagawa, T. Fukagawa, G. Almouzni & H. Kurumizaka (2014) Crystal structure and stable property of the cancer-associated heterotypic nucleosome containing CENP-A and H3.3. *Sci Rep,* 4**,** 7115.

Barnum, K. J. & M. J. O'Connell (2014) Cell cycle regulation by checkpoints. *Methods Mol Biol,* 1170**,** 29-40.

Basilico, F., S. Maffini, J. R. Weir, D. Prumbaum, A. M. Rojas, T. Zimniak, A. De Antoni, S. Jeganathan, B. Voss, S. van Gerwen, V. Krenn, L. Massimiliano, A. Valencia, I. R. Vetter, F. Herzog, S. Raunser, S. Pasqualato & A. Musacchio (2014) The pseudo GTPase CENP-M drives human kinetochore assembly. *Elife,* 3**,** e02978.

Bellizzi, J. J., 3rd, P. K. Sorger & S. C. Harrison (2007) Crystal structure of the yeast inner kinetochore subunit Cep3p. *Structure,* 15**,** 1422-30.

Biggins, S. (2013) The composition, functions, and regulation of the budding yeast kinetochore. *Genetics,* 194**,** 817-46.

Biggins, S. & A. W. Murray (2001) The budding yeast protein kinase Ipl1/Aurora allows the absence of tension to activate the spindle checkpoint. *Genes Dev,* 15**,** 3118-29.

Black, B. E., L. E. Jansen, D. R. Foltz & D. W. Cleveland (2010) Centromere identity, function, and epigenetic propagation across cell divisions. *Cold Spring Harb Symp Quant Biol,* 75**,** 403-18.

Bock, L. J., C. Pagliuca, N. Kobayashi, R. A. Grove, Y. Oku, K. Shrestha, C. Alfieri, C. Golfieri, A. Oldani, M. Dal Maschio, R. Bermejo, T. R. Hazbun, T. U. Tanaka & P. De Wulf (2012) Cnn1 inhibits the interactions between the KMN complexes of the yeast kinetochore. *Nat Cell Biol,* 14**,** 614-24.

Boettcher, B. & Y. Barral. 2013. The cell biology of open and closed mitosis. In *Nucleus*, 160-5.

Bouck, D. C. & K. S. Bloom (2005) The kinetochore protein Ndc10p is required for spindle stability and cytokinesis in yeast. *Proc Natl Acad Sci U S A,* 102**,** 5408-13.

Brown, M. T. (1995) Sequence similarities between the yeast chromosome segregation protein Mif2 and the mammalian centromere protein CENP-C. *Gene,* 160**,** 111-6.

Camahort, R., B. Li, L. Florens, S. K. Swanson, M. P. Washburn & J. L. Gerton (2007) Scm3 is essential to recruit the histone h3 variant cse4 to centromeres and to maintain a functional kinetochore. *Mol Cell,* 26**,** 853-65.

Carroll, C. W., K. J. Milks & A. F. Straight (2010) Dual recognition of CENP-A nucleosomes is required for centromere assembly. *J Cell Biol,* 189**,** 1143-55.

Carroll, C. W., M. C. Silva, K. M. Godek, L. E. Jansen & A. F. Straight (2009) Centromere assembly requires the direct recognition of CENP-A nucleosomes by CENP-N. *Nat Cell Biol,* 11**,** 896-902.

Cheeseman, I. M. (2014) The kinetochore. *Cold Spring Harb Perspect Biol,* 6**,** a015826.

Cheeseman, I. M., S. Anderson, M. Jwa, E. M. Green, J. Kang, J. R. Yates, 3rd, C. S. Chan, D. G. Drubin & G. Barnes (2002) Phospho-regulation of kinetochore-microtubule attachments by the Aurora kinase Ipl1p. *Cell,* 111**,** 163-72.

Cheeseman, I. M., J. S. Chappie, E. M. Wilson-Kubalek & A. Desai (2006) The conserved KMN network constitutes the core microtubule-binding site of the kinetochore. *Cell,* 127**,** 983-97.

Cheeseman, I. M. & A. Desai (2008) Molecular architecture of the kinetochore-microtubule interface. *Nat Rev Mol Cell Biol,* 9**,** 33-46.
Chen, Y., R. E. Baker, K. C. Keith, K. Harris, S. Stoler & M. Fitzgerald-Hayes (2000) The N terminus of the centromere H3-like protein Cse4p performs an essential function distinct from that of the histone fold domain. *Mol Cell Biol,* 20**,** 7037-48.
Chittori, S., J. Hong, H. Saunders, H. Feng, R. Ghirlando, A. E. Kelly, Y. Bai & S. Subramaniam (2018) Structural mechanisms of centromeric nucleosome recognition by the kinetochore protein CENP-N. *Science,* 359**,** 339-343.
Cho, U. S. & S. C. Harrison (2011) Ndc10 is a platform for inner kinetochore assembly in budding yeast. *Nat Struct Mol Biol,* 19**,** 48-55.
Cimini, D. (2008) Merotelic kinetochore orientation, aneuploidy, and cancer. *Biochim Biophys Acta,* 1786**,** 32-40.
Clarke, L. (1998) Centromeres: proteins, protein complexes, and repeated domains at centromeres of simple eukaryotes. *Curr Opin Genet Dev,* 8**,** 212-8.
Clarke, L. & M. P. Baum (1990) Functional analysis of a centromere from fission yeast: a role for centromere-specific repeated DNA sequences. *Mol Cell Biol,* 10**,** 1863-72.
Cohen, R. L., C. W. Espelin, P. De Wulf, P. K. Sorger, S. C. Harrison & K. T. Simons (2008) Structural and functional dissection of Mif2p, a conserved DNA-binding kinetochore protein. *Mol Biol Cell,* 19**,** 4480-91.
Connelly, C. & P. Hieter (1996) Budding yeast SKP1 encodes an evolutionarily conserved kinetochore protein required for cell cycle progression. *Cell,* 86**,** 275-85.
Cox, J. & M. Mann (2008) MaxQuant enables high peptide identification rates, individualized p.p.b.-range mass accuracies and proteome-wide protein quantification. *Nat Biotechnol,* 26**,** 1367-72.
De Wulf, P., A. D. McAinsh & P. K. Sorger (2003) Hierarchical assembly of the budding yeast kinetochore from multiple subcomplexes. *Genes Dev,* 17**,** 2902-21.
Delobel, P. & C. Tesnière (2014) A simple FCM method to avoid misinterpretation in Saccharomyces cerevisiae cell cycle assessment between G0 and sub-G1. *PLoS One,* 9**,** e84645.
DeLuca, J. G. & A. Musacchio (2012) Structural organization of the kinetochore-microtubule interface. *Curr Opin Cell Biol,* 24**,** 48-56.
Deshaies, R. J. (1999) SCF and Cullin/Ring H2-based ubiquitin ligases. *Annu Rev Cell Dev Biol,* 15**,** 435-67.
Dimitrova, Y. N., S. Jenni, R. Valverde, Y. Khin & S. C. Harrison (2016) Structure of the MIND Complex Defines a Regulatory Focus for Yeast Kinetochore Assembly. *Cell,* 167**,** 1014-1027 e12.
Doheny, K. F., P. K. Sorger, A. A. Hyman, S. Tugendreich, F. Spencer & P. Hieter (1993) Identification of essential components of the S. cerevisiae kinetochore. *Cell,* 73**,** 761-74.
Earnshaw, W. C. & N. Rothfield (1985) Identification of a family of human centromere proteins using autoimmune sera from patients with scleroderma. *Chromosoma,* 91**,** 313-21.
Espert, A., P. Uluocak, R. N. Bastos, D. Mangat, P. Graab & U. Gruneberg (2014) PP2A-B56 opposes Mps1 phosphorylation of Knl1 and thereby promotes spindle assembly checkpoint silencing. *J Cell Biol,* 206**,** 833-42.
Faesen, A. C., M. Thanasoula, S. Maffini, C. Breit, F. Müller, S. van Gerwen, T. Bange & A. Musacchio (2017) Basis of catalytic assembly of the mitotic checkpoint complex. *Nature,* 542**,** 498-502.
Falk, S. J., J. Lee, N. Sekulic, M. A. Sennett, T. H. Lee & B. E. Black (2016) CENP-C directs a structural transition of CENP-A nucleosomes mainly through sliding of DNA gyres. *Nat Struct Mol Biol,* 23**,** 204-208.
Fang, J., Y. Liu, Y. Wei, W. Deng, Z. Yu, L. Huang, Y. Teng, T. Yao, Q. You, H. Ruan, P. Chen, R. M. Xu & G. Li (2015) Structural transitions of centromeric chromatin regulate the cell cycle-dependent recruitment of CENP-N. *Genes Dev,* 29**,** 1058-73.
Fischbock-Halwachs, J., S. Singh, M. Potocnjak, G. Hagemann, V. Solis-Mezarino, S. Woike, M. Ghodgaonkar-Steger, F. Weissmann, L. D. Gallego, J. Rojas, J. Andreani, A. Kohler & F. Herzog (2019) The COMA complex interacts with Cse4 and positions Sli15/Ipl1 at the budding yeast inner kinetochore. *Elife,* 8.
Fitzgerald-Hayes, M., L. Clarke & J. Carbon (1982) Nucleotide sequence comparisons and functional analysis of yeast centromere DNAs. *Cell,* 29**,** 235-44.
Foley, E. A. & T. M. Kapoor (2013) Microtubule attachment and spindle assembly checkpoint signalling at the kinetochore. *Nat Rev Mol Cell Biol,* 14**,** 25-37.
Foltz, D. R., L. E. Jansen, B. E. Black, A. O. Bailey, J. R. Yates, 3rd & D. W. Cleveland (2006) The human CENP-A centromeric nucleosome-associated complex. *Nat Cell Biol,* 8**,** 458-69.
Francisco, L., W. Wang & C. S. Chan (1994) Type 1 protein phosphatase acts in opposition to IpL1 protein kinase in regulating yeast chromosome segregation. *Mol Cell Biol,* 14**,** 4731-40.

Fujimitsu, K., M. Grimaldi & H. Yamano (2016) Cyclin-dependent kinase 1-dependent activation of APC/C ubiquitin ligase. *Science,* 352**,** 1121-4.
Furth, N., O. Gertman, A. Shiber, O. S. Alfassy, I. Cohen, M. M. Rosenberg, N. K. Doron, A. Friedler & T. Ravid (2011) Exposure of bipartite hydrophobic signal triggers nuclear quality control of Ndc10 at the endoplasmic reticulum/nuclear envelope. *Mol Biol Cell,* 22**,** 4726-39.
Gascoigne, K. E., K. Takeuchi, A. Suzuki, T. Hori, T. Fukagawa & I. M. Cheeseman (2011) Induced ectopic kinetochore assembly bypasses the requirement for CENP-A nucleosomes. *Cell,* 145**,** 410-22.
Ghodgaonkar-Steger, M., M. Potocnjak, T. Zimniak, J. Fischböck-Halwachs, V. Solis-Mezarino, S. Singh, T. Speljko, G. Hagemann, D. J. Drexler, G. Witte & F. Herzog (2020) C-Terminal Motifs of the MTW1 Complex Cooperatively Stabilize Outer Kinetochore Assembly in Budding Yeast. *Cell Rep,* 32**,** 108190.
Goh, P. Y. & J. V. Kilmartin (1993) NDC10: a gene involved in chromosome segregation in Saccharomyces cerevisiae. *J Cell Biol,* 121**,** 503-12.
Guacci, V., D. Koshland & A. Strunnikov (1997) A direct link between sister chromatid cohesion and chromosome condensation revealed through the analysis of MCD1 in S. cerevisiae. *Cell,* 91**,** 47-57.
Guo, L. Y., P. K. Allu, L. Zandarashvili, K. L. McKinley, N. Sekulic, J. M. Dawicki-McKenna, D. Fachinetti, G. A. Logsdon, R. M. Jamiolkowski, D. W. Cleveland, I. M. Cheeseman & B. E. Black (2017) Centromeres are maintained by fastening CENP-A to DNA and directing an arginine anchor-dependent nucleosome transition. *Nat Commun,* 8**,** 15775.
Hamilton, G. E., L. A. Helgeson, C. L. Noland, C. L. Asbury, Y. N. Dimitrova & T. N. Davis (2020) Reconstitution reveals two paths of force transmission through the kinetochore. *Elife,* 9.
Hanahan, D. & R. A. Weinberg (2000) The hallmarks of cancer. *Cell,* 100**,** 57-70.
Hara, M. & T. Fukagawa (2020) Dynamics of kinetochore structure and its regulations during mitotic progression. *Cell Mol Life Sci,* 77**,** 2981-2995.
Hegemann, J. H. & U. N. Fleig (1993) The centromere of budding yeast. *Bioessays,* 15**,** 451-60.
Helgeson, L. A., A. Zelter, M. Riffle, M. J. MacCoss, C. L. Asbury & T. N. Davis (2018) Human Ska complex and Ndc80 complex interact to form a load-bearing assembly that strengthens kinetochore-microtubule attachments. *Proc Natl Acad Sci U S A,* 115**,** 2740-2745.
Hellwig, D., S. Emmerth, T. Ulbricht, V. Döring, C. Hoischen, R. Martin, C. P. Samora, A. D. McAinsh, C. W. Carroll, A. F. Straight, P. Meraldi & S. Diekmann (2011) Dynamics of CENP-N kinetochore binding during the cell cycle. *J Cell Sci,* 124**,** 3871-83.
Henikoff, S., K. Ahmad, J. S. Platero & B. van Steensel (2000) Heterochromatic deposition of centromeric histone H3-like proteins. *Proc Natl Acad Sci U S A,* 97**,** 716-21.
Herzog, F., A. Kahraman, D. Boehringer, R. Mak, A. Bracher, T. Walzthoeni, A. Leitner, M. Beck, F. U. Hartl, N. Ban, L. Malmstrom & R. Aebersold (2012) Structural probing of a protein phosphatase 2A network by chemical cross-linking and mass spectrometry. *Science,* 337**,** 1348-52.
Hieter, P., D. Pridmore, J. H. Hegemann, M. Thomas, R. W. Davis & P. Philippsen (1985) Functional selection and analysis of yeast centromeric DNA. *Cell,* 42**,** 913-21.
Hinshaw, S. M., A. N. Dates & S. C. Harrison (2019) The structure of the yeast Ctf3 complex. *Elife,* 8.
Hinshaw, S. M. & S. C. Harrison (2013) An Iml3-Chl4 heterodimer links the core centromere to factors required for accurate chromosome segregation. *Cell Rep,* 5**,** 29-36.
--- (2018) Kinetochore Function from the Bottom Up. *Trends Cell Biol,* 28**,** 22-33.
--- (2019) The structure of the Ctf19c/CCAN from budding yeast. *Elife,* 8.
Hori, T., M. Amano, A. Suzuki, C. B. Backer, J. P. Welburn, Y. Dong, B. F. McEwen, W. H. Shang, E. Suzuki, K. Okawa, I. M. Cheeseman & T. Fukagawa (2008) CCAN makes multiple contacts with centromeric DNA to provide distinct pathways to the outer kinetochore. *Cell,* 135**,** 1039-52.
Hornung, P., M. Maier, G. M. Alushin, G. C. Lander, E. Nogales & S. Westermann (2011) Molecular architecture and connectivity of the budding yeast Mtw1 kinetochore complex. *J Mol Biol,* 405**,** 548-59.
Hornung, P., P. Troc, F. Malvezzi, M. Maier, Z. Demianova, T. Zimniak, G. Litos, F. Lampert, A. Schleiffer, M. Brunner, K. Mechtler, F. Herzog, T. C. Marlovits & S. Westermann (2014) A cooperative mechanism drives budding yeast kinetochore assembly downstream of CENP-A. *J Cell Biol,* 206**,** 509-24.
Hyland, K. M., J. Kingsbury, D. Koshland & P. Hieter (1999) Ctf19p: A novel kinetochore protein in Saccharomyces cerevisiae and a potential link between the kinetochore and mitotic spindle. *J Cell Biol,* 145**,** 15-28.

Jiang, W., J. Lechner & J. Carbon (1993) Isolation and characterization of a gene (CBF2) specifying a protein component of the budding yeast kinetochore. *J Cell Biol,* 121**,** 513-9.
Joglekar, A. P. & P. Aravamudhan (2016) How the kinetochore switches off the spindle assembly checkpoint. *Cell Cycle,* 15**,** 7-8.
Joglekar, A. P., K. Bloom & E. D. Salmon (2009) In vivo protein architecture of the eukaryotic kinetochore with nanometer scale accuracy. *Curr Biol,* 19**,** 694-9.
Kagawa, N., T. Hori, Y. Hoki, O. Hosoya, K. Tsutsui, Y. Saga, T. Sado & T. Fukagawa (2014) The CENP-O complex requirement varies among different cell types. *Chromosome Res,* 22**,** 293-303.
Kaplan, K. B., A. A. Hyman & P. K. Sorger (1997) Regulating the yeast kinetochore by ubiquitin-dependent degradation and Skp1p-mediated phosphorylation. *Cell,* 91**,** 491-500.
Kato, H., J. Jiang, B. R. Zhou, M. Rozendaal, H. Feng, R. Ghirlando, T. S. Xiao, A. F. Straight & Y. Bai (2013) A conserved mechanism for centromeric nucleosome recognition by centromere protein CENP-C. *Science,* 340**,** 1110-3.
Keith, K. C., R. E. Baker, Y. Chen, K. Harris, S. Stoler & M. Fitzgerald-Hayes (1999) Analysis of primary structural determinants that distinguish the centromere-specific function of histone variant Cse4p from histone H3. *Mol Cell Biol,* 19**,** 6130-9.
Kelly, A. E. & H. Funabiki (2009) Correcting aberrant kinetochore microtubule attachments: an Aurora B-centric view. *Curr Opin Cell Biol,* 21**,** 51-8.
Killinger, K., M. Böhm, P. Steinbach, G. Hagemann, M. Blüggel, K. Jänen, S. Hohoff, P. Bayer, F. Herzog & S. Westermann (2020) Auto-inhibition of Mif2/CENP-C ensures centromere-dependent kinetochore assembly in budding yeast. *Embo j,* 39**,** e102938.
Kim, S. & H. Yu (2011) Mutual regulation between the spindle checkpoint and APC/C. *Semin Cell Dev Biol,* 22**,** 551-8.
Kitagawa, K., D. Skowyra, S. J. Elledge, J. W. Harper & P. Hieter (1999) SGT1 encodes an essential component of the yeast kinetochore assembly pathway and a novel subunit of the SCF ubiquitin ligase complex. *Mol Cell,* 4**,** 21-33.
Kiyomitsu, T., H. Murakami & M. Yanagida (2011) Protein interaction domain mapping of human kinetochore protein Blinkin reveals a consensus motif for binding of spindle assembly checkpoint proteins Bub1 and BubR1. *Mol Cell Biol,* 31**,** 998-1011.
Knockleby, J. & J. Vogel (2009) The COMA complex is required for Sli15/INCENP-mediated correction of defective kinetochore attachments. *Cell Cycle,* 8**,** 2570-7.
Kouprina, N., A. Kirillov, E. Kroll, M. Koryabin, B. Shestopalov, V. Bannikov, V. Zakharyev & V. Larionov (1993) Identification and cloning of the CHL4 gene controlling chromosome segregation in yeast. *Genetics,* 135**,** 327-41.
Kudalkar, E. M., E. A. Scarborough, N. T. Umbreit, A. Zelter, D. R. Gestaut, M. Riffle, R. S. Johnson, M. J. MacCoss, C. L. Asbury & T. N. Davis (2015) Regulation of outer kinetochore Ndc80 complex-based microtubule attachments by the central kinetochore Mis12/MIND complex. *Proc Natl Acad Sci U S A,* 112**,** E5583-9.
Lang, J., A. Barber & S. Biggins (2018) An assay for de novo kinetochore assembly reveals a key role for the CENP-T pathway in budding yeast. *Elife,* 7.
Lanini, L. & F. McKeon (1995) Domains required for CENP-C assembly at the kinetochore. *Mol Biol Cell,* 6**,** 1049-59.
Leber, V. 2018. Structural and functional studies of the budding yeast kinetochore complex CBF3. In *The Francis Crick Institute*. University College London: University College London.
Leber, V., A. Nans & M. R. Singleton (2018) Structural basis for assembly of the CBF3 kinetochore complex. *Embo j,* 37**,** 269-281.
Lechner, J. & J. Carbon (1991) A 240 kd multisubunit protein complex, CBF3, is a major component of the budding yeast centromere. *Cell,* 64**,** 717-25.
Lee, P. D., H. Wei, D. Tan & S. C. Harrison (2019) Structure of the Centromere Binding Factor 3 Complex from Kluyveromyces lactis. *J Mol Biol,* 431**,** 4444-4454.
Levan, A. F., K.; Sandberg, A. A. (1964) Nomenclature for centromeric position on chromosomes. *Hereditas,* 52**,** 201-220.
Li, R. & A. W. Murray (1991) Feedback control of mitosis in budding yeast. *Cell,* 66**,** 519-31.
Lingelbach, L. B. & K. B. Kaplan (2004) The interaction between Sgt1p and Skp1p is regulated by HSP90 chaperones and is required for proper CBF3 assembly. *Mol Cell Biol,* 24**,** 8938-50.
Liu, D., M. Vleugel, C. B. Backer, T. Hori, T. Fukagawa, I. M. Cheeseman & M. A. Lampson (2010) Regulated targeting of protein phosphatase 1 to the outer kinetochore by KNL1 opposes Aurora B kinase. *J Cell Biol,* 188**,** 809-20.

London, N. & S. Biggins (2014) Signalling dynamics in the spindle checkpoint response. *Nat Rev Mol Cell Biol,* 15**,** 736-47.
London, N., S. Ceto, J. A. Ranish & S. Biggins (2012) Phosphoregulation of Spc105 by Mps1 and PP1 regulates Bub1 localization to kinetochores. *Curr Biol,* 22**,** 900-6.
Lowary, P. T. & J. Widom (1998) New DNA sequence rules for high affinity binding to histone octamer and sequence-directed nucleosome positioning. *J Mol Biol,* 276**,** 19-42.
Luger, K., A. W. Mader, R. K. Richmond, D. F. Sargent & T. J. Richmond (1997) Crystal structure of the nucleosome core particle at 2.8 A resolution. *Nature,* 389**,** 251-60.
Malvezzi, F., G. Litos, A. Schleiffer, A. Heuck, K. Mechtler, T. Clausen & S. Westermann (2013) A structural basis for kinetochore recruitment of the Ndc80 complex via two distinct centromere receptors. *EMBO J,* 32**,** 409-23.
Mann, R. K. & M. Grunstein (1992) Histone H3 N-terminal mutations allow hyperactivation of the yeast GAL1 gene in vivo. *Embo j,* 11**,** 3297-306.
McKinley, K. L., N. Sekulic, L. Y. Guo, T. Tsinman, B. E. Black & I. M. Cheeseman (2015) The CENP-L-N Complex Forms a Critical Node in an Integrated Meshwork of Interactions at the Centromere-Kinetochore Interface. *Mol Cell,* 60**,** 886-98.
Meadows, J. C. & J. B. Millar (2015) Sharpening the anaphase switch. *Biochem Soc Trans,* 43**,** 19-22.
Measday, V., D. W. Hailey, I. Pot, S. A. Givan, K. M. Hyland, G. Cagney, S. Fields, T. N. Davis & P. Hieter (2002) Ctf3p, the Mis6 budding yeast homolog, interacts with Mcm22p and Mcm16p at the yeast outer kinetochore. *Genes Dev,* 16**,** 101-13.
Mellor, J., J. Rathjen, W. Jiang, C. A. Barnes & S. J. Dowell (1991) DNA binding of CPF1 is required for optimal centromere function but not for maintaining methionine prototrophy in yeast. *Nucleic Acids Res,* 19**,** 2961-9.
Meluh, P. B. & D. Koshland (1997) Budding yeast centromere composition and assembly as revealed by in vivo cross-linking. *Genes Dev,* 11**,** 3401-12.
Michaelis, C., R. Ciosk & K. Nasmyth (1997) Cohesins: chromosomal proteins that prevent premature separation of sister chromatids. *Cell,* 91**,** 35-45.
Migl, D., M. Kschonsak, C. P. Arthur, Y. Khin, S. C. Harrison, C. Ciferri & Y. N. Dimitrova (2020) Cryoelectron Microscopy Structure of a Yeast Centromeric Nucleosome at 2.7 Å Resolution. *Structure,* 28**,** 363-370.e3.
Milks, K. J., B. Moree & A. F. Straight (2009) Dissection of CENP-C-directed centromere and kinetochore assembly. *Mol Biol Cell,* 20**,** 4246-55.
Murray, A. W. (2004) Recycling the cell cycle: cyclins revisited. *Cell,* 116**,** 221-34.
Musacchio, A. (2015) The Molecular Biology of Spindle Assembly Checkpoint Signaling Dynamics. *Curr Biol,* 25**,** R1002-18.
Musacchio, A. & A. Desai (2017) A Molecular View of Kinetochore Assembly and Function. *Biology (Basel),* 6.
Musacchio, A. & E. D. Salmon (2007) The spindle-assembly checkpoint in space and time. *Nat Rev Mol Cell Biol,* 8**,** 379-93.
Nagpal, H. & T. Fukagawa (2016) Kinetochore assembly and function through the cell cycle. *Chromosoma,* 125**,** 645-59.
Nasmyth, K. (1996) At the heart of the budding yeast cell cycle. *Trends Genet,* 12**,** 405-12.
Ng, R. & J. Carbon (1987) Mutational and in vitro protein-binding studies on centromere DNA from Saccharomyces cerevisiae. *Mol Cell Biol,* 7**,** 4522-34.
Nicklas, R. B. (1997) How cells get the right chromosomes. *Science,* 275**,** 632-7.
Nishino, T., K. Takeuchi, K. E. Gascoigne, A. Suzuki, T. Hori, T. Oyama, K. Morikawa, I. M. Cheeseman & T. Fukagawa (2012) CENP-T-W-S-X forms a unique centromeric chromatin structure with a histone-like fold. *Cell,* 148**,** 487-501.
O'Connor, C. (2008) Chromosome segregation in mitosis: The role of centromeres. *Nature Education,* 1**,** 28.
Orlicky, S., X. Tang, A. Willems, M. Tyers & F. Sicheri (2003) Structural basis for phosphodependent substrate selection and orientation by the SCFCdc4 ubiquitin ligase. *Cell,* 112**,** 243-56.
Ortiz, J., O. Stemmann, S. Rank & J. Lechner (1999) A putative protein complex consisting of Ctf19, Mcm21, and Okp1 represents a missing link in the budding yeast kinetochore. *Genes Dev,* 13**,** 1140-55.
Pagliuca, C., V. M. Draviam, E. Marco, P. K. Sorger & P. De Wulf (2009) Roles for the conserved spc105p/kre28p complex in kinetochore-microtubule binding and the spindle assembly checkpoint. *PLoS One,* 4**,** e7640.

Pekgoz Altunkaya, G., F. Malvezzi, Z. Demianova, T. Zimniak, G. Litos, F. Weissmann, K. Mechtler, F. Herzog & S. Westermann (2016a) CCAN Assembly Configures Composite Binding Interfaces to Promote Cross-Linking of Ndc80 Complexes at the Kinetochore. *Curr Biol,* 26**,** 2370-8.
--- (2016b) CCAN Assembly Configures Composite Binding Interfaces to Promote Cross-Linking of Ndc80 Complexes at the Kinetochore. *Curr Biol*.
Pentakota, S., K. Zhou, C. Smith, S. Maffini, A. Petrovic, G. P. Morgan, J. R. Weir, I. R. Vetter, A. Musacchio & K. Luger (2017) Decoding the centromeric nucleosome through CENP-N. *Elife,* 6.
Perriches, T. & M. R. Singleton (2012) Structure of yeast kinetochore Ndc10 DNA-binding domain reveals unexpected evolutionary relationship to tyrosine recombinases. *J Biol Chem,* 287**,** 5173-9.
Pesenti, M. E., D. Prumbaum, P. Auckland, C. M. Smith, A. C. Faesen, A. Petrovic, M. Erent, S. Maffini, S. Pentakota, J. R. Weir, Y. C. Lin, S. Raunser, A. D. McAinsh & A. Musacchio (2018) Reconstitution of a 26-Subunit Human Kinetochore Reveals Cooperative Microtubule Binding by CENP-OPQUR and NDC80. *Mol Cell,* 71**,** 923-939.e10.
Pesenti, M. E., J. R. Weir & A. Musacchio (2016) Progress in the structural and functional characterization of kinetochores. *Curr Opin Struct Biol,* 37**,** 152-63.
Petrovic, A., S. Mosalaganti, J. Keller, M. Mattiuzzo, K. Overlack, V. Krenn, A. De Antoni, S. Wohlgemuth, V. Cecatiello, S. Pasqualato, S. Raunser & A. Musacchio (2014) Modular assembly of RWD domains on the Mis12 complex underlies outer kinetochore organization. *Mol Cell,* 53**,** 591-605.
Petrovic, A., S. Pasqualato, P. Dube, V. Krenn, S. Santaguida, D. Cittaro, S. Monzani, L. Massimiliano, J. Keller, A. Tarricone, A. Maiolica, H. Stark & A. Musacchio (2010) The MIS12 complex is a protein interaction hub for outer kinetochore assembly. *J Cell Biol,* 190**,** 835-52.
Pluta, A. F., A. M. Mackay, A. M. Ainsztein, I. G. Goldberg & W. C. Earnshaw (1995) The centromere: hub of chromosomal activities. *Science,* 270**,** 1591-4.
Pot, I., V. Measday, B. Snydsman, G. Cagney, S. Fields, T. N. Davis, E. G. Muller & P. Hieter (2003) Chl4p and iml3p are two new members of the budding yeast outer kinetochore. *Mol Biol Cell,* 14**,** 460-76.
Primorac, I., J. R. Weir, E. Chiroli, F. Gross, I. Hoffmann, S. van Gerwen, A. Ciliberto & A. Musacchio (2013) Bub3 reads phosphorylated MELT repeats to promote spindle assembly checkpoint signaling. *Elife,* 2**,** e01030.
Przewloka, M. R., Z. Venkei, V. M. Bolanos-Garcia, J. Debski, M. Dadlez & D. M. Glover (2011) CENP-C is a structural platform for kinetochore assembly. *Curr Biol,* 21**,** 399-405.
Purvis, A. & M. R. Singleton (2008) Insights into kinetochore-DNA interactions from the structure of Cep3Delta. *EMBO Rep,* 9**,** 56-62.
Qiao, R., F. Weissmann, M. Yamaguchi, N. G. Brown, R. VanderLinden, R. Imre, M. A. Jarvis, M. R. Brunner, I. F. Davidson, G. Litos, D. Haselbach, K. Mechtler, H. Stark, B. A. Schulman & J. M. Peters (2016) Mechanism of APC/CCDC20 activation by mitotic phosphorylation. *Proc Natl Acad Sci U S A,* 113**,** E2570-8.
Rodrigo-Brenni, M. C., S. Thomas, D. C. Bouck & K. B. Kaplan (2004) Sgt1p and Skp1p modulate the assembly and turnover of CBF3 complexes required for proper kinetochore function. *Mol Biol Cell,* 15**,** 3366-78.
Russell, I. D., A. S. Grancell & P. K. Sorger (1999) The unstable F-box protein p58-Ctf13 forms the structural core of the CBF3 kinetochore complex. *J Cell Biol,* 145**,** 933-50.
Schalch, T. & F. A. Steiner (2017) Structure of centromere chromatin: from nucleosome to chromosomal architecture. *Chromosoma,* 126**,** 443-455.
Schleiffer, A., M. Maier, G. Litos, F. Lampert, P. Hornung, K. Mechtler & S. Westermann (2012) CENP-T proteins are conserved centromere receptors of the Ndc80 complex. *Nat Cell Biol,* 14**,** 604-13.
Schmitzberger, F., M. M. Richter, Y. Gordiyenko, C. V. Robinson, M. Dadlez & S. Westermann (2017) Molecular basis for inner kinetochore configuration through RWD domain-peptide interactions. *EMBO J*.
Screpanti, E., A. De Antoni, G. M. Alushin, A. Petrovic, T. Melis, E. Nogales & A. Musacchio (2011) Direct binding of Cenp-C to the Mis12 complex joins the inner and outer kinetochore. *Curr Biol,* 21**,** 391-8.
Seol, J. H., A. Shevchenko, A. Shevchenko & R. J. Deshaies (2001) Skp1 forms multiple protein complexes, including RAVE, a regulator of V-ATPase assembly. *Nat Cell Biol,* 3**,** 384-91.
Sharp, L. W. 1921. *An introduction to cytology*. New York McGraw-Hill book company.

Sievers, F., A. Wilm, D. Dineen, T. J. Gibson, K. Karplus, W. Li, R. Lopez, H. McWilliam, M. Remmert, J. Söding, J. D. Thompson & D. G. Higgins (2011) Fast, scalable generation of high-quality protein multiple sequence alignments using Clustal Omega. *Mol Syst Biol,* 7**,** 539.

Song, K., B. Gronemeyer, W. Lu, E. Eugster & J. E. Tomkiel (2002) Mutational analysis of the central centromere targeting domain of human centromere protein C, (CENP-C). *Exp Cell Res,* 275**,** 81-91.

Spencer, F., S. L. Gerring, C. Connelly & P. Hieter (1990) Mitotic chromosome transmission fidelity mutants in Saccharomyces cerevisiae. *Genetics,* 124**,** 237-49.

Stemmann, O. & J. Lechner (1996) The Saccharomyces cerevisiae kinetochore contains a cyclin-CDK complexing homologue, as identified by in vitro reconstitution. *Embo j,* 15**,** 3611-20.

Stoler, S., K. C. Keith, K. E. Curnick & M. Fitzgerald-Hayes (1995) A mutation in CSE4, an essential gene encoding a novel chromatin-associated protein in yeast, causes chromosome nondisjunction and cell cycle arrest at mitosis. *Genes Dev,* 9**,** 573-86.

Strunnikov, A. V., J. Kingsbury & D. Koshland (1995) CEP3 encodes a centromere protein of Saccharomyces cerevisiae. *J Cell Biol,* 128**,** 749-60.

Sullivan, M. & D. O. Morgan (2007) Finishing mitosis, one step at a time. *Nat Rev Mol Cell Biol,* 8**,** 894-903.

Suzuki, A., T. Hori, T. Nishino, J. Usukura, A. Miyagi, K. Morikawa & T. Fukagawa (2011) Spindle microtubules generate tension-dependent changes in the distribution of inner kinetochore proteins. *J Cell Biol,* 193**,** 125-40.

Swartz, S. Z., L. S. McKay, K. C. Su, L. Bury, A. Padeganeh, P. S. Maddox, K. A. Knouse & I. M. Cheeseman (2019) Quiescent Cells Actively Replenish CENP-A Nucleosomes to Maintain Centromere Identity and Proliferative Potential. *Dev Cell,* 51**,** 35-48.e7.

Takeuchi, K., T. Nishino, K. Mayanagi, N. Horikoshi, A. Osakabe, H. Tachiwana, T. Hori, H. Kurumizaka & T. Fukagawa (2014) The centromeric nucleosome-like CENP-T-W-S-X complex induces positive supercoils into DNA. *Nucleic Acids Res,* 42**,** 1644-55.

Tanaka, T. U., N. Rachidi, C. Janke, G. Pereira, M. Galova, E. Schiebel, M. J. Stark & K. Nasmyth (2002) Evidence that the Ipl1-Sli15 (Aurora kinase-INCENP) complex promotes chromosome bi-orientation by altering kinetochore-spindle pole connections. *Cell,* 108**,** 317-29.

Tang, X., S. Orlicky, T. Mittag, V. Csizmok, T. Pawson, J. D. Forman-Kay, F. Sicheri & M. Tyers (2012) Composite low affinity interactions dictate recognition of the cyclin-dependent kinase inhibitor Sic1 by the SCFCdc4 ubiquitin ligase. *Proc Natl Acad Sci U S A,* 109**,** 3287-92.

Taylor, S. S., E. Ha & F. McKeon (1998) The human homologue of Bub3 is required for kinetochore localization of Bub1 and a Mad3/Bub1-related protein kinase. *J Cell Biol,* 142**,** 1-11.

Thakur, J. & S. Henikoff (2016) CENPT bridges adjacent CENPA nucleosomes on young human α-satellite dimers. *Genome Res,* 26**,** 1178-87.

Tian, T., X. Li, Y. Liu, C. Wang, X. Liu, G. Bi, X. Zhang, X. Yao, Z. H. Zhou & J. Zang (2018) Molecular basis for CENP-N recognition of CENP-A nucleosome on the human kinetochore. *Cell Res,* 28**,** 374-378.

Verdaasdonk, J. S. & K. Bloom (2011) Centromeres: unique chromatin structures that drive chromosome segregation. *Nat Rev Mol Cell Biol,* 12**,** 320-32.

Walczak, C. E., S. Cai & A. Khodjakov (2010) Mechanisms of chromosome behaviour during mitosis. *Nat Rev Mol Cell Biol,* 11**,** 91-102.

Walzthoeni, T., M. Claassen, A. Leitner, F. Herzog, S. Bohn, F. Forster, M. Beck & R. Aebersold (2012) False discovery rate estimation for cross-linked peptides identified by mass spectrometry. *Nat Methods,* 9**,** 901-3.

Wang, H. W., S. Long, C. Ciferri, S. Westermann, D. Drubin, G. Barnes & E. Nogales (2008) Architecture and flexibility of the yeast Ndc80 kinetochore complex. *J Mol Biol,* 383**,** 894-903.

Weaver, B. A. & D. W. Cleveland (2006) Does aneuploidy cause cancer? *Curr Opin Cell Biol,* 18**,** 658-67.

Weir, J. R., A. C. Faesen, K. Klare, A. Petrovic, F. Basilico, J. Fischbock, S. Pentakota, J. Keller, M. E. Pesenti, D. Pan, D. Vogt, S. Wohlgemuth, F. Herzog & A. Musacchio (2016) Insights from biochemical reconstitution into the architecture of human kinetochores. *Nature,* 537**,** 249-253.

Weiss, E. & M. Winey (1996) The Saccharomyces cerevisiae spindle pole body duplication gene MPS1 is part of a mitotic checkpoint. *J Cell Biol,* 132**,** 111-23.

Weissmann, F., G. Petzold, R. VanderLinden, P. J. Huis In 't Veld, N. G. Brown, F. Lampert, S. Westermann, H. Stark, B. A. Schulman & J. M. Peters (2016) biGBac enables rapid gene assembly for the expression of large multisubunit protein complexes. *Proc Natl Acad Sci U S A,* 113**,** E2564-9.

Westermann, S., I. M. Cheeseman, S. Anderson, J. R. Yates, 3rd, D. G. Drubin & G. Barnes (2003) Architecture of the budding yeast kinetochore reveals a conserved molecular core. *J Cell Biol,* 163**,** 215-22.
Westermann, S., H. W. Wang, A. Avila-Sakar, D. G. Drubin, E. Nogales & G. Barnes (2006) The Dam1 kinetochore ring complex moves processively on depolymerizing microtubule ends. *Nature,* 440**,** 565-9.
Willard, H. F. (1990) Centromeres of mammalian chromosomes. *Trends Genet,* 6**,** 410-6.
Wolffe, A. P. & J. J. Hayes (1999) Chromatin disruption and modification. *Nucleic Acids Res,* 27**,** 711-20.
Xiao, H., F. Wang, J. Wisniewski, A. K. Shaytan, R. Ghirlando, P. C. FitzGerald, Y. Huang, D. Wei, S. Li, D. Landsman, A. R. Panchenko & C. Wu (2017) Molecular basis of CENP-C association with the CENP-A nucleosome at yeast centromeres. *Genes Dev,* 31**,** 1958-1972.
Yan, K., J. Yang, Z. Zhang, S. H. McLaughlin, L. Chang, D. Fasci, A. E. Ehrenhofer-Murray, A. J. R. Heck & D. Barford (2019) Structure of the inner kinetochore CCAN complex assembled onto a centromeric nucleosome. *Nature,* 574**,** 278-282.
Yan, K., Z. Zhang, J. Yang, S. H. McLaughlin & D. Barford (2018) Architecture of the CBF3-centromere complex of the budding yeast kinetochore. *Nat Struct Mol Biol,* 25**,** 1103-1110.
Yoon, H. J. & J. Carbon (1999) Participation of Bir1p, a member of the inhibitor of apoptosis family, in yeast chromosome segregation events. *Proc Natl Acad Sci U S A,* 96**,** 13208-13.
Zaytsev, A. V., L. J. Sundin, K. F. DeLuca, E. L. Grishchuk & J. G. DeLuca (2014) Accurate phosphoregulation of kinetochore-microtubule affinity requires unconstrained molecular interactions. *J Cell Biol,* 206**,** 45-59.
Zhang, W., N. Lukoyanova, S. Miah, J. Lucas & C. K. Vaughan (2019) Insights into Centromere DNA Bending Revealed by the Cryo-EM Structure of the Core Centromere Binding Factor 3 with Ndc10. *Cell Rep,* 26**,** 1070.